

Colonization studies of *Clavibacter michiganensis* in fruit and xylem of diverse  
*Solanum* species

A Dissertation

Presented to the Faculty of the Graduate School  
of Cornell University

In Partial Fulfillment of the Requirements for the Degree of  
Doctor of Philosophy

by

Franklin Christopher Peritore

May 2020

© 2020 Franklin Christopher Peritore

Colonization studies of *Clavibacter michiganensis* in fruit and xylem of diverse  
*Solanum* species

Franklin Christopher Peritore, Ph. D.

Cornell University 2020

Bacterial canker of tomato is an economically devastating disease with a worldwide distribution caused by the gram-positive pathogen *Clavibacter michiganensis*. The seedborne pathogen systemically colonizes the tomato xylem, causing unilateral leaflet wilt, stem and petiole cankers, marginal leaf necrosis, and plant death. Splash dispersal of the bacterium onto fruit exteriors causes bird's-eye lesions, which are characterized as necrotic centers surrounded by white halos. The pathogen can colonize developing seeds systemically through the xylem and through penetration of fruit tissues from the exterior. There are no commercially available resistant tomato cultivars, and copper-based bactericides have limited efficacy for controlling the disease once the pathogen is in the xylem. This dissertation describes differences in pathogen colonization of xylem and fruit between tolerant and susceptible *Solanum* species, demonstrating that *C. michiganensis* is impeded in systemic and intravascular spread in the xylem, and is capable of causing bird's-eye lesions on wild tomato fruit. The size at which *S. lycopersicum* fruit inoculated with *C. michiganensis* and two additional bacterial pathogens begins developing lesions, peaks in susceptibility, and ceases developing lesions was determined in wildtype and ethylene-responsive mutants. Changes in chemical composition of xylem sap from susceptible *S. lycopersicum* and tolerant *S. habrochaites* plants during *C. michiganensis* infection

was determined using untargeted metabolomics. Finally, a high-resolution proteome of *C. michiganensis* pellets and supernatant samples was generated and used to refine the reference genome. Together, these data provide a deeper understanding of *C. michiganensis* colonization of diverse host tissues, as well as host responses that may contribute to symptom development.

## BIOGRAPHICAL SKETCH

Chris Peritore-Galve was born in Columbia, Missouri and was raised between there and his second home with his family in Mexico City. He received his Bachelors of Science in Biology with a minor in Spanish literature from the University of Missouri in 2015. There he was encouraged to pursue a career in science through the Initiative for Maximizing Student Diversity program, under the guidance of Brian Booton. This program provided him with funding and training to work in the laboratory of Dr. Douglas Randall under the mentorship of Dr. Elizabeth Hoyos, where he studied the role of genes encoding the plant mitochondrial pyruvate dehydrogenase complex on plant development. He began graduate school in 2015 at Cornell University in the section of Plant Pathology and Plant-Microbe biology conducting rotations in the laboratories of Dr. Christine Smart, Dr. Adam Bogdanove, and Dr. Michelle Heck with the support of a Dean's Excellence Fellowship. Dr. Christine Smart's patient mentorship allowed him to study various aspects of *Clavibacter michiganensis* biology and pathology in diverse host systems. During his time at Cornell, he held various leadership roles in the Plant Pathology Graduate Student Association, the School of Integrative Plant Science (SIPS) Graduate Student Council, and the Diversity Preview Weekend (DPW) organizing committee. He helped co-found the Cornell chapter of the Society for Advancement of Chicanos/Hispanics and Native Americans in Science, led efforts to organize DPW for SIPS, and worked to successfully change admissions processes in the PPPMB section. He was selected as a Graduate School Ambassador who was sent to the national SACNAS meeting to help recruit students during his time in graduate school.

A mi madre, que, sin sus sacrificios innumerables, su apoyo incondicional, y sus grandes sueños para sus hijos, nada de esto hubiera sido posible.

## ACKNOWLEDGMENTS

I thank my advisor, Dr. Christine Smart, who, despite my broad interests and inexperience with plant pathology gave me the opportunity to pursue a PhD in her lab. She gave me the freedom to pursue my scientific interests and to prioritize efforts for making SIPS and Cornell more inclusive and diverse. I will forever be grateful for her mentorship and guidance during my journey to becoming a scientist, communicator, and leader at Cornell.

I would like to thank my committee members, Dr. Magdalen Lindeberg, Dr. Anthony Hay, and Dr. Bryan Swingle, who have supported me and provided me with helpful insights about my dissertation research. I also thank Dr. Marc Fuchs, Dr. Tom Burr, and Dr. Kerik Cox, for their valuable mentorship and friendship throughout my PhD.

This PhD would not have been possible without an amazing research group. I am appreciative for the support, guidance, and fun times provided by Smart lab members past and present, especially Chase Crowell, Greg Vogel, Matt Tancos, Martha Sudermann, Ali Cala, Juan Luis González-Girón, Holly Lange, Colin Day, and Garrett Giles. I am also thankful for the amazing mentees, Erica Robinson, Alvin Han, Christine Miller, and Tatiana Ortiz Sanabria, whom I have had the pleasure of working with through the summer scholars program.

Thank you to the people who inspired me to pursue a PhD and who helped me each step of the way. In particular, I thank Brian Booton, who has dedicated his life to helping students from underrepresented backgrounds find a home at MU and helped countless of us flourish in academic careers. Gracias a mi mentora, Dra. Elizabeth Hoyos, quien dedico tanto de su tiempo entrenándome en el laboratorio. Pero también me enseñó que la familia siempre será más importante que el trabajo. Finally, thank

you to Anitra Douglas-McCarthy, who recruited me at the ABRCMS conference, guided me through applying to Cornell, and who has supported me personally and professionally while I was here.

On a personal note, I am beyond grateful for the community that I have built at home and at Cornell that has allowed me to grow into who I am today. I am especially thankful to my wonderful partner Angela Kruse for her love and support, and for always finding a way to make life exciting. I am thankful for my family who taught me to work hard but to always find the humor in life. I am very thankful for my brother, Michael Peritore, who has taught me to be both carefree in life, but to be strong in my convictions. To my father, who instilled the value of reading and learning a wide variety of topics. Finally, to my friends for their support and who have made my time here amazing: Chase Crowell, Katrin Ayer, Bill Weldon, Libby Cieniewicz, Greg Vogel, Matt Tancos, Zoë Dubrow, Juan Luis González-Girón, Andy Read, Josue San Emeterio, Ayah Almousa, Amanda Restrepo, Marysol Luna, Sarah Naiman, Amnon Blotch, Jamal Elkhader, Adam Brady, Marco Hinojosa, Emily Betz, Jon Wheeler, Steven Caratti, Austin Nelson, Adrienne Gorny, Victoria Hassebroek Mariko Alexander and Dave Alexander.

This work was supported in part by Federal Capacity Funds through the New York State Agricultural Experiment Station at Cornell AgriTech, and by a Schmittau-Novak small grant through the School of Integrative Plant Sciences.

## TABLE OF CONTENTS

<u>Biographical sketch</u> .....	v
<u>Table of contents</u> .....	ix
<u>Introduction</u> .....	1
<u>Chapter 1</u> : Characterizing colonization patterns of <i>Clavibacter michiganensis</i> during infection of tolerant wild <i>Solanum</i> species.....	41
<u>Chapter 2</u> : Tomato fruit development plays a critical role in susceptibility to three bacterial pathogens.....	81
<u>Chapter 3</u> : Understanding the effects of <i>Clavibacter michiganensis</i> infection on xylem sap of wild and cultivated tomato using untargeted metabolomics.....	138
<u>Chapter 4</u> : Proteome profile and genome refinement of the tomato-pathogenic bacterium <i>Clavibacter michiganensis</i> subsp. <i>michiganensis</i> .....	201
<u>Conclusions and future studies</u> .....	225
<u>Appendix 1</u> : Assessing the role of the uncharacterized OLD nuclease in <i>Xanthomonas campestris</i> pv. <i>campestris</i> .....	246
<u>Appendix 2</u> : Diversity Preview Weekend 2018 extension report.....	281

## INTRODUCTION

### **History, taxonomic classification and economic relevance of bacterial canker**

Bacterial canker of tomato is an economically destructive disease caused by the gram-positive actinomycete *Clavibacter michiganensis* (de León et al., 2011; Sen et al., 2015; Nandi et al., 2018). The first scientific report of bacterial canker, then known as the “Grand Rapids tomato disease,” was by Erwin Smith in the early 1900s (Smith 1910). Since the first isolation in 1909, this pathogen has been detected globally, becoming an economically challenging problem for tomato growers worldwide.

The first recorded Latin binomial names of the causal agent were *Bacterium michiganense*, and shortly after, *Aplanobacter michiganense*, which described the non-motile, rod-like bacterium isolated from tomato plants in Michigan (Smith 1914; Payne and Lacey 1922; Bryan 1930). It was later reclassified as *Corynebacterium michiganense*, based on its irregular cell shape, and then into its current genus *Clavibacter* based on its unique 2,4-diaminobutyric acid content in its cell wall peptidoglycan (Jensen 1934; Collins and Jones 1980; Davis et al., 1984). The genus *Clavibacter* contained pathogens now classified into the genera *Rathayibacter* and *Leifsonia*, and the sole species remaining was *Clavibacter michiganensis* (Zgurskaya et al., 1993; Suzuki et al., 1999; Evtushenko et al., 2000; Li et al., 2017). The species *Clavibacter michiganensis* was comprised of five economically damaging plant-pathogenic subspecies: *C. michiganensis* subsp. *michiganensis* (bacterial canker of tomato), *C. michiganensis* subsp. *sepedonicus* (ring rot of potato), *C. michiganensis* subsp. *insidiosus* (alfalfa wilt), *C. michiganensis* subsp. *nebraskensis* (Goss’ wilt of corn), and *C. michiganensis* subsp. *tessellarius* (leaf spot of wheat). Recent reclassification of the *Clavibacter* genus using whole genome sequences and multi-locus sequence typing raised all of the subspecies to species level (Li et al.,

2017). The current composition of this genus is *C. michiganensis*, *C. insidiosus*, *C. nebraskensis*, *C. sepedonicus*, *C. tessellarius*, and the new species *C. capsici* (bacterial canker of pepper) (Oh et al., 2016; Li et al., 2017; Nandi et al., 2018). New *Clavibacter* species including non-pathogenic endophytes have been proposed, highlighting the genetic and ecological differences within this genus (Osdaghi et al., 2020).

Few reports exist on the economic losses caused by bacterial canker in a given growing season. The first reported outbreak of bacterial canker caused \$8,000 to \$10,000 in economic losses for the grower, or \$218,000 to \$272,000 in today's US dollar (Smith 1910). Bacterial canker reports from Michigan estimated sporadic losses of up to \$300,000 for a tomato grower in any given year (Hausbeck et al., 2000). Yield losses can vary between 46 to 93 percent of plants lost, and approximately 50 percent decreases in average fruit weight during severe epidemics (Emmatty and John 1973; Poysa 1993; Chang et al., 1992). Over 4.8 million hectares of land around the world produce 180 million tons of tomato fruit per year (FAO, 2020). Outbreaks of bacterial canker are sporadic and the severity can depend on how much inoculum is introduced, the tomato cultivars grown, weather conditions, and how rapidly detection occurs (de León et al., 2011; Sen et al., 2015). Bacterial canker causes severe economic losses every year, but additional global data on losses caused by this disease are needed to understand distribution and severity of outbreaks.

### **Epidemiology – in the field and greenhouse**

*Clavibacter michiganensis* is a seed-borne pathogen that colonizes the vascular system and tomato fruit. Contaminated seeds can harbor 100 to 1000 CFU per seed, and the population threshold for disease induction is approximated to be as low as 100 CFU per seed (Fatmi and Schaad 1988; Hadas et al., 2005; de León et al., 2011). Prior to the 1990s, tomato transplants

were propagated in Georgia and Florida during late winter, and then shipped to growers in states with cooler climates, such as New York, Michigan, and provinces in Canada (Hausbeck et al., 2000). Propagation facilities would seed tomatoes into transplant beds, and the seedlings would be routinely clipped with a rotary mower to ensure uniformity and increase plant vigor for better survival through shipping and transplantation (Farley and Miller 1973; Chang et al., 1991).

In 1984, a severe outbreak of bacterial canker occurred in commercial tomato fields in Ontario, Canada from certified disease-free transplants with latent infections that were propagated in the southern USA (Gitaitis et al., 1991; Chang et al., 1991). Two important epidemiological lessons were learned as result of this outbreak. (1) Low rates of seed contamination (0.05%; or five seeds per 10,000) in transplant seedlings can cause up to 60% of plants in the field to become systemically infected with *C. michiganensis* through mechanical transmission (Chang et al., 1991). (2) High populations of *C. michiganensis* can proliferate in the xylem of seedlings, but symptoms may not be observed for up to 17 days post inoculation (Gitaitis et al., 1991). New methods to detect the pathogen prior to symptom development were employed, and tomato transplants were propagated in-house, preventing epidemics spreading from transplant facilities (Gitaitis et al., 1991; Hausbeck et al., 2000; de León et al., 2011).

After transplanting seedlings to the field, plants with latent infections can take between 35 and 42 days to develop symptoms (Chang et al., 1991). During this period, spread within the field can occur through pruning, trellising, and wind-blown rain (Chang et al., 1991; Gleason et al., 1993; Carlton et al., 1998). The pathogen can also be introduced to healthy transplants through wind-blown rain, leaf litter and volunteer plants harboring the bacterium, and infested material such as trellising stakes (Gleason et al., 1991, 1993; de León et al., 2011; Sen et al., 2015). A recent study reported white blister-like lesions formed on leaves colonized by *C.*

*michiganensis*, although the contribution of foliar colonization on plant health and fruit yield remains unexplored (Chalupowicz et al., 2017). The pathogen can survive in plant debris at the soil surface containing bacterial populations ranging from  $10^5$  to  $10^8$  CFU per leaflet or fruit, and these bacteria can cause infections for the next two years (Gleason et al., 1991). Pathogen survival is reduced to around seven months when the debris is buried 10 cm below the soil surface (Gleason et al., 1991). Without tomato plant debris, the pathogen only survives about three to four weeks in the soil (Basu 1970; Gleason et al., 1991). The practice of grafting scions onto rootstocks that provide increased resistance to soil-borne pathogens and improved horticultural traits has become increasingly common (Kubota et al., 2008; de León et al., 2011). The process of grafting is another route through which healthy hosts can be contaminated with *C. michiganensis*, therefore grafting tools should be thoroughly and routinely sterilized during the process (Xu et al., 2010; de León et al., 2011).

Early developmental stages of tomato growth are the most important for disease detection and mitigation. A high proportion (72 percent) of plants inoculated with *C. michiganensis* between two and 14-leaf stage wilt then die (Sharabani et al., 2013). This number decreases to 30 percent of plants wilting and dying when inoculated at 16- to 17-leaf stage, and no plant death when inoculated after the 19-leaf stage (Sharabani et al., 2013). Severe bacterial canker symptoms (Fig. 1) developed when infected seedlings were transplanted to the field, leading to an average of 50 percent decrease in fruit yield and lower average fruit weight (Chang et al., 1991). Fruit yield reduction is exacerbated by bird's-eye lesions developing on fruit through splash dispersal of the pathogen, secondary pathogen infections causing rotting symptoms, and horticultural conditions such as sun scald that occur on fruit of *C. michiganensis*-infected plants (Chang et al., 1991; de León et al., 2011).

The process of fruit infection is a critical stage where both the marketable product is affected and seed can become contaminated, perpetuating future outbreaks. Pathogen colonization of fruit exteriors causes bird's-eye lesions, which are necrotic spots surrounded by a white halo (Fig. 2). Fruit are susceptible as early as two days post anthesis (dpa), and cease to be susceptible around 20 dpa, or when the fruit are approximately 3 cm in diameter (Medina-Mora et al., 2001; Tancos et al., 2013; Peritore-Galve, Ch. 2). The bacteria are able to spread externally from the lesions into the developing fruit tissues, allowing the pathogen to colonize the seed (Tancos et al., 2013).



**FIGURE 1.** Tomato wilt symptoms during severe bacterial canker infection (top and bottom left). Stem canker at the inoculation site of *C. michiganensis* (bottom right).



**FIGURE 2.** Bird's-eye lesions on green-stage tomato fruit (top and bottom left). Fruit epidermal peel highlighting the necrotic center and white halo of bird's-eye lesions (bottom right).

## **Pathogenomics of *Clavibacter michiganensis***

*Clavibacter michiganensis* is in the phylum *Actinobacteria*, which consists of gram-positive bacteria with high guanine-plus-cytosine (GC) content in their genomes (Barka et al., 2016). The reference genome of *C. michiganensis*, NCPPB382, consists of a circular 3.298 Mb chromosome with 72.6% GC content, and two circular plasmids, pCM1 (27.4 kbp; 66.5% GC) and pCM2 (70.0 kbp, 67.6% GC) (Gartemann et al., 2008). This strain requires both plasmids and a 129-kb pathogenicity island (PAI), termed the *chp/tomA* PAI, for full pathogenicity (Gartemann et al., 2008; Chalupowicz et al., 2010). These mobile elements encode a variety of proteases, carbohydrate-active enzymes (CAZymes), expansins, and a tomatinase enzyme putatively secreted through the Sec/Tat pathways (Gartemann et al., 2008; Thapa et al., 2017; Nandi et al., 2018). Recently characterized virulent isolates have variable plasmid content, ranging from zero to three plasmids whose genetic composition remains to be studied (Tancos et al., 2015; Thapa et al., 2017, 2020). The targets and functions of many secreted proteins remain unknown (Hiery et al., 2015; Peritore-Galve et al., 2019), but functional genetics, genomics, and next generation technologies have provided insights into general roles of individual genes (Nandi et al., 2018).

Functional genetic studies of a plasmid-cured derivative (Cm100) of the reference strain found that the bacterium could still proliferate to the same density as pathogenic strains, but was impaired in systemic spread and caused no wilt symptoms (Meletzus et al., 1993; Chalupowicz et al., 2012). When one plasmid was added back at a time, colonization ability and wilt symptoms were recovered, but were delayed in onset and less severe (Meletzus et al., 1993; Chalupowicz et al., 2012). These experiments concluded that genes essential for pathogenicity of the reference strain were plasmid-borne. A spontaneous mutation of NCPPB382 deleted the *chp/tomA* PAI but

retained the plasmids (Chalupowicz et al., 2010). Functional assays revealed that without the *chp/tomA* PAI, *C. michiganensis* was impaired in systemic spread, *in vitro* aggregation, and virulence when inoculated into the vascular system and on leaves (Chalupowicz et al., 2012, 2017). These findings underscore the additive contributions of genes on the plasmids and *chp/tomA* PAI to both virulence and colonization.

The plasmid pCM2 contains a pathogenicity gene, *pat-1*, which encodes a serine protease from the chymotrypsin subfamily S1A (Table 1) (Dreier et al., 1997; Di Cera 2009; Nandi et al., 2018). Targeted deletion of the *pat-1* gene in the reference strain decreased virulence significantly, but did not abolish symptoms completely (Dreier et al., 1997). When expressed in avirulent isolates, the *pat-1* gene caused the isolates to become virulent (Dreier et al., 1997). Recent studies have identified virulent *C. michiganensis* strains in New York and California that naturally lack the *pat-1* gene, but nonetheless are able to cause symptoms (Tancos et al., 2015; Thapa et al., 2017). Homologues of the *pat-1* gene are present on pCM2 (*phpA&B*) and the *chp/tomA* PAI (*chpA-G*) (Dreier et al., 1997; Burger et al., 2005; Gartemann et al., 2008). Seven of nine homologues have been knocked out for functional characterization in the reference strain, and only one of those seven (*chpC*) demonstrated a role in colonization, wilt and foliar blister development (Table 1) (Stork et al., 2008; Chalupowicz et al., 2017). Eleven genes from the chymotrypsin family S1X, designated *ppaA-ppaJ* are present in pCM1, *chp/tomA* PAI and in other areas of the chromosome (Table 1) (Gartemann et al., 2008). Mutants of two genes, *ppaA* and *ppaC*, have been functionally characterized in the reference genome, where they had no contribution to wilt or foliar symptom development (Chalupowicz et al., 2017). The function and targets of these genes remain unknown, but infiltration of *Agrobacterium tumefaciens* expressing *chpG* was capable of causing the hypersensitive response in four *Nicotiana* species, suggesting a

potential role in interactions with the host immune system (Lu et al., 2015; Nandi et al., 2018).

Plasmid pCM1 contains the pathogenicity gene *celA*, which encodes a chimeric protein consisting of a cellulase, carbohydrate binding, and expansin domains (Jahr et al., 2000; Gartemann et al., 2008). Partial or full deletions of the *celA* gene in the moderately virulent Cm101 (Cm100 containing only pCM1) strain led to complete loss of virulence, establishing the essential role of each CelA domain in wilt symptom development (Table 1) (Jahr et al., 2000). Likewise, transient expression of *celA* in genetically altered and naturally endophytic strains of *C. michiganensis* was capable of restoring wilt and canker symptoms, but there was no difference in colonization density with or without *celA* (Jahr et al., 2000; Thapa et al., 2017). A recent genetic dissection of CelA domains demonstrated that the cellulase and carbohydrate-binding domains were the only essential components for wilt induction (Hwang et al., 2019). Furthermore, mutations of the catalytic cellulase domains completely abolished pathogenicity, highlighting the role of cellulase activity in wilt symptom development (Hwang et al., 2019). Another chimeric cellulase-carbohydrate-binding enzyme, *celB*, is encoded in the chromosome of NCPPB382 (Table 1) (Gartemann et al., 2008). However, *celB* lacks a secretion signal and is a hypothesized pseudogene due to a truncated C-terminal domain (Gartemann et al., 2008). Disruption of *celB* in NCPPB382 had no significant effect on wilt or blister symptom development (Chalupowicz et al., 2017). Functional analysis of CelB determined that it has no cellulase activity, and when modified to be secreted was not able to restore virulence in a *celA* mutant strain (Hwang et al., 2019). Despite the importance of CelA in pathogenicity of NCPPB382, virulent strains naturally lacking *celA* have been characterized (Tancos et al., 2015, 2018; Peritore-Galve et al., 2020; Thapa et al., 2020).

Cellulase activity is critical to symptom development caused by NCPPB382 and other *C.*

*michiganensis* strains (Jahr et al., 2000; Thapa et al., 2017; Hwang et al., 2019). The CelA protein contains an expansin domain, CmEXLX1, which has conflicting results on its contribution to virulence (Jahr et al., 2000; Hwang et al., 2019). Another expansin, CmEXLX2, is located on the chromosome of NCPPB382 and other strains (Table 1) (Gartemann et al., 2008; Thapa et al., 2017; Tancos et al., 2015, 2018). Expansin proteins were originally characterized in plants, where they loosen xyloglucan-cellulose bonds in the cell wall in a pH-dependent manner to allow for non-hydrolytic expansion during cell growth (Cosgrove 2000, 2015). Mutation of CmEXLX1 causes reductions of virulence or no effect on virulence, but disruption of CmEXLX2 in an isolate naturally lacking CelA (and thus also lacking CmEXLX1) led to threefold increased wilt symptoms, and increase in bird's-eye lesion severity on fruit (Tancos et al., 2018; Peritore-Galve et al., 2020).

The functions of CmEXLX1 and CmEXLX2 remain unknown. Expansins of *Bacillus subtilis* and *Ralstonia solanacearum* have weak plant cell wall extension activity *in vitro* and affect root binding capability (Kerff et al., 2008; Georgelis et al., 2014; Tancos et al., 2018). Localization studies of expansin proteins from the soft rot pathogen *Pectobacterium carotovorum* (PcEx11) and *B. subtilis* (BsEXLX1) in celery xylem found that PcEx11 preferentially bound to xylem vessels and adjacent parenchyma cells, whereas BsEXLX1 bound to most cell types (Tovar-Herrera et al., 2018). A more focused view inside xylem vessels determined that PcEx11 preferentially bound to annular and helical rings of tracheary elements (Tovar-Herrera et al., 2018). Finally, the presence of PcEx11 reduced cellulase and xylanase activity in the xylem, potentially by competing for cellulose and hemicellulose binding sites (Tovar-Herrera et al., 2018). These findings paired with the hypervirulent CmEXLX2 mutant phenotype in *C. michiganensis* suggest that CmEXLX2 may competitively bind cellulose and

hemicellulose in the xylem, reducing enzymatic hydrolysis by bacterial CAZymes. This association is less clear with phenotypes of mutant *CmEXLXI*, which may signify different roles for both expansins, highlighting the need for future studies on these proteins.

The genome of NCPPB382 encodes an array of secreted CAZymes with putative xylanase, pectinase, and endoglucanase activity (Table 1) (Gartemann et al., 2008; Thapa et al., 2017). Functional characterization of xylanase-encoding genes in the reference strain identified no effect on wilt or blister symptom development (Chalupowicz et al., 2017). Mutation of a polygalacturonase-encoding gene (*pgaA*) resulted in reduced blister formation but had no effect on wilt symptoms (Chalupowicz et al., 2017). Of the two pectate lyase-encoding genes that share high sequence similarity, only one (*pelA1*) caused a significant reduction in virulence when disrupted, but there was no significant difference in colonization density between the wildtype and mutant (Thapa et al., 2017). Finally, an endoglucanase (*endX/Y*) was demonstrated to have a role in blister formation but not in wilt induction (Chalupowicz et al., 2017). Glycome profiling of stem segments infected with pathogenic and non-pathogenic *C. michiganensis* determined that the presence of pathogenic *C. michiganensis* indeed leads to degradation of plant cell polysaccharides, consistent with the array of CAZymes encoded in the genome (Thapa et al., 2017).

Other genes have been tested for their roles in virulence. The *chp/tomA* PAI contains a secreted tomatinase enzyme, which deglycosylates the antimicrobial compound  $\alpha$ -tomatine to tomatidine, removing its growth inhibiting properties (Table 1) (Kaup et al., 2005). Three subtilase protease-encoding genes are present on the *chp/tomA* PAI and other areas of the chromosome (Table 1) (Gartemann et al., 2008). Mutation of the *chp/tomA* PAI-encoded subtilase, SbtA, resulted in reduced blister and systemic wilt symptoms, but disruption of the

other two genes had no significant effect (Chalupowicz et al., 2017). Exopolysaccharide (EPS) production is critical for colonization and virulence of the tomato vascular pathogen *R. solanacearum*; however, chemically mutated *C. michiganensis* that produced reduced amounts of EPS caused the same amount of symptoms and colonized to the same density as the wildtype (Bermpohl et al., 1996; Araud-Razou et al., 1998). Genomic analysis of NCPPB382 identified the *wcm* gene cluster as the production pathway for the major *C. michiganensis* EPS, and used direct mutagenesis of those genes to confirm that EPS reduction does not affect virulence or colonization (Gartemann et al., 2008). The putative pore forming perforin protein (PerF) and cell surface anchoring sortase protein (SrtA) were necessary for full virulence during leaf blister formation, but not for wilt symptom development (Hendrickx et al., 2011; Chalupowicz et al., 2017).

Genetics of *C. michiganensis* pathogenicity and virulence has been mostly understood through studies of the reference strain, NCPPB382. This strain and its derivatives are an excellent resource for investigating *C. michiganensis*-host interactions, but studies of genetic diversity have begun to describe pathogenic strains that do not require the same genetic repertoire as NCPPB382 to induce bacterial canker symptoms in tomato (Tancos et al., 2015; Thapa et al., 2017, 2020). More genome sequences and functional genetic analyses in diverse isolates can provide us with a more holistic understanding of *C. michiganensis*-tomato interactions. Moreover, few functional genetic studies have inoculated tomato fruit (Tancos et al., 2018; Peritore-Galve et al., 2020). Future mutational studies of *C. michiganensis* genes should include inoculations of leaves, xylem, and fruit to comprehensively study the contribution of individual genes to symptom development.

**Table 1. Putative virulence genes and bacterial canker disease severity phenotypes when each gene was mutated**

Location in NCPPB382 <sup>c</sup>	Gene	Mutant disease severity phenotype in tomato tissues	Reference(s)
<b>Chymotrypsin subfamily S1A proteases</b>			
PAI	<i>chpA</i>	-	
PAI	<i>chpB</i>	-	
PAI	<i>chpC</i>	Reduced (wilt and blisters)	Stork et al., 2008; Chalupowicz et al., 2017
PAI	<i>chpD</i>	-	
PAI	<i>chpE</i>	None (wilt and blisters)	Chalupowicz et al., 2017
PAI	<i>chpF</i>	None (wilt and blisters)	Chalupowicz et al., 2017
PAI	<i>chpG</i>	None (wilt and blisters)	Stork et al., 2008; Chalupowicz et al., 2017
pCM2	<i>pat-1</i>	Reduced (wilt) <sup>a</sup>	Dreier et al., 1997; Thapa et al., 2017
pCM2	<i>phpA</i>	None (wilt)	Burger et al., 2005
pCM2	<i>phpB</i>	None (wilt)	Burger et al., 2005
<b>Chymotrypsin-related serine proteases</b>			
PAI	<i>ppaA</i>	None (wilt and blisters)	Chalupowicz et al., 2017
PAI	<i>ppaB1</i>	-	
PAI	<i>ppaB2</i>	-	
PAI	<i>ppaC</i>	None (wilt and blisters)	Chalupowicz et al., 2017
PAI	<i>ppaD</i>	-	
PAI	<i>ppaE</i>	-	
Chrom	<i>ppaF</i>	-	
Chrom	<i>ppaG</i>	-	
Chrom	<i>ppaH</i>	-	
Chrom	<i>ppaI</i>	-	
pCM1	<i>ppaJ</i>	-	
<b>Subtilase proteases</b>			
PAI	<i>sbtA</i>	Reduced (wilt and blisters)	Chalupowicz et al., 2017
Chrom	<i>sbtB</i>	None (wilt and blisters)	Chalupowicz et al., 2017
Chrom	<i>sbtC</i>	None (wilt and blisters)	Chalupowicz et al., 2017

<b>Cellulases</b>			
pCM1	<i>celA</i>	Avirulent (wilt) <sup>a</sup>	Jahr et al., 2000; Tanco et al., 2015, 2018; Thapa et al., 2017; Hwang et al., 2019; Peritore-Galve et al., 2020
Chrom	<i>celB</i>	None (wilt and blisters) <sup>a</sup>	Chalupowicz et al., 2017; Hwang et al., 2019
<b>Xylanases</b>			
Chrom	<i>xysA</i>	None (wilt and blisters)	Chalupowicz et al., 2017
Chrom	<i>xysB</i>	None (wilt and blisters)	Chalupowicz et al., 2017
<b>Pectinases</b>			
Chrom	<i>pgaA</i>	Reduced (blisters); none (wilt)	Chalupowicz et al., 2017
PAI	<i>pelA1</i>	Reduced (wilt) <sup>b</sup>	Thapa et al., 2017
PAI	<i>pelA2</i>	Reduced (wilt) <sup>b</sup>	Thapa et al., 2017
<b>Endoglucanases</b>			
Chrom	<i>endX/Y</i>	Reduced (blisters); none (wilt)	Chalupowicz et al., 2017
<b>Expansins</b>			
pCM1	<i>CmEXLX1</i> (CelA domain)	Reduced (wilt) <sup>a</sup>	Jahr et al., 2000; Hwang et al., 2019
Chrom	<i>expA</i> ( <i>CmEXLX2</i> )	Increased (wilt and bird's-eye lesions) <sup>b</sup>	Tanco et al., 2018; Peritore-Galve et al., 2020
<b>Others</b>			
Chrom	<i>perF</i> (perforin)	Reduced (blisters); none (wilt)	Chalupowicz et al., 2017
Chrom	<i>srtA</i> (sortase)	Reduced (blisters); none (wilt)	Chalupowicz et al., 2017
PAI	<i>tomA</i> (tomatinase)	None (wilt)	Kaup et al., 2005

<sup>a</sup> Highlights genes that reduced virulence in NCPPB382 when knocked out, but have contrasting results when knocked out or absent in other virulent strains.

<sup>b</sup> Denotes genes whose virulence phenotype was determined in a strain other than in NCPPB382.

<sup>c</sup> PAI = *chp/tomA* pathogenicity island; Chrom = chromosomal region outside the PAI.

Dashes (-) in the third column means there are no reported functional genetic studies on that particular virulence gene.

## Colonization of xylem and fruit

The xylem is a flowing environment consisting of dead tracheary elements and xylem fibers, and living parenchyma cells. Together, these units provide plant structural stability and create conduits for passive transport of water and solutes from the roots to aerial organs. Xylem sap flows acropetally using negative tension generated by transpirational water loss and through positive pressure generated by water uptake in the roots (Venturas et al., 2017). Although the xylem is a relatively low nutrient environment, xylem sap maintains a constant flow of low concentrations of sugars, proteins, and metabolites that can be nutrient sources for pathogens (Buhtz et al., 2004; Iwai et al., 2003; Gonorazky et al., 2011; Lowe-Power et al., 2018a). Furthermore, pathogens affect xylem sap composition, which may create a more habitable environment for colonization (Dixon and Pegg 1972; Wang and Bergeson 1974; Lowe-Power et al., 2018a; Peritore-Galve, Ch. 3). Therefore, with the right adaptations, pathogens can exploit the xylem for a constant stream of nutrients.

Bacterial pathogens often use chemotaxis and motility systems to colonize their plant hosts (Lowe-Power et al., 2018b). To adapt to the flow of xylem sap, the vascular bacterial pathogens *R. solanacearum* and *Xylella fastidiosa* use adhesins and exopolysaccharides (EPS) for aggregation and biofilm formation, and type IV pili for twitching motility (Araud-Razou et al., 1998; Meng et al., 2005; De La Fuente et al., 2007; Lowe-Power et al., 2018b; Rapicavoli et al., 2018). In contrast to other vascular bacterial pathogens, *C. michiganensis* contains no canonical pili, chemotaxis or adhesin-encoding genes, and does not require EPS for successful colonization (Bermppohl et al., 1996; Gartemann et al., 2008). Despite the absence of known aggregation and motility genes, the pathogen forms biofilm-like aggregates in xylem vessels and *in vitro* in the presence of xylem sap (Chalupowicz et al., 2012; Tancos et al., 2018; Peritore-

Galve et al., 2020). The bacterium does not form aggregates when cultured in nutrient rich or minimal medium, but forms large aggregates of cells when cultured in xylem sap or media supplemented with sap (Chalupowicz et al., 2012; Tancos et al., 2018; Peritore-Galve et al., 2020). Bacterial attachment may be induced through chemical or physiological signals provided by xylem sap, but these signals and genes involved in attachment remain unknown. The xylem environment is constantly flowing with sap. Rates range as high as 8 mm<sup>3</sup> per second during the day and slow to 2.3 mm<sup>3</sup> per second at night, yet *C. michiganensis* NCPPB382 and its non-pathogenic PAI and plasmid-free derivatives are capable of spreading basipitally against the flow of xylem sap (Windt et al., 2006; Chalupowicz et al., 2012). These results suggest that *C. michiganensis* may have the capacity for active motility, and genes encoding this process are located on the chromosome.

How *C. michiganensis* causes wilt symptoms is still unknown. Studies of non-pathogenic strains have demonstrated that the pathogen can spread and colonize the vascular system to similar densities as pathogenic strains (Meletzus et al., 1993; Chalupowicz et al., 2012; Thapa et al., 2017). During early stages of infection, the pathogen preferentially colonizes protoxylem vessels (Chalupowicz et al., 2012). Protoxylem are narrower, early formed vessels that support water transport during early plant growth, with wider metaxylem vessels forming after plant elongation. As wilt symptoms progress, *C. michiganensis* spreads into metaxylem and parenchyma cells, presumably through maceration of pit membranes, a strategy used by other vascular wilt pathogens but has not been directly observed during bacterial canker (Chalupowicz et al., 2012; Rapicavoli et al., 2018; Tancos et al., 2018; Peritore-Galve et al., 2020). In tolerant wild tomatoes, *C. michiganensis* colonizes protoxylem vessels but does not spread laterally into metaxylem or parenchyma tissue (Peritore-Galve et al., 2020). Why *C. michiganensis*

preferentially colonizes protoxylem is undetermined, but colonizing protoxylem vessels may contribute to latency of disease symptoms and might serve as a route for the pathogen to spread from the seed throughout the developing plant (Gitaitis et al., 1991). Recent studies of xylem hydraulics determined that the sap flow could occur at rates up to 15% higher in narrower vessels (eg. protoxylem) compared to larger diameter vessels (eg. metaxylem), which would make protoxylem vessels an even more effective conduit for systemic spread (Bouda et al., 2019).

During early wilt symptom development, typically 8 to 12 dpi, the pathogen will have spread systemically and the host will have mounted a basal defense response (Balaji et al., 2008; Chalupowicz et al., 2012; Savidor et al., 2012; Nandi et al., 2018). This response includes an increase in pathogenesis-related proteins, production of reactive oxygen species, and increased ethylene production (Coaker et al., 2004; Balaji et al., 2008; Savidor et al., 2012; Nandi et al., 2018). Ethylene production plays an important role in wilt symptom development. When ethylene synthesis mutants and insensitive *Nr* plants were inoculated with *C. michiganensis*, the onset of symptoms was delayed by several days and wilt symptoms were less severe compared to wildtype plants (Balaji et al., 2008; Peritore-Galve, Ch. 2). Increased ethylene has been associated with the induction of vascular defenses including tyloses and pectin gels that physically occlude pathogen spread (VanderMolen et al., 1983; Fry and Milholland 1990; Pérez-Donoso et al., 2007). These occlusions can cause hydraulic dysfunction, leading to xylem vessel cavitation and embolism, processes that are known to contribute to *Fusarium* wilt, Pierce's disease, and pine wilt disease symptoms (VanderMolen et al., 1983; Pérez-Donoso et al., 2007; Venturas et al., 2017). Xylem embolisms can also occur through the accumulation of hydrophobic terpenes during pine wilt disease, and through the maceration of pit membranes that connect vessels to parenchyma cells (Kuroda et al., 1991; Utsuzawa et al., 2005; McElrone et al.,

2008; Lowe-Power et al., 2018b). Interestingly, maize protoxylem vessels were more resistant to artificially induced embolisms; this relative resistance would make protoxylem vessels a safer niche than metaxylem if *C. michiganensis* indeed induces embolisms and cavitation (Hwang et al., 2016). The impacts of *C. michiganensis* on xylem hydraulics remains to be studied, but may prove useful to uncovering mechanisms of unilateral wilt symptom development.

Tomato fruit colonization by *C. michiganensis* has not been as investigated as vascular infection. Fruit colonization is a critical step in bacterial canker epidemiology since the bacterium colonizes seed systemically and through fruit exteriors, resulting in further pathogen dispersal (Tancos et al., 2013). The hallmark of fruit infection by *C. michiganensis* are bird's-eye lesions, which are white halos on the fruit epidermis surrounding a necrotic lesion. These lesions develop when *C. michiganensis* is introduced onto fruit exteriors during early developmental stages (Medina-Mora et al., 2001; Peritore-Galve, Ch. 2). Fruit begin to be susceptible two dpa and there is a peak susceptibility period between five to seven dpa (Medina-Mora et al., 2001; Peritore-Galve, Ch. 2). Fruit from the cultivar Ailsa Craig are one centimeter in diameter during peak susceptibility (Peritore-Galve, Ch. 2). Fruit cease developing symptoms around 20 dpa, or around 3 centimeters diameter for the cultivar Ailsa Craig (Medina-Mora et al., 2001; Peritore-Galve, Ch. 2). The diameter in which fruit cease to be susceptible to *C. michiganensis* varies by *S. lycopersicum* cultivar and *Solanum* species, but the developmental stage (20 dpa) remains the same, suggesting a conserved change occurs in the fruit around 20 dpa that abolishes the ability for the pathogen to cause fruit symptoms (Peritore-Galve et al., 2020; Peritore-Galve, Ch. 2).

Bacteria forming the fruit lesion spread from the epidermis into the pericarp, where they can access fruit xylem vessels for systemic spread (Tancos et al., 2013). To enter fruit xylem vessels, the bacterium must navigate through the outer epidermis, collenchyma, and parenchyma

layers, which may be facilitated by a motility system (Matas et al., 2011). How the pathogen spreads through these tissues remains nebulous, but confocal microscopy of an eGFP-expressing isolate observed putative intracellular colonization of intact pericarp cells (Tancos et al., 2013). Intracellular colonization is a unique strategy rarely observed in plant pathogens, but has been documented in two other actinomycete pathogens, *Rhodococcus fasciens* and *Streptomyces turgidiscabies* (Cornelis et al., 2001; Hogenhout and Loria 2008). Therefore *C. michiganensis* may be using a combination of CAZymes and exploiting host processes to spread to fruit xylem from fruit exteriors, although the exact method remains to be studied.

### **Management strategies – breeding and therapeutics**

There are no commercially available cultivars resistant to bacterial canker, although some offer partial tolerance (Sen et al., 2015). Diverse wild tomato species are tolerant to *C. michiganensis*, developing few to no symptoms while harboring dense populations of the pathogen in the xylem (Vulkova and Sotirova 1993; van Heusden et al., 1999; Sotirova et al., 1999; Francis et al., 2001; Kabelka et al., 2002; Lara-Ávila et al., 2012; Sen et al., 2012). Bacterial canker tolerance is polygenic and complex, but breeding studies have identified quantitative trait loci in *S. habrochaites* accessions that provide tolerance through changes in vascular thickness and increases in reactive oxygen species accumulation (Francis et al., 2001; Coaker and Francis 2004; Coaker et al., 2002, 2004). Transgenic plants expressing antimicrobial products such as the peptide Snakin-2, the glycoprotein Extensin-like protein, and an endolysin protein from the bacteriophage CMP1 reduce bacterial populations *in planta* and reduce symptom severity (Balaji and Smart 2012; Wittmann et al., 2016). A more comprehensive understanding of host resistance can help identify genes critical to tolerance, and incorporate them into commercial cultivars through traditional breeding and transgenic approaches.

Cultural practices of using certified disease-free seed, sterilizing equipment, increasing plant spacing, and rotating crops are effective at preventing bacterial canker outbreaks (de León et al., 2011). However, once the pathogen is present in the field, management options are limited to rogueing symptomatic plants and use of copper-based and streptomycin-containing bactericidal sprays (de León et al., 2011). Bactericides are sprayed preventatively or after symptom development in the field, and they can reduce disease severity by lowering bacterial populations (Hausbeck et al., 2000). Application of bacteriophages to control plant disease have variable results, and effective control of bacterial canker using phages has not been achieved thus far, but remains a possibility through further investigation (Svircev et al., 2018).

### **Conclusion and dissertation focus**

Bacterial canker continues to cause significant economic damage to growers worldwide, and we do not have a complete understanding of how the pathogen colonizes and causes symptoms in the xylem and fruit. Wild tomato species can tolerate high populations of *C. michiganensis* without developing severe symptoms, but we also do not have a complete picture of differences in bacterial colonization and host responses in tolerant versus susceptible genotypes. The objectives of my thesis were divided into four chapters: (i) characterizing *C. michiganensis* colonization of xylem and fruit in tolerant wild tomato species, (ii) understanding the role of fruit development and ethylene-responsiveness on symptom severity, (iii) probing host xylem sap responses to *C. michiganensis* infection in tolerant and susceptible genotypes, and (iv) generating a high-quality proteome of *C. michiganensis* to improve the reference genome.

## **REFERENCES**

- Araud-Razou, I., Vasse, J., Montrozier, H., Etchebar, C., and Trigalet, A. 1998. Detection and visualization of the major acidic exopolysaccharide of *Ralstonia solanacearum* and its role in tomato root infection and vascular colonization. *Eur. J. Plant Pathol.* 104:795–809.
- Balaji, V., Mayrose, M., Sherf, O., Jacob-Hirsch, J., Eichenlaub, R., Iraki, N., Manulis-Sasson, S., Rechavi, G., Barash, I., and Sessa, G. 2008. Tomato transcriptional changes in response to *Clavibacter michiganensis* subsp. *michiganensis* reveal a role for ethylene in disease development. *Plant Physiol.* 146:1797–1809.
- Balaji, V., and Smart, C. D. 2012. Over-expression of *snakin-2* and *extensin-like* protein genes restricts pathogen invasiveness and enhances tolerance to *Clavibacter michiganensis* subsp. *michiganensis* in transgenic tomato (*Solanum lycopersicum*). *Transgenic Res.* 21:23–37.
- Barka, E. A., Vatsa, P., Sanchez, L., Gaveau-Vaillant, N., Jacquard, C., Klenk, H.-P., Clément, C., Ouhdouch, Y., and van Wezel, G. P. 2016. Taxonomy, physiology, and natural products of *Actinobacteria*. *Microbiol. Mol. Biol. Rev.* 80:1–43.
- Basu, P. K. 1970. Temperature, an important factor determining survival of *Corynebacterium michiganense* in soil. *Phytopathology.* 60:825.

- Bermppohl, A., Dreier, J., Bahro, R., and Eichenlaub, R. 1996. Exopolysaccharides in the pathogenic interaction of *Clavibacter michiganensis* subsp. *michiganensis* with tomato plants. *Microbiol. Res.* 151:391–399.
- Bouda, M., Windt, C. W., McElrone, A. J., and Brodersen, C. R. 2019. *In vivo* pressure gradient heterogeneity increases flow contribution of small diameter vessels in grapevine. *Nat. Commun.* 10:1–10.
- Bryan, M. K. 1930. Studies on bacterial canker of tomato. *J. Agric. Res.* 41(12):825-851
- Buhtz, A., Kolasa, A., Arlt, K., Walz, C., and Kehr, J. 2004. Xylem sap protein composition is conserved among different plant species. *Planta.* 219:610–618.
- Burger, A., Gräfen, I., Engemann, J., Niermann, E., Pieper, M., Kirchner, O., Gartemann, K-H., and Eichenlaub, R. 2005. Identification of homologues to the pathogenicity factor Pat-1, a putative serine protease of *Clavibacter michiganensis* subsp. *michiganensis*. *Microbiol. Res.* 160:417–427.
- Carlton, W. M., Braun, E. J., and Gleason, M. L. 1998. Ingress of *Clavibacter michiganensis* subsp. *michiganensis* into tomato leaves through hydathodes. *Phytopathology.* 88:525–529.

Chalupowicz, L., Barash, I., Reuven, M., Dror, O., Sharabani, G., Gartemann, K.-H., Eichenlaub, R., Sessa, G., and Manulis-Sasson, S. 2017. Differential contribution of *Clavibacter michiganensis* ssp. *michiganensis* virulence factors to systemic and local infection in tomato. *Mol. Plant Pathol.* 18:336–346.

Chalupowicz, L., Cohen-Kandli, M., Dror, O., Eichenlaub, R., Gartemann, K.-H., Sessa, G., Barash, I., and Manulis-Sasson, S. 2010. Sequential expression of bacterial virulence and plant defense genes during infection of tomato with *Clavibacter michiganensis* subsp. *michiganensis*. *Phytopathology.* 100:252–261.

Chalupowicz, L., Zellermann, E.-M., Fluegel, M., Dror, O., Eichenlaub, R., Gartemann, K.-H., Savidor, A., Sessa, G., Iraki, N., Barash, I., and Manulis-Sasson, S. 2011. Colonization and movement of GFP-labeled *Clavibacter michiganensis* subsp. *michiganensis* during tomato infection. *Phytopathology.* 102:23–31.

Chang, R. J., Ries, S. M., and Pataky, J. K. 1991. Dissemination of *Clavibacter michiganensis* subsp. *michiganensis* by practices used to produce tomato transplants. *Phytopathology.* 81:1276–1281.

Chang, R. J., Ries, S. M., and Pataky, J. K. 1992. Reductions in yield of processing tomatoes and incidence of bacterial canker. *Plant Dis.* 76:805-809

- Coaker, G. L., and Francis, D. M. 2004. Mapping, genetic effects, and epistatic interaction of two bacterial canker resistance QTLs from *Lycopersicon hirsutum*. *Theor. Appl. Genet.* 108:1047–1055.
- Coaker, G. L., Meulia, T., Kabelka, E. A., Jones, A. K., and Francis, D. M. 2002. A QTL controlling stem morphology and vascular development in *Lycopersicon esculentum* × *Lycopersicon hirsutum* (*Solanaceae*) crosses is located on chromosome 2. *Am. J. Bot.* 89:1859–1866.
- Coaker, G. L., Willard, B., Kinter, M., Stockinger, E. J., and Francis, D. M. 2004. Proteomic analysis of resistance mediated by Rcm 2.0 and Rcm 5.1, two loci controlling resistance to bacterial canker of tomato. *Mol. Plant-Microbe Interact.* 17:1019–1028.
- Collins, M. D., and Jones, D. 1980. Lipids in the classification and identification of coryneform bacteria containing peptidoglycans based on 2,4-diaminobutyric acid. *J. Appl. Bacteriol.* 48(3):459-470
- Cornelis, K., Ritsema, T., Nijssse, J., Holsters, M., Goethals, K., and Jaziri, M. 2001. the plant pathogen *Rhodococcus fascians* colonizes the exterior and interior of the aerial parts of plants. *Mol. Plant-Microbe Interact.* 14:599–608.
- Cosgrove, D. J. 2000. Loosening of plant cell walls by expansins. *Nature.* 407:321–326.

- Cosgrove, D. J. 2015. Plant expansins: diversity and interactions with plant cell walls. *Curr. Opin. Plant Biol.* 25:162–172.
- Davis, M. J., Gillaspie, A. G., Vidaver, A. K., and Harris, R. W. 1984. *Clavibacter*: a new genus containing some phytopathogenic coryneform bacteria, including *Clavibacter xyli* subsp. *xyli* sp. nov., subsp. nov. and *Clavibacter xyli* subsp. *cynodontis* subsp. nov., pathogens that cause ratoon stunting disease of sugarcane and bermudagrass stunting disease. *Int. J. Syst. Bacteriol.* 34(2):107-117
- De La Fuente, L., Burr, T. J., and Hoch, H. C. 2007. Mutations in type I and type IV pilus biosynthetic genes affect twitching motility rates in *Xylella fastidiosa*. *J. Bacteriol.* 189:7507-7510.
- Di Cera, E. 2009. Serine Proteases. *IUBMB Life.* 61:510–515.
- Dixon, G. R., and Pegg, G. F. 1972. Changes in amino-acid content of tomato xylem sap following infection with strains of *Verticillium albo-atrum*. *Ann. Bot.* 36:147–154.
- Dreier, J., Meletzus, D., and Eichenlaub, R. 1997. Characterization of the plasmid encoded virulence region pat-1 of phytopathogenic *Clavibacter michiganensis* subsp. *michiganensis*. *Mol. Plant-Microbe Interact.* 10:195–206.

Emmatty, D. A., and John, C. A. 1973. Comparison of yield loss to bacterial canker of tomato in a resistant and a susceptible variety. *Plant Dis. Rep.* 57:787-788

Evtushenko, L. I., Dorofeeva, L. V., Subbotin, S. A., Cole, J. R., and Tiedje, J. M. 2000.

*Leifsonia poae* gen. nov., sp. nov., isolated from nematode galls on *Poa annua*, and reclassification of '*Corynebacterium aquaticum*' Leifson 1962 as *Leifsonia aquatica* (ex Leifson 1962) gen. nov., nom. rev., comb. nov. and *Clavibacter xyli* Davis et al. 1984 with two subspecies as *Leifsonia xyli* (Davis et al. 1984) gen. nov., comb. nov. *Int. J. Syst. Evol. Microbiol.* 50(1):371–380

FAO, 2017. FAOSTAT. Food and Agriculture Data.

Farley, J. D., and Miller, T. D. 1973. Spread and control of *Corynebacterium michiganense* in tomato transplants during clipping. *Plant Dis. Rep.* 57:767-769

Fatmi, M., and Schaad, N. W. 1988. Semiselective agar medium for isolation of *Clavibacter michiganense* subsp. *michiganense* from tomato seed. *Phytopathology.* 78:121–126.

Francis, D. M., Kabelka, E., Bell, J., Franchino, B., and St. Clair, D. 2001. Resistance to bacterial canker in tomato (*Lycopersicon hirsutum* LA407) and its progeny derived from crosses to *L. esculentum*. *Plant Dis.* 85:1171–1176.

Fry, S. M., and Milholland, R. D. 1990. Response of resistant, tolerant and susceptible grapevine tissues to invasion by the Pierce's Disease bacterium, *Xylella fastidiosa*. *Phytopathology*. 80:66–69.

Gartemann, K.-H., Abt, B., Bekel, T., Burger, A., Engemann, J., Flügel, M., Gaigalat, L., Goesmann, A., Gräfen, I., Kalinowski, J., Kaup, O., Kirchner, O., Krause, L., Linke, B., McHardy, A., Meyer, F., Pohle, S., Rückert, C., Schneiker, S., Zellermann, E. M., Pühler, A., Eichenlaub, R., Kaiser, O., and Bartels, D. 2008. The genome sequence of the tomato-pathogenic actinomycete *Clavibacter michiganensis* subsp. *michiganensis* NCPPB382 reveals a large island involved in pathogenicity. *J. Bacteriol.* 190:2138–2149.

Georgelis, N., Nikolaidis, N., and Cosgrove, D. J. 2014. Biochemical analysis of expansin-like proteins from microbes. *Carbohydr. Polym.* 100:17–23.

Gitaitis, R. D., Beaver, R. W., and Voloudakis, A. E. 1991. Detection of *Clavibacter michiganensis* subsp. *michiganensis* in symptomless tomato transplants. *Plant Dis.* 75:834–838.

Gleason, M. L. 1993. Recent progress in understanding and controlling bacterial canker of tomato in Eastern North America. *Plant Dis.* 77:1069.

- Gleason, M. L., Braun, E. J., Carlton, W. M., and Peterson, R. H. 1991. Survival and dissemination of *Clavibacter michiganensis* subsp. *michiganensis* in tomatoes. *Phytopathology*. 81:1519–1523.
- Gonorazky, G., Laxalt, A. M., Dekker, H. L., Rep, M., Munnik, T., Testerink, C., and de la Canal, L. 2012. Phosphatidylinositol 4-phosphate is associated to extracellular lipoproteic fractions and is detected in tomato apoplastic fluids. *Plant Biol*. 14:41–49.
- Hadas, R., Kritzman, G., Klietman, F., Gefen, T., and Manulis, S. 2005. Comparison of extraction procedures and determination of the detection threshold for *Clavibacter michiganensis* ssp. *michiganensis* in tomato seeds. *Plant Pathol*. 54:643–649.
- Hausbeck, M. K., Bell, J., Medina-Mora, C., Podolsky, R., and Fulbright, D. W. 2000. Effect of bactericides on population sizes and spread of *Clavibacter michiganensis* subsp. *michiganensis* on tomatoes in the greenhouse and on disease development and crop yield in the field. *Phytopathology*. 90:38–44.
- Hendrickx, A. P. A., Budzik, J. M., Oh, S.-Y., and Schneewind, O. 2011. Architects at the bacterial surface — sortases and the assembly of pili with isopeptide bonds. *Nat. Rev. Microbiol*. 9:166–176.

- van Heusden, A. W., Koornneef, M., Voorrips, R. E., Brüggemann, W., Pet, G., Vrielink-van Ginkel, R., Chen, X., and Lindhout, P. 1999. Three QTLs from *Lycopersicon peruvianum* confer a high level of resistance to *Clavibacter michiganensis* ssp. *michiganensis*. *Theor. Appl. Genet.* 99:1068–1074.
- Hiery, E., Poetsch, A., Moosbauer, T., Amin, B., Hofmann, J., and Burkovski, A. 2015 A proteomic study of *Clavibacter michiganensis* subsp. *michiganensis* culture supernatants. *Proteomes.* 3:411-423
- Hogenhout, S. A., and Loria, R. 2008. Virulence mechanisms of Gram-positive plant pathogenic bacteria. *Curr. Opin. in Plant Biol.* 11:449–456.
- Hwang, B. G., Ryu, J., and Lee, S. J. 2016. Vulnerability of protoxylem and metaxylem vessels to embolisms and radial refilling in a vascular bundle of maize leaves. *Front. Plant Sci.* 7:941
- Hwang, I. S., Oh, E.-J., Lee, H. B., and Oh, C-S. 2018. Functional characterization of two cellulase genes in the Gram-positive pathogenic bacterium *Clavibacter michiganensis* for wilting in tomato. *Mol. Plant-Microbe Interact.* 32:491–501.
- Iwai, H., Usui, M., Hoshino, H., Kamada, H., Matsunaga, T., Kakegawa, K., Ishii, T., and Satoh, S. 2003. Analysis of sugars in squash xylem sap. *Plant Cell Physiol.* 44:582–587.

- Jahr, H., Dreier, J., Meletzus, D., Bahro, R., and Eichenlaub, R. 2000. The endo- $\beta$ -1,4-glucanase CelA of *Clavibacter michiganensis* subsp. *michiganensis* is a pathogenicity determinant required for induction of bacterial wilt of tomato. *Mol. Plant-Microbe Interact.* 13:703–714.
- Jensen, H. L. 1934. Studies on saprophytic Mycobacteria and Corynebacteria. Pages 19-61 in: *The Proceedings of the Linnean Society of New South Wales*. Australasian Medical Publishing Co., Sydney, Australia.
- Kabelka, E., Franchino, B., and Francis, D. M. 2002. Two loci from *Lycopersicon hirsutum* LA407 confer resistance to strains of *Clavibacter michiganensis* subsp. *michiganensis*. *Phytopathology.* 92:504–510.
- Kaup, O., Gräfen, I., Zellermann, E.-M., Eichenlaub, R., and Gartemann, K.-H. 2005. Identification of a tomatinase in the tomato-pathogenic actinomycete *Clavibacter michiganensis* subsp. *michiganensis* NCPPB382. *Mol. Plant-Microbe Interact.* 18:1090–1098.
- Kerff, F., Amoroso, A., Herman, R., Sauvage, E., Petrella, S., Filée, P., Charlier, P., Joris, B., Tabuchi, A., Nikolaidis, N., and Cosgrove, D. J. 2008. Crystal structure and activity of *Bacillus subtilis* YoaJ (EXLX1), a bacterial expansin that promotes root colonization. *Proc. Natl. Acad. Sci. U. S. A.* 105:16876–16881.

- Kubota, C., McClure, M. A., Kokalis-Burelle, N., Bausher, M. G., and Roskopf, E. N. 2008. Vegetable grafting: history, use, and current technology status in North America. HortSci. 43:1664–1669.
- Kuroda, K. 1991. Mechanism of cavitation development in the pine wilt disease. Eur. J. Forest Pathol. 21:82–89.
- Lara-Ávila, J. P., Isordia-Jasso, M. I., Castillo-Collazo, R., Simpson, J., and Alpuche-Solís, Á. G. 2012. Gene expression analysis during interaction of tomato and related wild species with *Clavibacter michiganensis* subsp. *michiganensis*. Plant Mol. Biol. Rep. 30:498–511.
- de León, L., Siverio, F., López, M. M., and Rodríguez, A. 2011. *Clavibacter michiganensis* subsp. *michiganensis*, a seedborne tomato pathogen: healthy seeds are still the goal. Plant Dis. 95:1328–1338.
- Li, X., Tambong, J., Yuan, K. X., Chen, W., Xu, H., Lévesque, C. A., and De Boer, S. H. 2018. Re-classification of *Clavibacter michiganensis* subspecies on the basis of whole-genome and multi-locus sequence analyses. Int. J. Syst. Evol. Microbiol. 68(1):234-240

- Lowe-Power, T. M., Hendrich, C. G., Roepenack-Lahaye, E. von, Li, B., Wu, D., Mitra, R., Dalsing, B. L., Ricca, P., Naidoo, J., Cook, D., Jancewicz, A., Masson, P., Thomma, B., Lahaye, T., Michael, A. J., and Allen, C. 2018a. Metabolomics of tomato xylem sap during bacterial wilt reveals *Ralstonia solanacearum* produces abundant putrescine, a metabolite that accelerates wilt disease. *Environ. Microbiol.* 20:1330–1349.
- Lowe-Power, T. M., Khokhani, D., and Allen, C. 2018b. How *Ralstonia solanacearum* exploits and thrives in the flowing plant xylem environment. *Trends Microbiol.* 26:929–942.
- Lu, Y., Hatsugai, N., Katagiri, F., Ishimaru, C. A., and Glazebrook, J. 2015. Putative serine protease effectors of *Clavibacter michiganensis* induce a hypersensitive response in the apoplast of *Nicotiana* species. *Mol. Plant-Microbe Interact.* 28:1216–1226.
- Matas, A. J., Yeats, T. H., Buda, G. J., Zheng, Y., Chatterjee, S., Tohge, T., et al. 2011. Tissue- and cell-type specific transcriptome profiling of expanding tomato fruit provides insights into metabolic and regulatory specialization and cuticle formation. *Plant Cell.* 23:3893–3910.
- McElrone, A. J., Jackson, S., and Habdas, P. 2008. Hydraulic disruption and passive migration by a bacterial pathogen in oak tree xylem. *J. Exp. Bot.* 59:2649–2657.

- Medina-Mora, C. M., Hausbeck, M. K., and Fulbright, D. W. 2001. Bird's eye lesions of tomato fruit produced by aerosol and direct application of *Clavibacter michiganensis* subsp. *michiganensis*. Plant Dis. 85:88–91.
- Meletzus, D., Bermphol, A., Dreier, J., and Eichenlaub, R. 1993. Evidence for plasmid-encoded virulence factors in the phytopathogenic bacterium *Clavibacter michiganensis* subsp. *michiganensis* NCPPB382. J. Bacteriol. 175:2131–2136.
- Meng, Y., Li, Y., Galvavni, C. D., Turner, J. N., Burr, T. J., and Hoch, H. C. 2005. Upstream migration of *Xylella fastidiosa* via pilus-driven twitching motility. J. Bacteriol. 187:5560-5567.
- Nandi, M., Macdonald, J., Liu, P., Weselowski, B., and Yuan, Z.-C. 2018. *Clavibacter michiganensis* ssp. *michiganensis*: bacterial canker of tomato, molecular interactions and disease management. Mol. Plant Pathol. 19:2036–2050.
- Oh, E. J., Bae, C., Lee, H. B., Hwang, I. S., Lee, H. I., Yea, M. C., Yim, K. O., Lee, S., Heu, S., Cha, J. S., and Oh, C. S. 2016. *Clavibacter michiganensis* subsp. *capsici* subsp. nov., causing bacterial canker disease in pepper. Int. J. Syst. Evol. Microbiol. 66(10):4065-4070

- Osdaghi, E., Rahimi, T., Taghavi, S. M., Ansari, M., Zarei, S. Portier, P., Briand, M., and Jacques, M.-A. 2020. Comparative genomics and phylogenetic analyses suggest several novel species within the genus *Clavibacter*, including nonpathogenic tomato-associated strains. *Appl. Environ. Microbiol.* 86, e02873-19
- Payne, S. G. and Lacey, M. S. 1922. Comparison of the “stripe disease” with the “Grand Rapids disease” of tomato. Pages 210-212 in: *Studies in Bacteriosis*, Vol. 7. Cambridge University Press, Cambridge, UK.
- Pérez-Donoso, A. G., Greve, L. C., Walton, J. H., Shackel, K. A., and Labavitch, J. M. 2007. *Xylella fastidiosa* infection and ethylene exposure result in xylem and water movement disruption in grapevine shoots. *Plant Physiol.* 143:1024–1036.
- Peritore-Galve, F. C., Schneider, D. J., Yang, Y., Thannhauser, T. W., Smart, C. D., and Stoghill, P. 2019. Proteome profile and genome refinement of the tomato-pathogenic bacterium *Clavibacter michiganensis* subsp. *michiganensis*. *Proteomics.* 19:1800224
- Peritore-Galve, F. C., Miller, C., and Smart, C. D. 2020. Characterizing colonization patterns of *Clavibacter michiganensis* during infection of tolerant wild *Solanum* species. *Phytopathology.* 110:574–581.

Poysa, V. 1993. Evaluation of tomato breeding lines resistant to bacterial canker. *Can. J. Plant Pathol.* 15:301-304.

Rapicavoli, J., Ingel, B., Blanco-Ulate, B., Cantu, D., and Roper, C. 2018. *Xylella fastidiosa*: an examination of a re-emerging plant pathogen. *Mol. Plant Pathol.* 19:786-800

Savidor, A., Teper, D., Gartemann, K.-H., Eichenlaub, R., Chalupowicz, L., Manulis-Sasson, S., Barash, I., Tews, H., Mayer, K., Giannone, R. J., Hettich, R. L., and Sessa, G. 2012. The *Clavibacter michiganensis* subsp. *michiganensis*–tomato interactome reveals the perception of pathogen by the host and suggests mechanisms of infection. *J. Proteome Res.* 11:736–750.

Sen, Y., Feng, Z., Vandenbroucke, H., van der Wolf, J., Visser, R. G. F., and van Heusden, A. W. 2012. Screening for new sources of resistance to *Clavibacter michiganensis* subsp. *michiganensis* (Cmm) in tomato. *Euphytica.* 190:309–317.

Sen, Y., van der Wolf, J., Visser, R. G. F., and van Heusden, S. 2015. Bacterial canker of tomato: current knowledge of detection, management, resistance, and interactions. *Plant Dis.* 99:4–13.

- Sharabani, G., Shtienberg, D., Borenstein, M., Shulhani, R., Lofthouse, M., Sofer, M., Chalupowicz, L., Barel, V. and Manulis-Sasson, S. 2013. Effects of plant age on disease development and virulence of *Clavibacter michiganensis* subsp. *michiganensis* on tomato. *Plant Pathol.* 62:1114–1122.
- Smith, E. F. 1910. A new tomato disease of economic importance. *Science.* 31 (803):794-796
- Smith, E. F. 1914. The Grand Rapids tomato disease. Pages 161-165 in: *Bacteria in Relation to Plant Diseases*, Vol. 3. Carnegie Institute, Washington, D.C.
- Sotirova, V., Shtereva, L., Zagorska, N., Dimitrov, B., and Bogatsevska, N. 1999. Resistance responses of plants regenerated from tomato anther and somatic tissue cultures to *Clavibacter michiganense* subsp *michiganense*. *Isr. J. Plant Sci.* 47:237–243.
- Stork, I., Gartemann, K-H., Burger, A., and Eichenlaub, R. 2008. A family of serine proteases of *Clavibacter michiganensis* subsp. *michiganensis*: *chpC* plays a role in colonization of the host plant tomato. *Mol. Plant Pathol.* 9:599–608.
- Suzuki, K. I., Suzuki, M., Sasaki, J., Park, Y. H., and Komagata, K. K. 1999. *Leifsonia* gen. nov., a genus for 2,4-diaminobutyric acid-containing Actinomycetes to accommodate "*Corynebacterium aquaticum*" Leifson 1962 and *Clavibacter xyli* subsp. *cynodontis* Davis et al. 1984. *J. Gen. Appl. Microbiol.* 45(5):253–262

- Svircev, A., Roach, D., and Castle, A. 2018. Framing the future with bacteriophages in agriculture. *Viruses*. 10, 218.
- Tancos, M. A., Chalupowicz, L., Barash, I., Manulis-Sasson, S., and Smart, C. D. 2013. Tomato fruit and seed colonization by *Clavibacter michiganensis* subsp. *michiganensis* through external and internal routes. *Appl. Environ. Microbiol.* 79:6948–6957.
- Tancos, M. A., Lange, H. W., and Smart, C. D. 2015. Characterizing the genetic diversity of the *Clavibacter michiganensis* subsp. *michiganensis* population in New York. *Phytopathology*. 105:169–179.
- Tancos, M. A., Lowe-Power, T. M., Peritore-Galve, F. C., Tran, T. M., Allen, C., and Smart, C. D. 2018. Plant-like bacterial expansins play contrasting roles in two tomato vascular pathogens. *Mol. Plant Pathol.* 19:1210–1221.
- Thapa, S. P., O’Leary, M., Jacques, M.-A., Gilbertson, R. L., and Coaker, G. 2019. Comparative genomics to develop a specific multiplex pcr assay for detection of *Clavibacter michiganensis*. *Phytopathology*. 110:556–566.
- Thapa, S. P., Pattathil, S., Hahn, M. G., Jacques, M.-A., Gilbertson, R. L., and Coaker, G. 2017. Genomic analysis of *Clavibacter michiganensis* reveals insight into virulence strategies and genetic diversity of a gram-positive bacterial pathogen. *Mol. Plant-Microbe Interact.* 30:786–802.

- Tovar-Herrera, O. E., Rodríguez, M., Olarte-Lozano, M., Sampedro-Guerrero, J. A., Guerrero, A., Pinto-Cámara, R., Alvarado-Affantranger, X., Wood, C. D., Moran-Mirabal, J. M., Pastor, N., Segovia, L., and Martínez-Anaya, C. 2018. Analysis of the binding of expansin Ex11, from *Pectobacterium carotovorum*, to plant xylem and comparison to EXLX1 from *Bacillus subtilis*. *ACS Omega*. 3:7008–7018.
- Utsuzawa, S., Fukuda, K., and Sakaue, D. 2005. Use of magnetic resonance microscopy for the nondestructive observation of xylem cavitation caused by pine wilt disease. *Phytopathology*. 95:737–743.
- VanderMolen, G. E., Labavitch, J. M., Strand, L. L., and DeVay, J. E. 1983. Pathogen-induced vascular gels: ethylene as a host intermediate. *Physiol. Plant.*. 59:573–580.
- Venturas, M. D., Sperry, J. S., and Hacke, U. G. 2017. Plant xylem hydraulics: What we understand, current research, and future challenges. *J. of Integr. Plant Biol.* 59:356–389.
- Vulkova, Z. V., and Sotirova, V. G. 1993. Study of the three-genome hybrid *Lycopersicon esculentum* Mill. —*L. chilense* Dun. —*L. peruvianum* var. ‘*humifusum*’ Mill. and its use as a source for resistance. *Theoret. Appl. Genetics*. 87:337–342.
- Wang, E. L. H., and Bergeson, G. B. 1974. Biochemical changes in root exudate and xylem sap of tomato plants infected with *Meloidogyne incognita*. *J Nematol.* 6:194–202.

- Windt, C. W., Vergeldt, F. J., Jager, P. A. D., and As, H. V. 2006. MRI of long-distance water transport: a comparison of the phloem and xylem flow characteristics and dynamics in poplar, castor bean, tomato and tobacco. *Plant Cell Environ.* 29:1715–1729.
- Wittmann, J., Brancato, C., Berendzen, K. W., and Dreiseikelmann, B. 2016. Development of a tomato plant resistant to *Clavibacter michiganensis* using the endolysin gene of bacteriophage CMP1 as a transgene. *Plant Pathol.* 65:496–502.
- Xu, X., Miller, S. A., Baysal-Gurel, F., Gartemann, K.-H., Eichenlaub, R., and Rajashekara, G. 2010. Bioluminescence imaging of *Clavibacter michiganensis* subsp. *michiganensis* infection of tomato seeds and plants. *Appl. Environ. Microbiol.* 76:3978–3988.
- Zgurskaya, H. I., Evtushenko, L. I., Akimov, V. N., and Kalakoutskii, L. V. 1993. *Rathayibacter* gen. nov., including the species *Rathayibacter rathayi* comb. nov., *Rathayibacter tritici* comb. nov., *Rathayibacter iranicus* comb. nov., and six strains from annual grasses. *Int. J. Syst. Evol. Micr.* 43(1):143-149

## CHAPTER 1

# **Characterizing colonization patterns of *Clavibacter michiganensis* during infection of tolerant wild *Solanum* species**

### ***ABSTRACT***

*Clavibacter michiganensis* is the gram-positive causal agent of bacterial canker of tomato, an economically devastating disease with a worldwide distribution. *Clavibacter michiganensis* colonizes the xylem, leading to unilateral wilt, stem canker, and plant death. The pathogen can also infect developing tomato fruit through splash dispersal, forming exterior bird's-eye lesions. There are no documented sources of qualitative resistance in *Solanum* spp., however, QTL conferring tolerance in *Solanum arcanum* and *S. habrochaites* have been identified. Mechanisms of tolerance and *C. michiganensis* colonization patterns in wild tomato species remain poorly understood. This study describes differences in symptom development and colonization patterns of wild type (WT) and a hypervirulent bacterial expansin knockout ( $\Delta$ CmEXLX2) in wild and cultivated tomato genotypes. Overall, WT and  $\Delta$ CmEXLX2 cause less severe symptoms in wild tomato species and are impeded in spread and colonization of the vascular system. Laser scanning confocal microscopy and scanning electron microscopy was used to observe preferential colonization of protoxylem vessels and reduced intravascular spread in wild tomatoes. Differences in *C. michiganensis in vitro* growth and aggregation were determined in xylem sap, which may suggest responses to pathogen colonization are occurring, leading to reduced colonization density in wild tomato species. Finally, wild tomato fruit were determined to be susceptible to *C. michiganensis* through *in vivo* inoculations and assessing lesion numbers and size. Fruit symptom severity was in some cases unrelated to severity of symptoms during vascular infection, suggesting different mechanisms for colonization of different tissues.

\*This chapter was published in: Peritore-Galve F.C., Miller C., and Smart C. D. 2020.

Characterizing colonization patterns of *Clavibacter michiganensis* during infection of tolerant wild *Solanum* species. *Phytopathology*, 110:574-581

## **INTRODUCTION**

Bacterial canker is one of the most economically damaging diseases affecting tomato production worldwide (de León et al. 2011; Nandi et al. 2018; Sen et al. 2014). *Clavibacter michiganensis*, formerly *Clavibacter michiganensis* subsp. *michiganensis*, is the gram-positive causal agent of bacterial canker within the genus *Clavibacter*, which has been recently undergone reclassification from subspecies to species rank (Thapa et al. 2019; Li et al. 2017). *Clavibacter michiganensis* systemically colonizes the tomato vascular system leading to unilateral wilt, marginal leaf necrosis, stem cankers, and plant death (Chalupowicz et al. 2012; Sen et al. 2015). Splash dispersal of *C. michiganensis* can infect the exterior of developing tomato fruit, producing bird's-eye lesions that affect fruit quality and can lead to seed contamination (Medina-Mora et al. 2001; Tancos et al. 2013). Systemic spread of *C. michiganensis* in the xylem makes it difficult to control with conventional products, and there is no commercially available resistance in tomato (de León et al. 2011; Sen et al. 2015). Quantitative trait loci (QTL) from wild tomato species that confer tolerance have been identified; however, the mechanisms of tolerance to *C. michiganensis* are poorly understood (Sen et al. 2014). Studying *C. michiganensis* colonization of tomatoes with varying susceptibility is a step towards deciphering how wild tomato species tolerate *C. michiganensis* infection.

Wild *Solanum* spp. harbor genetic diversity that can be exploited as sources for disease resistance. Several species including: *S. arcanum*, *S. chilense*, *S. glandulosum*, *S. habrochaites*,

*S. minutum*, *S. parviflorum*, *S. peruvianum*, and *S. pimpinellifolium* have demonstrated moderate to high tolerance to *C. michiganensis* (Francis et al. 2001; van Heusden et al. 1999; Kabelka et al. 2002; Lara-Ávila et al. 2012; Sen et al. 2012, 2015; Sotirova et al. 1999; Vulkova and Sotirova 1993). Genetic studies of *S. arcanum* LA2157 (formerly *Lycopersicon peruvianum*) identified additive and co-dominant QTL on different chromosomes of interspecific crosses and an F<sub>2</sub> population (van Heusden et al. 1999; Sotirova et al. 1999). Fine mapping of *S. habrochaites* LA407 (formerly *Lycopersicon hirsutum*) identified two QTL with additive tolerance on chromosomes 2 and 5 that contribute to vascular development, morphology, and H<sub>2</sub>O<sub>2</sub> defense responses in the xylem (Coaker and Francis 2004; Coaker et al. 2002, 2004; Francis et al. 2001). Despite low symptom development in wild *Solanum* spp., *C. michiganensis* is able to systemically colonize the vascular system to high densities (10<sup>4</sup>-10<sup>8</sup> CFU per 1 mg tissue) (Francis et al. 2001; Sen et al. 2012). To the best of our knowledge, there have been no published studies investigating wild tomato fruit susceptibility to *C. michiganensis*. The role of *C. michiganensis* colonization, spread, and plant response in the development of bacterial canker symptoms remains uncharacterized in these tolerant plant species.

*Clavibacter michiganensis* interacts with plant host tissues in a complex manner that is poorly understood (Chalupowicz et al. 2017; Nandi et al. 2018). Genomic analyses have revealed a pathogenicity island and two plasmids necessary for full virulence in the reference strain, NCPPB382 (Dreier et al. 1997; Gartemann et al. 2008; Jahr et al. 2000; Meletzus et al. 1993). These mobile elements contain multiple copies of genes encoding secreted serine proteases, carbohydrate active enzymes, expansins, and tomatinase (Gartemann et al. 2008). Genetic studies have demonstrated that *C. michiganensis* strains have variable gene and plasmid contents that contribute to virulence (Tancos et al. 2015; Thapa et al. 2017). In a previous study, a

hypervirulent *C. michiganensis* isolate was generated by knocking out a single-copy expansin gene encoding a secreted expansin-like protein (CmEXLX2) (Tancos et al. 2018). The role of secreted *C. michiganensis* expansin proteins during virulence and the mechanisms underlying hypervirulence remain unclear, but the hypervirulent strain  $\Delta$ CmEXLX2 can be used as a tool to further our understanding of host- *C. michiganensis* interactions.

*Clavibacter michiganensis* poses a major threat to tomato producers, and epidemics often begin through seedling transplants harboring latent infections (de León et al. 2011). The goals of this study were to understand differences in *C. michiganensis* colonization and host symptom development between susceptible domesticated tomato and tolerant wild tomato species. Results from this study can begin to delineate the complex relationship between *C. michiganensis* and the host tissues it colonizes.

## ***MATERIALS AND METHODS***

### **Disease severity assays**

Wild tomato seeds (*S. habrochaites* LA2128, *S. arcanum* LA2157, and *S. arcanum* LA2172) were washed in a 50% bleach solution for 15 min, rinsed with sterile deionized water, and then, germinated on wet sterile Whatman filter paper (Fisher Scientific, Pittsburgh, PA) in petri dishes for 8-10 days. Seedlings were then transferred to a Farfard professional formula growing mix in 72-cell flats (Sun Gro Horticulture, Agawam, MA) and *S. lycopersicum* ‘Mt. Fresh Plus’ seeds were started in the mix. When seedlings had two true leaves, they were transferred to four-inch pots and supplemented with Osmocote slow release fertilizer (Scotts Miracle-Gro Co., Marysville, OH). Plants were grown with a 16-hr light/8-hr dark photoperiod in an environmentally controlled greenhouse.

To characterize plant susceptibility to *C. michiganensis*, seedlings of *S. lycopersicum*

'Mt. Fresh', *S. habrochaites* LA2128, *S. arcanum* LA2157, and *S. arcanum* LA2172 between the two and three-true leaf stage were inoculated with wild-type (WT) *C. michiganensis* 0317 (hereafter WT) and *C. michiganensis* 0317 $\Delta$ CmEXLX2 (hereafter  $\Delta$ CmEXLX2) cultured in Lysogeny Broth (LB) medium and LB supplemented with gentamicin (40 $\mu$ g/ml), respectively, for 18 hours shaking at 160 rpm at 28°C (Tancos et al. 2018). Bacterial suspensions were adjusted to optical density 600 (OD<sub>600</sub>) = 0.8 through centrifugation for 12 min at 4,000 rpm, washing the pellet with sterile water, and resuspending in sterile water (Tancos et al. 2018). Tomato seedlings ( $n = 15$  per genotype) were arranged in three randomized blocks with two replicates of each plant genotype/*C. michiganensis* strain combination per block in the greenhouse. One mock-inoculated plant per genotype was included in each block as a control.

Plants were inoculated by dipping sterilized scissors into bacterial suspension and clipping the cotyledons (Tancos et al. 2018). Plants were assessed daily for leaflet wilting and stem canker formation. Observations continued until 21 days post inoculation (dpi). Disease severity was quantified by dividing the number of leaflets wilting each day by the total number of leaflets present on the oldest seven leaves at 21 dpi (Balaji et al. 2008; Chalupowicz et al. 2012; Tancos et al. 2018). The mean area under the disease progress curve (AUDPC) was calculated from disease severity measurements (Tancos et al. 2018). Differences in AUDPC were analyzed using a mixed effects model with strain, genotype, block, and the interaction between strain and genotype as explanatory variables, and a random effect to account for block effects using packages lme4, pbrktest, emmeans, and lsmeans in R v. 3.3.2 (Bates et al. 2015; Halekoh and Højsgaard 2014; Lenth 2016). Significant differences between treatment groups were tested using Tukey's honestly significant difference (HSD) test ( $P < 0.05$ ). The experiment was performed three times.

### **Bacterial movement and *in planta* growth**

To characterize spread and colonization density of *C. michiganensis* in the plant vascular system, 0.5cm sections of tomato stem tissue at the inoculation site (0cm), 5cm, and 10cm above were harvested at 21dpi ( $n = 3$  per genotype inoculated with WT or  $\Delta$ CmEXLX2). Tissues were weighed and homogenized in 1 ml of sterile water using a sterile 5-mm stainless steel grinding bead (Qiagen, Valencia, CA) in a 2-ml Eppendorf tube using a TissueLyser (Retsch, Newtown, PA) at 30 Hz for 4 min. One hundred microliters of the homogenate were transferred to a 96-well Falcon tissue culture plate (Corning Inc, Corning, NY), and 10 $\mu$ l were serial diluted into 90 $\mu$ l sterile water for seven dilutions. Ten microliters of each dilution was spot inoculated onto D2ANX or LB plates amended with gentamycin (40 $\mu$ g/ml) four times and incubated for two to three days at 28°C. Numbers of CFU were quantified at the dilution where there were between 20 and 200 CFU, and the average of four technical replicates per biological replicate was used for the final analysis. CFU counts were log<sub>10</sub> transformed and data from three individual experiments were analyzed separately and then pooled for the final analysis ( $n = 9$  biological replicates of a host genotype inoculated with WT or  $\Delta$ CmEXLX2 at 0, 5, and 10cm from the inoculation site). A mixed effects model was generated with log<sub>10</sub>CFU milligram<sup>-1</sup> of tissue as the response and distance by genotype by strain as the main effects, with random effects accounting for variation between experiments, blocks within experiments, and variability within a single plant. The analysis was performed using packages lme4, pbkrtest, emmeans, and lmerTest in R v. 3.3.2 (Bates et al. 2015; Halekoh and Højsgaard 2014; Lenth 2016). Significant differences between groups were tested using Tukey's HSD test ( $P < 0.05$ ).

### ***In vitro* growth and attachment of *C. michiganensis* in xylem sap**

Xylem sap for *in vitro* analyses was extracted from plants between the six- and eight-leaf

stage by heavy watering the night before and at dawn, cutting the stem at an angle ~1 cm above the cotyledons; then, we tilted the pots to allow sap to drain into 15-ml conical tubes for 1 hour. Sap was transferred into tubes on ice every 15 min. Sap from at least six plants was pooled and filtered through 0.2- $\mu$ m polyethersulfone syringe filters (Corning Inc.) and stored at -20°C.

To measure bacterial growth in xylem sap, WT and  $\Delta$ CmEXLX2 were grown as described above and resuspended to OD<sub>600</sub> = 0.1 in sterile water. Five microliters of three individual WT and  $\Delta$ CmEXLX2 cultures were inoculated into 12 wells (4 wells per bacterial culture) of a 96-well Falcon tissue culture plate containing 195  $\mu$ l sterile tomato sap. The plate was incubated at 28°C shaking in a BioTek microplate reader (Winooski, VT). Optical density was measured at 590 nm every 2 h for 48 h (Tancos et al. 2018). Optical density for bacterial growth samples were normalized to mock (sterile water)-inoculated sap from each genotype. Area under the growth curve was calculated for each sample, and statistical analyses were performed using a mixed effects model including bacterial cultures as random effects using packages lme4, pbkrtest, and emmeans in R v. 3.3.2 (Bates et al. 2015; Halekoh and Højsgaard 2014; Lenth 2016). Significant differences between treatment groups were tested using Tukey's HSD test ( $P < 0.05$ ). The experiment was performed twice.

To measure *C. michiganensis* attachment *in vitro*, WT and  $\Delta$ CmEXLX2 were grown as described above and adjusted to OD<sub>600nm</sub> = 0.8. Five microliters of three individual cultures of WT and  $\Delta$ CmEXLX2 were inoculated to 12 wells (4 wells per bacterial culture) of a 96-well Falcon tissue culture plate containing 95  $\mu$ l of filter-sterilized tomato sap. Plates were briefly shaken and statically incubated at 28°C for 5 days (Chalupowicz et al. 2012; Tancos et al. 2018; Tran et al. 2016). After incubation, the supernatant was gently removed through pipetting, and wells were washed twice with 150  $\mu$ l of sterile water. The samples were fixed at 60°C for 1 h,

and surface-attached bacteria were stained with 25  $\mu$ l of 0.1% crystal violet for 25 min at room temperature. The plate was washed twice with 200  $\mu$ l of sterile water and gently blotted on paper towels (Davey and O'toole 2000; Tancos et al. 2018; Tran et al. 2016). Crystal violet was solubilized by adding 100  $\mu$ l of 30% acetic acid followed by brief agitation and quantifying the absorbance at 590 nm using the BioTek microplate reader (Davey and O'toole 2000; Tancos et al. 2018; Tran et al. 2016). Statistical analyses were performed using a mixed effects model including bacterial cultures as random effects using packages lme4, pbkrtest, and emmeans in R v. 3.3.2 (Bates et al. 2015; Halekoh and Højsgaard 2014; Lenth 2016). Significant differences between treatment groups were tested using Tukey's HSD test ( $P < 0.05$ ). The experiment was performed twice.

### **Lateral *C. michiganensis* spread in primary vascular bundles**

Three seedlings of each of the four host genotypes were grown as described above. Strains of WT and  $\Delta$ CmEXLX2 with stable plasmids expressing eGFP were cultured as described in LB amended with kanamycin (100 $\mu$ g/ml; Fisher Scientific) or kanamycin and gentamicin (40 $\mu$ g/ml), respectively (Tancos et al. 2018). Cultures were adjusted to  $OD_{600} = 0.8$  and cotyledon clip inoculated into plants at the two- to three-true leaf stage ( $n = 3$  per genotype per strain). Mock-inoculated plants were included as controls.

To determine the number of xylem vessels colonized by *C. michiganensis*, transverse stem sections were excised 1 cm above the inoculation site at 21 dpi. Primary vascular bundles were imaged using scanning laser confocal microscopy (Olympus BX61; Fluoview FV-300; Olympus Corp., Tokyo, Japan) using argon (488-nm) and green helium neon (543-nm) lasers to excite eGFP-expressing bacteria and induce plant autofluorescence, respectively (Chalupowicz et al. 2012; Tancos et al. 2013, 2018). The number of infected and non-infected protoxylem and metaxylem vessels in

primary vascular bundles was quantified for each of three plants for each genotype/strain combination. Mock-inoculated plants were included as controls for plant autofluorescence. In total, 332 fields of view were imaged for quantification. Comparisons of percent infected xylem vessels were calculated with analysis of variance (ANOVA) and Tukey's HSD test ( $P < 0.05$ ) using packages agricolae and emmeans in R v 3.3.2 (Lenth 2016; Mendiburu 2015).

To visualize bacterial colonization of individual proto- and metaxylem vessels using scanning electron microscopy (SEM), transverse and longitudinal stem sections 1 cm above the inoculation site were excised 12 dpi from mock- and WT-inoculated plants ( $n = 2$  per genotype). Tissue sections were fixed in 3% glutaraldehyde in sterile phosphate-buffered saline followed by application of vacuum pressure to remove air from samples. Tissues were washed four times with Sørensen's phosphate buffer (pH=7.2) and dehydrated using an ethanol series. Solvents were removed through critical point drying (030 Critical point dryer; BAL-TEC, Canonsburg, PA) and samples were mounted on aluminum stubs and sputter coated twice with gold (EMS500x; Electron Microscopy Sciences, Hatfield, PA). Images were captured using a scanning electron microscope (S-530 SEM; Hitachi, Tokyo, Japan) equipped with a digital camera. Two hundred eight fields of view were imaged in total.

### **Fruit disease severity assays**

To assess susceptibility of wild tomato fruit to *C. michiganensis*, 6-week old plants were transferred to 3-gallon pots and fertilized with Osmocote slow release fertilizer. Eight-week old *S. lycopersicum* 'Mt. Fresh' plants were self-pollinated using a vibrating pollinator wand (VegiBee, Maryland Heights, MO). *S. habrochaites* LA2128 and both *S. arcanum* genotypes were manually pollinated. *Clavibacter michiganensis* strains were cultured and adjusted to  $OD_{600} = 0.8$  as described above. Water, WT, and  $\Delta$ CmEXLX2 were brush inoculated onto fruit between 7 and 9 days post anthesis (dpa;  $n = 10$  per treatment) of four plants of each genotype. To prevent

cross-contamination of treatments, fruit clusters on the same plant were required to be a minimum of 25 cm distance apart. Fruit were harvested 15 dpi, and the diameter and number of lesions per fruit was measured. To measure fruit lesion size, images of each fruit were taken using an Olympus SZX18 dissecting microscope (Olympus Corp.). Lesion diameter and diameter of the lesion's necrotic center were measured using Olympus cellSens software (Olympus Corp.;  $n = 100$  per treatment). Comparisons of number of lesions per fruit and differences in lesion size were calculated using ANOVA and Tukey's HSD test ( $P < 0.05$ ) with packages agricolae, emmeans, and lsmeans in R v 3.3.2 (Lenth 2016; Mendiburu 2015). The fruit susceptibility experiment was performed twice for a total of 20 fruit per host genotype/*C. michiganensis* strain combination.

## **RESULTS**

### **Wild tomato species express fewer bacterial canker symptoms**

Host susceptibility and movement of *C. michiganensis* in the vascular system were assessed by inoculating seedlings of cultivated and wild tomatoes with *C. michiganensis*. Wild tomato seedlings inoculated with WT and  $\Delta$ CmEXLX2 developed little to no leaflet wilt in comparison to *S. lycopersicum* 'Mt. Fresh' ( $P < 0.01$ ) (Fig. 1.1). Leaflet wilt appeared as early as 7 and 10 dpi in *S. lycopersicum* 'Mt. Fresh' plants inoculated with  $\Delta$ CmEXLX2 and WT, respectively. On average, wilt appeared on *S. arcanum* LA2172 plants inoculated with  $\Delta$ CmEXLX2 at 12dpi. Wilt symptoms of *S. habrochaites* LA2128 inoculated with both strains were delayed until 17dpi. The mutant  $\Delta$ CmEXLX2 strain was hypervirulent in seedlings of *S. lycopersicum* 'Mt. Fresh' as well as *S. arcanum* LA2172, but not in *S. habrochaites* LA2128 and *S. arcanum* LA2157 (Fig. 1.2).

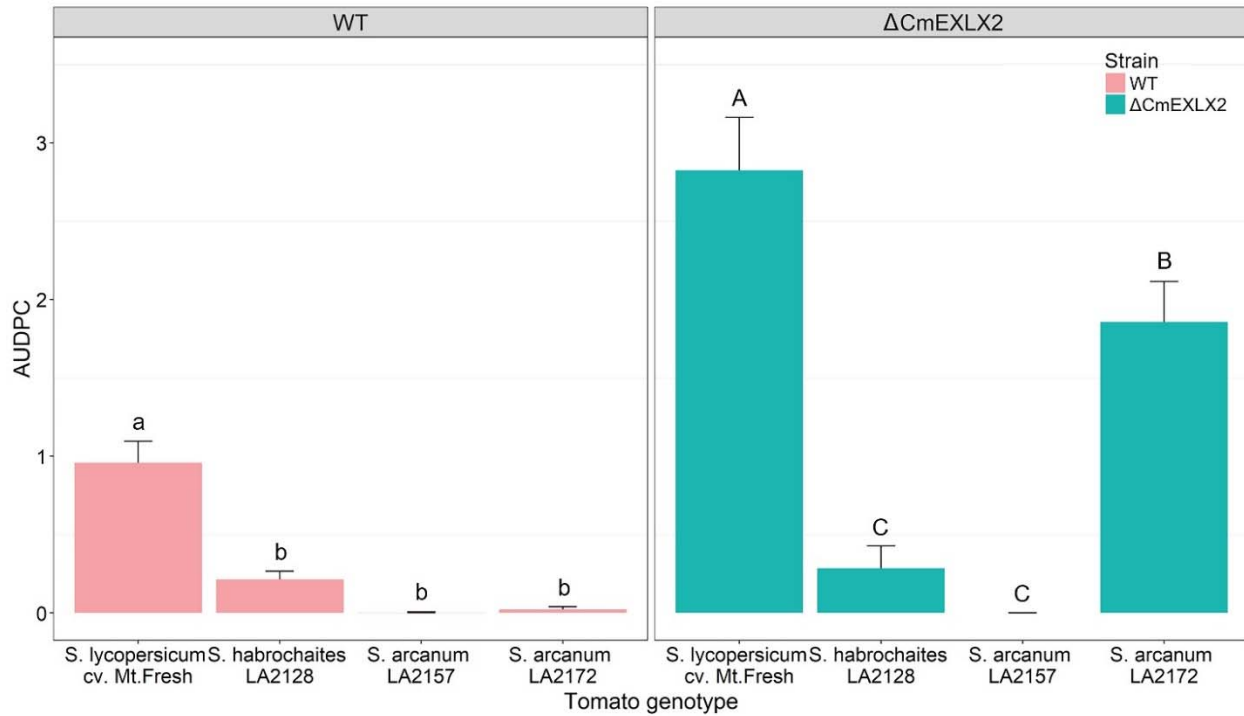


**FIGURE 1.1.** Disease severity as AUDPC of all four plant genotypes faceted by WT and  $\Delta$ CmEXLX2. Bars represent standard error and letters indicate significant differences ( $P < 0.05$ ) between genotypes inoculated with either WT or  $\Delta$ CmEXLX2. Differences were calculated using Tukey's pairwise comparisons.

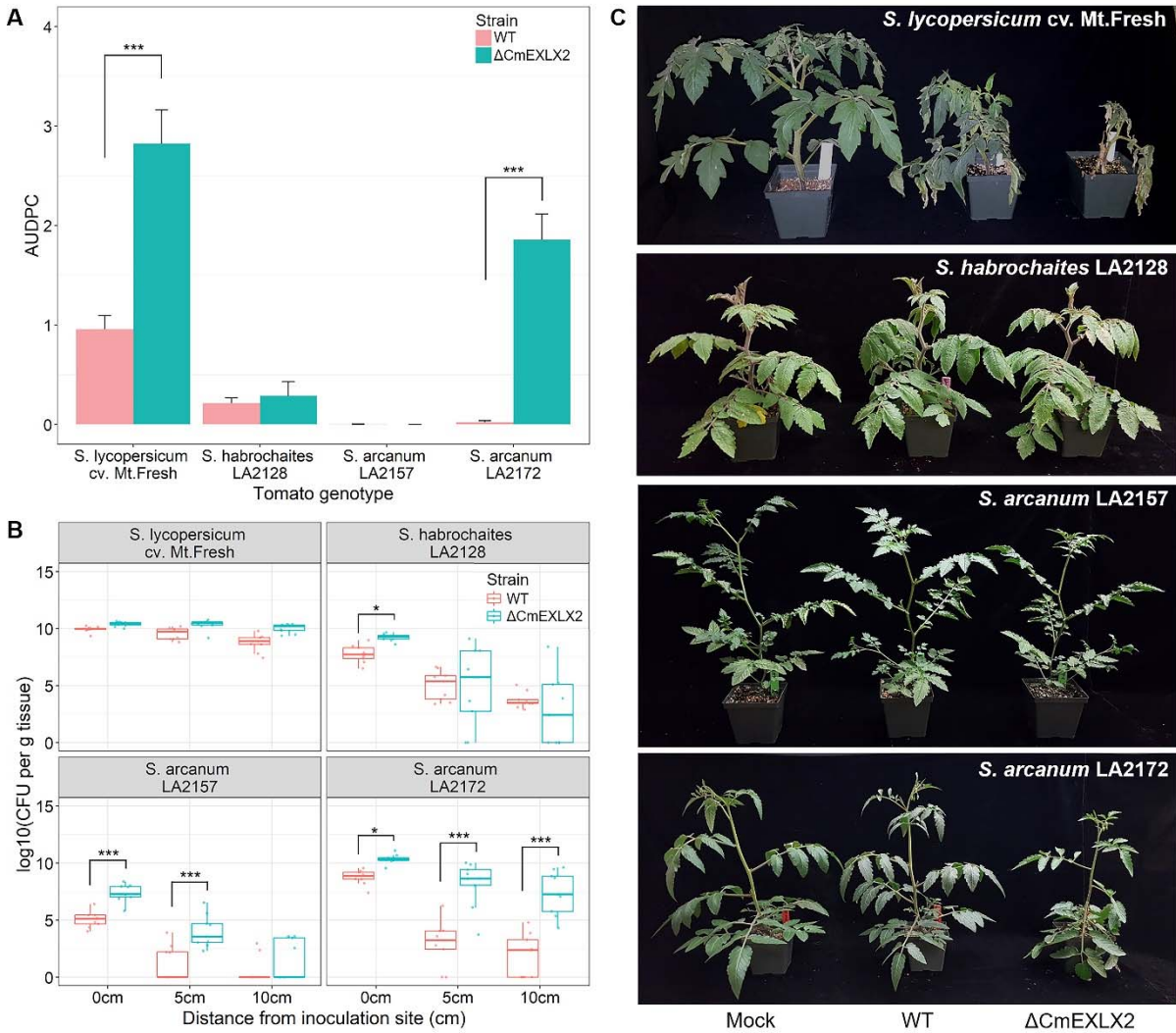


**Figure 1.2.** (A) Disease severity as area under the disease progress curve (AUDPC) of all four plant genotypes inoculated with WT and  $\Delta$ CmEXLX2. Bars represent standard error and asterisks indicate significant differences (\*  $P < 0.05$ , \*\*  $P < 0.01$ , \*\*\*  $P < 0.001$ ) between strains on a single host genotype. (B) Colonization density at the inoculation site and distally as  $\log_{10}$  colony forming units (CFU) per gram tissue. Asterisks represent significant differences in colonization density between strains at that site. (C) Representative mock (left), WT (middle) and  $\Delta$ CmEXLX2-inoculated (right) plants at 21dpi. Significant differences were calculated using Tukey's pairwise comparisons.

Differences in bacterial canker symptoms were observed between tomato genotypes. Severely affected leaflets of *S. arcanum* LA2172 wilted without marginal leaf necrosis, differing from typical wilt symptoms of bacterial canker in *S. lycopersicum* ‘Mt. Fresh’ (Figs. 1.1 and 1.3). *Solanum habrochaites* LA2128 leaflets would partially wilt before the development of chlorosis followed by marginal leaf necrosis (Fig. 1.3). Both *C. michiganensis* strains produced typical stem cankers at the inoculation site between 9-12dpi in *S. lycopersicum* ‘Mt. Fresh’ (Fig. 1.3). Only  $\Delta$ CmEXLX2 was able to form stem cankers at the inoculation site of *S. arcanum* LA2172. No cankers were present in *S. habrochaites* LA2128 and *S. arcanum* LA2157 plants inoculated with either *C. michiganensis* strain (Fig. 1.3).

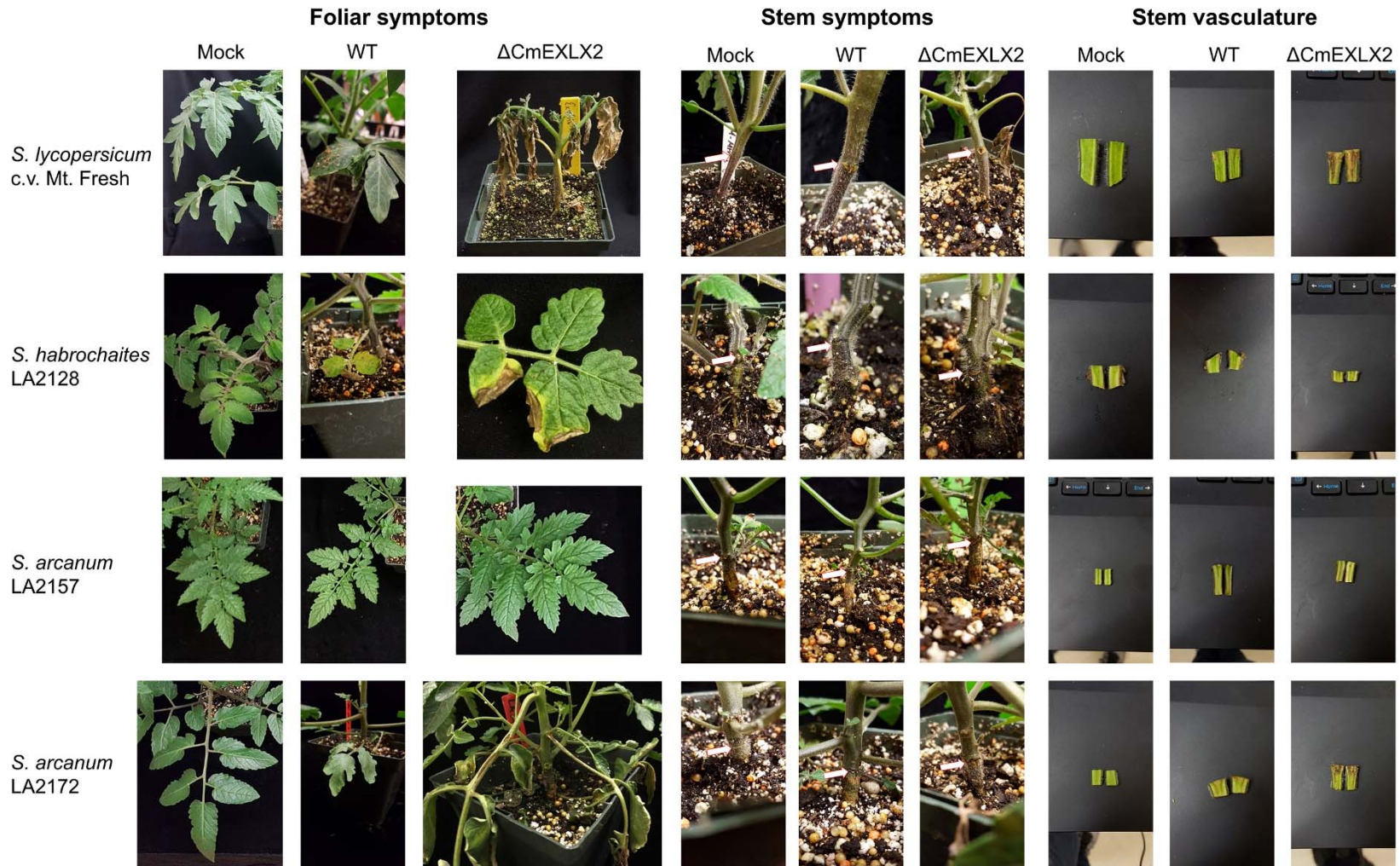


**FIGURE 1.3.** Foliar, stem and vascular symptoms and signs of all four tomato genotypes inoculated with water, WT, and  $\Delta$ CmEXLX2 at 21dpi.

### ***Clavibacter michiganensis* spread and colonization is reduced in wild tomatoes**

The ability for *C. michiganensis* to spread and densely colonize the vascular system is critical for systemic infection and symptom development. We quantified WT and  $\Delta$ CmEXLX2 colonization density of plant stem sections 21 dpi at the inoculation site (0), 5, and 10 cm above. Wild-type *C. michiganensis* was able to colonize to similarly high densities ( $10^9$  CFU per 1 g of tissue) at the inoculation site of *S. lycopersicum* ‘Mt. Fresh’ and *S. arcanum* LA2172, but not of *S. habrochaites* LA2128 and *S. arcanum* LA2157 (Figs. 1.2 and 1.4). Wild-type *C. michiganensis* populations were reduced at 5 and 10 cm above the inoculation site of all wild tomatoes (Figs. 1.2 and 1.4). The mutant  $\Delta$ CmEXLX2 strain only colonized at significantly higher densities relative to WT ( $P < 0.05$ ) at varying distances in *S. arcanum* accessions (Figs. 1.2 and 1.4). Populations of  $\Delta$ CmEXLX2 in wild tomatoes were also reduced as the distance from the inoculation site increased. Both WT and  $\Delta$ CmEXLX2 populations were lowest in the asymptomatic accession *S. arcanum* LA2157, but  $\Delta$ CmEXLX2 colonization of *S. arcanum* LA2172 was almost equal to  $\Delta$ CmEXLX2 titers in *S. lycopersicum* ‘Mt. Fresh’, suggesting that  $\Delta$ CmEXLX2 hypervirulence is specific to certain plant genotypes within a species (Fig. 1.2).

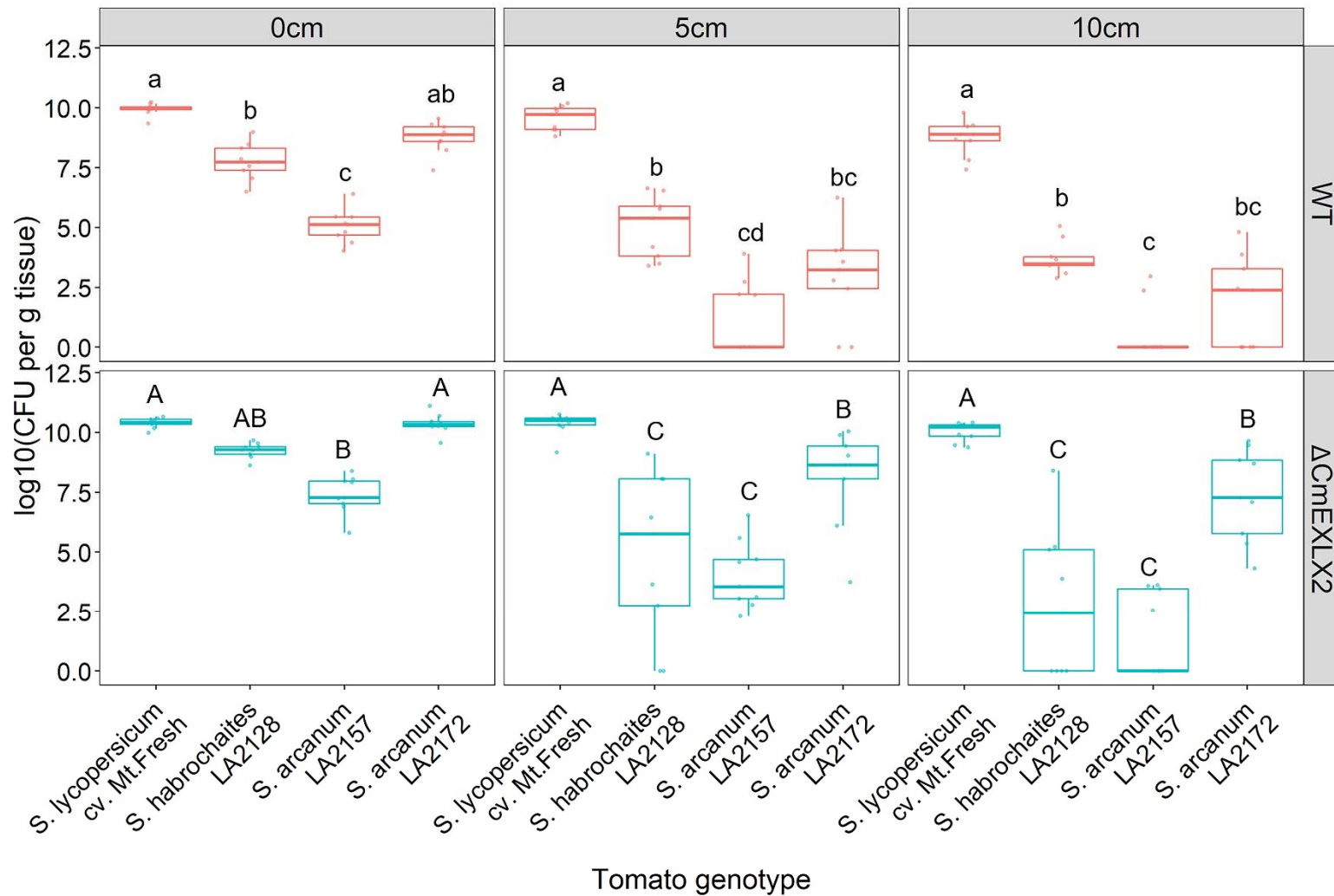


**FIGURE 1.4.** Colonization density at the inoculation site and distally separated by bacterial strain. Population density is measured as log<sub>10</sub> colony forming units (CFU) per gram of tissue. Letters denote significant differences (p < 0.05) between genotypes within a single site calculated using Tukey's pairwise comparisons.

## Composition of tomato xylem sap affects growth and biofilm formation

The xylem sap composition of wild tomatoes could be suboptimal for *C. michiganensis* growth, therefore reducing *in planta* growth and symptom development. We extracted sap from the four tomato genotypes and measured *in vitro* growth rates of WT and  $\Delta$ CmEXLX2 for 48 h. There were no differences in growth rates between WT and  $\Delta$ CmEXLX2 when cultured in sap from each of the four genotypes (Fig. 1.5) *Clavibacter michiganensis* grew to the highest density in sap from the most susceptible genotype, *S. lycopersicum* ‘Mt. Fresh’, and to the second highest density in sap from the asymptomatic genotype *S. arcanum* LA2157 (Fig. 1.5). *Clavibacter michiganensis* grew to lowest densities in sap from *S. habrochaites* LA2128.

Using the crystal violet attachment assay, we determined that WT *C. michiganensis* was able to aggregate to similar levels in sap from *S. lycopersicum* ‘Mt. Fresh’ and *S. arcanum* genotypes (Fig 1.6). Aggregation was severely reduced in sap from *S. habrochaites* LA2128, perhaps due to lower *in vitro* growth (Figs. 1.5 and 1.6). The mutant  $\Delta$ CmEXLX2 strain formed fewer aggregates in sap from both *S. arcanum* genotypes in comparison to WT, but was only significantly lower in sap from *S. arcanum* LA2157 ( $P = 0.0058$ ).

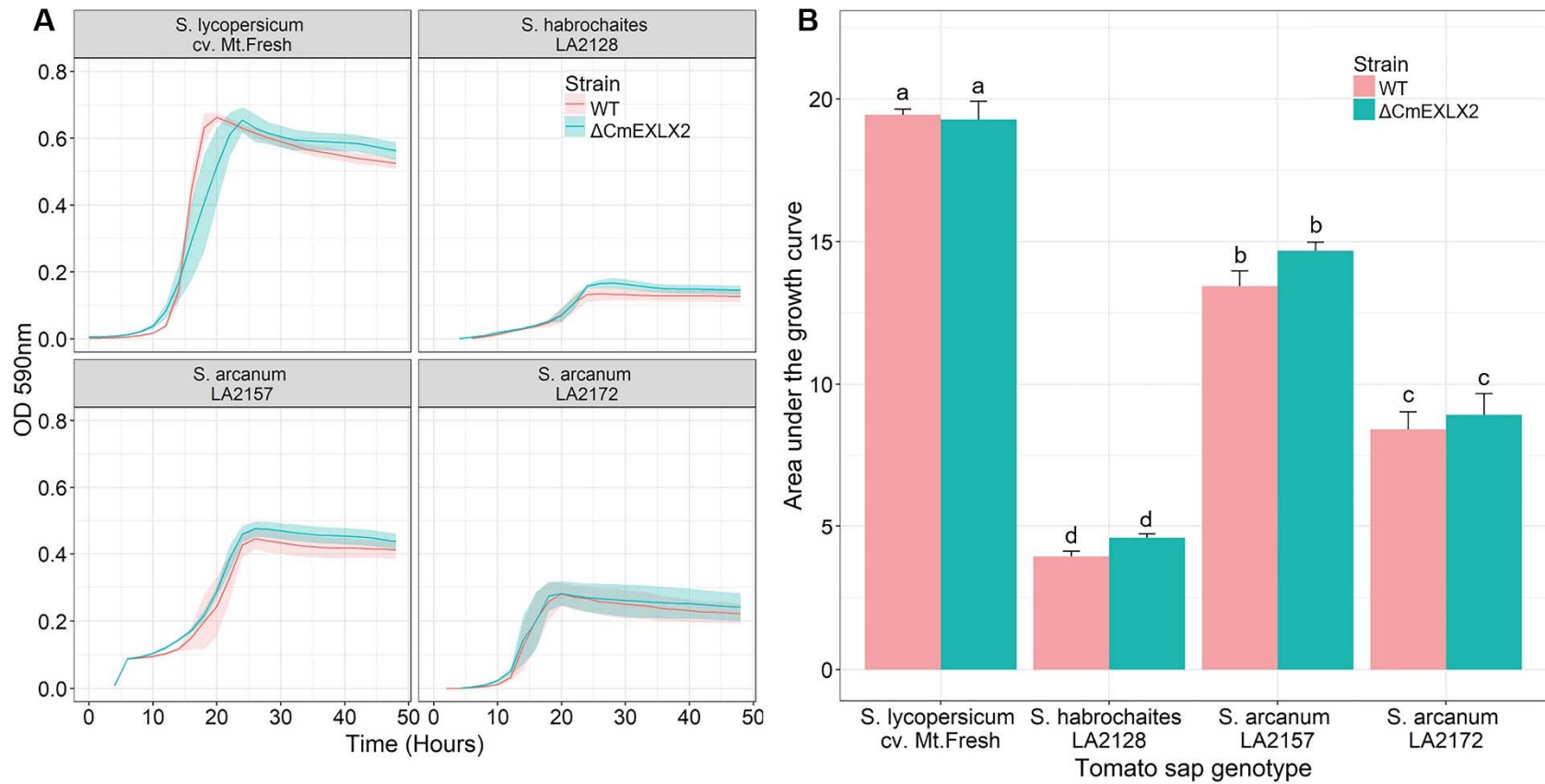


**FIGURE 1.5.** (A) Growth curves of WT and  $\Delta$ CmEXLX2 cultured in sterile xylem sap collected from healthy plants measured by optical density at absorbance 590. Ribbon corresponds to 95% confidence intervals. (B) Area under the growth curve of WT and  $\Delta$ CmEXLX2 cultured in sterile xylem sap. Bars denote standard error and letters represent significant differences ( $p < 0.05$ ) between treatment groups using Tukey's pairwise comparisons.

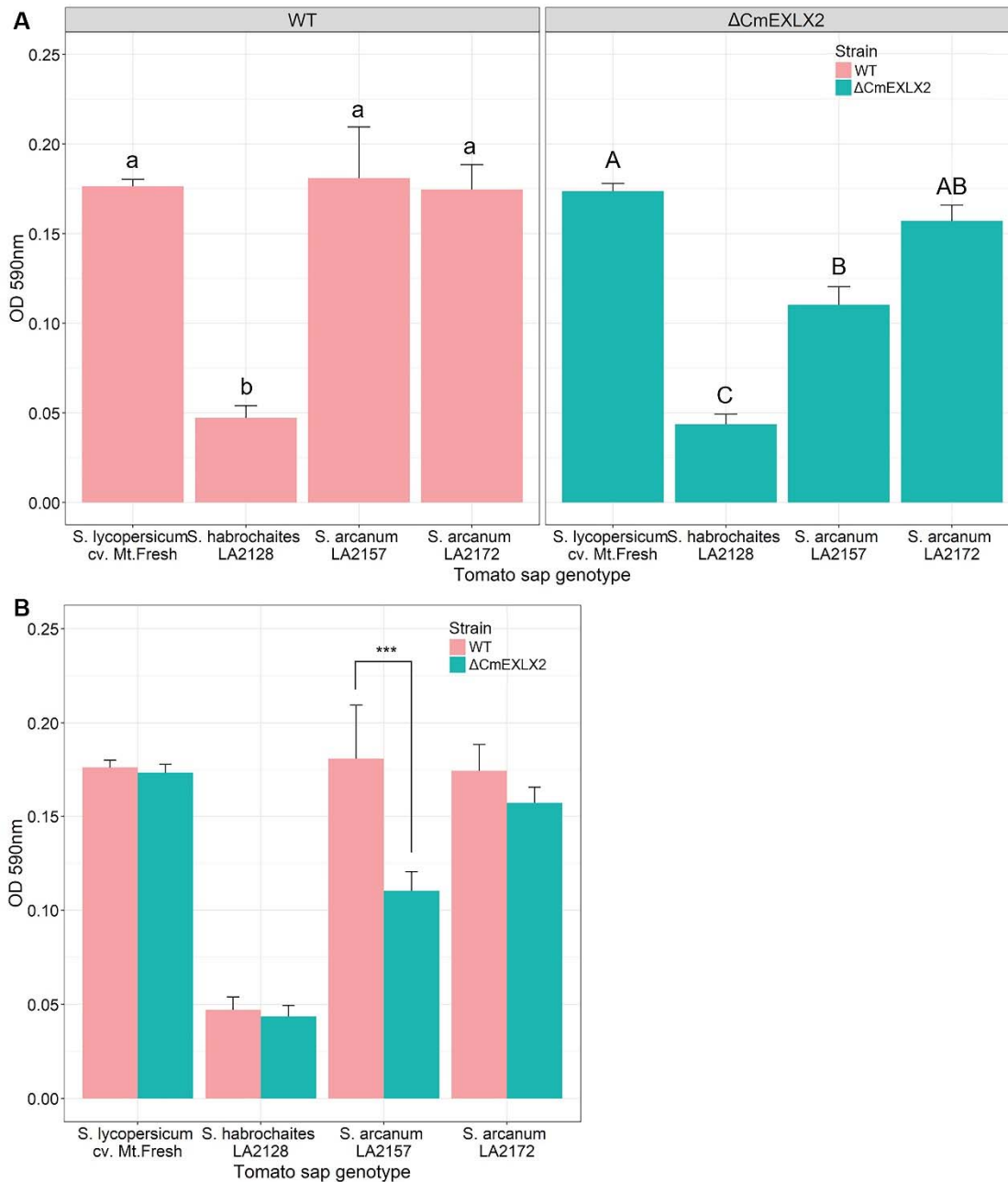


**FIGURE 1.6.** (A) Bacterial strain attachment in sterile xylem sap measured as optical density at absorbance 590. Letters denote significant differences ( $P < 0.05$ ) between genotypes inoculated with a single strain. (B) Bacterial attachment in sterile xylem sap. Asterisks represent significant differences ( $P < 0.001$ ) between strains within a single plant genotype. All bars represent standard error. Differences were calculated using Tukey's pairwise comparisons.

### ***Clavibacter michiganensis* is impeded in lateral spread in wild tomato vascular bundles**

The spread of *C. michiganensis* between xylem vessels of wild tomato species was studied by inoculating plants with eGFP-expressing WT and  $\Delta$ CmEXLX2 strains, and quantifying colonized proto- and metaxylem vessels in primary vascular bundles 21 dpi using laser scanning confocal microscopy (Fig. 1.7). Wild-type and  $\Delta$ CmEXLX2 strains colonized similar proportions of protoxylem vessels in all genotypes tested (Table 1.1). *Clavibacter michiganensis* was present in >50% of protoxylem vessels in primary vascular bundles of all four plant genotypes (Table 1.1). Spread to metaxylem vessels by *C. michiganensis* was highest in the most susceptible genotypes (*S. lycopersicum* ‘Mt. Fresh’ and *S. arcanum* LA2172), and lowest in the most tolerant genotypes (*S. habrochaites* LA2128 and *S. arcanum* LA2157) (Table 1.1). Spread of WT *C. michiganensis* to metaxylem vessels was significantly higher than  $\Delta$ CmEXLX2 in *S. lycopersicum* ‘Mt. Fresh’ ( $P = 0.0012$ ) and *S. arcanum* LA2172 ( $P = 0.0004$ ), the two genotypes that had more severe symptoms with  $\Delta$ CmEXLX2.

To achieve a closer view of biofilm-like structures in xylem vessels, we harvested transverse and longitudinal stem sections 1 cm above the inoculation site from plants (12dpi) inoculated with WT *C. michiganensis* for SEM. Bacterial aggregates were present in protoxylem vessels of all genotypes, and smaller aggregates were found less frequently in metaxylem vessels of *S. lycopersicum* ‘Mt. Fresh’, *S. habrochaites* LA2128 and *S. arcanum* LA2172 (Fig. 1.8) but not *S. arcanum* LA2157. *Clavibacter michiganensis* aggregates were present in xylem parenchyma and pith cells of *S. lycopersicum* ‘Mt. Fresh’ and *S. habrochaites* LA2128 (data not shown) but we cannot determine whether this was an artifact of sectioning or part of the natural infection process.

**TABLE 1.1.** Percentage of proto- and metaxylem vessels infected by eGFP-expressing WT and  $\Delta$ CmEXLX2 *C. michiganensis* across four tomato genotypes determined by laser scanning confocal microscopy.

Tomato genotype	Percentage of infected protoxylem vessels <sup>†</sup>		Percentage of infected metaxylem vessels <sup>†</sup>	
	WT	$\Delta$ CmEXLX2	WT	$\Delta$ CmEXLX2
<i>S. lycopersicum</i> ‘Mt. Fresh’	76.0 ± 11.7 a	69.6 ± 3.5 A	38.2 ± 6.5 c <sup>z</sup>	26.6 ± 3.8 C
<i>S. habrochaites</i> LA2128	57.2 ± 8.2 a	62.1 ± 7.7 A	9.7 ± 2.7 a	13.8 ± 2.7 B
<i>S. arcanum</i> LA2157	58.4 ± 12.7 a	62.3 ± 8.3 A	7.3 ± 4.2 a	5.2 ± 1.5 A
<i>S. arcanum</i> LA2172	71.4 ± 8.6 a	64.6 ± 8.0 A	27.7 ± 3.3 b <sup>z</sup>	14.7 ± 1.1 B

<sup>†</sup> Numbers presented are the mean percentage ± standard deviation. Letters represent significant differences ( $P < 0.05$ ) between plant genotypes inoculated with a single strain. Lowercase letters represent differences or lack thereof between genotypes inoculated with WT. Uppercase letters denote differences or lack thereof between genotypes inoculated with  $\Delta$ CmEXLX2.

<sup>z</sup> Significant differences ( $P < 0.05$ ) between strains within a single plant genotype.

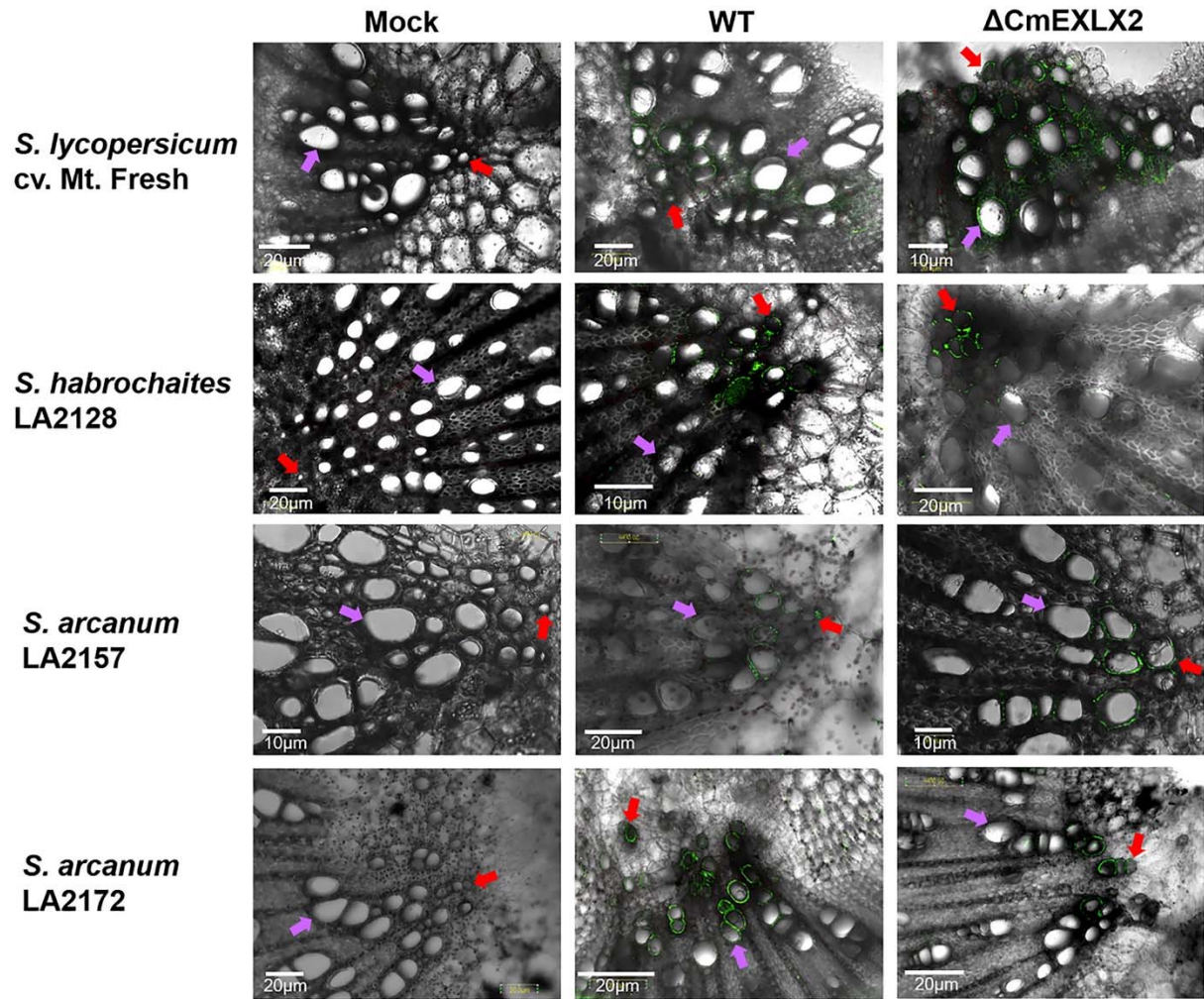


**FIGURE 1.7.** Intravascular colonization of xylem vessels from all four plant genotypes infected with WT and  $\Delta$ CmEXLX2 expressing eGFP at 21 days post inoculation. Red arrows highlight protoxylem and purple arrows highlight metaxylem vessels.

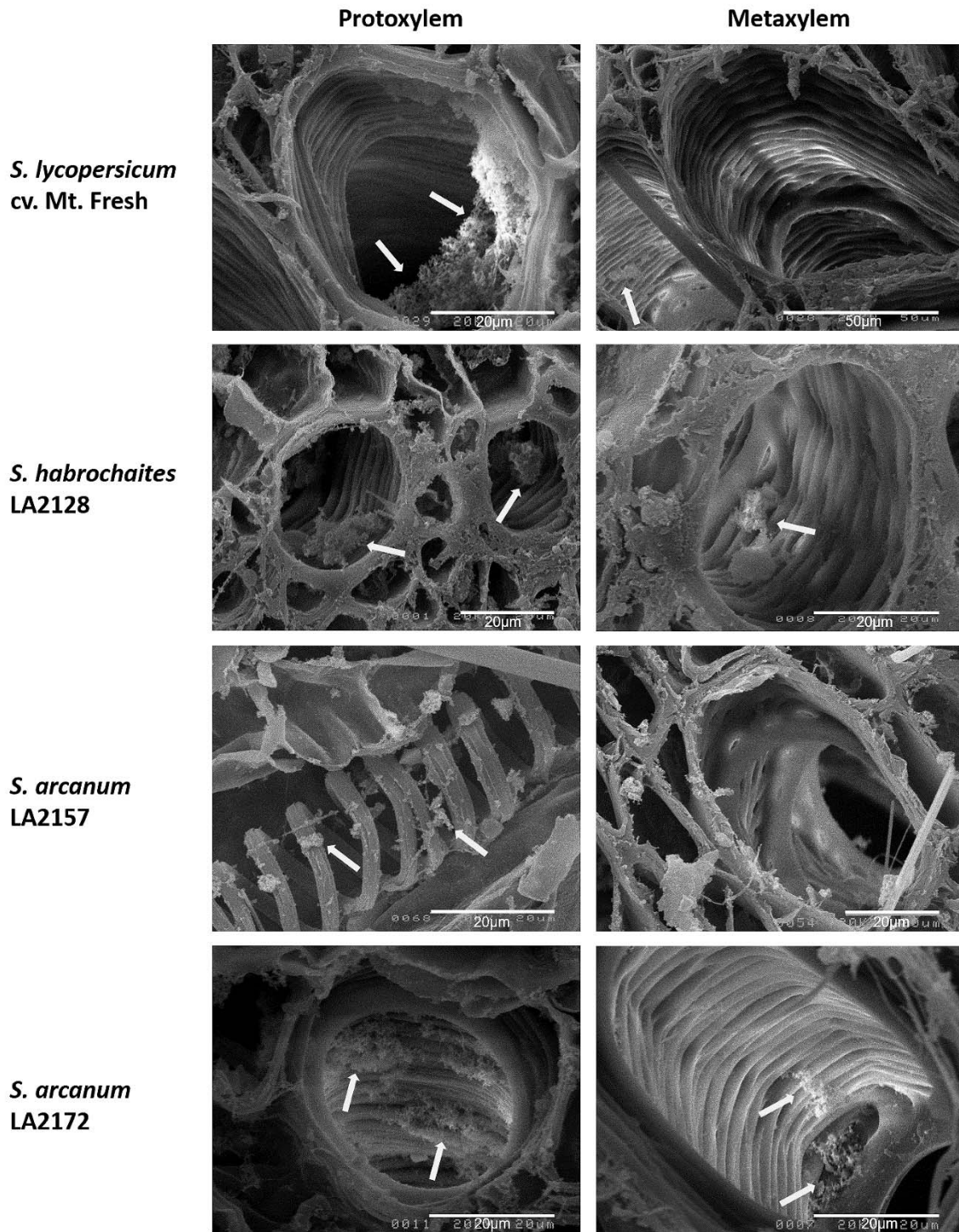


**FIGURE 1.8.** Scanning electron microscope images of WT *C. michiganensis* aggregates in individual proto- and metaxylem vessels of all four plant genotypes. White arrows highlight bacterial aggregates.

### **Fruit susceptibility assays demonstrate that susceptibility to Cm is tissue specific**

The ability for *C. michiganensis* strains to produce bird's eye lesions on wild tomato fruit was tested between 7 and 9 dpa. Both WT and  $\Delta$ CmEXLX2 caused characteristic symptoms, which appear as a necrotic center surrounded by a white halo, although the phenotype varied by plant genotype (Fig. 1.11). *Clavibacter michiganensis* formed two- to threefold more lesions in *S. lycopersicum* 'Mt. Fresh' fruit in comparison to wild genotypes (Fig. 1.9). Lesion severity was determined by measuring the diameter of whole lesions and their necrotic centers. Both WT and  $\Delta$ CmEXLX2 formed the largest lesions (approximately 1.3-mm diameter) on *S. lycopersicum* 'Mt. Fresh' and *S. arcanum* LA2157 fruit (Figs. 1.9, 1.10, and 1.11). Lesion diameter of WT *C. michiganensis* was significantly larger ( $P < 0.05$ ) in comparison to  $\Delta$ CmEXLX2 lesions in *S. habrochaites* LA2128 and *S. arcanum* LA2172 fruit (Fig. 1.9). The mutant  $\Delta$ CmEXLX2 strain produced significantly larger necrotic lesions in *S. lycopersicum* 'Mt. Fresh' as previously reported (Tancos et al., 2018), but the size of the necrotic lesion was reduced relative to WT in *S. habrochaites* LA2128 and *S. arcanum* LA2172 (Fig. 1.9).

Fruit from all four genotypes formed bird's eye lesions only when inoculated at early stages of development (7 to 15 dpa). Lesion phenotypes differed between genotypes, with the most striking difference being raised lesions in *S. habrochaites* LA2128 identified in 96% of lesions measured (Fig. 1.9 and Fig. 1.11).

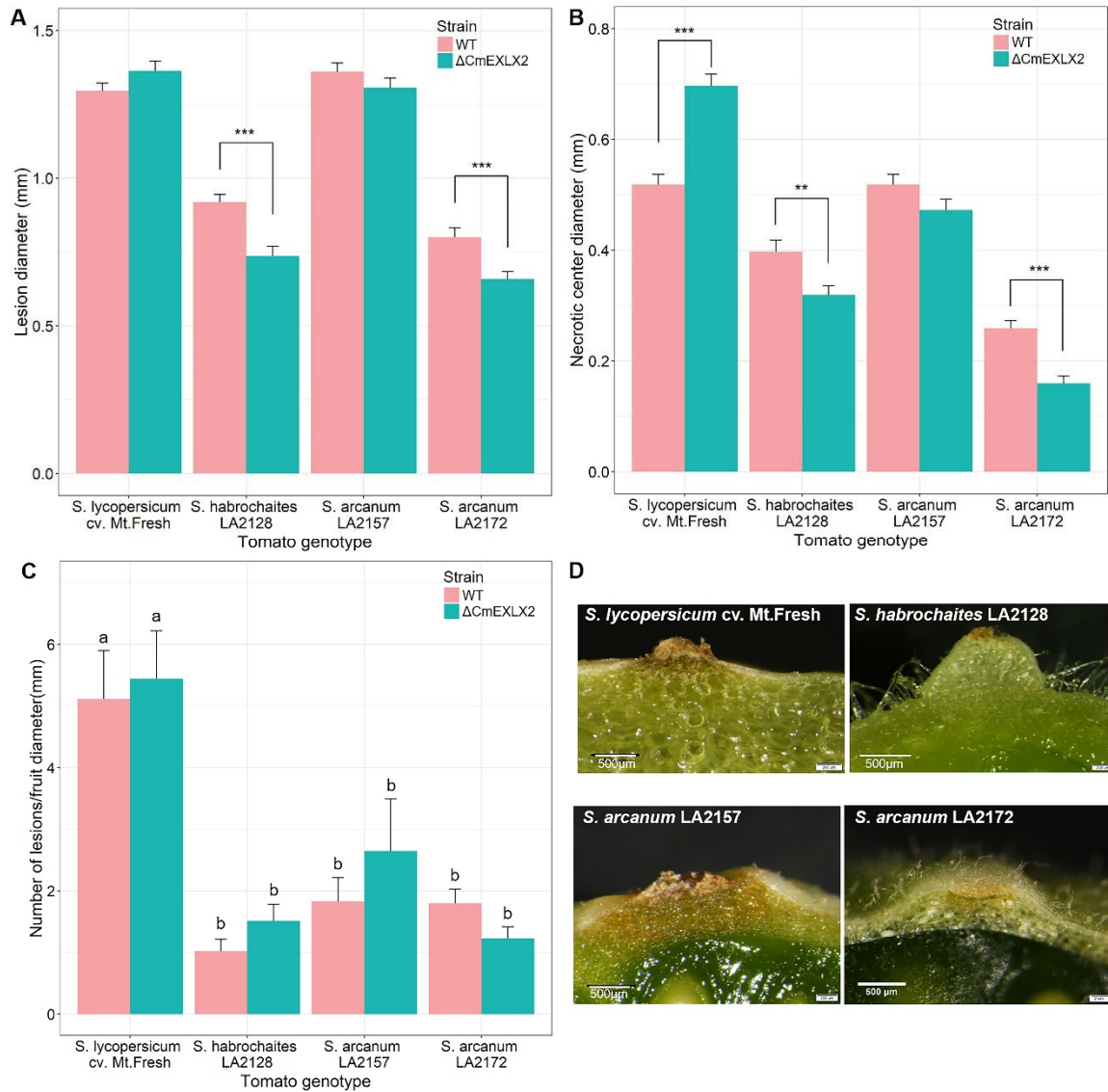


**FIGURE 1.9.** (A) Mean diameter (millimeters) of bird's eye lesions caused by WT and  $\Delta$ CmEXLX2 on fruit from all four genotypes. (B) Mean diameter (millimeters) of necrotic centers of bird's eye lesions. (C) Disease severity on fruit represented as number of lesions per fruit divided by fruit diameter (millimeters). Bars for all graphs represent standard error. Asterisks denote significant differences between strains and letters denote significant differences ( $P < 0.05$ ) across all treatments as calculated through Tukey's pairwise comparisons. (D) Transverse cross sections of fruit lesions on all four genotypes caused by WT *C. michiganensis* demonstrating phenotypic differences of lesions. Scale bar is 500 $\mu$ m. \*\* $P < 0.01$ ; \*\*\*  $P < 0.001$ .

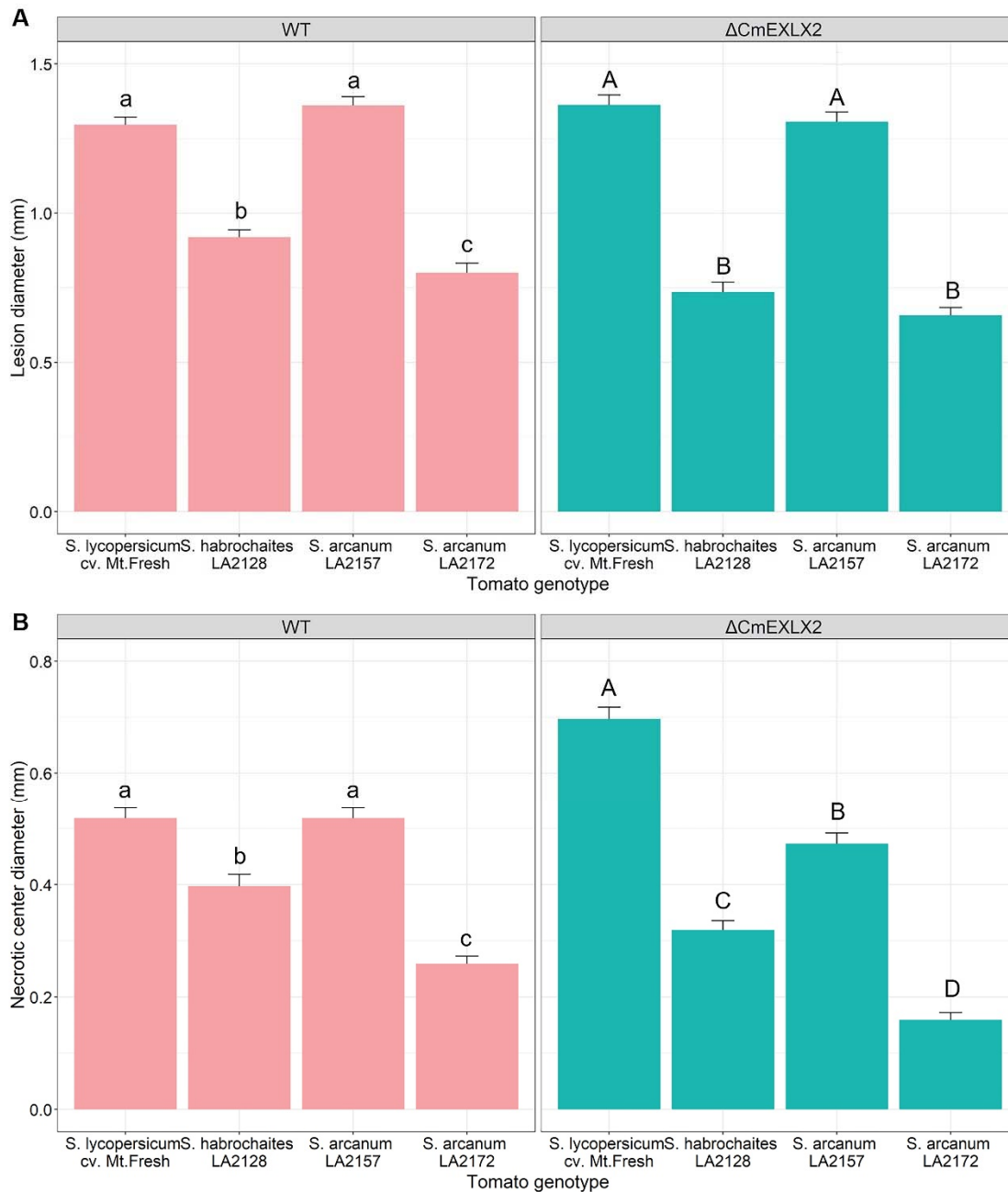


**FIGURE 1.10.** (A) Lesion diameter (millimeters) of WT and  $\Delta$ CmEXLX2 inoculated tomato fruit separated by strain. (B) Necrotic center diameter (millimeters) of WT and  $\Delta$ CmEXLX2 inoculated tomato fruit separated by strain. Bars for both graphs represent standard error and letters represent significant differences ( $P < 0.05$ ) between genotypes within a single bacterial strain calculated using Tukey's pairwise comparisons.

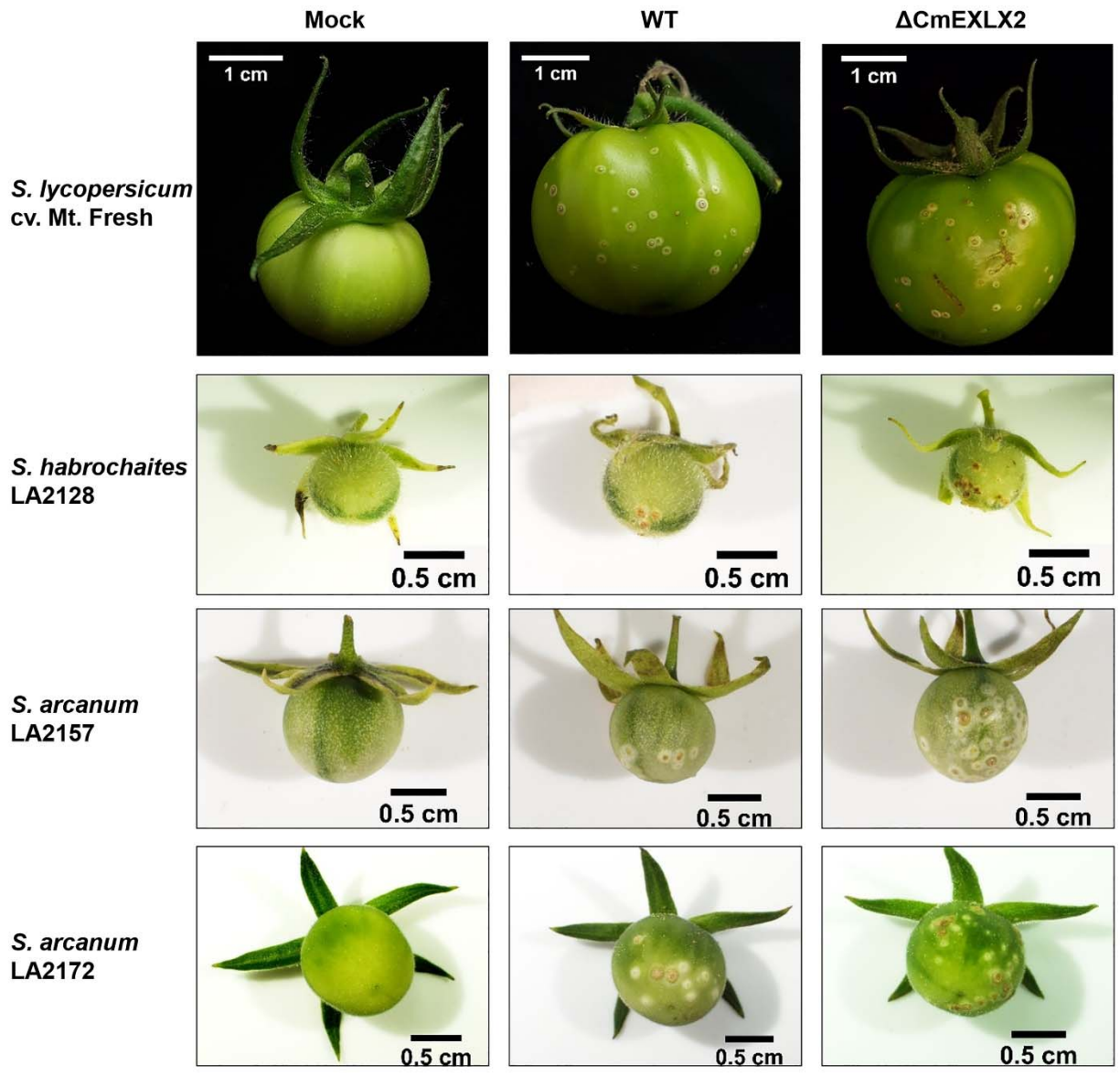


**FIGURE 1.11.** Tomato fruit from all four genotypes inoculated with WT and  $\Delta$ CmEXLX2 15 days post inoculation.

## **DISCUSSION**

There are no commercially available sources of resistance to bacterial canker of tomato, and we are just beginning to understand the complex interactions between *C. michiganensis* and its hosts. Here, we examined colonization patterns of WT and a hypervirulent mutant *C. michiganensis* strain in xylem and fruit of tolerant wild tomato species. Previous studies characterizing wild tomato tolerance to *C. michiganensis* have inoculated older plants between 4-10-true leaf stages, which may prevent more severe symptoms from developing (Sen et al. 2012; Sharabani et al. 2013). To reduce the effect of plant age on assessing tolerance, we inoculated wild tomatoes seedlings during early development (two- to three-true leaf stage). Disease severity assays demonstrated that  $\Delta$ CmEXLX2 was hypervirulent in *S. lycopersicum* ‘Mt. Fresh’ and *S. arcanum* LA2172 but not in *S. habrochaites* LA2128 and *S. arcanum* LA2157. The mutant  $\Delta$ CmEXLX2 strain colonized both *S. arcanum* accessions to higher densities than WT at several distances from the inoculation site, but stem cankers were only present in *S. arcanum* LA2172 inoculated with  $\Delta$ CmEXLX2. The lack of necrotic cankers in *S. arcanum* LA2157 and *S. habrochaites* LA2128 might suggest that *C. michiganensis* is impaired in its ability to macerate stem tissue in some wild tomato genotypes. We still do not understand the molecular mechanisms underlying hypervirulence, but these results suggest that secreted CmEXLX2 (Peritore-Galve et al. 2019) interacts with specific hosts, slowing disease onset and lowering severity of symptoms (Tancos et al. 2018). Functional analysis of a secreted *Pectobacterium carotovorum* expansin protein (PcEx11) determined that cellulolytic and xylanolytic activities of commercial cellulase and xylanase were reduced in celery vascular tissue in the presence of purified PcEx11 (Tovar-Herrera et al. 2018). Taken together, these results suggest that CmEXLX2 may bind plant polysaccharides to prevent hydrolysis. This may be a conserved

strategy to slow disease progress or to prevent activation of damage associated molecular pattern-triggered immunity (Choi and Klessig, 2016; Gust et al., 2017)

Previous studies of wild tomato tolerance have suggested that vascular morphology may play a role in tolerance to *C. michiganensis* (Coaker et al. 2002). A colonization study in cultivated tomato also demonstrated that *C. michiganensis* preferentially colonized protoxylem vessels during early infection and moved into metaxylem and parenchyma cells at later stages (Chalupowicz et al. 2012). Spread and colonization by WT and  $\Delta$ CmEXLX2 varied by host genotype. Wild-type and  $\Delta$ CmEXLX2 colonized *S. lycopersicum* 'Mt. Fresh' to a high density at the inoculation site and distally, whereas colonization and spread was reduced in wild tomato genotypes. The association between *C. michiganensis* populations and symptom severity remains unclear. For example, the plasmid free derivative, Cmm100, is able to colonize and spread in *S. lycopersicum* to similar rates as the pathogenic strain Cmm382 (Meletzus et al. 1993), and other studies of wild tomato tolerance have shown that *C. michiganensis* can colonize stem tissue to high densities without causing severe symptoms (Francis et al. 2001; Sen et al. 2012).

Assessment of systemic spread found that WT and  $\Delta$ CmEXLX2 colonizes stem tissue to lower densities distally from the inoculation site in wild tomato species. We were unable to identify any tyloses or gels that may be obstructing the movement of *C. michiganensis* through the xylem through SEM and confocal microscopy; however, this does not rule out their presence.

Confocal microscopy revealed that both WT and  $\Delta$ CmEXLX2 were present mainly in protoxylem vessels of wild tomato plants during later stages of infection (21 dpi), which has been observed in *S. lycopersicum* and hypothesized as a strategy to keep its host alive longer (Chalupowicz et al. 2012). SEM images identified larger *C. michiganensis* aggregates in protoxylem vessels relative to metaxylem at 12 dpi for all genotypes except *S. arcanum* LA2157,

where *C. michiganensis* was only found in protoxylem vessels. The ability for *C. michiganensis* to colonize higher proportions of metaxylem vessels correlated with disease severity between genotypes but not for differences between strains within a single genotype. A significantly higher proportion of metaxylem vessels were colonized by WT compared to  $\Delta$ CmEXLX2 in *S. lycopersicum* ‘Mt. Fresh’ and *S. arcanum* LA2172, which contradicts our hypothesis that metaxylem colonization is correlated to symptom severity. These data highlight the need for additional studies because the way in which  $\Delta$ CmEXLX2 causes more severe symptoms than WT is unknown. Microscopy data suggest that *C. michiganensis* is impaired in its ability to spread through the vascular system of wild tomatoes and it is possible that the restriction of *C. michiganensis* movement between xylem vessels and into other stem tissues may contribute to a reduction or elimination of symptoms in wild tomato species. However, further studies are required to delineate *C. michiganensis* colonization of xylem elements.

Biofilms play an important role in bacterial colonization and disease induction. Previous studies have shown that *C. michiganensis* is able to form biofilm-like aggregates *in vitro* when cultured in *S. lycopersicum* xylem sap, but not in LB or minimal medium (Chalupowicz et al. 2012; Tancos et al. 2018). We hypothesized that wild tomato sap composition would hinder growth and aggregate formation *in vitro*. Xylem sap from wild tomato species sustained lower populations of *C. michiganensis in vitro*. *In vivo* bacterial populations did not correlate with growth in sap. For example, *C. michiganensis* grew to the lowest densities in *S. arcanum* LA2157 plants, but sap was able to sustain *C. michiganensis* growth at the second highest rate. The inverse was true in *S. habrochaites* LA2128, where sap was only able to sustain low levels of growth of *C. michiganensis in vitro* but populations were only slightly reduced *in planta* in comparison to *S. lycopersicum* ‘Mt. Fresh’. Contrasting the results of *in vitro* and *in planta*

growth of *C. michiganensis* in wild tomato accessions suggests that host- *C. michiganensis* interactions are occurring in the xylem, affecting pathogen colonization. Aggregate formation was seemingly growth dependent, but attachment *in vitro* suggests that sap from wild tomato species provide similar conditions as sap from *S. lycopersicum* that triggers *C. michiganensis* attachment. We hypothesize that host proteins or metabolites are transported into xylem sap in response to *C. michiganensis* infection, which may lead to a reduction of bacterial growth as seen in *S. arcanum* LA2157. Metabolomics of *S. lycopersicum* xylem sap during infection by *Ralstonia solanacearum* found that the pathogen was secreting the polyamine putrescine as a virulence metabolite that altered host physiology (Lowe-Power et al. 2018). Findings in *R. solanacearum* support the idea that the xylem is an environment where pathogen and host interact to determine pathogen colonization.

Tomato fruit infection is an important disease stage for bacterial canker as it causes economic losses by blemishing fruit, and can serve as a route for *C. michiganensis* infection of developing seed (Tancos et al. 2013). We tested if *C. michiganensis* would cause lesions on wild tomato fruit and found that wild tomatoes were susceptible to *C. michiganensis* infection and formed similar bird's eye lesions. Moreover, *C. michiganensis* was able to form bird's eye lesions on *S. arcanum* LA2157, which did not develop any symptoms when *C. michiganensis* was inoculated into the vascular system, demonstrating that *C. michiganensis* susceptibility can vary between fruit and vascular infections. Bird's eye lesions forming on fruit from all genotypes seem to suggest that there is a conserved tomato fruit response that causes the lesion phenotype. Interestingly, bird's eye lesions on *S. habrochaites* LA2128 manifested as raised bumps, which under a microscope, seemed to be caused by host cell proliferation at the infection site. Raised lesions that we are hypothesizing to be caused by host cell proliferation might be caused by

perturbations in tomato fruit by compounds produced by *C. michiganensis* or through indirect alteration of host physiology as has been observed in other gram-positive pathogens (Thapa et al. 2019).

In conclusion, our data provide evidence that *C. michiganensis* colonizes vascular and fruit tissues of wild tomato species but is reduced in systemic spread. *Clavibacter michiganensis* growth in sap and *in planta* was not correlated, suggesting that interactions between host and *C. michiganensis* impact pathogen growth in xylem vessels. Confocal microscopy was used to observe preferential protoxylem colonization and reduced spread to metaxylem in wild tomato genotypes, which may play a role in reducing disease severity. Finally, fruit inoculations revealed that asymptomatic responses to *C. michiganensis* can be specific to the inoculated tissue in wild tomato species. This is important to know since breeding efforts have focused largely on susceptibility of plants to *C. michiganensis* when inoculated into the vascular system but not onto fruit. Bacterial canker continues to be one of the largest threats to the tomato industry; therefore, understanding the pathology of this gram-positive bacterium in tolerant and susceptible tomato genotypes can begin to untangle the complex interactions between host and pathogen.

### ***ACKNOWLEDGMENTS***

Thank you to Smart lab members, David Francis, and Angela Kruse for helpful discussions and critical feedback. Thank you to Holly Lange, Taylere Herrmann, Juan Luis González Girón, Mariami Bekauri, and Mary Jean Welser for technical support. Thank you to the Rick Tomato Genetics Resource Center and USDA-GRIN for wild tomato seed and advice on how to grow them. Thank you to Stephen Parry from the Cornell Statistical Consulting Unit for advice and support on statistical analyses.

## **REFERENCES**

- Balaji, V., Mayrose, M., Sherf, O., Jacob-Hirsch, J., Eichenlaub, R., Iraki, N., Manulis-Sasson, S., Rechavi, G., Barash, I., and Sessa, G. 2008. Tomato transcriptional changes in response to *Clavibacter michiganensis* subsp. *michiganensis* reveal a role for ethylene in disease development. *Plant Physiol.* 146:1797–1809.
- Bates, D., Mächler, M., Bolker, B., and Walker, S. 2015. Fitting linear mixed-effects models using lme4. *J. Stat. Softw.* 67:1–48.
- Chalupowicz, L., Barash, I., Reuven, M., Dror, O., Sharabani, G., Gartemann, K.-H., Eichenlaub, R., Sessa, G., and Manulis-Sasson, S. 2017. Differential contribution of *Clavibacter michiganensis* ssp. *michiganensis* virulence factors to systemic and local infection in tomato. *Mol. Plant Pathol.* 18:336–346.
- Chalupowicz, L., Zeller, E.-M., Fluegel, M., Dror, O., Eichenlaub, R., Gartemann, K.-H., Savidor, A., Sessa, G., Iraki, N., Barash, I., and Manulis-Sasson, S. 2012. Colonization and movement of GFP-labeled *Clavibacter michiganensis* subsp. *michiganensis* during tomato infection. *Phytopathology.* 102:23–31.
- Choi, H. W. and Klessig, D. F. 2016. DAMPs, MAMPs, and NAMPs in plant innate immunity. *BMC Plant Biol.* 16:232

- Coaker, G. L., and Francis, D. M. 2004. Mapping, genetic effects, and epistatic interaction of two bacterial canker resistance QTLs from *Lycopersicon hirsutum*. *Theor. Appl. Genet.* 108:1047–1055.
- Coaker, G. L., Meulia, T., Kabelka, E. A., Jones, A. K., and Francis, D. M. 2002. A QTL controlling stem morphology and vascular development in *Lycopersicon esculentum* × *Lycopersicon hirsutum* (Solanaceae) crosses is located on chromosome 2. *Am. J. Bot.* 89:1859–1866.
- Coaker, G. L., Willard, B., Kinter, M., Stockinger, E. J., and Francis, D. M. 2004. Proteomic analysis of resistance mediated by Rcm 2.0 and Rcm 5.1, two loci controlling resistance to bacterial canker of tomato. *Mol. Plant Microbe Interact.* 17:1019–1028.
- Davey, M. E., and O'toole, G. A. 2000. Microbial biofilms: from ecology to molecular genetics. *Mol. Biol. Rev.* 64:847–867.
- Dreier, J., Meletzus, D., and Eichenlaub, R. 1997. Characterization of the plasmid encoded virulence region *pat-1* of phytopathogenic *Clavibacter michiganensis* subsp. *michiganensis*. *Mol Plant Microbe Interact.* 10:195–206.

- Francis, D. M., Kabelka, E., Bell, J., Franchino, B., and St. Clair, D. 2001. Resistance to bacterial canker in tomato (*Lycopersicon hirsutum* LA407) and its progeny derived from crosses to *L. esculentum*. *Plant Dis.* 85:1171–1176.
- Gartemann, K.-H., Abt, B., Bekel, T., Burger, A., Engemann, J., Flügel, M., Gaigalat, L., Goesmann, A., Gräfen, I., Kalinowski, J., Kaup, O., Kirchner, O., Krause, L., Linke, B., McHardy, A., Meyer, F., Pohle, S., Rückert, C., Schneiker, S., Zeller, E. M., Pühler, A., Eichenlaub, R., Kaiser, O., and Bartels, D. 2008. The genome sequence of the tomato-pathogenic actinomycete *Clavibacter michiganensis* subsp. *michiganensis* NCPPB382 reveals a large island involved in pathogenicity. *J. Bacteriol.* 190:2138–2149.
- Gust, A. A., Pruitt, R., and Nürnberger, T. 2017. Sensing danger: key to activating plant immunity. *Trends Plant Sci.* 22:779-791.
- Halekoh, U., and Højsgaard, S. 2014. A Kenward-Roger approximation and parametric bootstrap methods for tests in linear mixed models the R package pbkrtest. *J. Stat. Softw.* 59:1–32.
- Heusden, A. W. van, Koornneef, M., Voorrips, R. E., Brüggemann, W., Pet, G., Ginkel, R. V., Chen, X., and Lindhout, P. 1999. Three QTLs from *Lycopersicon peruvianum* confer a high level of resistance to *Clavibacter michiganensis* ssp. *michiganensis*. *Theor. Appl. Genet.* 99:1068–1074.

- Jahr, H., Dreier, J., Meletzus, D., Bahro, R., and Eichenlaub, R. 2000. The endo- $\beta$ -1,4-glucanase CelA of *Clavibacter michiganensis* subsp. *michiganensis* is a pathogenicity determinant required for induction of bacterial wilt of tomato. *Mol. Plant Microbe Interact.* 13:703–714.
- Kabelka, E., Franchino, B., and Francis, D. M. 2002. Two loci from *Lycopersicon hirsutum* LA407 confer resistance to strains of *Clavibacter michiganensis* subsp. *michiganensis*. *Phytopathology.* 92:504–510.
- Lara-Avila, J. P., Isordia-Jasso, M. I., Castillo-Collazo, R., Simpson, J., and Alpuche-Solis, A. G. 2012. Gene expression analysis during interaction of tomato and related wild species with *Clavibacter michiganensis* subsp. *michiganensis*. *Plant Mol. Biol. Rep.* 30:498–511.
- Lenth, R. V. 2016. Least-squares means: the R package lsmeans. *J. of Stat. Softw.* 69:1–33.
- de León, L., Siverio, F., López, M. M., and Rodríguez, A. 2011. *Clavibacter michiganensis* subsp. *michiganensis*, a seedborne tomato pathogen: healthy seeds are still the goal. *Plant Dis.* 95:1328–1338.
- Li, X., Tambong, J., Yuan, K. (Xiaoli), Chen, W., Xu, H., Lévesque, C. A., and De Boer, S. H. 2018. Re-classification of *Clavibacter michiganensis* subspecies on the basis of whole-genome and multi-locus sequence analyses. *Int. J. Syst. Evol. Microbiol.* 68(1):234-40.

- Lowe-Power, T. M., Hendrich, C. G., Roepenack-Lahaye, E. von, Li, B., Wu, D., Mitra, R., Dalsing, B. L., Ricca, P., Naidoo, J., Cook, D., Jancewicz, A., Masson, P., Thomma, B., Lahaye, T., Michael, A. J., and Allen, C. 2018. Metabolomics of tomato xylem sap during bacterial wilt reveals *Ralstonia solanacearum* produces abundant putrescine, a metabolite that accelerates wilt disease. *Environ Microbiol.* 20:1330–1349.
- Medina-Mora, C. M., Hausbeck, M. K., and Fulbright, D. W. 2001. Bird's eye lesions of tomato fruit produced by aerosol and direct application of *Clavibacter michiganensis* subsp. *michiganensis*. *Plant Dis.* 85:88–91.
- Meletzus, D., Bermphol, A., Dreier, J., and Eichenlaub, R. 1993. Evidence for plasmid-encoded virulence factors in the phytopathogenic bacterium *Clavibacter michiganensis* subsp. *michiganensis* NCPPB382. *J. Bacteriol.* 175:2131–2136.
- Mendiburu, F. D. 2015. *Agricolae*: statistical procedures for agricultural research. R Package. <https://CRAN.R-project.org/package=agricolae>
- Nandi, M., MacDonald, J., Liu, P., Weselowski, B., and Yuan, Z.-C. 2018. *Clavibacter michiganensis* ssp. *michiganensis*: bacterial canker of tomato, molecular interactions and disease management. *Mol. Plant Pathol.* 19:2036–2050.

- Peritore-Galve, F. C., Schneider, D. J., Yang, Y., Thannhauser, T. W., Smart, C. D., and Stodghill, P. 2019. Proteome profile and genome refinement of the tomato-pathogenic bacterium *Clavibacter michiganensis* subsp. *michiganensis*. *Proteomics*. 19:1800224.
- Sen, Y., Feng, Z., Vandenbroucke, H., van der Wolf, J., Visser, R. G. F., and van Heusden, A. W. 2012. Screening for new sources of resistance to *Clavibacter michiganensis* subsp. *michiganensis* (*Cmm*) in tomato. *Euphytica*. 190:309–317.
- Sen, Y., van der Wolf, J., Visser, R. G. F., and van Heusden, S. 2014. Bacterial canker of tomato: current knowledge of detection, management, resistance, and interactions. *Plant Dis*. 99:4–13.
- Sharabani, G., Shtienberg, D., Borenstein, M., Shulhani, R., Lofthouse, M., Sofer, M., Chalupowicz, L., Barel, V., and Manulis-Sasson, S. 2013. Effects of plant age on disease development and virulence of *Clavibacter michiganensis* subsp. *michiganensis* on tomato. *Plant Pathol*. 62:1114–1122.
- Sotirova, V., Shtereva, L., Zagorska, N., Dimitrov, B., and Bogatsevska, N. 1999. Resistance responses of plants regenerated from tomato anther and somatic tissue cultures to *Clavibacter michiganense* subsp *michiganense*. *Isr. J. Plant Sci*. 47:237–243.

- Tancos, M. A., Chalupowicz, L., Barash, I., Manulis-Sasson, S., and Smart, C. D. 2013. Tomato fruit and seed colonization by *Clavibacter michiganensis* subsp. *michiganensis* through external and internal routes. *Appl. Environ. Microbiol.* 79:6948–6957.
- Tancos, M. A., Lange, H. W., and Smart, C. D. 2015. Characterizing the genetic diversity of the *Clavibacter michiganensis* subsp. *michiganensis* population in New York. *Phytopathology.* 105:169–179.
- Tancos, M. A., Lowe-Power, T. M., Peritore-Galve, F. C., Tran, T. M., Allen, C., and Smart, C. D. 2018. Plant-like bacterial expansins play contrasting roles in two tomato vascular pathogens. *Mol. Plant Pathol.* 19:1210–1221.
- Thapa, S. P., Davis, E. W., Lyu, Q., Weisberg, A. J., Stevens, D. M., Clarke, C. R., Coaker, G., and Chang, J. H. 2019. The evolution, ecology, and mechanisms of infection by Gram-positive, plant-associated bacteria. *Annu. Rev. Phytopathol.* 57:341-365.
- Thapa, S. P., Pattathil, S., Hahn, M. G., Jacques, M.-A., Gilbertson, R. L., and Coaker, G. 2017. Genomic analysis of *Clavibacter michiganensis* reveals insight into virulence strategies and genetic diversity of a Gram-positive bacterial pathogen. *Mol. Plant Microbe Interact.* 30:786–802.

Tovar-Herrera, O. E., Rodríguez, M., Olarte-Lozano, M., Sampedro-Guerrero, J. A., Guerrero, A., Pinto-Cámara, R., Alvarado-Affantranger, X., Wood, C. D., Moran-Mirabal, J. M., Pastor, N., Segovia, L., and Martínez-Anaya, C. 2018. Analysis of the binding of expansin Ex11, from *Pectobacterium carotovorum*, to plant xylem and comparison to EXLX1 from *Bacillus subtilis*. *ACS Omega*. 3:7008–7018.

Tran, T. M., MacIntyre, A., Hawes, M., and Allen, C. 2016. Escaping underground nets: extracellular DNases degrade plant extracellular traps and contribute to virulence of the plant pathogenic bacterium *Ralstonia solanacearum*. *PLOS Pathog*. 12:e1005686.

Vulkova, Z. V. and Sotirova, V. G. 1993. Study of the three-genome hybrid *Lycopersicon esculentum* Mill. —*L. chilense* Dun. —*L. peruvianum* var ‘*humifusum*’ Mill. and its use as a source for resistance. *Theoret. Appl. Genet*. 87:337–342.

## CHAPTER 2

### **Tomato fruit development plays a critical role in susceptibility to three bacterial pathogens**

#### ***ABSTRACT***

Tomato (*Solanum lycopersicum*) fruit are fleshy climacteric fruit that are cultivated worldwide as a source of essential vitamins, nutrients, and flavors. To attain the ripe red stage that is popular for consumption, tomato fruit go through complex development and ripening processes. During development, fruit are susceptible to a variety of bacterial diseases. Among those that cause economically impacting diseases are the bacterial canker pathogen *Clavibacter michiganensis*, bacterial speck pathogen *Pseudomonas syringae* pv. tomato, and bacterial spot pathogen *Xanthomonas gardneri*. Previous studies have described a decrease in symptom severity as fruit mature, but the exact stages where fruit are most susceptible and cease to be susceptible are unknown. Our objective was to describe patterns of susceptibility of tomato fruit to three bacterial pathogens. In many species, fruit ripening and development is in part governed by the plant hormone ethylene. Therefore, we used tomato mutants impaired in ripening, ethylene synthesis, and ethylene perception to understand how susceptibility to bacterial pathogen shifts according to fruit ethylene phenotypes. Overall, fruit in the Ailsa Craig background inoculated with these three pathogens exhibited a peak in disease severity at 0.5, 1 or 1.5cm diameter and ceased developing symptoms between 2.5-3.5cm diameters. Disease severity phenotypes differed by pathogen and tomato genotype. We confirmed that *Never ripe* plants had lower disease severity when inoculated with a New York isolate of *C. michiganensis*, and demonstrated that the *high pigment-1* mutant was hyper susceptible to *C. michiganensis* relative to wildtype Ailsa Craig.

## **INTRODUCTION**

Tomato (*Solanum lycopersicum*) is among the most widely grown vegetable crops worldwide with approximately 180 million tons produced across 4.8 million hectares in 2017 (FAO, 2020). Tomato fruit are a source of essential vitamins and nutrients such as carotenoids, potassium, vitamins A and C, and its flavors are a staple in diverse cuisines. High yields and ease of cultivation have made it a popular crop for both subsistence and commercial growers. However, both the plant and its fruit are susceptible to a variety of diseases, threatening food security and grower income. Bacterial pathogens of tomato reduce overall yield, and during severe epidemics can cause total loss of a field (Yunis et al. 1980; de León et al. 2011; Sen et al. 2014; Potnis et al. 2015). Some pathogens cause lesions on plant tissues and tomato fruit, affecting plant yield, rendering the fruit unmarketable and in some cases contaminating seed. Such economically devastating bacterial diseases that affect both plant and fruit are: bacterial canker caused by *Clavibacter michiganensis*, bacterial speck caused by *Pseudomonas syringae* pv. tomato, and bacterial spot caused by *Xanthomonas* species.

The bacterial canker pathogen *C. michiganensis* colonizes tomato vasculature through seed-borne infections or through mechanical inoculation (de Leon et al. 2011; Sen et al. 2014). The pathogen spreads systemically through the xylem leading to unilateral wilt, marginal leaf necrosis, stem cankers, internal colonization of seed and fruit tissue, and during severe infections plant death (de Leon et al. 2011; Sen et al. 2014). Splash dispersal of the pathogen onto the exterior of developing tomato fruit causes bird's-eye lesions characterized by a necrotic center surrounded by a white halo (Medina-Mora et al. 2001; de Leon et al. 2011; Tancos et al. 2013; Peritore-Galve et al. 2020). Furthermore, *C. michiganensis* can spread from the fruit exterior to interior tissues, colonizing tomato fruit xylem and developing seed, thus perpetuating future

epidemics (Tancos et al. 2013).

The bacterial speck pathogen *P. syringae* pv. tomato is often introduced through infected seed or transplants and can overwinter in plant debris and weeds (McCarter et al. 1983; Jones et al. 2014). Plant-to-plant spread occurs through wind-blown rain, which can lead to severe epidemics during cool, wet growing seasons (Yunis et al. 1980). This pathogen typically colonizes the leaf apoplast through natural openings or mechanical wounds, and is hypothesized to colonize fruit through natural openings exposed during trichome shedding (Getz et al. 1983a; Xin and He 2013). Typical symptoms appear as small necrotic lesions of leaflets, stems, sepals and fruit that affect plant health and reduce fruit yield and marketability (Roberts et al. 2019; Xin and He 2013).

Bacterial spot of tomato and pepper can be caused by four *Xanthomonas* species: *X. euvesicatoria*, *X. gardneri*, *X. perforans*, and *X. vesicatoria* (Jones et al. 2000; Timilsina et al. 2015). Geographic populations of xanthomonads causing bacterial spot shift dynamically, with *X. gardneri* recently emerging as a threat to tomato and pepper growers in the Northeast USA, perhaps due to its preference for cooler climates (Araújo et al. 2011; Ma et al. 2011; Timilsina et al. 2015). The pathogen is often introduced through infected seed and can persist in leaf litter and weeds, with outbreaks often occurring during humid and rainy growing seasons (Jones et al. 1986; Potnis et al. 2015). Bacteria can be spread within a field through wind-blown rain and mechanical wounding, where they colonize the leaf apoplast through stomates or wounds (McInnes et al. 1988; Potnis et al. 2015). Water soaked lesions that turn necrotic appear on leaves after infection with *X. gardneri*, and black necrotic lesions develop on fruit, affecting quality and yield (Potnis et al. 2015).

Previous greenhouse and field studies have reported that mature fruit develop less severe

symptoms or none at all during bacterial canker, spot and speck outbreaks (Gardner and Kendrick 1923; Bryan 1930; Yunis et al. 1980; Getz, et al. 1983b; Scott et al. 1989; Pohronezny et al. 1993; Tancos et al. 2013; Peritore-Galve et al. 2020). Disease incidence of bacterial spot on pepper fruit increased between 0 and 14 days post anthesis (dpa), then reduced to completely asymptomatic around 40 dpa (Scott et al. 1989). Bacterial speck disease severity peaked when fruit were between the open corolla stage and green fruit less than 3cm diameter, and no longer developed lesions at pink to red stages (Getz et al. 1983b). Moreover, a high percentage of fruit inoculated with *P. syringae* pv. tomato at the open corolla stage produced small deformed fruit that ripened prematurely (Getz et al. 1983b). Studies of *C. michiganensis* showed that developing fruit begin to exhibit symptoms when inoculated 5 dpa, and flowers inoculated with *C. michiganensis* typically abscise (Medina-Mora et al. 2001; Tancos et al. 2013; Peritore-Galve et al. 2020). Tomato fruit from both wild accessions and commercially available cultivars developed lesions until 15-20 dpa, regardless of the genetic background, fruit size, or morphology (Peritore-Galve et al. 2020). One hypothesis for the reduction and cessation of fruit symptom development to *P. syringae* pv. tomato is that the pathogen cannot colonize red mature fruit tissue because of the lower pH of the epidermis relative to that of green developing fruit (Yunis et al. 1980). Fruit ripening is a dynamic process that reshapes fruit cell content and cell wall structure; therefore, epidermal pH may not completely explain fruit susceptibility phenotypes.

Tomato fruit undergo a complex ripening process leading to changes in color, nutrient content, acidity, texture, and cell wall composition (Giovannoni et al. 2017). Changes that occur during ripening are coordinated by multiple factors including the diffusible plant hormone ethylene (Klee and Giovannoni 2011; Giovannoni et al. 2017). The genetics of tomato fruit

ripening have largely been understood through the study of tomato genotypes with mutations affecting key transcription factors in addition to ethylene synthesis, regulation, and perception (Klee and Giovannoni 2011; Giovannoni et al. 2017). Tools such as the Tomato Expression Atlas have incorporated spatiotemporal transcriptomics data to understand gene expression at the tissue level during ripening (Fernandez-Pozo et al. 2017). Despite advances in understanding the changes that occur during ripening and maturation, the factors involved in fruit susceptibility to pathogens during development remain unknown.

The goal of this study was to determine the relationship between fruit size and developmental stage at inoculation and susceptibility to bacterial pathogens using six tomato ripening, ethylene perception and ethylene synthesis mutants. Experiments were designed to test the hypothesis that tomato fruit developed more lesions on fruit at a younger developmental stage, and that this phenotype would change based on the mutant tested. Fruit were inoculated with New York isolates of *C. michiganensis*, *P. syringae* pv. tomato and *X. gardneri*, and symptoms were assessed. We also measured disease severity in foliar tissues of select mutant genotypes inoculated with *C. michiganensis*. This study provides novel information on fruit developmental stages in mutant and wildtype tomato genotypes where bacterial canker, speck and spot disease severity is at its peak, and stages where fruit are no longer susceptible. Current methods of controlling bacterial plant pathogens are limited to copper based products and biocontrol agents. Therefore, understanding the association between fruit development and symptom severity of bacterial disease can improve management practices (de Leon et al. 2011; Sen et al. 2014; Potnis et al. 2015).

**TABLE 2.1.** Pathogen strains and tomato genotypes used in this study

<b>Pathogen strain</b>	<b>Disease caused</b>	<b>Year collected in New York</b>	<b>Reference(s)</b>
<i>Clavibacter michiganensis</i> 0317	Bacterial canker	2003	Tancos et al., 2013; Tancos et al., 2018; Peritore-Galve et al., 2020
<i>Pseudomonas syringae</i> pv. tomato NYT1	Bacterial speck	2009	Jones et al., 2014; Kraus et al. 2017
<i>Xanthomonas gardneri</i> 16-156	Bacterial spot	2016	This study
<b>Tomato genotype</b>	<b>Mutation</b>	<b>Ethylene phenotype</b>	<b>Reference(s)</b>
Ailsa Craig (AC)	Wildtype background		
<i>Colorless nonripening (Cnr)</i>	Epimutation of SQUAMOSA promoter binding protein	Reduced ethylene synthesis and responsiveness related to ripening	Manning et al., 2006; Giovannoni, 2007
<i>Green ripe (Gr)</i>	Ectopic expression of an unknown protein that inhibits ripening	Fruit-specific ethylene insensitivity	Barry et al., 2005; Barry and Giovannoni, 2006
<i>high-pigment 1 (hp1)</i>	Loss of function of UV-DAMAGED DNA BINDING PROTEIN 1	Delayed and reduced ethylene synthesis	Kilambi et al., 2013; Wang et al., 2019
<i>nonripening (nor)</i>	Mutation in non-ripening control region	No ripening-associated ethylene synthesis	Giovannoni et al., 1995; Klee and Giovannoni, 2011; Wang et al., 2018
<i>Never ripe (Nr)</i>	Single amino acid change in NEVER RIPE ethylene receptor	Global ethylene insensitivity	Lanahan et al., 1994; Wilkinson et al., 1995
<i>ripening inhibitor (rin)</i>	Partial C-terminal deletion of MADS-box protein	Reduced ethylene synthesis and responsiveness related to ripening	Vrebalov et al., 2002; Giovannoni, 2007
Pearson	Wildtype background		
<i>Never ripe<sup>Pearson</sup> (Nr<sup>P</sup>)</i>	Single amino acid change in NEVER RIPE ethylene receptor	Global ethylene insensitivity	Lanahan et al., 1994

## **MATERIALS AND METHODS**

### **Fruit disease severity assays**

Seeds of wildtype tomato (*S. lycopersicum*) cultivars Ailsa Craig (AC) and Pearson, along with the mutant genotypes *Colorless nonripening* (*Cnr*), *Green ripe* (*Gr*), *high-pigment 1* (*hp1*), *nonripening* (*nor*), *Never ripe* (*Nr*), *ripening inhibitor* (*rin*), and *Never ripe*<sup>Pearson</sup> (*Nr*<sup>Pearson</sup>) were germinated on wet sterile Whatman filter paper (Fisher Scientific, Pittsburgh, PA) in petri dishes for 8-10 days (Table 2.1). Seedlings were transferred to a Farfard professional formula growing mix in 50-cell flats (Sun Gro Horticulture, Agawam, MA). When seedlings had three true leaves they were transferred to four-inch pots, then repotted again at the six-leaf stage in five-gallon pots supplemented with Osmocote slow release fertilizer (Scotts Miracle-Gro Co., Maryville, OH). Six plants per genotype were randomly arranged in an environmentally controlled greenhouse with a 16-hr light/8-hr dark photoperiod.

*Clavibacter michiganensis* 0317 and *Xanthomonas gardneri* 16-156 were cultured in liquid Lysogeny Broth (LB) medium for 18 hours shaking at 160RPM at 28°C (Bertani 1951; Lange et al. 2015; Tancos et al. 2015). *Pseudomonas syringae* pv. tomato NYT1 was cultured in liquid King's B (KB) medium for 18 hours shaking at 160RPM at 28°C (King et al., 1954; Jones et al. 2014; Kraus et al. 2017). Bacterial suspensions were adjusted to OD<sub>600</sub>=0.8 through centrifugation for 12 minutes at 4,000RPM, followed by washing the pellet with sterile water, then re-suspending in sterile water (Kraus et al. 2017; Tancos et al. 2018; Peritore-Galve et al. 2020).

To characterize wildtype and mutant fruit susceptibility at different developmental stages, fruit diameter was measured using digital calipers (Mitutoyo, Sakado, Japan) and mutant and wildtype fruit from AC and Pearson backgrounds with diameters ranging from 0.15-6.8cm were paintbrush inoculated with bacterial suspensions of *C. michiganensis*, *P. syringae* pv. tomato, and *X. gardneri* (Getz et al. 1983b; Medina-Mora et al. 2001; Tancos et al. 2013; Peritore-Galve et al. 2020). The entire surface of the fruit was gently painted with bacterial suspension using a No. 2 horsehair brush until completely covered. Fruit were harvested fifteen days post inoculation (dpi) where diameter, number of lesions, and phenotypic information was recorded. Fruit were classified as stunted if they were inoculated at diameters smaller than 1cm and grew less than 1cm in diameter after 15 days. Exact numbers of fruit inoculated with each pathogen can be found in Tables 2.2, 2.3 and 2.4, and the number of fruit analyzed are presented in Figs. 2.1 and 2.6.

Comparisons of fruit disease severity between mutant genotypes and the wildtype background were performed using two model types: a negative binomial generalized linear mixed-effects model designed to test overall disease severity between genotypes without accounting for size (GLMM1), and a more complex negative binomial generalized linear mixed-effects model that tests interactions between fruit diameter and disease severity (GLMM2). The GLMM1 models were used to test for overall differences in disease severity between mutant genotypes and the wildtype AC background, or between  $Nr^{Pearson}$  and its wildtype Pearson background. These GLMM1 models were generated using number of lesions per fruit as the response, with tomato genotype as the sole main effect. Random effect variables were included for plant replicate and the date when fruit were inoculated. Individual GLMM1s were generated and analyzed by pathogen, and by wildtype tomato background.

The experimental design was continuous for fruit diameter, and lesion count data from AC background fruit increased then decreased with size. Therefore, we generated GLMM2 models to test differences in symptom severity between AC and mutant genotypes based on fruit diameter at inoculation. Individual GLMM2 models were generated and analyzed by pathogen. These GLMM2 models contained number of lesions per fruit as the response. The main effects were: tomato genotype, the interaction between tomato genotype and fruit diameter at inoculation, and the interaction between tomato genotype and fruit diameter at inoculation squared. Fruit diameter at inoculation squared was included as a quadratic term to fit the bell shaped trend of disease severity. These GLMM2 models also included random effect variables for plant replicate and date when fruit were inoculated. Mean number of lesions per fruit and standard errors were derived from the GLMM2s and are presented unless stated otherwise. Differences in disease severity between and within genotypes for various diameters at inoculation were tested using Dunnett's and Tukey's post-hoc tests. Statistical modeling and analyses were performed in R v.3.6.2 using packages lme4, glmmTMB and emmeans, and graphs were generated using ggplot2 (Wickham 2009; Bates et al. 2015; Lenth 2016; Brooks et al. 2017).

### **Bacterial canker disease severity and *in planta* colonization density**

To assess bacterial canker disease severity of whole plants, AC, *hp1* and *Nr* seedlings with two true leaves were transferred to four-inch pots and supplemented with Osmocote slow release fertilizer. Tomato seedlings at the three-leaf stage (n=9 per genotype) were arranged in three randomized blocks with three replicates of each plant genotype per block. One water-inoculated plant per genotype was included in each block as a mock-inoculated control.

Plants were inoculated by submerging sterilized scissors into *C. michiganensis* bacterial

suspension ( $OD_{600}=0.8$ , prepared as described above) and clipping the cotyledons as previously described (Tancos et al. 2018; Peritore-Galve et al. 2020). Leaflet wilting and canker formation was recorded daily until 21 days post inoculation. Disease severity was quantified by dividing the number of leaflets wilting daily by the total number of leaflets present on the oldest five leaves at 21dpi (Balaji et al. 2008; Chalupowicz et al. 2011; Peritore-Galve et al. 2020). The mean area under the disease progress curve (AUDPC) was calculated from percent wilt measurements. Differences in AUDPC were assessed using a linear mixed effects model with AUDPC as the response, plant genotype as the main effect, and block as a random effect using packages lme4 and emmeans, in R. v.3.6.2 (Halekoh and Højsgaard 2014; Bates et al. 2015; Lenth 2016; Kuznetsova et al. 2017). Graphs were produced using package ggplot2 (Wickham 2009). Disease severity differences between genotypes were tested using ANOVA and Tukey's pairwise comparisons ( $P<0.05$ ). The experiment was performed twice.

*In planta* populations of *C. michiganensis* were determined by sectioning 0.5cm of stem tissue 1cm above the inoculation site from the same plants used for one replicate of disease severity assays at 21dpi ( $n=9$  per genotype). Stem tissues were weighed and homogenized in 1mL sterile water using a sterile 5mm stainless steel grinding bead (Qiagen, Valencia, CA) in a 2mL Eppendorf tube using a TissueLyser (Retsch, Newton, PA) at 30Hz for 4 minutes. One hundred microliters of the homogenate were transferred to a sterile 96-well falcon tissue culture plate (Corning Inc, Corning, NY) and ten microliters were serial diluted into ninety microliters sterile water for seven dilutions. Ten microliters of each dilution was spot inoculated onto D2ANX semi-selective medium four times and incubated for 2-3 days at 28°C. Colony forming units (CFUs) were counted at the dilution where there were between 20 and 200 CFUs, and the average of four technical replicates per biological replicate were  $\log_{10}$  transformed and used for

statistical analysis. A linear model was generated with  $\log_{10}$  CFU/g tissue as the response, and genotype, plant number and block as main effects. Differences in bacterial colonization density between plant genotypes were tested using ANOVA and Tukey's pairwise comparisons ( $P < 0.05$ ) using package emmeans in R v.3.6.2, and graphs were made using ggplot2 (Lenth 2016; Wickham 2009).

## **RESULTS**

### **Fruit disease severity assays**

#### ***Clavibacter michiganensis***

To determine the association between fruit size at inoculation and disease severity, AC, *Cnr*, *Gr*, *hp1*, *nor*, *Nr*, and *rin* fruit of different sizes were measured and paintbrush inoculated with *C. michiganensis* until the fruit were completely covered (Tables 2.1 and 2.2). Since the fruit size measurements were continuous, we categorized fruit by 0.5cm increments from 0 to 4cm to interpret symptom severity phenotypes. We observed that inoculating fruit at sizes smaller than 1cm diameter caused other disease related phenotypes such as stunting (less than 1cm growth in diameter after 15 days) and abscission. Inoculating fruit smaller than 0.5cm diameter caused fruit abscission that varied from 0 to 33 percent of fruit based on genotype. Abscission was not observed at sizes larger than 0.5cm diameter. Zero *hp1* and *Nr* fruit abscised, and the highest percentages of abscission were in AC (18%) and *rin* (33%) fruit (Table 2.2). The smallest fruit class, 0-0.5cm diameter, also had a high proportion of stunted fruit (35 to 93 percent based on genotype) that grew less than 1cm in diameter after inoculation (Table 2.2). Stunting was rarely observed in inoculated fruit greater than 1cm. Ailsa Craig and *nor* had the lowest percentage of stunted fruit (both 35 percent), and *Cnr* and *Gr* fruit had the highest percentage of stunting (93 and 88 percent of fruit, respectively) (Table 2.2).

The first analysis with GLMM1 compared genotype-level differences in fruit disease severity based on the number of lesions developed. Statistical analyses of data using this model captured some of the overall differences between genotypes without incorporating fruit size at inoculation (Fig. 2.2). Fruit from the genotype *nor* developed significantly fewer lesions relative to AC ( $P=0.035$ ) (Fig. 2.2).

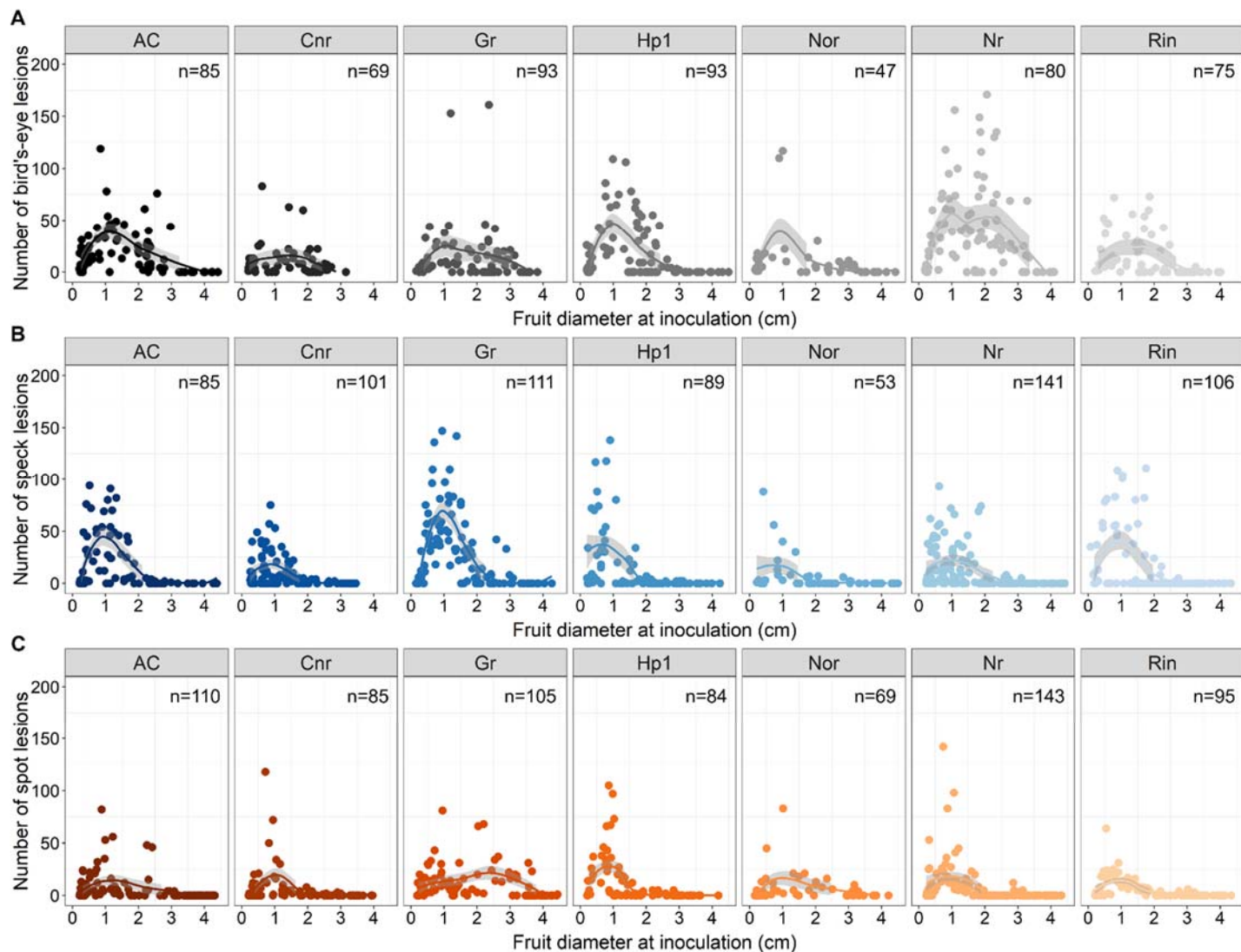


**FIGURE 2.1.** (A-C) Scatterplots depicting the number of *C. michiganensis* (A), *P. syringae* pv. tomato (B) and *X. gardneri* (C) lesions present on fruit harvested 15 days post inoculation. Plots are faceted by tomato genotype and the number of fruit assessed per pathogen per genotype is at the top right corner of each graph. Line and shaded area represent a locally estimated scatterplot smoothing curve to highlight disease severity trends.

**TABLE 2.2. Fruit inoculated with *Clavibacter michiganensis***

		AC	<i>Cnr</i>	<i>Gr</i>	<i>hp1</i>	<i>nor</i>	<i>Nr</i>	<i>rin</i>	Pearson	<i>Nr</i> <sup>Pearson</sup>
<b>Total fruit inoculated</b>		90	70	95	93	49	93	80	34	21
<b>0-0.5cm</b>	# fruit inoculated	28	19	26	15	19	13	15	7	-
	# fruit abscised	5	1	2	0	2	0	5	1	-
	% fruit abscised	18%	5%	8%	0%	11%	0%	33%	14%	-
	# fruit stunted	8/23	13/18	21/24	6/15	6/17	8/13	6/10	3/6	-
	% fruit stunted	35%	93%	88%	40%	35%	62%	60%	50%	-
	# fruit with lesions	21/23	17/18	22/24	7/15	17/17	10/13	10/10	6/6	-
	% fruit with lesions	91%	94%	92%	47%	100%	77%	100%	100%	-
<b>0.5-1cm</b>	# fruit inoculated	11	9	10	13	2	12	14	-	-
	# fruit stunted	1/11	4/9	6/13	1/13	0/2	1/12	6/14	-	-
	% fruit stunted	9%	44%	46%	8%	0%	8%	43%	-	-
	# fruit with lesions	11/11	6/9	10/10	13/13	2/2	12/12	13/14	-	-
	% fruit with lesions	100%	67%	100%	100%	100%	100%	93%	-	-
<b>1-1.5cm</b>	# fruit inoculated	12	10	13	8	3	12	7	-	2
	# fruit with lesions	11/12	9/10	12/13	5/8	3/3	11/12	7/7	-	1/2
	% fruit with lesions	92%	90%	92%	62%	100%	92%	100%	-	50%
<b>1.5-2cm</b>	# fruit inoculated	5	8	7	19	4	19	14	6	7
	# fruit with lesions	5/5	8/8	3/7	12/19	2/4	14/19	9/14	6/6	6/7
	% fruit with lesions	100%	100%	43%	63%	50%	74%	64%	100%	86%

		<i>AC</i>	<i>Cnr</i>	<i>Gr</i>	<i>hp1</i>	<i>nor</i>	<i>Nr</i>	<i>rin</i>	<b>Pearson</b>	<i>Nr</i> <sup>Pearson</sup>
<b>2-2.5cm</b>	# fruit inoculated	16	14	15	17	5	18	7	1	6
	# fruit with lesions	15/16	7/14	9/15	8/17	4/5	17/18	5/7	1/1	3/6
	% fruit with lesions	94%	50%	60%	47%	80%	94%	71%	100%	50%
<b>2.5-3cm</b>	# fruit inoculated	6	9	14	7	4	6	10	2	1
	# fruit with lesions	5/6	9/9	11/14	5/7	3/4	6/6	0/10	1/2	0/1
	% fruit with lesions	83%	100%	79%	71%	75%	100%	0%	50%	0%
<b>3-3.5cm</b>	# fruit inoculated	4	1	6	4	6	7	9	4	-
	# fruit with lesions	0/4	0/1	3/6	0/4	4/6	4/7	1/9	4/4	-
	% fruit with lesions	0%	0%	50%	0%	67%	57%	11%	100%	-
<b>3.5-4cm</b>	# fruit inoculated	3	-	4	6	4	4	3	2	-
	# fruit with lesions	0/3	-	0/4	0/6	0/4	0/4	0/3	1/2	-
	% fruit with lesions	0%	-	0%	0%	0%	0%	0%	50%	0%
<b>4-4.5cm</b>	# fruit inoculated	5	-	-	4	2	2	1	1	1
	# fruit with lesions	0/5	-	-	0/4	0/2	0/2	0/1	0/1	0/1
	% fruit with lesions	0%	0%	0%	0%	0%	0%	0%	0%	0%
<b>4.5-5cm</b>	# fruit inoculated	-	-	-	-	-	-	-	3	-
	# fruit with lesions	-	-	-	-	-	-	-	0/3	-
	% fruit with lesions	-	-	-	-	-	-	-	0%	-

		<i>AC</i>	<i>Cnr</i>	<i>Gr</i>	<i>hpl</i>	<i>nor</i>	<i>Nr</i>	<i>rin</i>	<b>Pearson</b>	<i>Nr</i> <sup>Pearson</sup>
<b>5+cm</b>	# fruit inoculated	-	-	-	-	-	-	-	8	4
	# fruit with lesions	-	-	-	-	-	-	-	0/8	0/4
	% fruit with lesions	-	-	-	-	-	-	-	0%	0%

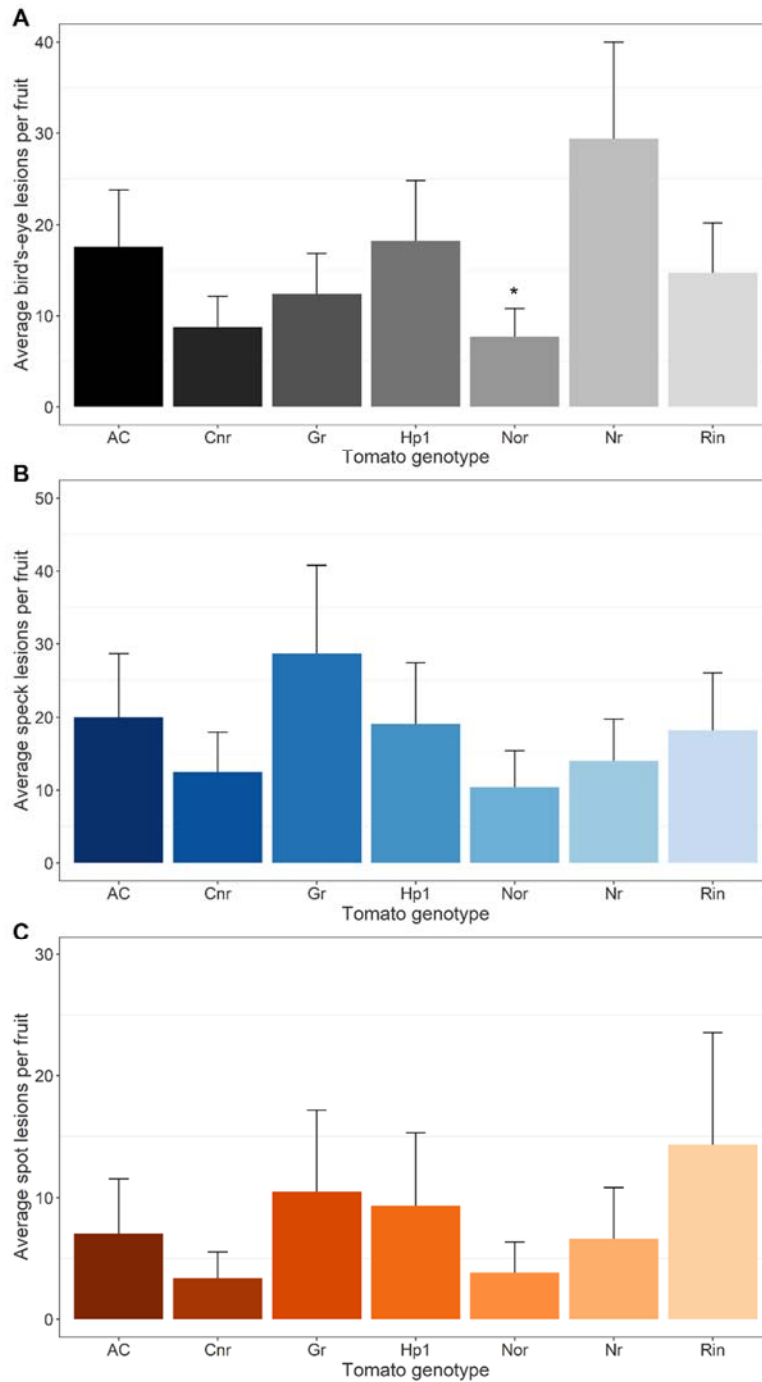


**FIGURE 2.2.** Average number of (A) *C. michiganensis*, (B) *P. syringae* pv. tomato, and (C) *X. gardneri* lesions per genotype as derived from GLMM1 models with genotype as the sole main effect. Error bars represent one standard error, also derived from the model, and asterisks denote significant differences between mutant genotypes and the wildtype AC background (\* $P < 0.05$ ) calculated using Dunnett's test.

To understand the effect of ethylene-related mutations on fruit disease severity, we evaluated differences in the number of bird's-eye lesions developed between genotypes on fruit inoculated from 0.5 to 4cm in diameter. There were significantly fewer lesions on inoculated 0.5 cm *Gr* fruit (9 lesions avg.,  $P=0.047$ ) relative to AC (18 lesions avg.) (Fig. 2.3). Although there were numerical differences between the number of lesions developed at peak disease severity (1.5cm diameter), there were no statistical differences between genotypes (Fig. 2.3). At peak disease severity, the highest number of lesions per fruit occurred on *Nr* (53 lesions per fruit;  $P=0.745$ ), and the lowest on *Cnr* (18 lesions per fruit;  $P=0.177$ ) relative to AC (39 lesions per fruit) (Fig. 2.3). Symptom severity continued to decrease as fruit size increased, and significant differences between genotypes were apparent on 2.5cm fruit, where *Nr* continued to have high disease severity (30 lesions per fruit,  $P=0.015$ ), and *Cnr* developed fewer symptoms (3 lesions avg.,  $P=0.003$ ) relative to AC (12 lesions avg.) (Figs. 2.3 and 2.5). Disease severity remained significantly higher in *Nr* fruit (13 lesions avg.,  $P=0.003$ ) inoculated at 3cm in diameter, whereas most other genotypes presented very few symptoms or none at all (Figs. 2.1, 2.3 and 2.5).

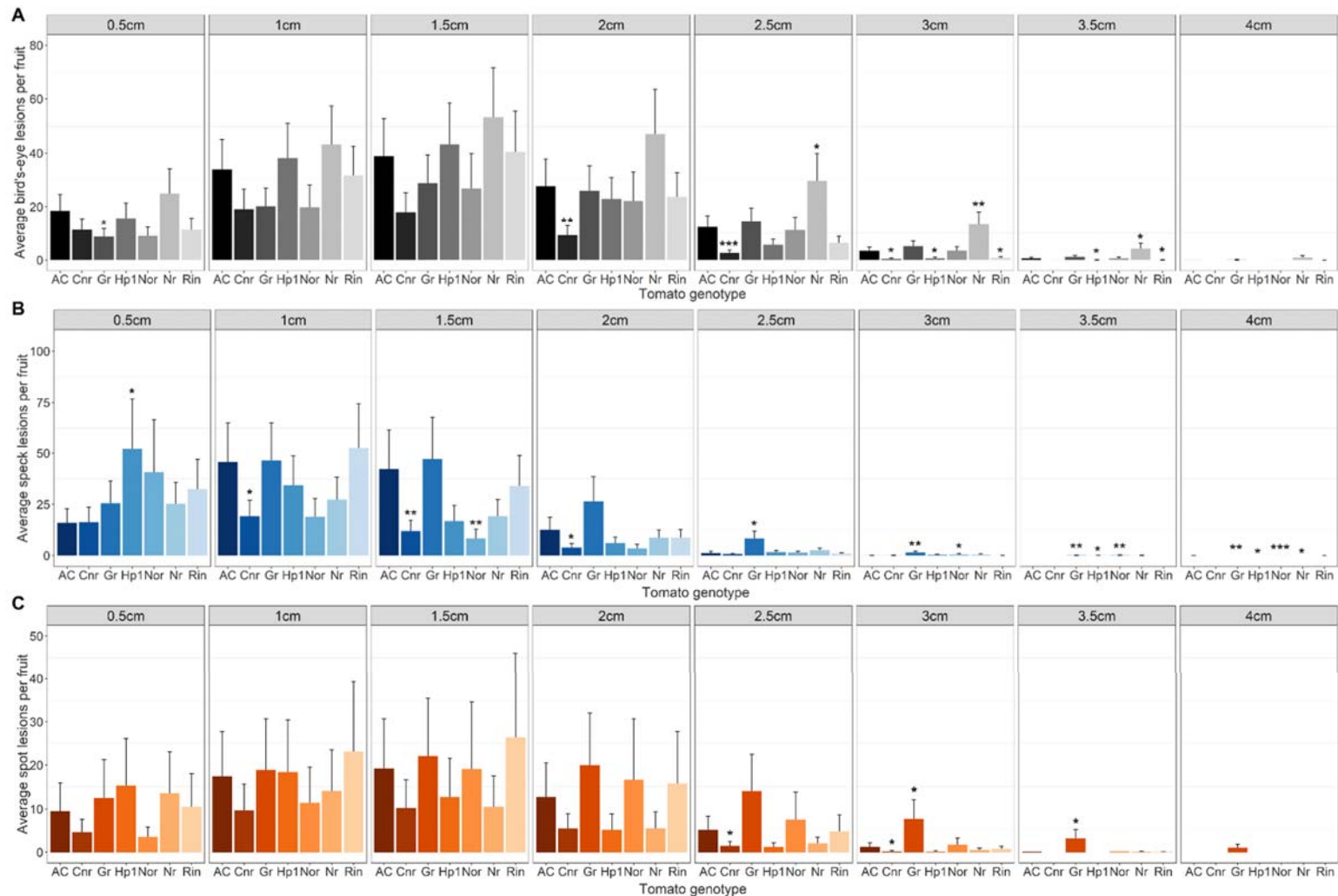


**FIGURE 2.3.** (A-C) Average lesions per fruit inoculated with *C. michiganensis* (A), *P. syringae* pv. tomato (B), and *X. gardneri* (C) at various diameters (cm) derived from GLMM2 statistical models. Bars denote one standard error and asterisks represent significant differences in the number of lesions developed when inoculated at specific diameters between mutant genotypes and the wildtype AC background (\* $P < 0.05$ , \*\* $P < 0.01$ , \*\*\* $P < 0.001$ ). Significant differences were calculated using Dunnett's test.

Disease severity data demonstrated that there was an interaction between the diameter at inoculation and the number of lesions developed (Fig. 2.1 and Fig. 2.4). The GLMM2 model was used to test effects of fruit diameter on disease severity within genotypes. Within genotypes there was a significant increase in the number of lesions developed between 0.5cm and 1cm in AC (18 to 34 lesions,  $P=0.03$ ), *Gr* (9 to 20 lesions,  $P=0.0001$ ), *hp1* (16 to 38 lesions,  $P=0.0001$ ), *nor* (9 to 20 lesions,  $P=0.021$ ), *Nr* (25 to 43 lesions,  $P=0.05$ ) and *rin* (11 to 32 lesions,  $P=0.0001$ ) (Figs. 2.1 and 2.4). The peak in symptom severity was observed on inoculated 1.5cm diameter fruit across all genotypes (Figs. 2.1 and 2.4). Number of lesions per fruit gradually decreased between 1.5 and 2cm in genotypes *Gr* (29 to 26 lesions,  $P=0.732$ ), *nor* (27 to 22 lesions,  $P=0.326$ ), and *Nr* (53 to 47 lesions,  $P=0.607$ ). Then decreased drastically in AC (39 to 28 lesions,  $P=0.0007$ ), *Cnr* (18 to 9 lesions,  $P=0.0001$ ), *hp1* (43 to 23 lesions,  $P<0.0001$ ), and *rin* (40 to 24 lesions,  $P<0.0001$ ) (Fig. 2.4). Fruit inoculated at diameters  $>2$ cm had fewer lesions overall, and the size of the lesions themselves were reduced relative those on smaller diameter fruit (Figs 2.4 and 2.5). Disease severity continued to decrease as fruit diameter increased, until bird's-eye lesions no longer developed on fruit between 3 to 3.5cm (Figs 2.1 and 2.4).

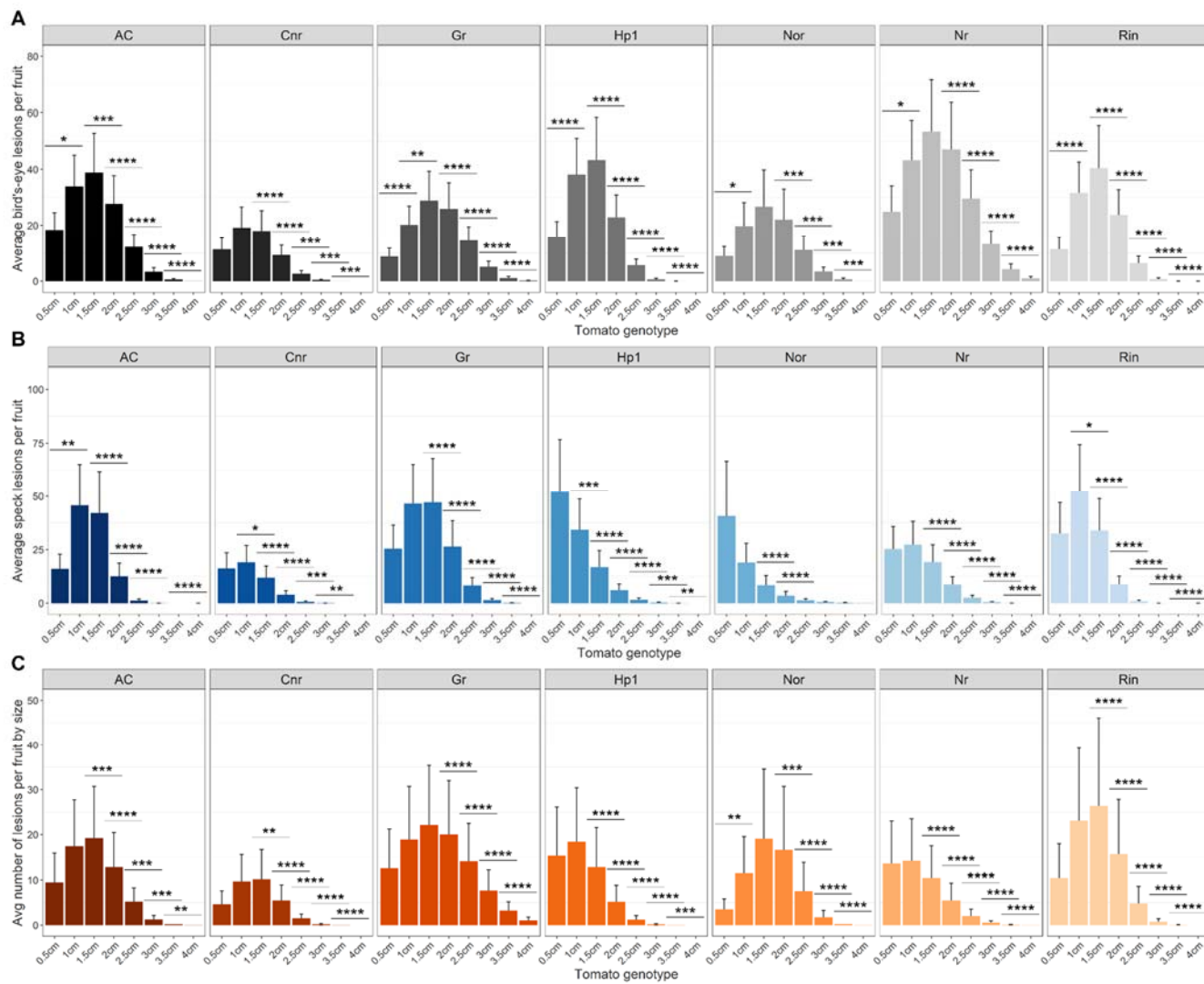


**FIGURE 2.4.** Model based mean number of (A) *C. michiganensis*, (B) *P. syringae* pv. tomato, and (C) *X. gardneri* lesions developed on fruit inoculated at different diameters calculated using GLMM2 models. Error bars denote one standard error and asterisks (\* $P < 0.05$ , \*\* $P < 0.01$ , \*\*\* $P < 0.001$ , \*\*\*\* $P < 0.0001$ ) represent significant differences in the number of lesions between different sized fruit within a genotype calculated using Tukey's pairwise comparison.

The experiment was concurrently performed with *S. lycopersicum* cv. ‘Pearson’ and  $Nr^{\text{Pearson}}$  since the *Nr* mutation has been shown to be more effective at blocking ripening in the Pearson background. These two genotypes had a smaller sample size due to lower fruit set, making it a better fit for the GLMM1 model that used genotype as the sole main effect. Overall, there was no significant difference ( $P=0.976$ ) in the average number of lesions per fruit between Pearson and  $Nr^{\text{Pearson}}$  (Fig. 2.6). The trend of increasing then decreasing disease severity based on fruit diameter was observed, with the disease severity peak at fruit inoculated at 3cm for Pearson, and 2cm for  $Nr^{\text{Pearson}}$  (Fig. 2.6). Pearson ceased developing lesions in fruit inoculated at 4cm diameter, and  $Nr^{\text{Pearson}}$  ceased at 2.5cm diameter (Fig. 2.6). These fruit diameter trends for peak disease severity and cessation of bird’s-eye lesion development were different from those observed in AC background fruit.



**FIGURE 2.5.** Individual fruit inoculated with *C. michiganensis* at various sizes between 0.6 and 2.8cm from wildtype genotype AC (top row), less susceptible *Cnr* (middle row), and more susceptible *Nr* (bottom row). White bars represent 1cm diameter.

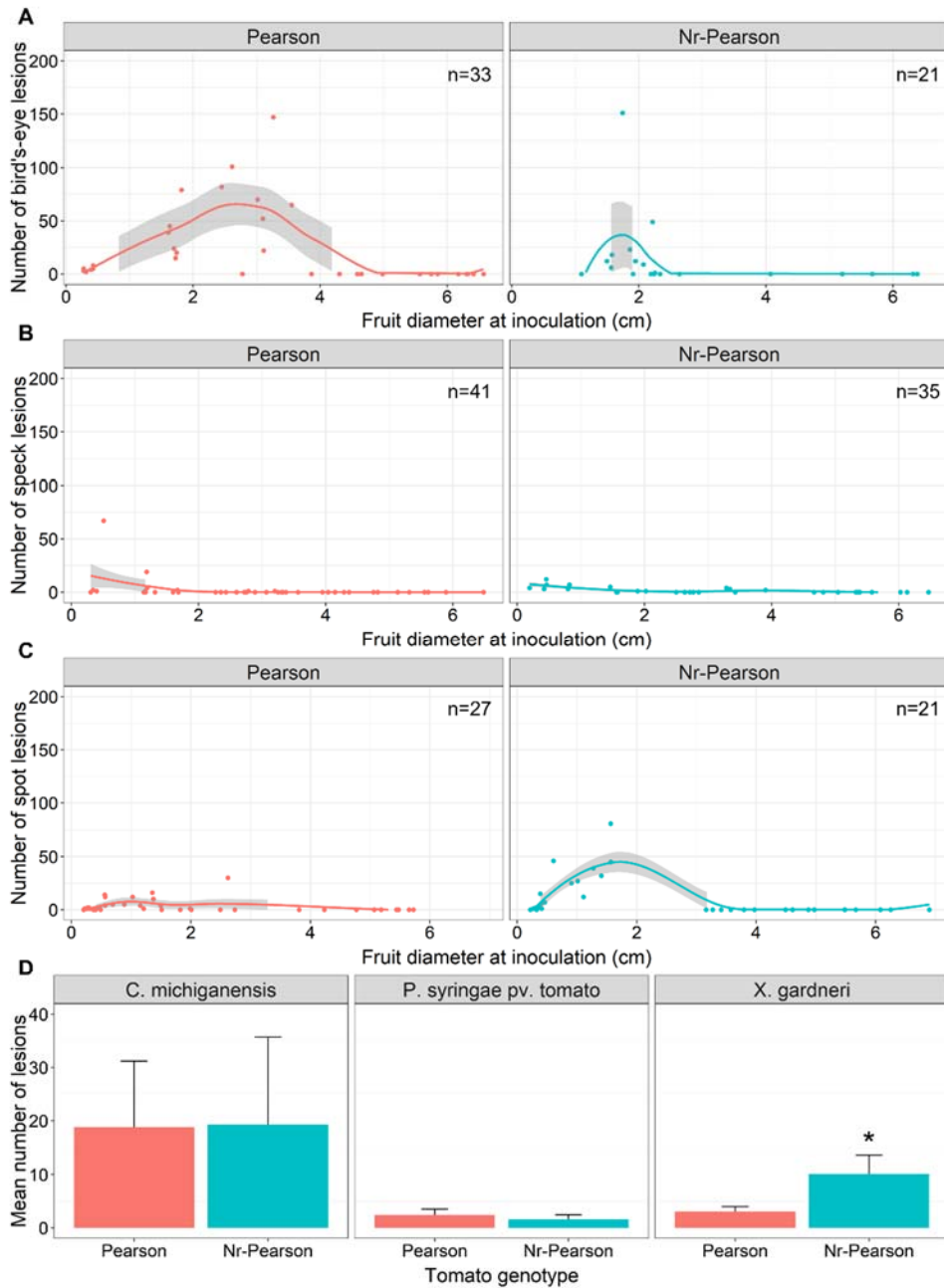


**FIGURE 2.6.** (A-C) Scatterplots depicting the number of *C. michiganensis* (A), *P. syringae* pv. tomato (B) and *X. gardneri* (C) lesions per fruit when harvested 15 days post inoculation by the fruit diameter (cm) when inoculated. Plots are faceted by Pearson and Nr in the Pearson background. Line and shaded area represent a locally estimated scatterplot smoothing (LOESS) curve. The number of fruit assessed per pathogen per genotype is in the top right of each plot.

(D) Bar plots comparing the model-derived mean number of fruit lesions between Pearson and  $Nr^{Pearson}$  for *C. michiganensis* (Cm), *P. syringae* pv. tomato (Pst), and *X. gardneri* (Xg) derived from GLMM1 models. Bars represent one standard error. Asterisk denotes significant differences ( $*P<0.05$ ) between the mutant and wildtype background calculated using Dunnett's test

### ***Pseudomonas syringae* pv. tomato**

The relationship between fruit size and bacterial speck symptom severity was tested in different sized AC, *Cnr*, *Gr*, *hp1*, *nor*, *Nr*, and *rin* fruit (Tables 2.1 and 2.3). Fruit were classified by 0.5cm increments from 0 to 4cm to determine disease severity phenotypes. Abscission and stunting occurred in inoculated smaller fruit classes. Variable percentages ranging from 0 to 50 percent of inoculated 0-0.5cm fruit abscised based on genotype (Table 2.3). Fruit from AC, *Cnr*, *Gr*, and *Nr* genotypes between 0-0.5cm diameter at inoculation had low rates of abscission (4, 0, 8 and 4 percent, respectively), while *hp1*, *nor*, and *rin* fruit had higher percentages of abscised fruit (33, 50, and 29 percent, respectively) (Table 2.3). Fruit <0.5cm that did not abscise exhibited high rates of stunting by genotype, ranging from 30 to 73 percent (Table 2.3). The genotype *hp1* had the lowest percentage of stunting (30%), while *Cnr* and *nor* had the highest percentages (73 and 71 percent fruit stunted, respectively) (Table 2.3).

**TABLE 2.3. Fruit inoculated with *Pseudomonas syringae* pv. tomato**

		AC	<i>Cnr</i>	<i>Gr</i>	<i>hpI</i>	<i>nor</i>	<i>Nr</i>	<i>rin</i>	Pearson	<i>Nr</i> <sup>Pearson</sup>
<b>Total fruit inoculated</b>		86	101	113	94	60	142	112	45	33
<b>0-0.5cm</b>	# fruit inoculated	25	15	26	15	14	26	21	7	4
	# fruit abscised	1	0	2	5	7	1	6	4	0
	% fruit abscised	4%	0%	8%	33%	50%	4%	29%	57%	0%
	# fruit stunted	16/24	11/15	16/24	3/10	5/7	12/25	10/15	3/3	3/4
	% fruit stunted	67%	73%	67%	30%	71%	48%	67%	100%	75%
	# fruit with lesions	15/24	12/15	17/24	8/10	4/7	21/25	13/15	2/3	4/4
	% fruit with lesions	63%	80%	71%	80%	57%	84%	87%	67%	100%
<b>0.5-1cm</b>	# fruit inoculated	11	27	22	16	4	25	11	1	2
	# fruit stunted	1/11	10/27	1/22	2/16	0/4	3/25	3/11	0/1	0/2
	% fruit stunted	9%	37%	5%	13%	0%	12%	27%	0%	0%
	# fruit with lesions	11/11	17/27	22/22	15/16	4/4	23/25	8/11	1/1	2/2
	% fruit with lesions	100%	63%	100%	94%	100%	92%	73%	100%	100%
<b>1-1.5cm</b>	# fruit inoculated	15	17	15	10	5	22	12	6	1
	# fruit with lesions	13/15	14/17	15/15	6/10	4/5	18/22	7/12	3/6	1/1
	% fruit with lesions	87%	82%	100%	60%	80%	82%	58%	50%	100%
<b>1.5-2cm</b>	# fruit inoculated	11	15	19	9	7	13	18	3	3
	# fruit with lesions	10/11	10/15	16/19	6/9	2/7	8/13	6/18	1/3	1/3
	% fruit with lesions	91%	67%	84%	67%	29%	62%	33%	33%	33%

		<i>AC</i>	<i>Cnr</i>	<i>Gr</i>	<i>hp1</i>	<i>nor</i>	<i>Nr</i>	<i>rin</i>	<i>Pearson</i>	<i>Nr</i> <sup>Pearson</sup>
<b>2-2.5cm</b>	# fruit inoculated	7	5	11	15	6	13	10	3	1
	# fruit with lesions	2/7	3/5	5/11	7/15	1/6	4/13	3/10	0/3	1/1
	% fruit with lesions	29%	60%	45%	47%	17%	31%	30%	0%	100%
<b>2.5-3cm</b>	# fruit inoculated	8	8	6	7	5	15	17	5	6
	# fruit with lesions	4/8	3/8	3/6	2/7	1/5	5/15	2/17	1/5	0/6
	% fruit with lesions	50%	38%	50%	29%	20%	33%	12%	20%	0%
<b>3-3.5cm</b>	# fruit inoculated	2	14	6	9	5	9	16	6	3
	# fruit with lesions	0/2	0/14	1/6	3/9	3/5	1/9	0/16	1/6	2/3
	% fruit with lesions	0%	0%	17%	33%	60%	11%	0%	17%	67%
<b>3.5-4cm</b>	# fruit inoculated	4	-	5	8	6	8	4	2	1
	# fruit with lesions	0/4	-	0/5	0/8	0/6	0/8	0/4	0/2	1/1
	% fruit with lesions	0%	-	0%	0%	0%	0%	0%	0%	100%
<b>4-4.5cm</b>	# fruit inoculated	2	-	2	1	4	9	3	4	-
	# fruit with lesions	0/2	-	0/2	0/1	0/4	0/9	0/3	0/4	-
	% fruit with lesions	0%	-	0%	0%	0%	0%	0%	0%	-
<b>4.5-5cm</b>	# fruit inoculated	1	-	-	4	2	2	-	2	2
	# fruit with lesions	0/1	-	-	0/4	0/2	0/2	-	0/2	0/2
	% fruit with lesions	0%	-	-	0%	0%	0%	-	0%	0%

		<i>AC</i>	<i>Cnr</i>	<i>Gr</i>	<i>hpl</i>	<i>nor</i>	<i>Nr</i>	<i>rin</i>	<b>Pearson</b>	<i>Nr</i> <sup>Pearson</sup>
<b>5+cm</b>	# fruit inoculated	-	-	1	-	2	-	-	6	10
	# fruit with lesions	-	-	0/1	-	0/2	-	-	0/6	0/10
	% fruit with lesions	-	-	0%	-	0%	-	-	0%	0%

The GLMM1 model that compared genotype-level differences in fruit disease severity identified no overall differences in disease severity ( $P < 0.05$ ) between mutant genotypes and the wildtype AC background (Fig. 2.2). Differences in disease severity between genotypes at various sizes were assessed using a GLMM2 model. At 0.5cm – the peak symptom severity for genotypes *hp1* and *nor* – significantly more lesions developed on *hp1* tomatoes (52 lesions avg.,  $P = 0.015$ ) compared to AC fruit (16 lesions avg.) (Fig. 2.3). At 1cm – the peak symptom severity size for genotypes AC, *Cnr*, *Gr*, *Nr*, and *rin* – there were significantly fewer lesions on *Cnr* fruit (19 lesions avg.,  $P = 0.022$ ) relative to AC (46 lesions avg.) (Fig. 2.3). Inoculated fruit from genotypes *Cnr* and *nor* developed significantly fewer lesions relative to AC (42 lesions avg.) at 1.5cm (*Cnr* 12 lesions avg.,  $P = 0.007$ ; *nor* 8 lesions avg.,  $P = 0.006$ ) (Fig. 2.3). At 2.5cm the only remaining susceptible genotype was *Gr*. On average, *Gr* developed eight speck lesions in comparison to one average lesion per fruit in AC ( $P = 0.003$ ) (Fig. 2.3).

The GLMM2 model was also used to assess differences in symptom severity between diameters within a tomato genotype (Fig. 2.4). The peak in bacterial speck disease severity occurred in fruit inoculated at either 0.5 or 1cm depending on genotype (Figs. 2.1 and 2.4). Symptom severity increased from 0.5 to 1cm in AC fruit (16 to 46 lesions avg.,  $P = 0.002$ ), and peaked at 1cm diameter in AC, *Cnr*, *Gr*, *Nr*, and *rin* (Fig. 2.4). Disease severity peaked at 0.5cm in *hp1*, and *nor*, and began to decrease at 1cm (Fig. 2.4). Fruit that peaked in disease severity at 0.5cm had significant reductions in the number of lesions developed between 1 and 1.5cm (*hp1* 34 to 17 lesions avg.,  $P = 0.0003$ ; *nor* 22 to 8 lesions avg.,  $P = 0.025$ ) (Fig. 2.4). Fruit from all genotypes experienced significant reduction in disease severity from 1.5cm to 2cm (Figs. 2.1 and 2.4). Raw data and model-based means demonstrated that zero to three lesions developed on fruit from all genotypes when inoculated at 2.5cm diameter or larger (Fig. 2.1 and 2.4). There was one

genotype that was an exception. *Green ripe*, the genotype with the highest disease severity, continued to develop lesions until fruit were 3cm in diameter (Figs. 2.1, 2.4, and 2.7).

The *P. syringae* pv. tomato inoculations were also performed on genotypes Pearson and *Nr<sup>Pearson</sup>*, and was subject to the same low sample size as in the Pearson-*C. michiganensis* experiment (Table 2.3). Differences in overall symptom severity between genotypes were calculated using a GLMM1 model. There was no significant difference in overall symptom severity between mutant and wildtype ( $P=0.564$ ) (Fig. 2.6). In fact, Pearson and *Nr<sup>Pearson</sup>* fruit were not very susceptible to the NYT1 isolate of *P. syringae* pv. tomato used in this study. The overall model-derived mean number per fruit was two for both Pearson and *Nr<sup>Pearson</sup>* (Table 2.3 and Fig. 2.6).



**FIGURE 2.7.** Individual fruit inoculated *P. syringae* pv. tomato at various sizes between 0.19 and 2.58cm from wildtype genotype AC (top row), less susceptible *Cnr* (middle row), and more susceptible *Gr* (bottom row). White bars represent 1cm diameter.

### *Xanthomonas gardneri*

The effect of fruit size on bacterial spot disease severity was tested in AC, *Cnr*, *Gr*, *hp1*, *nor*, *Nr*, and *rin* fruit. Fruit were again classified by 0.5cm increments from 0 to 4cm to determine disease severity phenotypes. Similar to the previous two pathogens, abscission and stunting were also observed in smaller fruit. Lower rates (0 to 26 percent) of inoculated fruit abscising at this early stage in development were observed in comparison to the previous two pathogens (Table 2.4). No inoculated *Cnr* or *Gr* fruit between 0-0.5cm abscised, and *nor* fruit had the highest rate of abscission at 26% (Table 2.4). Despite the relatively low abscission rates, 42 to 80 percent of fruit across genotypes inoculated between 0-0.5cm stunted (Table 2.4). The genotype *hp1* had the lowest percentage of stunted fruit (42%), and *Cnr* the highest at 80% (Table 2.4).

**TABLE 2.4. Fruit inoculated with *Xanthomonas gardneri***

		<i>AC</i>	<i>Cnr</i>	<i>Gr</i>	<i>hpl</i>	<i>nor</i>	<i>Nr</i>	<i>rin</i>	<i>Pearson</i>	<i>Nr</i> <sup>Pearson</sup>
<b>Total fruit inoculated</b>		112	85	105	87	81	144	97	27	21
<b>0-0.5cm</b>	# fruit inoculated	35	30	23	15	47	21	17	18	10
	# fruit abscised	2	0	0	3	12	1	2	0	0
	% fruit abscised	6%	0%	0%	20%	26%	5%	12%	0%	0%
	# fruit stunted	24/33	24/30	15/23	5/12	24/35	12/20	9/15	9/18	6/10
	% fruit stunted	73%	80%	65%	42%	69%	60%	60%	50%	60%
	# fruit with lesions	21/33	12/30	18/23	10/12	10/35	10/20	7/15	13/18	8/10
	% fruit with lesions	64%	40%	78%	83%	29%	50%	47%	72%	80%
<b>0.5-1cm</b>	# fruit inoculated	16	14	15	15	6	13	15	5	2
	# fruit stunted	2/16	7/14	2/15	0/15	0/6	1/13	1/15	0/5	0/2
	% fruit stunted	13%	50%	13%	0%	0%	8%	7%	0%	0%
	# fruit with lesions	15/16	10/14	15/15	15/15	5/6	13/13	15/15	5/5	2/2
	% fruit with lesions	94%	71%	100%	100%	83%	100%	100%	100%	100%
<b>1-1.5cm</b>	# fruit inoculated	11	10	12	14	8	21	17	6	4
	# fruit with lesions	10/11	9/10	10/12	10/14	6/8	21/21	17/17	6/6	4/4
	% fruit with lesions	91%	90%	83%	71%	75%	100%	100%	100%	100%
<b>1.5-2cm</b>	# fruit inoculated	6	5	6	10	3	15	8	3	2
	# fruit with lesions	3/6	3/5	5/6	5/10	2/3	11/15	7/8	1/3	2/2
	% fruit with lesions	50%	60%	83%	50%	67%	73%	88%	33%	100%

		<i>AC</i>	<i>Cnr</i>	<i>Gr</i>	<i>hpl</i>	<i>nor</i>	<i>Nr</i>	<i>rin</i>	<i>Pearson</i>	<i>Nr</i> <sup>Pearson</sup>
<b>2-2.5cm</b>	# fruit inoculated	7	6	6	5	4	10	10	2	-
	# fruit with lesions	5/7	3/6	6/6	4/5	4/4	0/10	4/10	0/2	-
	% fruit with lesions	71%	50%	100%	80%	100%	0%	40%	0%	-
<b>2.5-3cm</b>	# fruit inoculated	4	12	5	14	3	15	5	2	-
	# fruit with lesions	2/4	7/12	5/5	3/14	1/3	2/15	1/5	1/2	-
	% fruit with lesions	50%	58%	100%	21%	33%	13%	20%	50%	-
<b>3-3.5cm</b>	# fruit inoculated	10	8	7	10	7	15	14	-	3
	# fruit with lesions	3/10	0/8	4/7	0/10	4/7	3/15	4/14	-	0/3
	% fruit with lesions	30%	0%	57%	0%	57%	20%	29%	-	0%
<b>3.5-4cm</b>	# fruit inoculated	14	8	17	3	2	22	7	1	3
	# fruit with lesions	0/14	0/8	4/17	0/3	0/2	0/22	0/7	0/1	0/3
	% fruit with lesions	0%	0%	24%	0%	0%	0%	0%	0%	0%
<b>4-4.5cm</b>	# fruit inoculated	9	-	7	1	1	12	4	1	1
	# fruit with lesions	0/9	-	1/7	0/1	0/1	0/12	0/4	0/1	0/1
	% fruit with lesions	0%	-	14%	0%	0%	0%	0%	0%	0%
<b>4.5-5cm</b>	# fruit inoculated	-	-	7	-	-	-	-	1	3
	# fruit with lesions	-	-	0/7	-	-	-	-	0/1	0/3
	% fruit with lesions	-	-	0	-	-	-	-	0%	0%

		<i>AC</i>	<i>Cnr</i>	<i>Gr</i>	<i>hpl</i>	<i>nor</i>	<i>Nr</i>	<i>rin</i>	Pearson	$Nr^{\text{Pearson}}$
<b>5+cm</b>	# fruit inoculated	-	-	-	-	-	-	-	6	6
	# fruit with lesions	-	-	-	-	-	-	-	0/6	0/6
	% fruit with lesions	-	-	-	-	-	-	-	0%	0%

There were no significant differences ( $P < 0.05$ ) in genotype-level *X. gardneri* disease severity between mutants and the AC background when analyzed using the GLMM1 model (Fig. 2.2). Therefore, disease severity between genotypes at various sizes was tested using GLMM2. Although there were numerical differences in the number of spot lesions between mutant genotypes and the AC background, there were no significant differences in fruit inoculated at 0.5, 1, 1.5, and 2cm diameters (Fig. 2.3). At 2.5cm, *Cnr* fruit developed significantly fewer lesions (1 lesion avg.,  $P = 0.031$ ) compared to AC (5 lesions avg.), and maintained lower symptom severity until AC ceased developing lesions at 3.5cm (Fig. 2.3). *Green ripe* fruit inoculated at 3cm and 3.5cm diameters developed significantly more lesions than AC (3cm: *Gr* 8, AC 1 lesion(s) avg.,  $P = 0.013$ ) (3.5cm: *Gr* 3, AC 0 lesions avg.,  $P = 0.029$ ). *Green ripe* fruit continued developing lesions at larger sizes compared to other genotypes (Figs. 2.1 and 2.3).

The GLMM2 model was used to investigate interactions between sizes within a genotype (Fig. 2.4). There was a significant increase in the average number of lesions between 0.5 and 1cm in the genotype *nor* (3 to 11 lesions avg.,  $P = 0.003$ ) (Fig. 2.4). The highest number of lesions were developed on 1cm diameter fruit for genotypes *hpl* and *Nr*, and on 1.5cm fruit for AC, *Cnr*, *Gr*, *nor*, and *rin* (Figs. 2.1 and 2.4). After peak disease severity for *hpl* and *Nr* at 1cm, the number of lesions gradually decreased between 1 and 1.5cm (*hpl* 18 to 13 lesions avg.,

$P=0.365$ ; *Nr* 14 to 11 lesions avg.,  $P=0.294$ ) (Fig. 2.4). Then symptom severity significantly decreased between 1.5 and 2cm for those two genotypes (*hp1* 13 to 5 lesions avg.,  $P<0.0001$ ; *Nr* 11 to 5 lesions avg.,  $P<0.0001$ ) (Fig. 2.4). Peak disease severity for genotypes *AC*, *Cnr*, *Gr*, *nor*, and *rin* occurred at 1.5cm diameter (Fig. 2.4). Three of those genotypes (*AC*, *Cnr*, and *rin*) experienced significant reductions in susceptibility between 1.5 and 2cm (*AC* 19 to 13 lesions avg.,  $P=0.0004$ ; *Cnr* 10 to 5 lesions avg.,  $P=0.004$ ; *rin* 26 to 16 lesions avg.,  $P<0.0001$ ) (Fig. 2.4). The remaining two genotypes, *Gr* and *nor*, experienced gradual reductions in the number of lesions per fruit between 1.5 and 2cm (*Gr* 22 to 20 lesions avg.  $P=0.943$ ; *nor* 19 to 17 lesions avg.,  $P=0.900$ ), that then significantly reduced between 2 and 2.5cm (*Gr* 20 to 14 lesions avg.,  $P<0.0001$ ; *nor* 16 to 7 lesions avg.,  $P=0.0002$ ) (Fig. 2.4). Fruit from the *Gr* genotype continued to develop lesions up to 4cm in diameter (Figs. 2.1, 2.4, and 2.8).

The *X. gardneri* experiment was performed with Pearson and *Nr<sup>Pearson</sup>* genotypes. Smaller sample sizes of these tomato genotypes were obtained as with the previous two pathogens (Table 2.4). Genotype-level contrasts were calculated using a GLMM1 model with genotype as the sole main effect. Overall, *Nr<sup>Pearson</sup>* developed significantly more spot lesions relative to Pearson ( $P=0.014$ ). The model-derived average number of lesions on *Nr<sup>Pearson</sup>* was 10 lesions per fruit, and three lesions per fruit on Pearson (Fig. 2.6). The relationship of increasing and decreasing disease severity based on fruit size was not observed in Pearson fruit, but was present in *Nr<sup>Pearson</sup>*. Disease severity peaked in fruit inoculated between 1.5 and 2cm, and ceased developing symptoms at 3cm, which is similar to what was observed in *AC* fruit inoculated with *X. gardneri* (Fig. 2.6).



**FIGURE 2.8.** Individual fruit inoculated with *X. gardneri* at various sizes between 0.26 and 3.45cm from wildtype genotype AC (top row), less susceptible *Cnr* (middle row), and more susceptible *Gr* (bottom row). White bars represent 1cm diameter.

### **Bacterial canker disease severity and *in planta* colonization density**

Bacterial canker disease severity and bacterial colonization of two mutant genotypes was determined by inoculating seedlings of AC, *hp1*, and *Nr* with *C. michiganensis* and water as a control, then measuring leaflet wilt for 21 days. Overall, *hp1* plants developed more severe wilt symptoms relative to AC ( $P=0.0001$ ), and *Nr* plants exhibited significantly fewer symptoms ( $P=0.010$ ) (Fig. 2.9). Leaflet wilt appeared as early as five days post inoculation (dpi) in *hp1* plants, and were delayed to 7dpi in AC and 10dpi in *Nr* (Fig. 2.10). Wilt symptoms in *hp1* developed more rapidly than those in AC and *Nr*, rising from 0% (4dpi) to over 50% (10dpi) of leaflets wilted in all plants over the course of six days (Fig. 2.10). In contrast, AC plants did not pass the 50% wilt threshold until 16dpi, and the maximum average percent wilt for *Nr* plants was 41% (Fig. 2.10). At 17dpi, *hp1* plants were almost 100% wilted (Fig. 2.10). Since dense colonization of the vascular system is critical to infection, we quantified *C. michiganensis* populations 1cm above the inoculation site at 21dpi. Bacterial populations were similar ( $10^{10}$  CFU per 1g tissue) at 1cm above the inoculation site in all three genotypes. This suggests that bacterial populations reached saturation in tissues close to the inoculation site despite the difference in wilt symptoms (Fig. 2.9). None of the control plants developed symptoms or contained *C. michiganensis* when plated on semi-selective medium (data not shown).

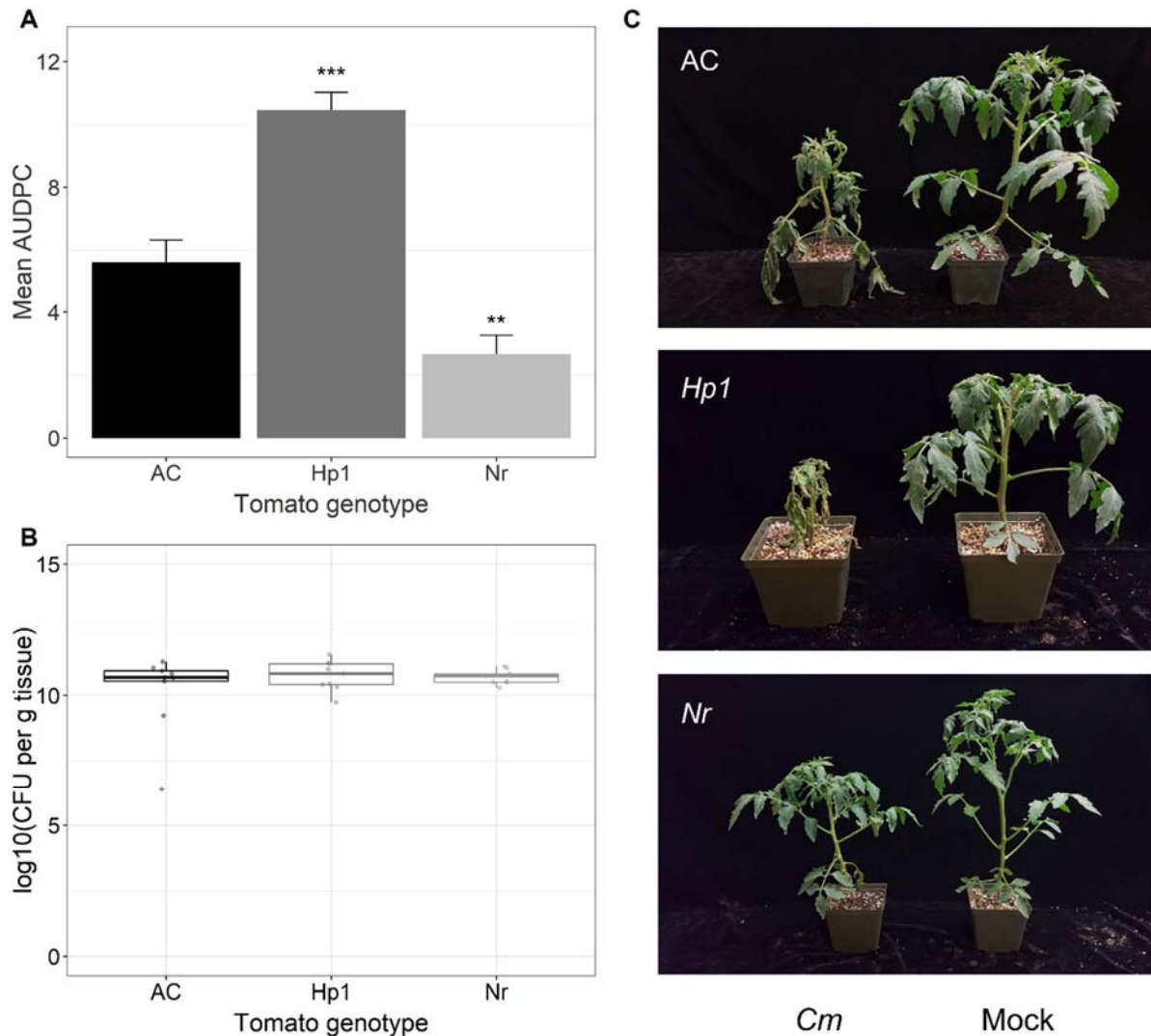


**FIGURE 2.9.** (A) Bacterial canker plant disease severity over time represented as mean area under the disease progress curve (AUDPC). Error bars represent the standard error of the mean (SEM). Both mean AUDPC and SEM were calculated directly from observational data. Asterisks denote significant differences (\*\*  $P < 0.01$ , \*\*\*  $P < 0.001$ ) relative to the wildtype (AC) calculated using Tukey's pairwise comparisons. (B) Colonization density of *C. michiganensis* 1cm above the inoculation site as log<sub>10</sub> colony forming units (CFU) per gram tissue. There were no significant differences in colonization between genotypes. (C) Representative *C. michiganensis* (Cm) and water-inoculated (mock) plants 21 days post inoculation.

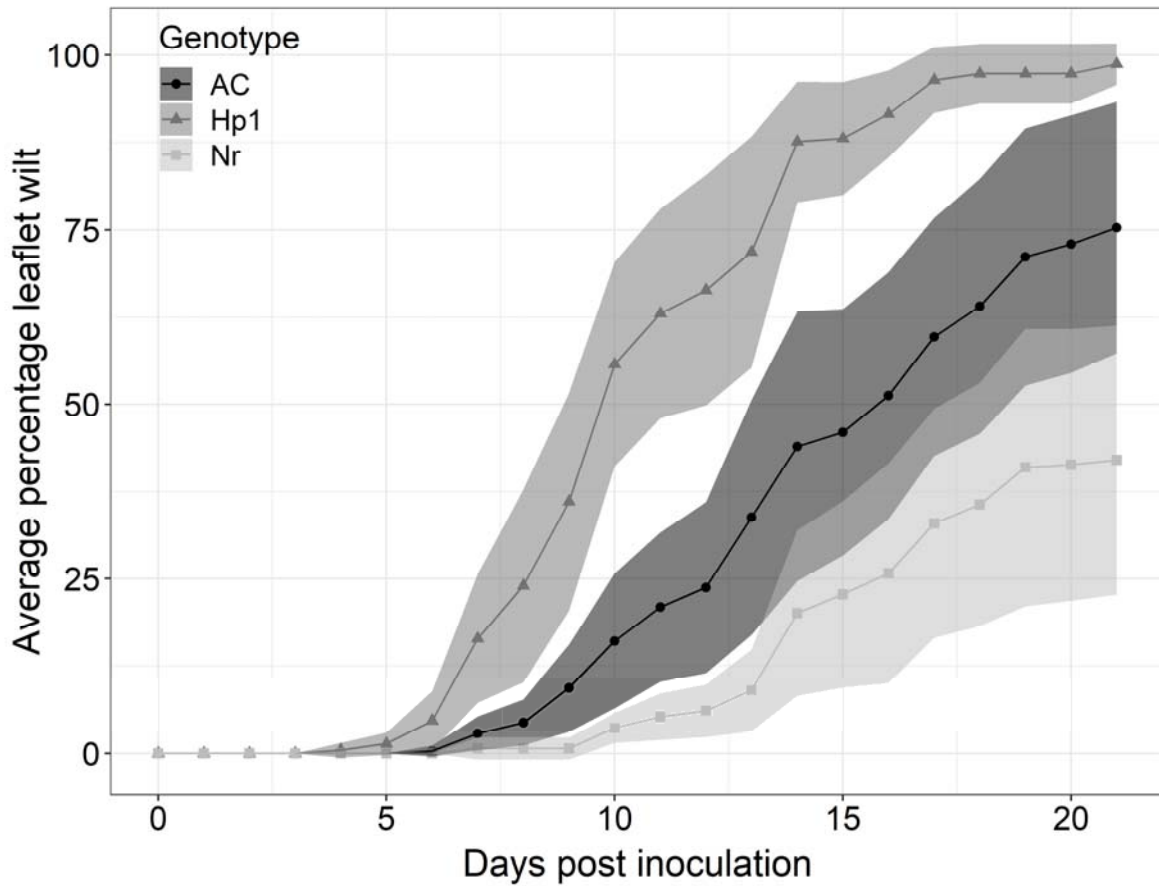


**FIGURE 2.10.** Average leaflet wilt over time in AC, *hp1*, and *Nr* plants inoculated with *C. michiganensis*. Leaflet wilt was calculated as the number of leaflets wilting on the first five leaves divided by the total number of leaflets on the first five leaves. Points indicate the average percentage wilt of nine plants at each time point, and the shaded regions correspond to the 95% confidence interval at each time point.

## ***DISCUSSION***

Bacterial pathogens of tomato continue to inflict significant crop damage and economic losses to growers worldwide. The pathogens *C. michiganensis*, *P. syringae* pv. tomato, and *X. gardneri* cause three destructive diseases and are able to cause symptoms on all aerial parts of the plant including tomato fruit. Previous studies demonstrated that tomato fruit are only susceptible to bacterial pathogens during a broad developmental window spanning approximately from the open corolla stage to mature green fruit around 3cm in diameter (Gardner and Kendrick 1923; Bryan 1930; Yunis et al. 1980; Getz et al. 1983b; Medina-Mora et al. 2001; Tancos et al. 2013; Peritore-Galve et al. 2020). Our goal was to delineate the relationship between fruit size and development at inoculation and the severity of symptoms developed, which would enable us to further identify factors involved in bacterial fruit infection. Ethylene plays an integral role in fruit development and ripening. Therefore, we characterized disease severity patterns in ripening, ethylene synthesis, and ethylene-responsive mutant and wildtype tomatoes, providing us with tools to improve our understanding on how ripening and development affect susceptibility to bacterial pathogens.

Inoculating pre-anthesis flowers with *C. michiganensis* or *P. syringae* pv. tomato typically causes flower abscission (Getz et al. 1983b; Medina-Mora et al. 2001). We inoculated fruit post-anthesis, but found that fruit smaller than 0.5cm exhibited variable rates of abscission when inoculated with bacterial pathogens. A high proportion of surviving 0-0.5cm fruit across genotypes and pathogens exhibited stunted and deformed phenotypes. High titers of bacteria may disrupt early fruit development processes, or abscission and stunting might be host-derived responses that can prevent further contamination and pathogen spread to seed.

Previous studies demonstrated that fruit were only susceptible to bacterial pathogens until

the mature green stage (Yunis et al. 1980; Getz et al. 1983b; Scott et al. 1989; Medina-Mora et al. 2001; Peritore-Galve et al. 2020). Disease severity patterns differed between genotypes when inoculated with each pathogen. Fruit inoculated with *C. michiganensis* and *X. gardneri* peaked in symptom severity at 1.5cm and ceased developing symptoms at 3cm. Peak disease severity of fruit inoculated with *P. syringae* pv. tomato was at 0.5 or 1cm depending on fruit genotype, with a cessation of symptom development at 2.5cm. Stages of peak symptom severity and cessation of lesion development occurred in ethylene synthesis and perception mutants, as well as in mutants impaired in ripening, suggesting that fruit developmental processes independent of ripening affect susceptibility to bacterial pathogens. The observed susceptibility patterns approximate cuticle deposition, which changes in both thickness and chemical composition during fruit development (Leide et al., 2007; Mintz-Oron et al., 2008; Leide et al., 2010).

Fruit undergo complex modifications during early development including cell division, cell structural modifications, and changes in chemical composition (Fishman et al. 2002; Bertin et al. 2003; Bargel and Neinhuis 2005; Leide et al., 2007; Ruiz-May and Rose 2013; España et al. 2014; Martin and Rose 2014). Tomato fruit cell division initiates after bloom and continues until 15 to 20 days post bloom, when cells cease to divide and begin elongation (Fishman et al. 2002; Bertin et al. 2003, 2007). To accommodate intensive fruit growth and dynamic changes in shape and size during the period of cell division, fruit have developed a waxy cuticle that maintains structural integrity of the fruit, controls transpiration rates, and protects against biotic and abiotic stresses (Bargel and Neinhuis 2005; Bertin et al. 2007; España et al. 2014; Martin and Rose 2014). During early development, the cuticular membrane is more elastic and hydrophobic, allowing for higher rates of evapotranspiration (Bargel and Neinhuis 2005; Montanaro et al. 2012; España et al. 2014; Martin and Rose 2014). Cuticular thickness, rigidity

and chemical composition change between immature green, mature green and mature red stages, mainly driven by flavonoid accumulation and cuticular wax deposition (Bargel and Neinhuis 2005; Leide et al., 2007; España et al. 2014).

Scanning electron microscopy of *P. syringae* pv. tomato fruit colonization showed bacteria aggregating around the bases of broken or shedded trichomes, and confocal microscopy of eGFP-expressing *C. michiganensis* provided evidence for bacterial spread from the exterior into fruit tissues (Getz et al. 1983a; Tancos et al. 2013). However, we do not know how phytopathogenic bacteria penetrate and colonize astomatous fruit, or how they cause lesions that affect fruit health and marketability. It is possible that rapid cell division and fruit expansion paired with a more elastic cuticle may create physical apertures that bacteria can exploit as routes of entry. If bacteria can only colonize fruit during early development, then cessation of symptom development may coincide with the transition from cell division to elongation around the mature green fruit stage. Different factors involved in maturation may also play a role, such as trichome shedding, cuticle thickness and fruit chemical composition (Leide et al., 2007; Mintz-Oron et al., 2008; Leide et al., 2010). Indeed, fruit from cutin-deficient tomato mutants were more susceptible to opportunistic microbes and the fungal pathogen *Botrytis cinerea* (Isaacson et al. 2009). Further studies are needed to understand both tomato fruit host and bacterial pathogen factors that influence pathogen colonization and host symptom development.

Ethylene plays crucial roles in complex development and ripening processes (Klee and Giovannoni 2011; Giovannoni et al. 2017). There were differences in disease severity between ethylene-mutant genotypes: *Cnr* fruit with reduced ethylene synthesis and responsiveness developed fewer lesions than AC and were susceptible for a shorter window on average to all three pathogens. In contrast, some genotypes had higher disease severity and were susceptible

until larger diameters. *Nr* fruit, impaired in ethylene perception, were susceptible to *C. michiganensis* until larger diameters compared to AC, and developed significantly more lesions than AC at several sizes. The ethylene insensitive mutant *Gr* exhibited similar trends of continuing to be susceptible until larger diameters than AC and developing significantly more lesions when inoculated with *P. syringae* pv. tomato and *X. gardneri*. We did not observe a direct link between ethylene synthesis or perception on fruit susceptibility. Since these mutations alter fruit developmental processes involved in ripening, it is possible that disease severity phenotypes and extended windows of susceptibility might be due to pleiotropic effects on development. It had previously been hypothesized that changes in fruit pH that occur during ripening was affecting the ability for *P. syringae* pv. tomato to colonize and cause speck symptoms on fruit (Yunis et al., 1980). In contrast to this hypothesis, mutant tomato genotypes assessed in this study were susceptible during a developmental time-frame that was unaffected by fruit ripening processes and unchanged between the wildtype AC background and ripening-impaired mutants.

Impairments in ethylene synthesis and perception have been demonstrated to slow and reduce overall wilt symptom development in tomato plants inoculated with the reference strain of *C. michiganensis* (NCPB382) (Balaji et al. 2008). Here we confirmed the phenotype of delayed and reduced wilt symptoms to a New York strain of *C. michiganensis* in *Nr* tomato plants. In contrast, the *hp1* mutant exhibited rapid onset of symptoms that were significantly more severe in comparison to AC and *Nr*. Pathogen populations 1cm above the inoculation site were the same densities at 21 dpi in all genotypes, but further studies will have to be conducted to test differences in spread and colonization of *C. michiganensis* in *hp1* to better understand why this genotype is more susceptible. Comparing the reduction in symptom wilt symptom severity

displayed in *Nr* plants inoculated with *C. michiganensis* to the increased bird's-eye lesion symptom severity of *Nr* fruit inoculated with *C. michiganensis* highlights the differences in host responses by tissue type described in wild tomato plants and fruit (Peritore-Galve et al. 2020).

Fruit inoculations were performed on Pearson and *Nr*<sup>Pearson</sup> genotypes because the *Nr* mutation more effectively blocks ripening in Pearson fruit compared to AC (Lanahan et al., 1994). Different patterns of increasing and decreasing symptom severity and overall susceptibility differed between Pearson and AC fruit when inoculated with each pathogen. The different patterns may suggest that disease severity trends based on fruit size differ between tomato genotypes. Due to size differences between medium sized (~4oz at maturity) AC and larger (~7oz) Pearson fruit, it is likely that Pearson fruit cease cell division and begin elongation at larger diameters than AC fruit. If cell division and elongation stages play a role in cessation of susceptibility, then that might explain why Pearson fruit were susceptible until around 4.5cm diameter when inoculated with *C. michiganensis*. Interestingly, *P. syringae* pv. tomato NYT1 caused few lesions on Pearson tomato fruit. This phenotype may be due to differences in cuticle thickness and composition between AC and Pearson fruit, or in the mechanisms of infection of *P. syringae* pv. tomato on fruit from different genotypes, which remain to be tested.

In conclusion, tomato fruit in the Ailsa Craig background develop lesions caused by *C. michiganensis*, *P. syringae* pv. tomato, and *X. gardneri* broadly between 0.15 and 3cm in diameter. Fruit undergo a peak in disease severity and cessation of symptom development at different sizes depending on pathogen and ethylene mutant tested, which is not governed by ripening, ethylene production or ethylene perception. Questions remain about what those processes and host responses might be, as well as how bacteria can exploit host development to successfully colonize fruit. Through these experiments we identified ethylene and ripening

mutant tomato lines that are more or less susceptible and that are susceptible until larger sizes. These mutant genotypes can be used as tools to begin dissecting mechanisms of bacterial colonization and fruit resistance.

### ***ACKNOWLEDGEMENTS***

Funding for this project was provided by Cornell AgriTech and USDA Federal Capacity Funds. Thank you to Jim Giovannoni for tomato seed and guidance on this project; to Holly Lange, Tatiana Sanabria Ortiz, Colin Day, Garrett Giles, Juan Luis González Girón for technical support; and Stephen Parry from the Cornell Statistical Consulting Unit for support on statistical analyses.

### ***REFERENCES***

- Araújo, E. R., Pereira, R. C., Ferreira, M. A. S. V., Café-Filho, A. C., Moita, A. W., and Quezado-Duval, A. M. 2011. Effect of temperature on pathogenicity components of tomato bacterial spot and competition between *Xanthomonas perforans* and *X. gardneri*. *Acta Hortic.* 914:39–42.
- Balaji, V., Mayrose, M., Sherf, O., Jacob-Hirsch, J., Eichenlaub, R., Iraki, N., Manulis-Sasson, S., Rechavi, G., Barash, I., and Sessa, G. 2008. Tomato transcriptional changes in response to *Clavibacter michiganensis* subsp. *michiganensis* reveal a role for ethylene in disease development. *Plant Physiol.* 146:1797–1809.

- Bargel, H., and Neinhuis, C. 2005. Tomato (*Lycopersicon esculentum* Mill.) fruit growth and ripening as related to the biomechanical properties of fruit skin and isolated cuticle. *J. Exp. Bot.* 56:1049–1060.
- Barry, C. S., McQuinn, R. P., Thompson, A. J., Seymour, G. B., Grierson, D., and Giovannoni, J. J. Ethylene insensitivity conferred by the *Green-ripe* and *Never-ripe 2* ripening mutants of tomato. *Plant Physiol.* 138:267-275
- Barry, C. S. and Giovannoni, J. J. Ripening in the tomato *Green-ripe* mutant is inhibited by ectopic expression of a protein that disrupts ethylene signalling. *Proc. Natl. Acad. Sci. U.S.A.* 103:7923-7928
- Bates, D., Mächler, M., Bolker, B., and Walker, S. 2015. Fitting linear mixed-effects models using lme4. *J. Stat. Softw.* 67:1–48.
- Bertani, G. 1951. Studies on lysogenesis. *J. Bacteriol.* 62:293-300.
- Bertin, N., Génard, M., and Fishman, S. 2003. A model for an early stage of tomato fruit development: cell multiplication and cessation of the cell proliferative activity. *Ann. Bot.* 92:65–72.

Bertin, N., Lecomte, A., Brunel, B., Fishman, S., and Génard, M. 2007. A model describing cell polyplodization in tissues of growing fruit as related to cessation of cell proliferation. *J. Exp. Bot.* 58:1903–1913.

Brooks, M. E., Kristensen, K., Benthem, K. J. van, Magnusson, A., Berg, C. W., Nielsen, A., Skaug, H. J., Mächler, M., and Bolker, B. M. 2017. glmmTMB balances speed and flexibility among packages for zero-inflated generalized linear mixed modeling. *The R Journal.* 9:378–400.

Bryan, M. K. 1930. Studies on bacterial canker of tomato. *J. Agric. Res.* 41:825–851.

Chalupowicz, L., Zellermann, E.-M., Fluegel, M., Dror, O., Eichenlaub, R., Gartemann, K.-H., Savidor, A., Sessa, G., Iraki, N., Barash, I., and Manulis-Sasson, S. 2011. Colonization and movement of GFP-labeled *Clavibacter michiganensis* subsp. *michiganensis* during tomato infection. *Phytopathology.* 102:23–31.

España, L., Heredia-Guerrero, J. A., Segado, P., Benítez, J. J., Heredia, A., and Domínguez, E. 2014. Biomechanical properties of the tomato (*Solanum lycopersicum*) fruit cuticle during development are modulated by changes in the relative amounts of its components. *New Phytol.* 202:790–802.

FAO, 2017. FAOSTAT. Food and Agriculture Data.

- Fernandez-Pozo, N., Zheng, Y., Snyder, S. I., Nicolas, P., Shinozaki, Y., Fei, Z., Catala, C., Giovannoni, J. J., Rose, J. K. C., and Mueller, L. A. 2017. The Tomato Expression Atlas. *Bioinformatics*. 33:2397–2398.
- Fishman, S., Bertin, N., and Génard, M. 2002. Cell division and cessation of cell proliferation in growing fruit. *Acta Hortic.* :125–131.
- Gardner, M. W., and Kendrick, J. B. 1923. Bacterial spot of tomato and pepper. *Phytopathology*. 13:307–315.
- Getz, S., Fulbright, D. W., and Stephens, C. T. 1983a. Scanning electron microscopy of infection sites and lesion development on tomato fruit infected with *Pseudomonas syringae* pv. *tomato*. *Phytopathology*. 73:39–43.
- Getz, S., Stephens, C. T., and Fulbright, D. W. 1983b. Influence of developmental stage on susceptibility of tomato fruit to *Pseudomonas syringae* pv. *tomato*. *Phytopathology*. 73:36.
- Giovannoni, J. J., Noensie, E. N., Ruezinsky, D. M., Lu, X., Tracy, S. L., Ganal, M. W., Martin, G. B., Pillen, K., Alpert, K., and Tanksley, S. D. 1995. Molecular genetic analysis of the *ripening-inhibitor* and *non-ripening* loci of tomato: a first step in genetic map-based cloning of fruit ripening genes. *Mol. Gen. Genet.* 248:195-206

Giovannoni, J. J. 2007 Fruit ripening mutants yield insights into ripening control. *Curr. Opin. Plant Biol.* 10:283-289

Giovannoni, J., Nguyen, C., Ampofo, B., Zhong, S., and Fei, Z. 2017. The epigenome and transcriptional dynamics of fruit ripening. *Annu. Rev. Plant Biol.* 68:61–84.

Isaacson, T., Kosma, D. K., Matas, A. J., Buda, G. J., He, Y., Yu, B., et al. 2009. Cutin deficiency in the tomato fruit cuticle consistently affects resistance to microbial infection and biomechanical properties, but not transpirational water loss. *Plant J.* 60:363–377.

Halekoh, U., and Højsgaard, S. 2014. A Kenward-Roger Approximation and parametric bootstrap methods for tests in linear mixed models - the R package pbkrtest. *J. Stat. Softw.* 59:132.

Jones, J. B., Bouzar, H., Stall, R. E., Almira, E. C., Roberts, P. D., Bowen, B. W., et al. 2000. Systematic analysis of xanthomonads (*Xanthomonas* spp.) associated with pepper and tomato lesions. *Int. J. Syst. Evol. Microbiol.* 50:1211–1219.

Jones, J. B., Pohronezny, K. L., Stall, R. E., and Jones, J. P. 1986. Survival of *Xanthomonas campestris* pv. *vesicatoria* in Florida on tomato crop residue, weeds, seeds, and volunteer tomato plants. *Phytopathology.* 76:430–434.

- Jones, L. A., Saha, S., Collmer, A., Smart, C. D., and Lindeberg, M. 2014. Genome-assisted development of a diagnostic protocol for distinguishing high virulence *Pseudomonas syringae* pv. tomato strains. *Plant Dis.* 99:527–534.
- Kilambi, H. V., Kumar, R., Sharma, R., and Sreelakshmi, Y. 2013. Chromoplast-specific carotenoid-associated protein appears to be important for enhanced accumulation of carotenoids in *hp1* tomato fruits. *Plant Physiol.* 161:2085-2101
- King, E. O., Ward, M. K., and Raney, D. E. 1954. Two simple media for the demonstration of pyocyanin and fluorescin. *J. Lab. Clin. Med.* 44:301-307
- Klee, H. J., and Giovannoni, J. J. 2011. Genetics and control of tomato fruit ripening and quality attributes. *Annu. Rev. Genet.* 45:41–59.
- Kraus, C. M., Mazo-Molina, C., Smart, C. D., and Martin, G. B. 2017. *Pseudomonas syringae* pv. tomato strains from New York exhibit virulence attributes intermediate between typical race 0 and race 1 strains. *Plant Dis.* 101:1442–1448.
- Kuznetsova, A., Brockhoff, P., and Christensen, R. 2017. lmerTest package: tests in linear mixed effects models. *J. Stat. Softw.* 82:1–26.
- Lanahan, M. B., Yen, H-C., Giovannoni, J. J., and Klee, H. J. 1994. The *Never ripe* mutation blocks ethylene perception in tomato. *Plant Cell.* 6:521-530.

- Lange, H. W., Tancos, M. A., Carlson, M. O., and Smart, C. D. 2015. Diversity of *Xanthomonas campestris* isolates from symptomatic crucifers in New York State. *Phytopathology*. 106:113–122.
- Lenth, R. V. 2016. Least-Squares Means: The R Package lsmeans. *J. of Stat. Softw.* 69:1–33.
- Leide, J., Hildebrandt, U., Reussing, K., Riederer, M., and Vogg, G. 2007. The developmental pattern of tomato fruit wax accumulation and its impact on cuticular transpiration barrier properties: effects of a deficiency in a  $\beta$ -ketoacyl-coenzyme A synthase (LeCER6). *Plant Physiol.* 144:1667-1679.
- Leide, J., Hildebrandt, U., Vogg, G., and Riederer, M. 2010. The *positional sterile (ps)* mutation affects cuticular transpiration and wax biosynthesis of tomato fruits. *J. Plant Physiol.* 168:871-877.
- de León, L., Siverio, F., López, M. M., and Rodríguez, A. 2011. *Clavibacter michiganensis* subsp. *michiganensis*, a seedborne tomato pathogen: healthy seeds are still the goal. *Plant Dis.* 95:1328–1338.
- Ma, X., Lewis Ivey, M. L., and Miller, S. A. 2011. First report of *Xanthomonas gardneri* causing bacterial spot of tomato in Ohio and Michigan. *Plant Dis.* 95:1584–1584.

- Manning, K., Mahmut, T., Poole, M., Hong, Y., Thompson, A. J., King, G. J., Giovannoni, J. J., and Seymour, G. B. 2006. A naturally occurring epigenetic mutation in a gene encoding an SBP-box transcription factor inhibits tomato fruit ripening. *Nat. Genet.* 38:948-952
- Martin, L. B. B., and Rose, J. K. C. 2014. There's more than one way to skin a fruit: formation and functions of fruit cuticles. *J. Exp. Bot.* 65:4639–4651.
- McCarter, S. M., Jones, J. B., Gitaitis, R. D., and Smitley, D. R. 1983. Survival of *Pseudomonas syringae* pv. tomato in association with tomato seed, soil, host tissue, and epiphytic weed hosts in Georgia. *Phytopathology.* 73:1393–1398.
- McInnes, T. B., Gitaitis, R. D., McCarter, S. M., Jaworski, C. A., and Phatak, S. C. 1988. Airborne dispersal of bacteria in tomato and pepper transplant fields. *Plant Dis.* 72:575–579.
- Medina-Mora, C. M., Hausbeck, M. K., and Fulbright, D. W. 2001. Bird's eye lesions of tomato fruit produced by aerosol and direct application of *Clavibacter michiganensis* subsp. *michiganensis*. *Plant Disease.* 85:88–91.
- Mintz-Oron, S., Mandel, T., Rogachev, I., Feldberg, L., Lotan, O., Yativ, M., Wang, Z., Jetter, R., Venger, I., Adato, A., and Aharoni, A. 2008. Gene expression and metabolism in tomato fruit surface tissues. *Plant Physiol.* 147: 823-851.

- Montanaro, G., Dichio, B., and Xiloyannis, C. 2012. Fruit transpiration: mechanisms and significance for fruit nutrition and growth. In: Montanaro, G., Dichio, B., eds. *Advances in Selected Plant Physiology Aspects*. InTech.
- Peritore-Galve, F. C., Miller, C., and Smart, C. D. 2020. Characterizing colonization patterns of *Clavibacter michiganensis* during infection of tolerant wild *Solanum* species. *Phytopathology*. 110:574-581.
- Pohronezny, K., Hewitt, M., and Infante, J. 1993. Susceptibility of pepper fruit to infection by *Xanthomonas campestris* pv. *vesicatoria*. *Can. J. Plant Pathol.* 15:107–109.
- Potnis, N., Timilsina, S., Strayer, A., Shantharaj, D., Barak, J. D., Paret, M. L., Vallad, G. E., and Jones, J. B. 2015. Bacterial spot of tomato and pepper: diverse *Xanthomonas* species with a wide variety of virulence factors posing a worldwide challenge. *Mol. Plant Pathol.* 16:907–920.
- Roberts, R., Mainiero, S., Powell, A. F., Liu, A. E., Shi, K., Hind, S. R., et al. 2019. Natural variation for unusual host responses and flagellin-mediated immunity against *Pseudomonas syringae* in genetically diverse tomato accessions. *New Phytol.* 223:447–461.

- Ruiz-May, E., and Rose, J. K. C. 2013. Cell wall architecture and metabolism in ripening fruit and the complex relationship with softening. In: Giovannoni, J.J., Poole, M., Seymour, G.B., Tucker, G.A., eds. *The molecular biology and biochemistry of fruit ripening*. Chichester, UK: Wiley, 163–187.
- Scott, J. W., Somodi, G. C., and Jones, J. B. 1989. Resistance to bacterial spot fruit infection in tomato. *HortSci*. 24:825–827.
- Sen, Y., van der Wolf, J., Visser, R. G. F., and van Heusden, S. 2014. Bacterial canker of tomato: current knowledge of detection, management, resistance, and interactions. *Plant Dis*. 99:4–13.
- Tancos, M. A., Chalupowicz, L., Barash, I., Manulis-Sasson, S., and Smart, C. D. 2013. Tomato fruit and seed colonization by *Clavibacter michiganensis* subsp. *michiganensis* through external and internal routes. *Appl. Environ. Microbiol.* 79:6948–6957.
- Tancos, M. A., Lange, H. W., and Smart, C. D. 2015. Characterizing the genetic diversity of the *Clavibacter michiganensis* subsp. *michiganensis* population in New York. *Phytopathology*. 105:169–179.
- Tancos, M. A., Lowe-Power, T. M., Peritore-Galve, F. C., Tran, T. M., Allen, C., and Smart, C. D. 2018. Plant-like bacterial expansins play contrasting roles in two tomato vascular pathogens. *Mol. Plant Pathol.* 19:1210–1221.

- Timilsina, S., Jibrin, M. O., Potnis, N., Minsavage, G. V., Kebede, M., Schwartz, A., Bart, R., Staskawicz, B., Boyer, C., Vallad, G. E., Pruvost, O., Jones, J. B., and Goss, E. M. 2015. Multilocus sequence analysis of *Xanthomonas* causing bacterial spot of tomato and pepper plants reveals strains generated by recombination among species and recent global spread of *Xanthomonas gardneri*. *Appl. Environ. Microbiol.* 81:1520–1529.
- Vrebalov, J., Ruezinsky, D., Padmanabhan, V., White, R., Medrano, D., Drake, R., Schuch, W., and Giovannoni, J. 2002. A MADS-Box gene necessary for fruit ripening at the tomato *Ripening-inhibitor (Rin)* locus. *Science.* 296:343-346
- Wang, A., Chen, D., Ma, Q., Rose, J. K. C., Fei, Z., Liu, Y., and Giovannoni, J. J. 2019. The tomato *HIGH PIGMENT1/DAMAGED DNA PROTEIN 1* gene contributes to regulation of fruit ripening. *Hortic. Res.* 6:15
- Wang, N., Chen, H., Nonaka, S., Sato-Izawa, K., Kusano, M., and Ezura, H. 2018. Ethylene biosynthesis controlled by *NON-RIPENING*: a regulatory conflict between wounding and ripening. *Plant Physiol. Bioch.* 132:720-726
- Wickham, H. 2009. *ggplot2: Elegant Graphics for Data Analysis*. New York: Springer-Verlag.
- Wilkinson, J. Q., Lanahan, M. B., Yen, H-C., Giovannoni, J. J., and Klee, H. J. 1995 An ethylene-inducible component of signal transduction encoded by *Never-ripe*. *Science.* 270:1807-1809

Xin, X.-F., and He, S. Y. 2013. *Pseudomonas syringae* pv. tomato DC3000: a model pathogen for probing disease susceptibility and hormone signaling in plants. *Annu. Rev. Phytopathol.* 51:473–498.

Yunis, H., Bashan, Y., Okon, Y., and Henis, Y. 1980. Weather dependence, yield losses, and control of bacterial speck of tomato caused by *Pseudomonas tomato*. *Plant Dis.* 64:937–939.

## CHAPTER 3

### **Understanding the effects of *Clavibacter michiganensis* infection on xylem sap of wild and cultivated tomato using untargeted metabolomics**

#### ***INTRODUCTION***

The gram-positive bacterium *Clavibacter michiganensis* is the causal agent of tomato bacterial canker, an economically damaging disease for tomato growers worldwide (de León et al., 2011; Sen et al., 2014). The pathogen systemically colonizes the xylem, which is a nutrient limited, hypoxic and acidic environment (Fatima and Senthil-Kumar, 2015; Dalsing et al., 2015). During pathogenesis, *C. michiganensis* causes unilateral leaflet wilt, stem cankers, marginal leaf necrosis and plant death (de León et al., 2011; Sen et al., 2014). This seed-borne bacterium also uses the xylem as a route to colonize developing seeds, leading to new outbreaks of the disease (Tancos et al., 2013). At later stages of infection, *C. michiganensis* macerates tissues surrounding the vascular bundles, leading to increased wilt and canker symptoms, and plant death (Chalupowicz et al., 2011).

Wild tomato accessions are able to harbor varying amounts of *C. michiganensis* in the vascular systems while developing fewer symptoms compared to cultivated tomato (Sen et al., 2014; Peritore-Galve et al., 2020). This is in part due to the pathogen's inability to spread from colonized protoxylem vessels into larger metaxylem (Peritore-Galve et al., 2020). The bacterium also grows to lower densities in xylem sap harvested from wild tomato species compared to cultivated species (Peritore-Galve et al., 2020). At the cellular level, host responses to the presence of *C. michiganensis* is poorly understood; therefore, studying chemical responses in the xylem of wild and cultivated tomato may provide insights into host responses and plant tolerance against bacterial canker.

Genomics and functional analyses have provided insights into *C. michiganensis* virulence genes critical for host colonization. The reference strain, NCPPB382 (Cm382), contains a pathogenicity island (*chp/tomA* PAI) and two plasmids, pCM1 and pCM2, that are necessary for full virulence (Gartemann et al., 2008; Nandi et al., 2018). These mobile elements contain multiple copies of genes encoding secreted serine proteases, cell wall degrading enzymes (CWDEs), expansins, and a tomatinase enzyme (Kaup et al., 2005; Gartemann et al., 2008; Tancos et al., 2018; Nandi et al., 2018). The chimeric, pCM1-borne protein CelA consists of a cellulase, carbohydrate-binding module, and an expansin domain (CmEXLX1), which is necessary for pathogenicity in the reference strain, but not in the pathogenic New York isolate, *C. michiganensis* 0317 (Jahr et al., 2000; Tancos et al., 2015; Tancos et al., 2018). The virulence plasmid pCM2 encodes a serine protease, Pat-1, which is required for full virulence in Cm382 (Dreier et al., 1997). Chromosomal genes encoding CWDEs, serine proteases, perforin, and an expansin (CmEXLX2) have also been implicated in virulence (Gartemann et al., 2008; Chalupowicz et al., 2017; Thapa et al., 2017; Tancos et al., 2018; Peritore-Galve et al., 2020).

Further ‘omics analyses of plant tissue have provided us with insights into host responses to infection by *C. michiganensis* (Nandi et al., 2018). Proteomic analyses of *S. lycopersicum* x *S. habrochaites* LA407 tolerant breeding lines at two and four days post *C. michiganensis*-inoculation identified an accumulation of proteins involved in oxidative stress responses (Coaker et al., 2004). Transcriptomics of susceptible cultivated tomatoes at four and eight days post-*C. michiganensis* inoculation helped determine a role for increased ethylene production during pathogen colonization (Balaji et al., 2008). A second proteomics experiment of susceptible *S. lycopersicum* stem tissue eight days post inoculation detected both virulence proteins secreted by the pathogen and increased accumulation of host proteins involved in ethylene production,

pathogenesis-related (PR) proteins, and antimicrobial activity (Savidor et al., 2012). Recently, untargeted metabolomics of xylem sap was used to determine the effects of the tomato wilt pathogen *Ralstonia solanacearum* on the host xylem environment (Lowe-Power et al., 2018). Those experiments revealed that *Ralstonia solanacearum* uses xylem sap metabolites as carbon and nitrogen sources, and it secretes the polyamine putrescine, leading to accelerated wilt symptoms (Lowe-Power et al., 2018). Insights into *Ralstonia*-tomato interactions in the xylem led us to hypothesize that *C. michiganensis* may also alter host xylem sap composition, which may provide further insight into the molecular host-microbe interactions during bacterial canker disease.

We used untargeted metabolomics of xylem sap in a discovery-oriented approach to answer the following questions: (1) how does *C. michiganensis* infection affect xylem sap metabolite composition, and do those metabolite changes differ between tolerant wild, and susceptible cultivated tomato species? In addition, (2) what are the core differences in xylem sap metabolites between healthy *S. lycopersicum* and *S. habrochaites*? Concurrently, we sequenced the genome of *C. michiganensis* 0317 to compare its repertoire of virulence genes to other sequenced isolates, and to probe the genome for production pathways of metabolites in the datasets that may be bacterially derived.

## ***MATERIALS AND METHODS***

### **Plant growth conditions and inoculation with *C. michiganensis***

*Solanum habrochaites* LA2128 seeds were washed in a 50% bleach solution for 15 min, rinsed with sterile water, and then germinated on moist sterile Whatman filter paper (Fisher Scientific, Hampton, NH) in Petri dishes for 8 to 10 days (Peritore-Galve et al., 2020). Germinated seedlings were transferred to a Farfard professional formula growing mix in 72-cell

flats (Sun Gro Horticulture, Agawam, MA) and *S. lycopersicum* ‘Mt. Fresh’ seeds were planted in the mix. When seedlings had two true leaves, they were transferred to four-inch pots and supplemented with Osmocote slow release fertilizer (Scotts Miracle-Gro Co., Marysville, OH). Plants were grown in an environmentally controlled greenhouse with a 16-hr light/8-hr dark photoperiod.

To collect sap from healthy and infected plants, *S. lycopersicum* ‘Mt. Fresh’ and *S. habrochaites* LA2128 plants at the two- to three-true leaf stage were inoculated with *C. michiganensis* 0317 or sterile water. The bacterium was cultured in Lysogeny Broth (LB) medium for 18 hours shaking at 160 rpm at 28°C (Tancos et al., 2018; Peritore-Galve et al., 2020). Bacterial suspensions were adjusted to optical density 600 ( $OD_{600}$ ) = 0.8 through centrifugation for 12 min at 4,000 rpm, washing the pellet with sterile water, then re-suspending in sterile water (Tancos et al., 2018; Peritore-Galve et al., 2020). Tomato seedlings ( $n = 60$  per genotype) were inoculated by dipping sterilized scissors into either *C. michiganensis* suspension ( $n = 30$  plants per genotype) or sterile water ( $n = 30$  plants per genotype) and clipping the cotyledons (Tancos et al., 2018; Peritore-Galve et al., 2020).

### **Sap collection and sample selection for untargeted metabolomics**

Plants were observed daily for wilt and canker symptoms. Xylem sap was collected at 12 days post inoculation (dpi), when *S. lycopersicum* ‘Mt. Fresh’ on average began presenting leaflet wilt symptoms. All plants were watered adequately the evening before collection. Xylem sap was collected 1-2 hr after sunrise to control for diurnal changes in sap flow rate and composition (Siebrecht et al., 2003; Lowe-Power et al., 2018). Plants were de-topped at a 30 to 45 degree angle 2 cm above the inoculation site with individual sterile razor blades and gently blotted dry with sterile Kimwipes (Fisher Scientific) (Goodger et al., 2005; Lowe-Power et al.,

2018). De-topped plants were then tilted so that stems were parallel to the bench or pointing slightly downward, and a 2 ml Eppendorf tube was gently placed on the stem to collect sap. For the next ninety minutes, sap was transferred into pre-chilled 2 ml Eppendorf tubes on ice every ten minutes. After ninety minutes, the total volume of sap collected per plant was measured using pipetting, and 40 µl of sap from each plant was transferred into individual wells of 96-well Falcon tissue culture plates (Corning Inc., Corning, NY) for bacterial density measurements. Sap samples were stored at -80°C until the LC-MS analysis.

To quantify bacterial density, 10 µl of the 40-µl sap that was set aside in 96-well Falcon tissue culture plates were serially diluted into 90 µl of sterile water for seven dilutions. Ten microliters of each dilution were spot inoculated onto D2ANX semi-selective medium three times and incubated for two to three days at 28°C. Number of CFUs were counted and the average of three technical replicates was calculated into CFU per milliliter of sap. Differences in sap flow and CFU ml<sup>-1</sup> between groups were calculated using analysis of variance (ANOVA) and Tukey's pairwise comparisons ( $P < 0.05$ ) in R v. 3.6.2 using package emmeans (Lenth 2016). Graphs were generated using ggplot2 (Wickham 2009).

Sap from *C. michiganensis* and water-inoculated *S. lycopersicum* 'Mt. Fresh' and *S. habrochaites* LA2128 were selected for untargeted metabolomics analysis. The experiment was designed to compare differences in sap metabolite accumulation between healthy tomato plants, and those infected with *C. michiganensis*. The experiment was also designed to compare overall sap metabolite composition between healthy *S. lycopersicum* 'Mt. Fresh' and *S. habrochaites* LA2128 plants. Sap selected for metabolomics met the following criteria: *S. lycopersicum* 'Mt. Fresh' healthy sap samples had zero CFU per ml sap, and 'infected' samples had between 1.04 x 10<sup>9</sup> to 1.7 x 10<sup>9</sup> CFU per ml sap. *Solanum habrochaites* LA2128 healthy sap samples had zero

CFU per ml sap, and ‘infected’ samples had between  $3 \times 10^6$  to  $1 \times 10^7$  CFU per ml sap. To reduce the effect of sap flow rates on metabolite concentration, samples close to the median sap flow rate for each treatment and genotype were selected for pooling. To generate the pools, selected samples were thawed on ice, and then centrifuged for 1 min at 14,000 rpm at 4°C to remove bacteria and debris (Lowe-Power et al., 2018). Then, 200 µl of sap per treatment (healthy or infected) per genotype from three biological replicates were transferred to sterile 1.5 ml Eppendorf tubes to yield three pools per treatment per tomato genotype ( $n = 12$  pools total).

### **LC-MS analysis**

Healthy and infected sap samples from *S. lycopersicum* ‘Mt. Fresh’ and *S. habrochaites* LA2128 were analyzed using a Vanquish UHPLC system coupled to a Q Exactive Hybrid Quadrupole-Orbitrap High Resolution Mass spectrometer (Thermo Fisher Scientific, Waltham, MA), operated on both positive and negative electrospray ionization (ESI) modes. To prepare the samples, 300 µl of sap from each pool were dried using a SpeedVac concentrator at room temperature. Samples were reconstituted in 150 µl acetonitrile/water/formic acid (50/50/0.1) containing an internal standard of sulfadimethoxine,  $^{13}\text{C}$  pyruvate, and  $^{13}\text{C}$  valine (1.5 ppm final concentration) for controlling LC-MS machine performance. Ten microliters of each sample were pooled into four independent quality control (QC) samples used for downstream analyses. Samples were run on two different columns in two independent experiments; to separate hydrophobic compounds, an Accucore Vanquish C18+ column (Thermo Fisher Scientific; 2.1mm x 100mm, 1.5-µm) was used, and to separate hydrophilic compounds, a SeQuant ZIC pHILIC column (Millipore Sigma, Burlington, MA; 2.1 mm x 150 mm, 5-µm) was used.

In the experiment that utilized the C18 column, the mobile phase A consisted of 0.1% formic acid in water, and mobile phase B was 0.1% formic acid in 60% acetonitrile and 40%

H<sub>2</sub>O with 0.1% formic acid. The liquid chromatography elution gradient was 0-2.0 min (0% B), 19-19.1 min (50-100% B), 19.1-21 min (100% B), 21-21.1 min (100-0% B), 21.1-25 min (0% B) followed by 4 min of column re-equilibration prior to the next run. The flow rate was 320  $\mu$ l per min and the injection volumes were 2- $\mu$ l. For the HILIC column experiment, mobile phase A was 10 mM ammonium acetate in water (pH = 9.8) and mobile phase B consisted of acetonitrile and water (60/40). The elution gradient for the HILIC column was 0-1 min (90% B), 15-18.9 min (30% B), 19-39 min (90% B) followed by 4 min of column re-equilibration prior to the next run. The injection volumes were 2- $\mu$ l and the flow rate was 250- $\mu$ l per min. To avoid sample biases, the sequence of injections was randomized in both C18 and HILIC experiments, and QC samples were run at the beginning, middle, and end of the sequence.

After chromatographic separation, samples were analyzed using positive and negative ESI in data-dependent MS/MS mode. Nitrogen as sheath gas, auxiliary gas, and sweep gas were set to 50, 10 and 1 arbitrary units, respectively. Full MS scans were acquired from 67-1000  $m/z$  at 120k resolution. Automatic gain control (AGC) target was  $3 \times 10^6$  and the maximum injection time (MIT) was 100 ms. Other parameters included spray voltage of 3.5kV, capillary temperature of 275°C, auxiliary gas heater temperature of 375°, and S-lens radio frequency level 55% (Vidavsky et al., 2019). Data-dependent MS/MS (DDMS2) spectra were acquired at 15k resolution, AGC target  $1 \times 10^5$  ions, MIT 50 ms, isolation window 0.4  $m/z$ , and normalized collision energy 20, 30, 40 (Vidavsky et al., 2019). All data were acquired using the Xcalibur 3.1 software (Thermo Fisher Scientific).

### **Data processing and statistical analyses**

Metabolite identification and relative quantification was performed using mass matching and MS/MS matching in Compound Discoverer<sup>TM</sup> 3.0 software (Thermo Fisher Scientific).

Blank samples from C18 and HILIC experiments were used for background subtraction and noise removal during data processing. ChemSpider, BioCyc, Human Metabolome Database, The Food Metabolome, MassBank, LIPID MAPS and mzCloud databases were used for mass matching and MS/MS matching using Compound Discoverer™ software (Karp et al., 2019; Wishart et al., 2018; Scalbert et al., 2014; Horai et al., 2010; Fahy et al., 2007). For each biological replicate, the peak area of each detected metabolite was normalized against QC sample peaks (Godzien et al., 2015). Identified metabolites and their normalized peak areas were uploaded to MetaboAnalyst 4.0 as unpaired columns and were log<sub>2</sub> transformed (Chong et al., 2018).

Statistical and multivariate analyses were conducted to test differential accumulation of metabolites between infected and healthy sap samples within a species, or metabolite abundance differences between healthy sap samples of *S. lycopersicum* ‘Mt. Fresh’ and *S. habrochaites* LA2128. All analyses were performed by column and ESI mode (e.g. *S. lycopersicum* ‘Mt. Fresh’ infected vs. healthy sap within C18, negative mode). To identify differentially accumulated sap metabolites, a Student’s *t*-test was conducted to generate the average fold change and *p*-value of each metabolite (Hao et al., 2016, 2018). False discovery rate (FDR) correction was used to correct for multiple hypothesis testing using the Benjamini-Hochberg algorithm (Hao et al., 2016, 2018). Metabolites with an FDR corrected *p*-value lower than 0.1, and fold change greater than one were considered statistically significant. Partial least squares (PLS)-discriminant analyses were conducted to determine within- and between-group variance. Graphs were generated in MetaboAnalyst 4.0 or in R v. 3.6.2 using ggplot2 (Wickham 2009).

### **Genome sequencing and analysis**

*Clavibacter michiganensis* 0317 was cultured as described above. Two mL of liquid

culture ( $OD_{600}=2.294$ ) was centrifuged, the pellet was washed with sterile deionized water, then DNA was extracted using the MasterPure Gram-Positive DNA Purification Kit (Epicentre, Madison, WI, USA) according to the manufacturer's protocol. Quality (260/280 ratio) and quantity of DNA was measured using a NanoDrop ND 1000 (NanoDrop Technologies, Wilmington, DE, USA) and a Qubit 2.0 Fluorometer (Invitrogen, Carlsbad, CA, USA). Library preparations were performed by the Cornell Biotechnology Resource Center using the Illumina TruSeq PCR-free library kit (Illumina, Inc, San Diego, CA, USA) then run on the Illumina MiSeq platform as paired end 250 bp reads using the MiSeq Reagent Nano v2 kit. Quality of reads were assessed using FASTQC, then adapter clipping and quality filtering was performed with Trimmomatic (Andrews, 2010; Bolger et al. 2014). *De novo* assembly was performed using SPAdes, and assembly statistics were calculated using QUAST and BUSCO (Bankevich et al. 2012; Gurevich et al. 2013; Simão et al. 2015).

The polished assembly was then annotated using Rapid Annotation and Subsystem Technology (RAST) and Prokka (Aziz et al. 2008; Overbeek et al. 2014; Seemann 2014; Brettin et al. 2015; Kurtz et al. 2004). The *C. michiganensis* 0317 assembly was aligned to the reference *C. michiganensis* genome, NCPPB382 (i.e. Cm382) (AM711867) and the pCM2 (AM711866) plasmid using MUMmer 3.0 (Kurtz et al., 2004; Gartemann et al., 2008). The assembly was then compared to Cm382 and two sequenced isolates, CASJ002 (NZ\_MDHC00000000.1) and CASJ009 (NZ\_MDHJ00000000.1) using BRIG (Alikhan et al. 2011; Thapa et al., 2017). Carbohydrate active enzymes (CAZymes) were predicted using dbCAN2 and annotated to the genome (Zhang et al. 2018). Motifs for translocation through the general secretory (Sec) and twin-arginine translocation (Tat) pathways were predicted using SignalP 5.0 and annotated to the genome (Almagro Armenteros et al. 2019).

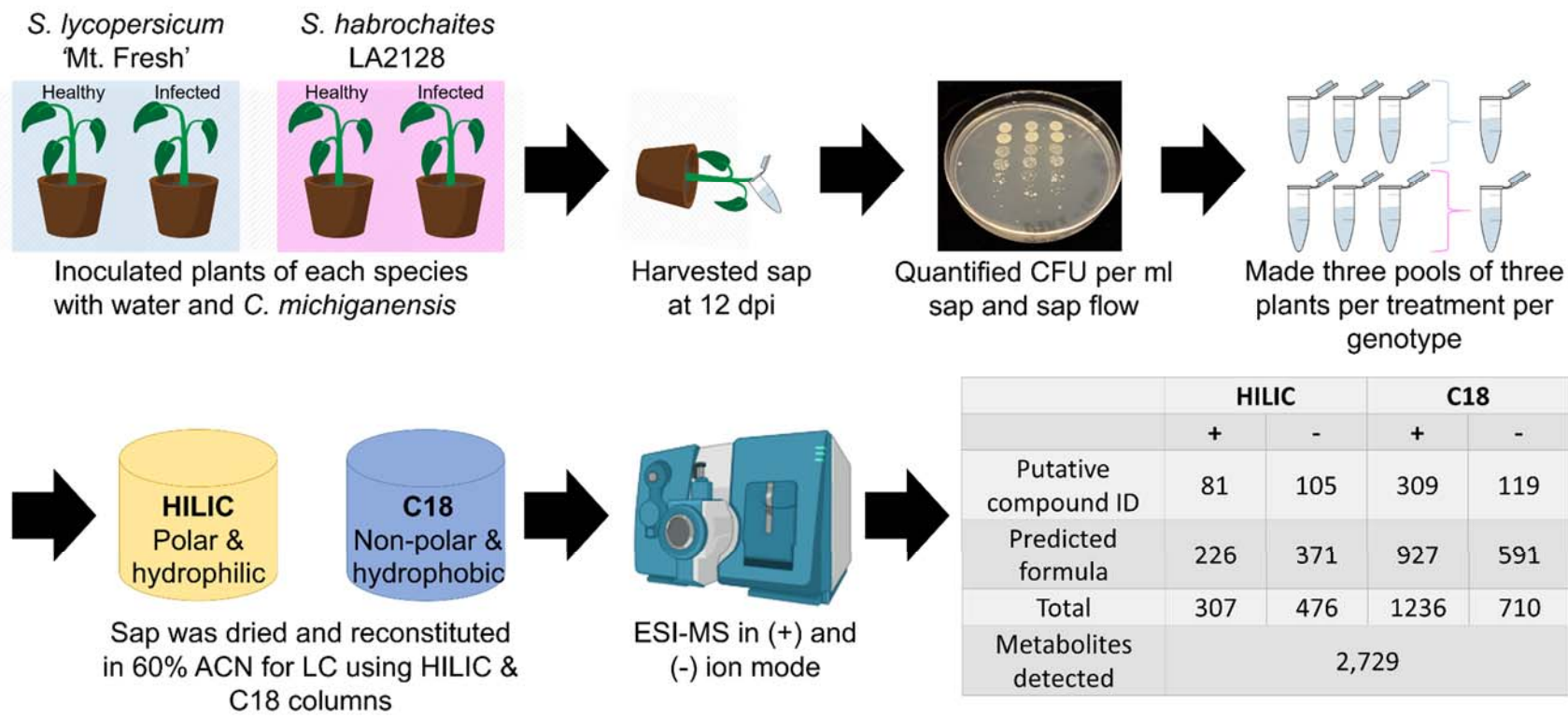


**FIGURE 3.1.** Visual abstract of sample preparation, collection, and LC-MS workflow. The table depicts how many metabolites were identified in each column experiment by ionization mode (+ positive, or - negative mode).

## **RESULTS**

### **Sap collection**

Seedlings of *S. lycopersicum* ‘Mt. Fresh’ and *S. habrochaites* LA2128 were cotyledon clip inoculated with *C. michiganensis* 0317, and sap was harvested 12 days post inoculation, from *S. lycopersicum* plants showing their first wilting symptoms (Fig. 3.1). Plants were observed daily, and wilt and canker symptoms were recorded. At 12 dpi, sap from nine plants of each treatment (*C. michiganensis* or water-inoculated) within a genotype was selected based on present wilt symptoms, sap flow rate, and CFU ml<sup>-1</sup> (Fig. 3.1). Only *S. lycopersicum* ‘Mt. Fresh’ were expected to present leaflet wilt in at least one leaflet since *S. habrochaites* LA2128 does not develop full leaflet wilt symptoms (Peritore-Galve et al., 2020). Sap from plants that met those criteria were pooled into three individual pools per treatment per genotype to increase total volume of sap necessary for LC-MS, and to reduce individual plant variation to capture biological effects (Fig. 3.1).

### **Sap flow and populations of *C. michiganensis* in sap**

Since *C. michiganensis* colonizes the xylem it is possible that bacterial aggregates impeding sap flow may cause wilt symptoms. As a criterion for sap from a plant to be selected for LC-MS analysis, we measured the sap flow as total volume of sap divided by the time collected (1.5 hr) (Fig. 3.2). Plants close to the median sap flow rate for its treatment-genotype combination were selected for further analysis (Fig. 3.2). Sap flow varied between plants within the same treatment-genotype combination, and plants that no sap was collected from were removed from the analysis. Sap flow did not lead to wilt symptoms as there were no significant differences between sap flow of *C. michiganensis* and water-inoculated plants at 12 dpi (*S. lycopersicum* ‘Mt. Fresh’,  $P = 0.06$ ; *S. habrochaites* LA2128,  $P = 0.25$ ) (Fig. 3.2).

Population density of *C. michiganensis* was determined in harvested sap as a measure for bacterial colonization of both symptomatic *S lycopersicum* ‘Mt. Fresh’, and asymptomatic *S. habrochaites* LA2128 at 12dpi. The pathogen typically colonizes to densities of  $10^{10}$  CFU g<sup>-1</sup> of tissue in *S. lycopersicum* ‘Mt. Fresh’ and  $10^8$  CFU g<sup>-1</sup> of tissue in stem segments of *S. habrochaites* LA2128 near the inoculation site at 21 dpi (Peritore-Galve et al., 2020). In sap extracted from *S. lycopersicum* ‘Mt. Fresh’ at 12 dpi, the mean bacterial density was  $2.7 \times 10^8$  CFU per ml sap (Fig. 3.3), indicating high amounts of planktonic *C. michiganensis* during early stages of symptom development. Bacterial density in *S. habrochaites* LA2128 sap at 12 dpi was significantly reduced ( $P < 0.0001$ ) by two orders of magnitude to  $4.7 \times 10^6$  CFU per ml sap compared to bacterial density in *S. lycopersicum* ‘Mt. Fresh’ (Fig. 3.3).

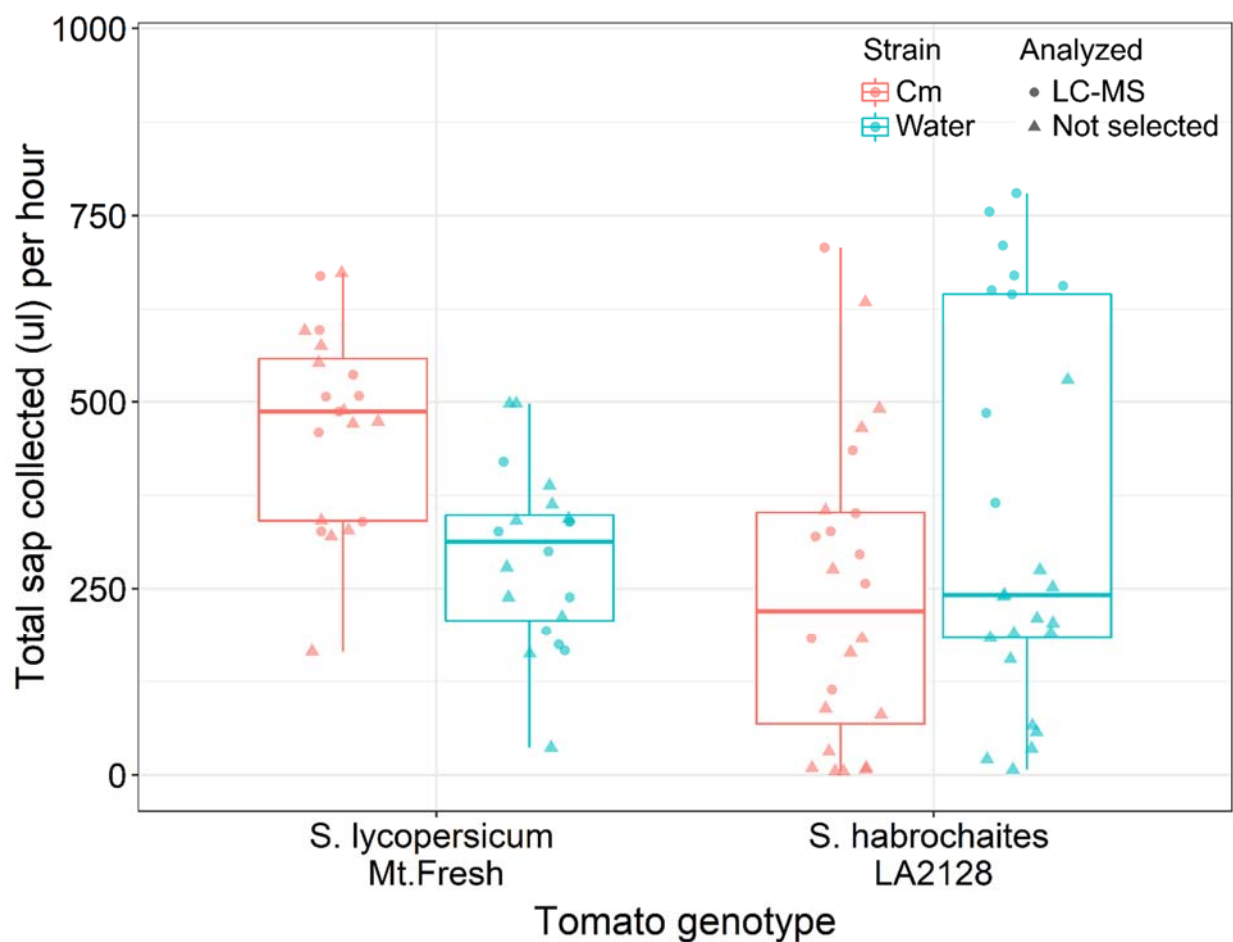


**FIGURE 3.2.** Total amount of sap collected from *S. lycopersicum* ‘Mt. Fresh’ and *S. habrochaites* LA2128 plants inoculated with *C. michiganensis* or water at 12 dpi divided by collection time (1.5 h). Red boxes represent *C. michiganensis*-inoculated plants and blue boxes represent water-inoculated plants. Circular points are individual plants selected for LC-MS analysis and triangle points were not analyzed using LC-MS. There were no significant differences between treatment groups within a genotype ( $P < 0.05$ ).

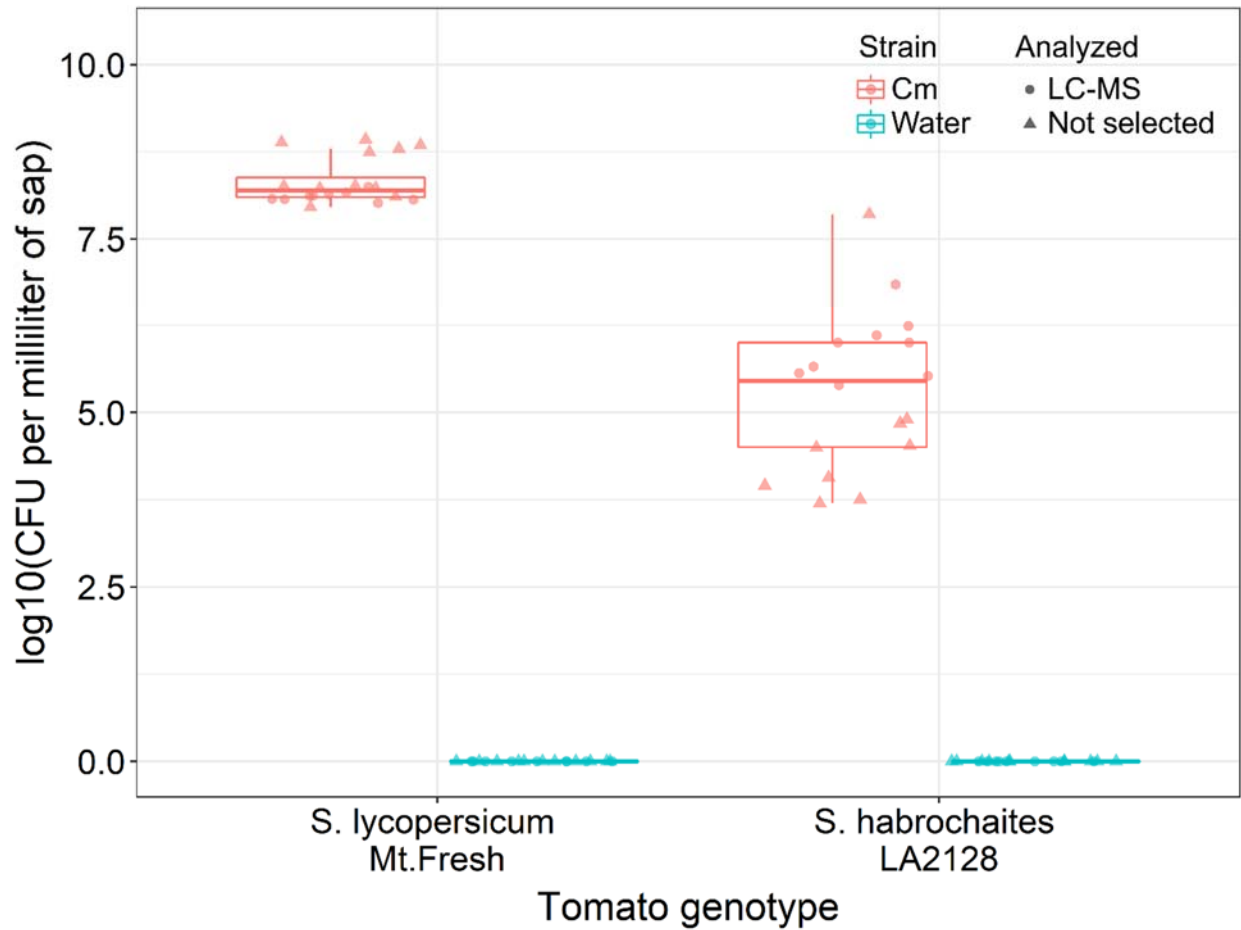


**FIGURE 3.3.** Bacterial density of *C. michiganensis* in *S. lycopersicum* ‘Mt. Fresh’ and *S. habrochaites* LA2128 sap at 12 dpi. Red boxes are from inoculated plants and blue boxes are from mock-inoculated plants. Circular points represent plants that were selected for LC-MS analysis. Triangle points were plants not selected for further analysis.

## Differential metabolite accumulation in *S. lycopersicum* ‘Mt. Fresh’ sap during *C. michiganensis* infection

To identify differentially accumulated xylem sap metabolites of *C. michiganensis* – infected cultivated tomato, we performed untargeted metabolomics to compare the chemical composition of sap between healthy and early symptomatic plants. Our approach used C18 and HILIC liquid chromatography columns in independent experiments to enrich for hydrophobic and hydrophilic compounds, respectively, and mass spectrometry was performed in both ESI positive and negative modes. Results from this experiment determined that *C. michiganensis* infection changes the chemical composition of xylem sap during early stages of disease (Fig. 3.4). Overall, 2,729 metabolites were detected using LC-MS, with 614 annotated compounds and 2,110 unknown compounds with predicted chemical structures (Fig. 3.1).

To determine differences in metabolite accumulation between healthy and infected *S. lycopersicum* ‘Mt. Fresh’ plants, PLS discriminant analyses of log<sub>2</sub>-transformed data were performed. Significant differences between healthy and infected *S. lycopersicum* ‘Mt. Fresh’ sap were identified in C18 ESI-, HILIC ESI- and HILIC ESI+ modes (Fig. 3.4 and 3.5). A Student’s *t*-test was performed on each dataset to determine which metabolites were significantly differentially accumulated ( $P_{\text{adj}} < 0.1$ ,  $\text{FC} > 1$ ) in *C. michiganensis*-infected samples (Fig. 3.5 and Table 3.1). Five of 55 significantly differentially accumulated metabolites were known compounds (Table 3.1). Among those five were tomatidine, the aglycone derivative of the defense alkaloid  $\alpha$ -tomatine (Arwiyanto et al., 1994; Kozukue et al., 2004; Kaup et al., 2005). Tomatidine was increased 106-fold in *C. michiganensis*-infected samples and was detected with the HILIC column in ESI- mode (Fig. 3.5 and Table 1). The nucleoside analog sangivamycin was reduced 0.258-fold in infected samples and was detected using the HILIC column in ESI+

mode (Fig. 3.5 and Table 1) (McCarty and Bandarian, 2008). The majority of differentially accumulated metabolites in infected *S. lycopersicum* 'Mt. Fresh' sap were negatively charged hydrophobic molecules detected using the C18 column in ESI- mode (Fig. 3.5). A majority of those metabolites (47 of 55) were increased in concentration during *C. michiganensis* infection (Fig. 3.5 and Table 3.1). Three annotated metabolites that significantly increased in C18 ESI-mode were the dipeptide  $\gamma$ -glutamylmethionine (59.5-fold increase;  $P_{\text{adj}} = 0.008$ ), the pyrimidine glycoside convicine (40.9-fold increase;  $P_{\text{adj}} = 0.055$ ), and the saccharide 2-(1-Hydroxy-4-oxo-2,5-cyclohexadien-1-yl) ethyl  $\beta$ -L-glucofuranoside (14.5-fold increase;  $P_{\text{adj}} = 0.077$ ) (Fig. 3.5 and Table 3.1).

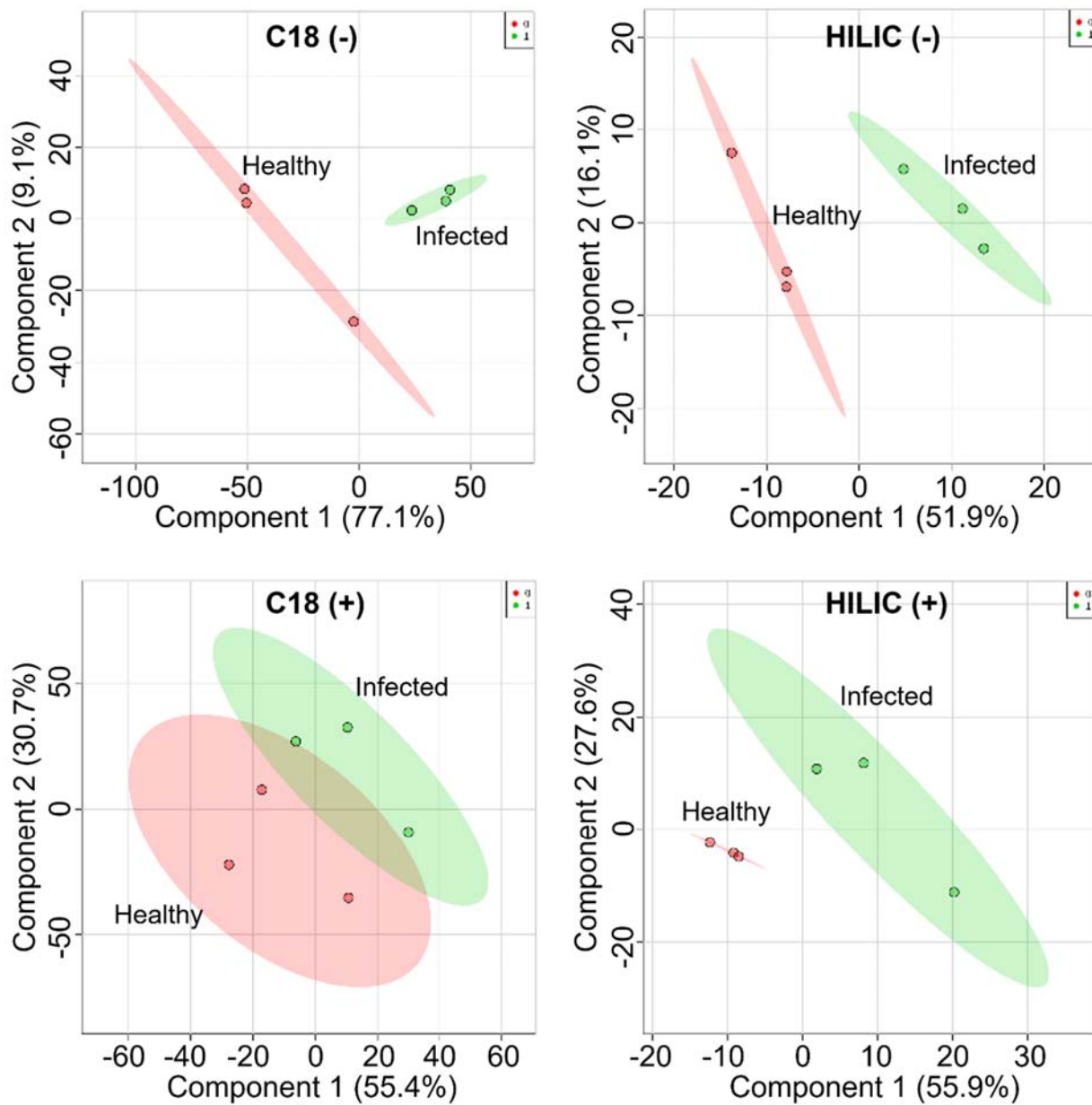


**FIGURE 3.4.** Partial least squares discriminant analysis between *S. lycopersicum* 'Mt. Fresh' healthy and infected samples by column and ionization mode ( $n = 3$  pools per treatment within column and ionization mode). Shaded areas represent 95% confidence intervals.

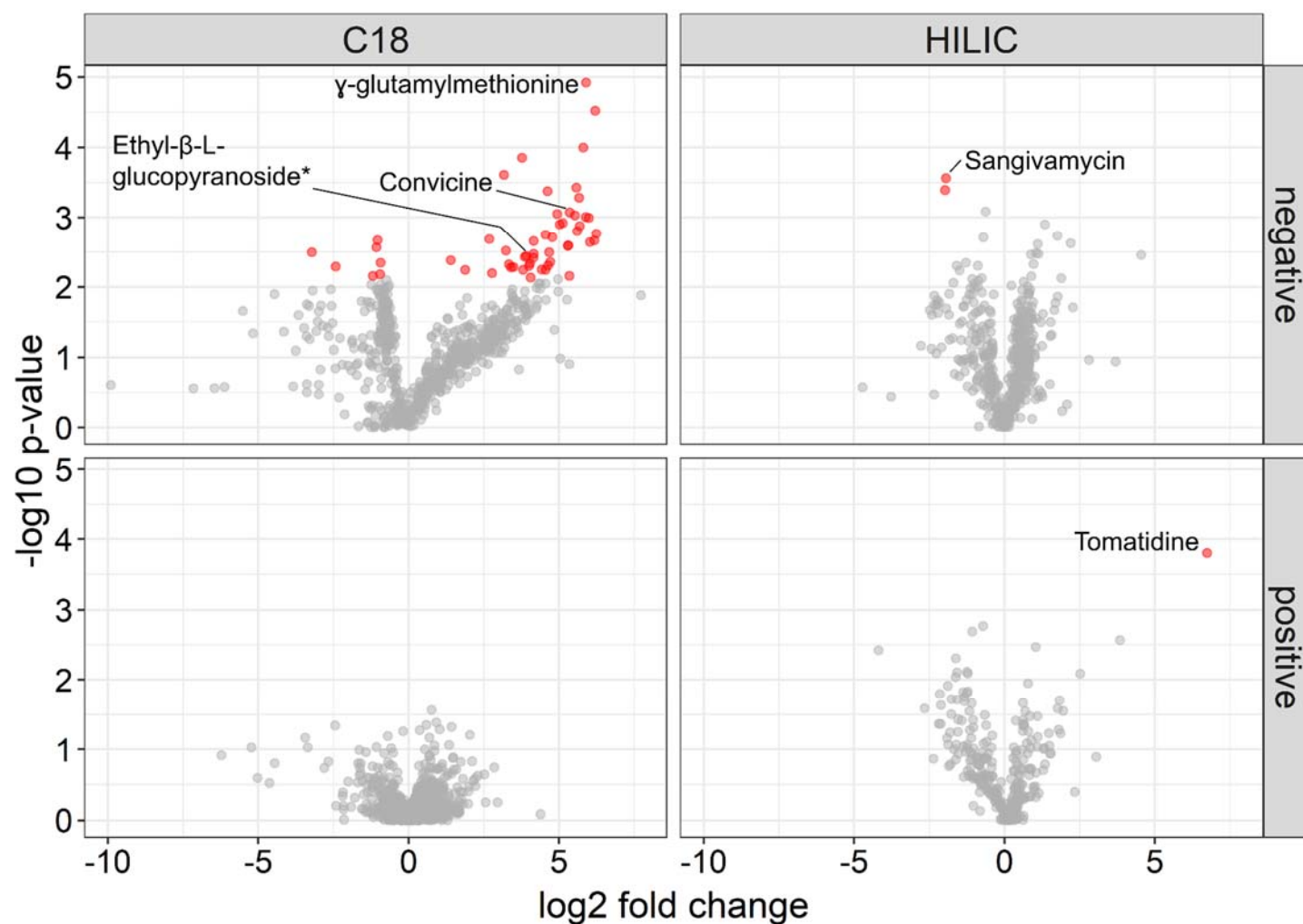


**FIGURE 3.5.** Differentially accumulated metabolites between infected and healthy *S. lycopersicum* ‘Mt. Fresh’ sap at 12 dpi. Red dots are metabolites that increased or decreased significantly ( $P_{\text{adj}} < 0.1$  and  $\log_2$  fold change  $> 1$ ) in infected sap relative to healthy sap. Grey dots represent metabolites that were not significantly differentially accumulated between treatments. Negative  $\log_{10} p$ -values shown in this graph were not FDR adjusted. Red dots without labels are metabolites with predicted formulas found in table 3.1. \*Full name of Ethyl- $\beta$ -L-glucopyranoside is located in table 3.1.

**TABLE 3.1.** Significantly differentially accumulated metabolites in infected *S. lycopersicum* ‘Mt. Fresh’ sap relative to healthy sap 12 days post inoculation.

Mass ID	Detected MW	RT <sub>min</sub>	Column	Ion mode	FC	Log <sub>2</sub> FC	P <sub>adj</sub>
Tomatidine	415.344	1.414	HILIC	ESI+	105.96	6.72	0.048
C <sub>5</sub> H <sub>2</sub> NO <sub>2</sub> P <sub>3</sub> S <sub>3</sub>	296.845	1.109	C18	ESI-	75.45	6.23	0.064
C <sub>11</sub> H <sub>7</sub> Cl <sub>2</sub> O <sub>16</sub> P <sub>3</sub> S <sub>5</sub>	717.692	1.103	C18	ESI-	73.32	6.19	0.010
C <sub>4</sub> H <sub>2</sub> NO <sub>5</sub> P <sub>3</sub> S <sub>4</sub>	364.802	1.107	C18	ESI-	72.22	6.17	0.064
C <sub>3</sub> H <sub>2</sub> NO <sub>4</sub> P <sub>3</sub> S <sub>3</sub>	304.834	1.111	C18	ESI-	64.86	6.01	0.064
C <sub>3</sub> H <sub>5</sub> ClN <sub>2</sub> O <sub>6</sub> P <sub>2</sub> S <sub>5</sub>	421.793	1.109	C18	ESI-	63.25	5.98	0.055
γ-glutamylmethionine	278.093	2.759	C18	ESI-	59.52	5.89	0.008
C <sub>5</sub> H <sub>2</sub> NOP <sub>3</sub> S <sub>4</sub>	312.823	1.111	C18	ESI-	59.10	5.88	0.055
C <sub>6</sub> H <sub>2</sub> N <sub>6</sub> O <sub>3</sub>	206.018	8.676	C18	ESI-	55.74	5.80	0.023
C <sub>4</sub> H <sub>2</sub> ClN <sub>4</sub> O <sub>5</sub> P <sub>3</sub> S <sub>5</sub>	473.745	1.111	C18	ESI-	51.22	5.67	0.058
C <sub>2</sub> H <sub>3</sub> N <sub>2</sub> O <sub>3</sub> PS <sub>5</sub>	293.849	1.108	C18	ESI-	50.58	5.6	0.046
C <sub>2</sub> H <sub>6</sub> Cl <sub>3</sub> OP <sub>3</sub> S	275.849	1.108	C18	ESI-	48.40	5.59	0.064
C <sub>7</sub> HN <sub>3</sub> O <sub>2</sub> P <sub>2</sub>	220.953	8.673	C18	ESI-	47.61	5.57	0.042
C <sub>7</sub> H <sub>4</sub> NO <sub>2</sub> P <sub>3</sub> S <sub>2</sub>	290.889	1.102	C18	ESI-	46.04	5.52	0.055
Convicine	305.085	2.709	C18	ESI-	40.90	5.35	0.055
C <sub>5</sub> H <sub>4</sub> BrCl <sub>2</sub> OP	259.857	1.145	C18	ESI-	40.53	5.34	0.093
C <sub>12</sub> H <sub>5</sub> ClO <sub>12</sub> P <sub>2</sub> S <sub>5</sub>	597.756	1.104	C18	ESI-	39.39	5.29	0.068
C <sub>45</sub> H <sub>86</sub> Cl <sub>3</sub> N	745.581	1.107	C18	ESI-	39.09	5.28	0.068
C <sub>9</sub> H <sub>3</sub> ClO <sub>2</sub> S <sub>5</sub>	337.842	1.142	C18	ESI-	34.80	5.12	0.058
C <sub>2</sub> H <sub>6</sub> ClO <sub>6</sub> P <sub>3</sub> S	285.878	1.103	C18	ESI-	32.46	5.02	0.058
C <sub>14</sub> H <sub>2</sub> BrO <sub>2</sub> P <sub>3</sub> S	405.815	1.104	C18	ESI-	30.55	4.93	0.055
C <sub>6</sub> HO <sub>9</sub> P <sub>3</sub> S <sub>4</sub>	437.770	1.106	C18	ESI-	27.33	4.77	0.064
C <sub>26</sub> H <sub>30</sub> N <sub>2</sub> O <sub>12</sub> S	594.153	2.791	C18	ESI-	26.08	4.70	0.082
C <sub>3</sub> H <sub>3</sub> ClN <sub>2</sub> O <sub>10</sub> P <sub>2</sub> S <sub>5</sub>	355.868	1.099	C18	ESI-	25.49	4.67	0.072
C <sub>7</sub> H <sub>3</sub> ClO <sub>3</sub> S <sub>2</sub>	233.921	18.60	C18	ESI-	24.72	4.62	0.082
C <sub>9</sub> H <sub>2</sub> O <sub>6</sub> S	237.956	8.671	C18	ESI-	24.42	4.61	0.042
C <sub>23</sub> H <sub>22</sub> N <sub>4</sub> O <sub>5</sub>	434.157	8.718	C18	ESI-	23.44	4.55	0.082
C <sub>13</sub> H <sub>9</sub> Cl <sub>2</sub> O <sub>16</sub> P <sub>3</sub> S <sub>4</sub>	711.736	1.096	C18	ESI-	23.42	4.54	0.064
C <sub>2</sub> H <sub>7</sub> ClO <sub>11</sub> P <sub>2</sub> S <sub>3</sub>	399.833	1.127	C18	ESI-	21.40	4.41	0.082
C <sub>4</sub> H <sub>3</sub> Cl <sub>2</sub> N <sub>4</sub> P <sub>3</sub>	269.893	1.134	C18	ESI-	17.80	4.15	0.064
C <sub>49</sub> H <sub>96</sub> Cl <sub>2</sub> NO <sub>3</sub> P	847.650	1.102	C18	ESI-	17.74	4.14	0.074
C <sub>6</sub> HO <sub>14</sub> PS <sub>3</sub>	423.8252	1.100	C18	ESI-	17.60	4.13	0.077
C <sub>5</sub> H <sub>4</sub> ClN <sub>2</sub> O <sub>7</sub> P <sub>3</sub>	331.893	1.127	C18	ESI-	16.59	4.05	0.096
CHClN <sub>2</sub> O <sub>5</sub> P <sub>2</sub>	217.905	1.152	C18	ESI-	16.38	4.03	0.082
C <sub>2</sub> H <sub>4</sub> ClN <sub>4</sub> O <sub>9</sub> P <sub>3</sub> S <sub>4</sub>	483.775	1.108	C18	ESI-	15.92	3.99	0.082
C <sub>2</sub> HN <sub>2</sub> O <sub>4</sub> P <sub>3</sub> S	241.887	1.111	C18	ESI-	15.08	3.91	0.077
2-(1-Hydroxy-4-oxo-2,5-cyclohexadien-1-yl)ethyl β-L-glucopyranoside	316.115	6.829	C18	ESI-	14.46	3.85	0.077

C <sub>5</sub> H <sub>8</sub> N <sub>5</sub> O <sub>4</sub> PS	265.004	2.782	C18	ESI-	13.90	3.79	0.082
C <sub>3</sub> H <sub>2</sub> N <sub>4</sub> O <sub>7</sub> P <sub>2</sub> S <sub>3</sub>	363.856	1.102	C18	ESI-	13.58	3.76	0.024
C <sub>3</sub> H <sub>4</sub> NP <sub>3</sub>	146.955	1.186	C18	ESI-	11.14	3.47	0.082
C <sub>4</sub> H <sub>8</sub> O <sub>6</sub>	152.032	2.544	C18	ESI-	10.51	3.39	0.082
C <sub>4</sub> H <sub>8</sub> ClO <sub>5</sub> P <sub>3</sub>	263.928	1.149	C18	ESI-	10.07	3.33	0.082
C <sub>8</sub> H <sub>2</sub> O <sub>8</sub> P <sub>2</sub> S <sub>4</sub>	415.810	1.132	C18	ESI-	9.38	3.23	0.072
C <sub>9</sub> H <sub>2</sub> O <sub>6</sub> P <sub>2</sub> S <sub>3</sub>	363.849	1.133	C18	ESI-	8.99	3.16	0.034
C <sub>4</sub> H <sub>5</sub> Cl <sub>2</sub> N <sub>4</sub> O <sub>2</sub> P	241.953	1.167	C18	ESI-	6.83	2.77	0.090
C <sub>6</sub> H <sub>2</sub> N <sub>6</sub> P <sub>2</sub> S <sub>4</sub>	347.871	1.128	C18	ESI-	6.39	2.67	0.064
C <sub>19</sub> H <sub>26</sub> N <sub>4</sub> O <sub>3</sub>	358.198	9.215	C18	ESI-	3.65	1.87	0.082
C <sub>19</sub> H <sub>32</sub> O <sub>9</sub>	404.204	9.217	C18	ESI-	2.62	1.39	0.081
C <sub>10</sub> H <sub>18</sub> O <sub>6</sub>	234.109	6.976	C18	ESI-	0.486	-1.04	0.064
C <sub>3</sub> H <sub>5</sub> ClN <sub>8</sub> O	204.027	1.199	C18	ESI-	0.473	-1.07	0.068
C <sub>11</sub> H <sub>11</sub> N <sub>2</sub> O <sub>8</sub> P <sub>3</sub> S <sub>3</sub>	487.888	1.055	C18	ESI-	0.435	-1.19	0.093
Sangivamycin	308.106	7.508	HILIC	ESI-	0.258	-1.95	0.960
C <sub>7</sub> H <sub>18</sub> ClN <sub>9</sub> O <sub>4</sub>	327.116	7.644	HILIC	ESI-	0.253	-1.98	0.960
C <sub>12</sub> H <sub>23</sub> ClN <sub>2</sub> O <sub>4</sub> P <sub>2</sub> S	388.052	1.200	C18	ESI-	0.185	-2.43	0.082
C <sub>12</sub> H <sub>6</sub> ClO <sub>14</sub> PS <sub>2</sub>	503.862	1.107	C18	ESI-	0.107	-3.22	0.072

MW = Molecular weight; RT = retention time; FC = fold change;  $P_{\text{adj}}$  = FDR-adjusted  $P$  values calculated within each column-ion mode combination.

## Differential metabolite accumulation in *S. habrochaites* LA2128 sap during *C. michiganensis* infection

Untargeted metabolomics was performed on sap samples of healthy and infected *S. habrochaites* LA2128 plants to detect differentially accumulated xylem sap metabolites. This experiment was designed to gain insight into the chemical responses of tolerant, wild tomatoes to *C. michiganensis* infection and how these responses differ to those of susceptible *S. lycopersicum*. *Solanum habrochaites* LA2128 sap samples were analyzed with C18 and HILIC columns in ESI positive and negative modes. Results from this experiment determined that there are changes in sap metabolite concentrations despite no wilt or canker symptoms developing at 12 dpi (Figs. 3.6 and 3.7).

To determine statistical differences in xylem sap metabolite accumulation between healthy and infected *S. habrochaites* LA2128 plants, PLS discriminant analyses of log<sub>2</sub>-transformed data were performed. The only class of significantly differentially accumulated metabolites were negatively charged, hydrophobic molecules detected with the C18 column in ESI negative mode (Figs. 3.6 and 3.7). Contrary to what was observed in *C. michiganensis*-infected *S. lycopersicum* ‘Mt. Fresh’ sap, the majority of significantly differentially accumulated *S. habrochaites* LA2128 sap metabolites (82 of 87) decreased in concentration in plants infected with *C. michiganensis* (Fig. 3.7 and Table 3.2). A Student’s *t*-test was performed on each dataset to determine which metabolites were significantly differentially accumulated ( $P_{\text{adj}} < 0.1$ ,  $\text{FC} > 1$ ) in *C. michiganensis*-infected samples (Fig. 3.7 and Table 3.2). Eight of 87 significantly differentially accumulated metabolites had predicted compounds (Fig. 3.7 and Table 3.2). Five acidic molecules had significantly reduced concentrations in sap from *C. michiganensis*-infected *S. habrochaites* LA2128 plants: the amino acid derivative L-pyroglutamic acid (0.41-fold

decrease;  $P_{\text{adj}} = 0.047$ ); phosphor-1-aminoethyl-2-carboxypropylphosphinic acid (0.02-fold decrease;  $P_{\text{adj}} = 0.017$ ); ( $\pm$ )-malic acid (0.03-fold decrease;  $P_{\text{adj}} = 0.019$ ); N-acetyl-L-glutamic acid (0.12-fold decrease;  $P_{\text{adj}} = 0.074$ ); and trans-aconitic acid (0.04-fold decrease;  $P_{\text{adj}} = 0.098$ ) (Fig. 3.7 and Table 3.2). The remaining three differentially accumulated molecules were the terpene sweroside (0.12-fold decrease;  $P_{\text{adj}} = 0.061$ ), the antimicrobial sulfadimethoxine (0.26-fold decrease;  $P_{\text{adj}} = 0.098$ ), and 4-butoxy methyl-2-methoxyphenol (i.e. vanillyl butyl ether) (0.10-fold decrease;  $P_{\text{adj}} = 0.056$ ) (Fig. 3.7 and Table 3.2).

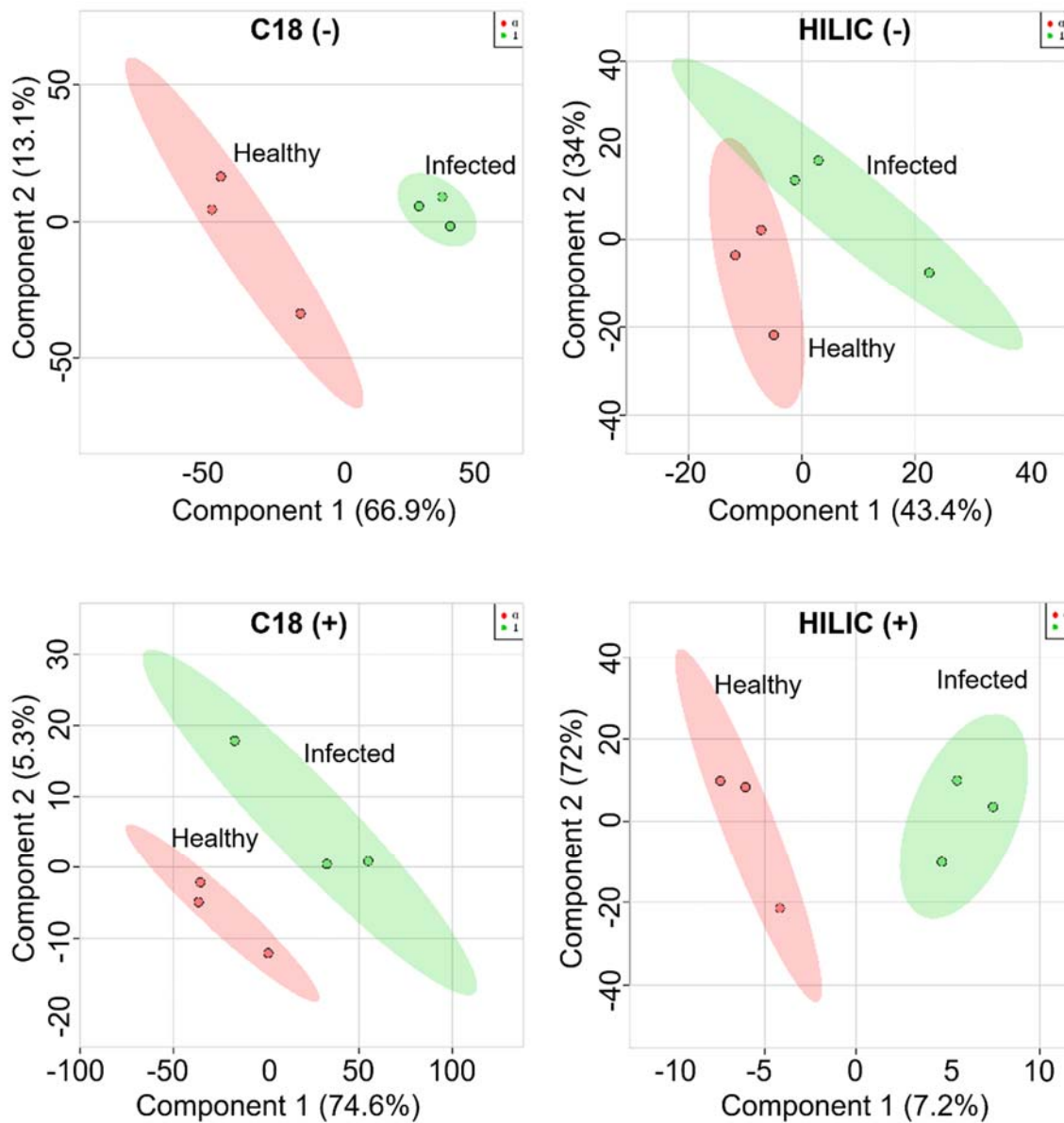


**FIGURE 3.6.** Partial least squares discriminant analysis between *S. habrochaites* LA2128 healthy and infected samples by column and ionization mode ( $n = 3$  per treatment within column and ionization mode). Shaded areas represent 95% confidence intervals.

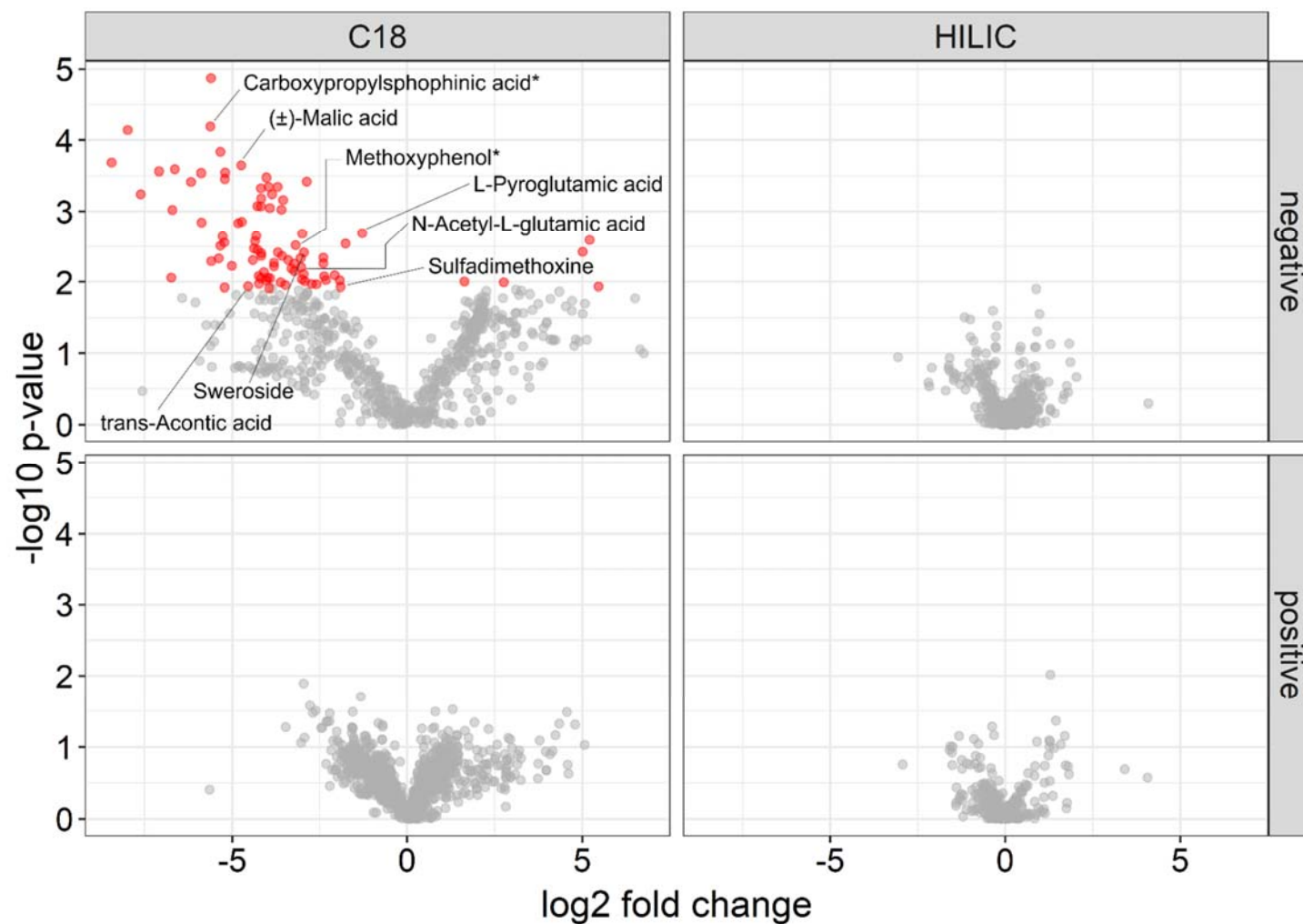


**FIGURE 3.7.** Differentially accumulated metabolites between infected and healthy *S. habrochaites* LA2128 sap at 12 dpi. Red dots are metabolites that increased or decreased significantly ( $P_{\text{adj}} < 0.1$  and  $\log_2$  fold change  $> 1$ ) in infected sap relative to healthy sap. Grey dots represent metabolites that were not significantly differentially accumulated between treatments. Negative  $\log_{10} p$ -values shown in this graph were not FDR adjusted. Red dots without labels are metabolites with predicted formulas found in table 3.1. \*Full name of metabolites with asterisks are located in table 3.2.

**TABLE 3.2.** Significantly differentially accumulated metabolites in infected *S. habrochaites* LA2128 sap relative to healthy sap 12 days post inoculation.

Mass ID	Detected MW	RT <sub>min</sub>	Column	Ion mode	FC	Log <sub>2</sub> FC	P <sub>adj</sub>
C <sub>7</sub> H <sub>18</sub> N <sub>6</sub> O <sub>8</sub>	314.120	1.185	C18	ESI-	44.00	5.45	0.098
C <sub>2</sub> H <sub>6</sub> O <sub>17</sub>	301.960	1.184	C18	ESI-	37.08	5.21	0.053
C <sub>2</sub> H <sub>5</sub> CIN <sub>2</sub> O <sub>18</sub>	379.921	1.109	C18	ESI-	32.20	5.00	0.061
C <sub>9</sub> H <sub>18</sub> N <sub>4</sub> O <sub>6</sub>	278.122	1.191	C18	ESI-	6.782	2.76	0.092
C <sub>19</sub> H <sub>28</sub> O <sub>12</sub>	448.157	6.917	C18	ESI-	3.105	1.63	0.092
L-Pyroglutamic acid	129.042	2.35	C18	ESI-	0.410	-1.28	0.047
C <sub>6</sub> H <sub>3</sub> N <sub>9</sub> O <sub>7</sub> S	344.988	1.232	C18	ESI-	0.294	-1.76	0.055
Sulfadimethoxine	310.073	9.068	C18	ESI-	0.267	-1.90	0.098
C <sub>13</sub> H <sub>14</sub> N <sub>6</sub> O <sub>10</sub> S	446.04	9.069	C18	ESI-	0.263	-1.92	0.091
C <sub>8</sub> H <sub>10</sub> CIN <sub>7</sub> S <sub>4</sub>	366.95	1.232	C18	ESI-	0.238	-2.06	0.089
C <sub>3</sub> H <sub>9</sub> N <sub>4</sub> OP	148.051	2.814	C18	ESI-	0.199	-2.32	0.091
C <sub>4</sub> H <sub>12</sub> CIN <sub>3</sub> O <sub>12</sub>	329.010	1.24	C18	ESI-	0.193	-2.37	0.089
C <sub>14</sub> H <sub>9</sub> O <sub>4</sub> P <sub>3</sub> S	365.944	1.173	C18	ESI-	0.190	-2.39	0.069
C <sub>13</sub> H <sub>14</sub> N <sub>4</sub> O <sub>5</sub> S	338.068	8.917	C18	ESI-	0.189	-2.39	0.066
CH <sub>3</sub> CIN <sub>2</sub> O <sub>11</sub> P <sub>2</sub>	315.890	1.144	C18	ESI-	0.165	-2.59	0.094
C <sub>3</sub> H <sub>11</sub> N <sub>3</sub> O <sub>13</sub> S	329.001	1.256	C18	ESI-	0.150	-2.73	0.094
C <sub>10</sub> H <sub>22</sub> N <sub>8</sub> O <sub>6</sub> S <sub>4</sub>	478.054	1.228	C18	ESI-	0.136	-2.87	0.019
C <sub>8</sub> H <sub>17</sub> N <sub>2</sub> OP <sub>3</sub>	250.05	2.798	C18	ESI-	0.131	-2.92	0.092
Sweroside	358.126	7.995	C18	ESI-	0.129	-2.95	0.061
C <sub>11</sub> H <sub>5</sub> NO <sub>3</sub> S	230.998	1.828	C18	ESI-	0.128	-2.95	0.087
C <sub>6</sub> H <sub>10</sub> N <sub>6</sub> O <sub>4</sub>	230.076	6.432	C18	ESI-	0.124	-3.00	0.047
C <sub>7</sub> H <sub>12</sub> N <sub>6</sub> O <sub>4</sub>	244.091	7.553	C18	ESI-	0.124	-3.00	0.091
N-Acetyl-L-glutamic acid	189.062	1.830	C18	ESI-	0.122	-3.03	0.074
C <sub>8</sub> H <sub>16</sub> N <sub>2</sub> O <sub>9</sub>	284.085	1.349	C18	ESI-	0.120	-3.04	0.066
4-(Butoxymethyl)-2-methoxyphenol	210.124	9.462	C18	ESI-	0.109	-3.18	0.056
C <sub>13</sub> H <sub>18</sub> N <sub>2</sub> O <sub>10</sub>	362.095	2.547	C18	ESI-	0.107	-3.22	0.082
C <sub>4</sub> H <sub>2</sub> CIN <sub>6</sub> OP <sub>3</sub> S <sub>5</sub>	437.779	1.130	C18	ESI-	0.106	-3.22	0.069
C <sub>22</sub> H <sub>36</sub> O <sub>10</sub>	460.230	9.223	C18	ESI-	0.100	-3.30	0.077
C <sub>12</sub> H <sub>28</sub> N <sub>2</sub> O <sub>3</sub> P <sub>2</sub> S	342.131	7.161	C18	ESI-	0.094	-3.40	0.067
CHCIN <sub>2</sub> O <sub>5</sub> P <sub>2</sub>	217.905	1.152	C18	ESI-	0.089	-3.48	0.096
C <sub>5</sub> H <sub>8</sub> NO <sub>9</sub> PS	288.964	1.874	C18	ESI-	0.085	-3.54	0.023
C <sub>23</sub> H <sub>36</sub> N <sub>4</sub> O <sub>10</sub>	528.241	6.761	C18	ESI-	0.083	-3.57	0.065
C <sub>5</sub> H <sub>8</sub> O <sub>9</sub> S	243.988	1.816	C18	ESI-	0.083	-3.59	0.025
C <sub>7</sub> HO <sub>6</sub> P <sub>3</sub> S <sub>3</sub>	369.813	1.374	C18	ESI-	0.081	-3.61	0.092
C <sub>8</sub> H <sub>22</sub> N <sub>4</sub> O <sub>10</sub> P <sub>2</sub> S	428.052	1.227	C18	ESI-	0.077	-3.69	0.061
C <sub>16</sub> H <sub>24</sub> N <sub>4</sub> O <sub>3</sub> S <sub>2</sub>	384.129	2.538	C18	ESI-	0.076	-3.70	0.019
C <sub>12</sub> H <sub>19</sub> N <sub>4</sub> O <sub>2</sub> P <sub>3</sub>	344.071	2.62	C18	ESI-	0.071	-3.80	0.069
CH <sub>4</sub> N <sub>2</sub> O <sub>8</sub> S <sub>5</sub>	331.857	1.371	C18	ESI-	0.071	-3.81	0.074

C <sub>8</sub> H <sub>5</sub> N <sub>3</sub> O <sub>6</sub> P <sub>2</sub>	300.964	1.868	C18	ESI-	0.068	-3.86	0.021
C <sub>7</sub> H <sub>8</sub> N <sub>2</sub> O <sub>3</sub> S <sub>2</sub>	231.997	1.6	C18	ESI-	0.066	-3.91	0.09
C <sub>12</sub> H <sub>2</sub> ClOP <sub>3</sub> S <sub>3</sub>	385.817	1.133	C18	ESI-	0.065	-3.92	0.025
C <sub>6</sub> H <sub>14</sub> N <sub>2</sub> O <sub>5</sub> S <sub>2</sub>	258.034	2.555	C18	ESI-	0.064	-3.94	0.099
C <sub>59</sub> H <sub>124</sub> N <sub>5</sub> O <sub>3</sub> P <sub>3</sub> S <sub>4</sub>	1171.78	2.273	C18	ESI-	0.064	-3.96	0.019
C <sub>5</sub> H <sub>4</sub> N <sub>6</sub> O <sub>2</sub> P <sub>2</sub>	241.987	2.625	C18	ESI-	0.062	-3.99	0.090
C <sub>13</sub> H <sub>6</sub> N <sub>2</sub> O <sub>9</sub> P <sub>2</sub> S <sub>5</sub>	555.815	1.082	C18	ESI-	0.061	-4.02	0.091
C <sub>6</sub> H <sub>12</sub> N <sub>4</sub> O <sub>8</sub> S <sub>3</sub>	363.982	1.236	C18	ESI-	0.061	-4.02	0.019
C <sub>5</sub> H <sub>8</sub> N <sub>5</sub> O <sub>4</sub> PS	265.004	2.782	C18	ESI-	0.058	-4.09	0.083
C <sub>3</sub> H <sub>4</sub> ClPS	137.946	1.111	C18	ESI-	0.055	-4.16	0.065
C <sub>6</sub> H <sub>7</sub> N <sub>3</sub> O <sub>10</sub> P <sub>2</sub>	342.960	1.817	C18	ESI-	0.055	-4.17	0.062
C <sub>19</sub> H <sub>15</sub> N <sub>2</sub> O <sub>7</sub> PS <sub>2</sub>	478.004	2.777	C18	ESI-	0.055	-4.17	0.023
C <sub>8</sub> H <sub>10</sub> O <sub>5</sub> P <sub>2</sub>	248.001	2.833	C18	ESI-	0.055	-4.17	0.025
C <sub>6</sub> H <sub>11</sub> O <sub>12</sub> P	305.998	1.605	C18	ESI-	0.055	-4.18	0.090
C <sub>20</sub> H <sub>12</sub> N <sub>7</sub> O <sub>3</sub> P	429.074	2.826	C18	ESI-	0.055	-4.18	0.019
C <sub>2</sub> H <sub>3</sub> ClP <sub>2</sub> S	155.912	1.144	C18	ESI-	0.053	-4.23	0.094
C <sub>2</sub> H <sub>4</sub> ClN <sub>2</sub> PS <sub>3</sub>	217.895	1.143	C18	ESI-	0.052	-4.24	0.089
C <sub>4</sub> H <sub>6</sub> Cl <sub>2</sub> OP <sub>2</sub>	201.927	1.15	C18	ESI-	0.051	-4.27	0.060
C <sub>25</sub> H <sub>21</sub> P	352.139	2.816	C18	ESI-	0.051	-4.28	0.025
C <sub>3</sub> H <sub>6</sub> N <sub>2</sub> O <sub>2</sub> P <sub>2</sub> S <sub>2</sub>	227.934	1.138	C18	ESI-	0.050	-4.31	0.048
C <sub>3</sub> H <sub>5</sub> OP <sub>3</sub> S	181.92	1.152	C18	ESI-	0.049	-4.35	0.053
C <sub>2</sub> H <sub>4</sub> Cl <sub>2</sub> O <sub>3</sub> P <sub>2</sub> S	239.874	1.15	C18	ESI-	0.048	-4.37	0.060
C <sub>7</sub> H <sub>10</sub> N <sub>2</sub> O <sub>12</sub>	314.024	1.82	C18	ESI-	0.046	-4.41	0.067
trans-Aconitic acid	174.015	2.284	C18	ESI-	0.042	-4.54	0.098
C <sub>3</sub> H <sub>3</sub> N <sub>6</sub> O <sub>12</sub> P	345.954	1.813	C18	ESI-	0.037	-4.72	0.035
(±)-Malic Acid	134.021	1.613	C18	ESI-	0.037	-4.74	0.019
C <sub>3</sub> H <sub>4</sub> N <sub>2</sub> O <sub>5</sub> S <sub>2</sub>	211.956	1.135	C18	ESI-	0.035	-4.82	0.035
CH <sub>3</sub> N <sub>2</sub> O <sub>10</sub> P <sub>3</sub>	295.899	1.098	C18	ESI-	0.031	-5.00	0.074
C <sub>6</sub> H <sub>13</sub> N <sub>4</sub> O <sub>12</sub> PS <sub>2</sub>	427.969	2.279	C18	ESI-	0.027	-5.20	0.019
C <sub>9</sub> H <sub>2</sub> O <sub>8</sub> P <sub>2</sub> S <sub>3</sub>	395.838	1.126	C18	ESI-	0.026	-5.21	0.019
C <sub>6</sub> H <sub>10</sub> O <sub>11</sub> S iso	289.994	2.275	C18	ESI-	0.026	-5.21	0.098
C <sub>5</sub> H <sub>11</sub> ClN <sub>8</sub> O <sub>12</sub> S <sub>3</sub>	505.934	2.279	C18	ESI-	0.026	-5.22	0.054
CH <sub>3</sub> N <sub>2</sub> O <sub>9</sub> P <sub>3</sub> S	311.877	1.103	C18	ESI-	0.025	-5.27	0.048
C <sub>19</sub> H <sub>17</sub> N <sub>5</sub> O <sub>8</sub> S	475.080	2.794	C18	ESI-	0.024	-5.33	0.019
C <sub>13</sub> H <sub>10</sub> N <sub>2</sub> O <sub>14</sub> P <sub>2</sub> S	511.932	2.272	C18	ESI-	0.024	-5.33	0.056
C <sub>13</sub> H <sub>16</sub> N <sub>10</sub> O <sub>15</sub> P <sub>2</sub>	614.027	2.288	C18	ESI-	0.023	-5.38	0.066
C <sub>5</sub> H <sub>16</sub> N <sub>9</sub> O <sub>6</sub> P <sub>3</sub>	391.043	2.313	C18	ESI-	0.020	-5.60	0.068

C <sub>8</sub> H <sub>27</sub> ClN <sub>10</sub> O <sub>9</sub> P <sub>2</sub> S <sub>4</sub>	632.000	2.309	C18	ESI-	0.020	-5.60	0.009
Phospho(1-aminoethyl)(2-carboxypropyl)phosphinic acid	275.032	1.608	C18	ESI-	0.020	-5.62	0.017
CHN <sub>2</sub> O <sub>3</sub> P <sub>3</sub>	181.919	1.115	C18	ESI-	0.017	-5.87	0.035
C <sub>11</sub> H <sub>9</sub> N <sub>3</sub> O <sub>18</sub> S <sub>2</sub>	534.932	2.276	C18	ESI-	0.016	-5.88	0.019
C <sub>54</sub> H <sub>107</sub> N <sub>10</sub> P	926.841	2.276	C18	ESI-	0.013	-6.18	0.019
C <sub>30</sub> H <sub>17</sub> NO <sub>7</sub> P <sub>2</sub> S <sub>2</sub>	628.991	2.273	C18	ESI-	0.010	-6.63	0.019
C <sub>23</sub> H <sub>13</sub> N <sub>3</sub> O <sub>16</sub> S <sub>2</sub>	650.973	2.279	C18	ESI-	0.009	-6.71	0.025
CH <sub>3</sub> N <sub>2</sub> O <sub>8</sub> P <sub>3</sub>	263.909	1.115	C18	ESI-	0.009	-6.74	0.09
C <sub>26</sub> H <sub>9</sub> N <sub>2</sub> O <sub>13</sub> P <sub>3</sub> S	681.903	2.276	C18	ESI-	0.007	-7.08	0.019
C <sub>6</sub> H <sub>3</sub> N <sub>3</sub> O <sub>15</sub>	356.954	1.819	C18	ESI-	0.005	-7.61	0.021
C <sub>6</sub> H <sub>8</sub> N <sub>6</sub> O <sub>5</sub> S	276.028	1.611	C18	ESI-	0.003	-7.98	0.017
C <sub>2</sub> H <sub>8</sub> N <sub>7</sub> O <sub>18</sub> P	448.965	2.285	C18	ESI-	0.002	-8.44	0.019

MW = Molecular weight; RT = retention time; FC = fold change;  $P_{adj}$  = FDR-adjusted  $P$  values calculated within each column-ion mode combination.

## Sap metabolite differences between species

A secondary aim of this experiment was to describe the core chemical differences in healthy xylem sap composition between the wild tomato accession *S. habrochaites* LA2128 and the cultivated tomato *S. lycopersicum* ‘Mt. Fresh’. This analysis was conducted on the untargeted metabolomics data of healthy sap from both plant species. Metabolites with significantly different concentrations were identified in HILIC ESI positive and negative experiments, as well as C18 ESI negative mode (Figs. 3.8 and 3.9). In total, 192 metabolites had significantly different ( $P_{adj} < 0.1$ ,  $FC > 1$ ) concentrations in *S. lycopersicum* ‘Mt. Fresh’ sap relative to *S. habrochaites* LA2128 sap (Table 3.3).

*Solanum lycopersicum* ‘Mt. Fresh’ sap was relatively enriched in negatively charged hydrophilic molecules when compared to *S. habrochaites* LA2128 sap (Fig. 3.9). Known metabolites with the highest relative abundance ( $FC > 50$ ) in *S. lycopersicum* ‘Mt. Fresh’ sap were camphorsulfonic acid ( $FC = 216$ ,  $P_{adj} = 0.0023$ ), 4-formyl-2-methoxyphenyl hydrogen sulfate (i.e. vanillin 4-sulfate) ( $FC = 185$ ,  $P_{adj} = 0.0019$ ), uric acid ( $FC = 179$ ,  $P_{adj} = 0.0028$ ), and the plant hormone phaseic acid ( $FC = 75$ ,  $P_{adj} = 0.0045$ ) (Fig. 3.9 and Table 3.3). Twenty two metabolites were increased between 25 and 49-fold concentrations in *S. lycopersicum* ‘Mt. Fresh’ sap; notably among those were dehydroascorbic acid ( $FC = 47$ ,  $P_{adj} = 0.0017$ ), dihydrouridine ( $FC = 43$ ,  $P_{adj} = 0.0028$ ), L-threonine O-phosphate ( $FC = 43$ ,  $P_{adj} = 0.0044$ ), thymolsulfate ( $FC = 36$ ,  $P_{adj} = 0.0033$ ), 2E-abscisic acid ( $FC = 33$ ,  $P_{adj} = 0.0030$ ) (Fig. 3.9 and Table 3.3). An additional 117 metabolites were increased between 2 and 24-fold concentrations in *S. lycopersicum* ‘Mt. Fresh’ sap, 32 of which were known compounds (Table 3.3).

Metabolites that had significantly decreased concentrations in this analysis meant that they were detected in significantly higher concentrations in *S. habrochaites* LA2128 sap relative

to what was identified in *S. lycopersicum* 'Mt. Fresh' sap. Only 40 metabolites had significantly increased concentrations in *S. habrochaites* LA2128 sap, 11 of which were known compounds (Fig. 3.9 and Table 3.3). Compounds with the largest increase in *S. habrochaites* LA2128 sap were benzylmethanoate (i.e. benzyl formate) (FC = 0.035,  $P_{adj}$  = 0.068) followed by N-Acetylneuraminic acid (FC = 0.043,  $P_{adj}$  = 0.029) (Table 3.3). A full list of metabolites with significantly increased concentrations in *S. habrochaites* LA2128 sap can be found in table 3.3.

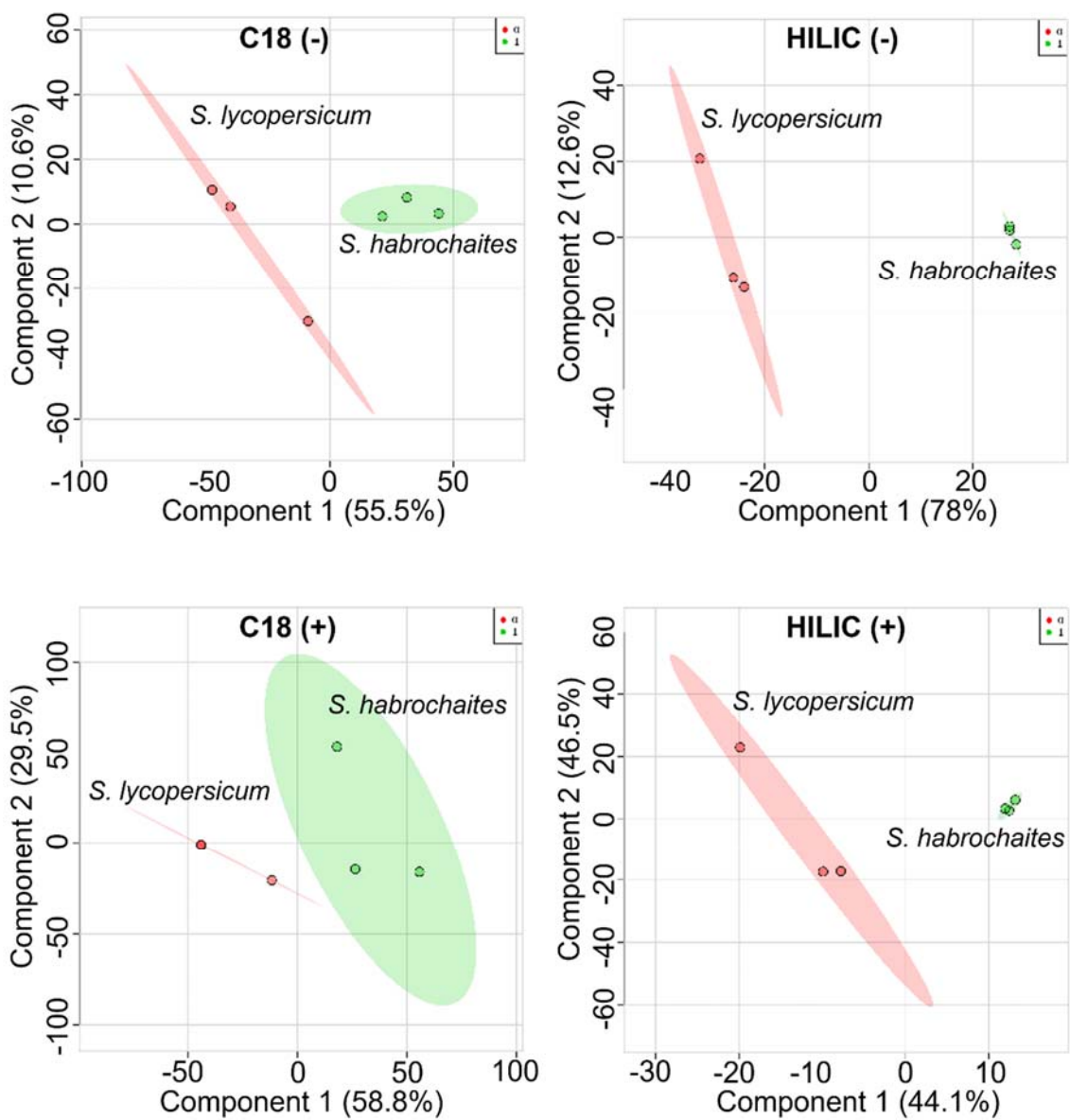


**FIGURE 3.8.** Partial least squares discriminant analysis between *S. lycopersicum* ‘Mt. Fresh’ and *S. habrochaites* LA2128 healthy sap samples by column and ionization mode ( $n = 3$  per treatment within column and ionization mode). Shaded areas represent 95% confidence intervals.

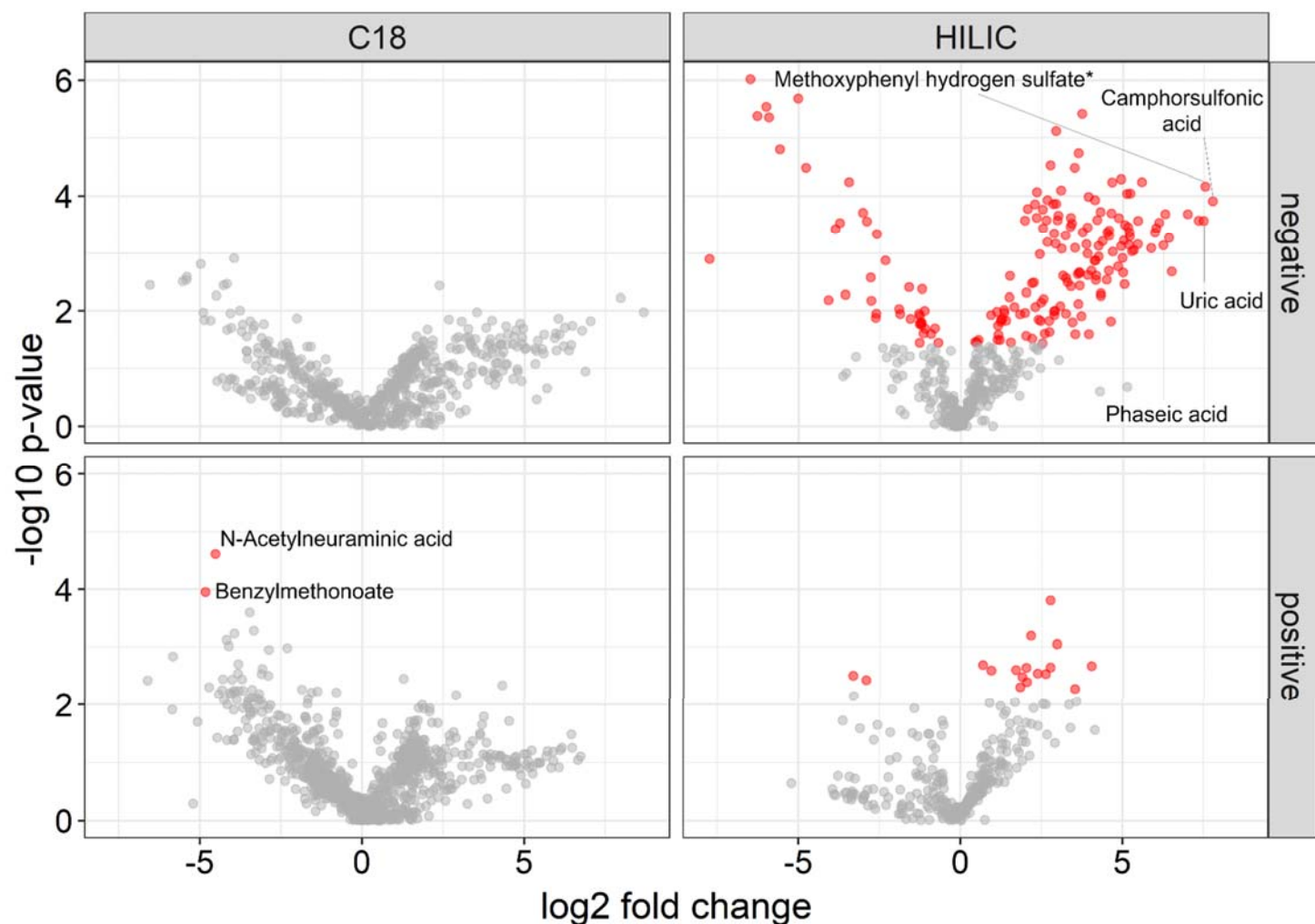


**FIGURE 3.9.** Differential abundance of metabolites between healthy *S. habrochaites* LA2128 and *S. lycopersicum* ‘Mt. Fresh’ sap. Red dots are metabolites that had significantly ( $P_{\text{adj}} < 0.1$  and  $\log_2$  fold change  $> 1$ ) higher or lower concentrations in *S. lycopersicum* ‘Mt. Fresh’ relative to *S. habrochaites* LA2128. Grey dots represent metabolites that did not have significantly different concentrations between species. Negative  $\log_{10} p$ -values shown in this graph were not FDR adjusted. Labels are only present on metabolites with significantly increased or decreased concentrations at fold change  $>50$  or  $>-50$ . All metabolite IDs can be found in table 3.3. \*Full name with an asterisk is located in table 3.3.

**TABLE 3.3.** Metabolites with significantly different concentrations in healthy sap of *S. lycopersicum* ‘Mt. Fresh’ relative to *S. habrochaites* LA2128 (eg. A positive fold change equals a higher abundance in *S. lycopersicum* ‘Mt. Fresh’ sap compared to the concentration of that metabolite in *S. habrochaites* LA2128 sap. Fold change < 1 means the metabolite was significantly more abundant in *S. habrochaites* LA2128 sap relative to *S. lycopersicum* ‘Mt. Fresh’ sap.)

Mass ID	Detected MW	RT <sub>min</sub>	Column	Ion mode	FC	Log <sub>2</sub> FC	P <sub>adj</sub>
Camphorsulfonic acid	232.076	1.344	HILIC	ESI-	216.6	7.75	0.0023
4-Formyl-2-methoxyphenyl hydrogen sulfate	232.003	1.399	HILIC	ESI-	185.3	7.53	0.0019
Uric acid	168.027	8.218	HILIC	ESI-	179.0	7.48	0.0028
C <sub>10</sub> H <sub>20</sub> O <sub>5</sub> S	252.103	1.529	HILIC	ESI-	160.4	7.32	0.0028
C <sub>8</sub> H <sub>17</sub> N <sub>2</sub> O <sub>10</sub> P	332.062	9.058	HILIC	ESI-	127.6	6.99	0.0028
C <sub>6</sub> H <sub>7</sub> ClO <sub>6</sub> iso	209.992	2.324	HILIC	ESI-	89.95	6.49	0.0103
C <sub>10</sub> H <sub>18</sub> O <sub>4</sub> S	234.092	1.314	HILIC	ESI-	84.98	6.40	0.0037
C <sub>13</sub> H <sub>17</sub> ClO <sub>7</sub>	320.066	2.403	HILIC	ESI-	78.55	6.29	0.0028
Phaseic acid	280.131	2.304	HILIC	ESI-	75.45	6.23	0.0045
C <sub>15</sub> H <sub>6</sub> N <sub>4</sub> O <sub>8</sub>	370.018	9.060	HILIC	ESI-	69.22	6.11	0.0028
C <sub>10</sub> H <sub>20</sub> N <sub>6</sub> O <sub>7</sub> S	368.112	7.621	HILIC	ESI-	64.80	6.01	0.0031
C <sub>8</sub> H <sub>6</sub> ClN <sub>8</sub> O <sub>8</sub> P	407.974	9.051	HILIC	ESI-	63.21	5.98	0.0033
C <sub>8</sub> H <sub>18</sub> O <sub>6</sub> P <sub>2</sub> S	304.030	9.207	HILIC	ESI-	58.17	5.86	0.0048
Dehydroascorbic acid	174.015	7.731	HILIC	ESI-	47.87	5.58	0.0017
Dihydrouridine	246.085	5.592	HILIC	ESI-	43.88	5.45	0.0028
L-Threonine O-phosphate	199.024	7.377	HILIC	ESI-	43.76	5.45	0.0044
C <sub>14</sub> H <sub>22</sub> N <sub>3</sub> PS	295.126	7.553	HILIC	ESI-	40.17	5.32	0.0050
C <sub>18</sub> H <sub>30</sub> O <sub>8</sub>	374.194	2.216	HILIC	ESI-	38.57	5.26	0.0052
C <sub>7</sub> H <sub>18</sub> ClN <sub>9</sub> O <sub>4</sub>	327.116	7.644	HILIC	ESI-	37.30	5.22	0.0020
C <sub>8</sub> H <sub>7</sub> Cl <sub>2</sub> N <sub>8</sub> O <sub>8</sub> P	443.950	9.069	HILIC	ESI-	36.79	5.20	0.0036
Thymol sulfate	230.060	1.384	HILIC	ESI-	36.58	5.19	0.0033
C <sub>7</sub> H <sub>15</sub> N <sub>2</sub> O <sub>10</sub> P	318.046	9.143	HILIC	ESI-	36.12	5.17	0.0045
C <sub>18</sub> H <sub>30</sub> O <sub>7</sub>	358.199	2.278	HILIC	ESI-	35.58	5.15	0.0031
C <sub>9</sub> H <sub>21</sub> NO <sub>5</sub> P <sub>2</sub> S	317.062	9.048	HILIC	ESI-	34.66	5.112	0.0020
2E-Abscisic acid	264.136	2.112	HILIC	ESI-	33.34	5.05	0.0030
C <sub>14</sub> H <sub>18</sub> N <sub>2</sub> P <sub>2</sub>	276.095	7.820	HILIC	ESI-	32.90	5.04	0.0147
C <sub>8</sub> H <sub>18</sub> O <sub>5</sub> S	226.087	1.898	HILIC	ESI-	32.48	5.02	0.0041
Prostaglandin G22-glycerylester	442.256	2.278	HILIC	ESI-	31.90	4.99	0.0105
C <sub>10</sub> H <sub>14</sub> O <sub>6</sub> S	262.051	1.556	HILIC	ESI-	31.52	4.97	0.0065
C <sub>7</sub> H <sub>14</sub> O <sub>5</sub> S	210.055	1.372	HILIC	ESI-	30.55	4.93	0.0045

2,6-Bis(2-methyl-2-propanyl)-1,4-benzoquinone	220.146	2.112	HILIC	ESI-	30.53	4.93	0.0017
C <sub>4</sub> H <sub>7</sub> ClN <sub>10</sub> O <sub>2</sub> S	294.017	8.366	HILIC	ESI-	29.22	4.86	0.0028
C <sub>6</sub> H <sub>7</sub> N <sub>2</sub> OP	154.029	1.870	HILIC	ESI-	28.72	4.84	0.0086
C <sub>10</sub> H <sub>14</sub> O <sub>5</sub> S	246.056	2.218	HILIC	ESI-	25.63	4.68	0.0053
C <sub>7</sub> H <sub>14</sub> ClNO <sub>4</sub>	210.055	1.372	HILIC	ESI-	25.27	4.65	0.0017
345-Trihydroxy-1-cyclohexenecarboxylic acid	174.052	8.774	HILIC	ESI-	24.85	4.63	0.0028
Kresoxim-methyl	313.131	1.599	HILIC	ESI-	24.54	4.61	0.0465
C <sub>20</sub> H <sub>17</sub> N <sub>5</sub> O	343.141	1.542	HILIC	ESI-	23.79	4.57	0.0035
C <sub>10</sub> H <sub>12</sub> N <sub>7</sub> OP	277.084	7.553	HILIC	ESI-	23.77	4.57	0.0033
N-lactoyl ethanolamine phosphate	213.039	7.382	HILIC	ESI-	23.60	4.56	0.0100
3-O-3-Methylbutanoyl-beta-D-fructofuranosyl2-O-acetyl-3-O-2-methylbutanoyl-alpha-D-glucopyranoside	594.288	1.346	HILIC	ESI-	22.79	4.51	0.0033
Alpha-methyl D-mannoside	194.078	7.832	HILIC	ESI-	22.52	4.49	0.0128
C <sub>2</sub> H <sub>5</sub> Cl <sub>3</sub> N <sub>8</sub> O <sub>17</sub>	517.883	9.065	HILIC	ESI-	20.60	4.36	0.0041
C <sub>8</sub> H <sub>16</sub> O <sub>5</sub> S	224.071	1.425	HILIC	ESI-	19.85	4.31	0.02011
C <sub>13</sub> H <sub>15</sub> ClP <sub>2</sub>	268.035	2.000	HILIC	ESI-	19.82	4.30	0.0219
C <sub>8</sub> H <sub>10</sub> N <sub>10</sub> S	278.080	7.572	HILIC	ESI-	19.75	4.30	0.0028
C <sub>11</sub> H <sub>5</sub> ClO <sub>13</sub>	379.942	9.218	HILIC	ESI-	18.97	4.24	0.0045
C <sub>7</sub> H <sub>4</sub> ClN <sub>8</sub> O <sub>8</sub> P	393.958	9.142	HILIC	ESI-	18.90	4.24	0.0062
C <sub>6</sub> H <sub>14</sub> N <sub>3</sub> O <sub>9</sub> P	303.046	9.192	HILIC	ESI-	18.33	4.19	0.0028
C <sub>10</sub> H <sub>12</sub> O <sub>15</sub>	372.016	9.062	HILIC	ESI-	17.95	4.16	0.0113
C <sub>10</sub> H <sub>24</sub> O <sub>2</sub> P <sub>2</sub> S	270.098	7.387	HILIC	ESI-	17.82	4.15	0.0129
C <sub>12</sub> H <sub>15</sub> N <sub>5</sub> O <sub>6</sub>	325.100	7.693	HILIC	ESI-	17.78	4.15	0.0070
Sangivamycin	309.106	7.508	HILIC	ESI-	17.48	4.12	0.0023
Hexyl salicylate	222.125	1.390	HILIC	ESI-	17.31	4.11	0.0070
3,4-Dihydroxybenzoate	153.019	7.369	HILIC	ESI+	16.29	4.02	0.0789
Oxaceprol	173.068	8.321	HILIC	ESI-	16.21	4.01	0.0100
C <sub>9</sub> H <sub>18</sub> N <sub>2</sub> O <sub>8</sub>	282.106	6.530	HILIC	ESI-	15.39	3.94	0.0708
3-O-sulfo-D-glucose	260.020	10.12	HILIC	ESI-	15.24	3.93	0.0022
C <sub>5</sub> H <sub>10</sub> N <sub>6</sub> O <sub>11</sub> S	362.014	8.358	HILIC	ESI-	15.03	3.91	0.0113

C <sub>11</sub> H <sub>8</sub> Cl <sub>2</sub> N <sub>9</sub> P <sub>3</sub>	428.950	9.061	HILIC	ESI-	14.97	3.90	0.0056
Elaidolinolenic acid	278.224	1.343	HILIC	ESI-	14.96	3.90	0.0031
45-Dihydroxy-3-oxo-1-cyclohexene-1-carboxylic acid	172.036	7.975	HILIC	ESI-	14.61	3.86	0.0044
(12S)-12-hydroxy-16-heptadecynoic acid	282.219	1.562	HILIC	ESI-	13.50	3.75	0.0033
C <sub>3</sub> H <sub>11</sub> N <sub>3</sub> OS <sub>2</sub>	169.034	9.064	HILIC	ESI-	13.37	3.74	0.0003
C <sub>7</sub> H <sub>16</sub> N <sub>2</sub> O <sub>4</sub>	192.110	8.302	HILIC	ESI-	13.11	3.71	0.0404
C <sub>5</sub> H <sub>4</sub> N <sub>10</sub> O <sub>5</sub>	284.037	8.348	HILIC	ESI-	12.64	3.66	0.01074
2-Acetamido-2-deoxyglucose	221.089	7.862	HILIC	ESI-	12.63	3.65	0.0153
3,4-Dihydroxy-5-(1,2,3-trihydroxypropyl)dihydro-2(3H)-furanone	208.057	4.798	HILIC	ESI-	12.47	3.64	0.0105
CH <sub>3</sub> CIN <sub>7</sub> O <sub>4</sub> P	242.967	9.050	HILIC	ESI-	12.36	3.62	0.0009
C <sub>5</sub> H <sub>15</sub> CIN <sub>6</sub> O <sub>2</sub> P <sub>2</sub> S	320.013	8.326	HILIC	ESI-	12.30	3.62	0.0285
C <sub>5</sub> H <sub>9</sub> ClO <sub>5</sub>	184.013	4.797	HILIC	ESI-	12.10	3.59	0.0110
Sanguinarine	332.090	7.707	HILIC	ESI-	11.46	3.51	0.0708
C <sub>19</sub> H <sub>18</sub> N <sub>10</sub> O <sub>3</sub>	434.157	1.493	HILIC	ESI-	11.46	3.51	0.0048
C <sub>13</sub> H <sub>19</sub> O <sub>6</sub> P	302.092	2.124	HILIC	ESI+	11.43	3.51	0.0966
C <sub>6</sub> H <sub>3</sub> N <sub>5</sub> OP <sub>2</sub>	222.982	9.056	HILIC	ESI-	11.33	3.50	0.0013
C <sub>13</sub> H <sub>19</sub> NO <sub>7</sub> S	333.086	7.703	HILIC	ESI-	10.83	3.43	0.0478
C <sub>10</sub> H <sub>15</sub> N <sub>4</sub> O <sub>7</sub> P	334.066	9.570	HILIC	ESI-	10.69	3.41	0.0028
Daminozide	160.084	7.384	HILIC	ESI-	10.46	3.38	0.0157
C <sub>8</sub> H <sub>18</sub> N <sub>3</sub> O <sub>9</sub> P	331.078	9.040	HILIC	ESI-	10.45	3.38	0.0028
C <sub>11</sub> H <sub>20</sub> O <sub>6</sub> P <sub>2</sub> S	342.046	5.493	HILIC	ESI-	10.42	3.38	0.0031
C <sub>6</sub> H <sub>11</sub> N <sub>8</sub> O <sub>8</sub> P	354.044	9.063	HILIC	ESI-	9.76	3.28	0.01392
Geranyl phosphate	234.101	2.148	HILIC	ESI-	9.47	3.24	0.0121
C <sub>16</sub> H <sub>11</sub> CIN <sub>6</sub> O	338.068	2.111	HILIC	ESI-	9.41	3.23	0.0380
C <sub>5</sub> H <sub>2</sub> BrNO <sub>10</sub> P <sub>2</sub> S	408.804	9.030	HILIC	ESI-	9.33	3.22	0.0035
C <sub>11</sub> H <sub>8</sub> N <sub>10</sub> O	296.089	1.646	HILIC	ESI-	8.87	3.14	0.0113
C <sub>7</sub> H <sub>11</sub> N <sub>7</sub> O <sub>9</sub> S	369.034	9.031	HILIC	ESI-	8.60	3.10	0.0048
Uridine	244.069	5.497	HILIC	ESI-	8.51	3.08	0.0020

C <sub>23</sub> H <sub>38</sub> N <sub>2</sub> O <sub>13</sub> S	582.210	1.335	HILIC	ESI-	8.35	3.06	0.0312
C <sub>6</sub> H <sub>13</sub> Cl <sub>2</sub> N <sub>7</sub> O <sub>8</sub> P <sub>2</sub>	442.966	9.037	HILIC	ESI-	8.00	3.00	0.0028
C <sub>11</sub> H <sub>19</sub> ClN <sub>2</sub> S <sub>2</sub>	278.066	2.938	HILIC	ESI-	7.85	2.97	0.0028
C <sub>12</sub> H <sub>9</sub> ClN <sub>9</sub> P <sub>3</sub>	406.990	9.038	HILIC	ESI+	7.81	2.96	0.0789
C <sub>5</sub> H <sub>12</sub> NO <sub>8</sub> P	245.030	9.072	HILIC	ESI-	7.65	2.93	0.0023
C <sub>3</sub> H <sub>3</sub> Cl <sub>2</sub> N <sub>7</sub> P <sub>2</sub> S <sub>2</sub>	332.874	9.052	HILIC	ESI-	7.63	2.93	0.0005
C <sub>9</sub> H <sub>19</sub> ClN <sub>5</sub> O <sub>3</sub> P <sub>3</sub> S	405.010	9.037	HILIC	ESI-	7.54	2.91	0.0044
C <sub>14</sub> H <sub>26</sub> ClN <sub>6</sub> O <sub>5</sub> P <sub>3</sub>	486.088	8.828	HILIC	ESI-	7.45	2.89	0.0356
C <sub>28</sub> H <sub>48</sub> ClN <sub>8</sub> O <sub>3</sub> P <sub>3</sub>	672.275	1.280	HILIC	ESI-	7.34	2.87	0.03929
C <sub>3</sub> H <sub>6</sub> N <sub>3</sub> O <sub>2</sub> P <sub>3</sub>	208.966	9.199	HILIC	ESI-	7.32	2.87	0.0034
C <sub>19</sub> H <sub>15</sub> N <sub>5</sub> O	329.126	1.994	HILIC	ESI-	7.26	2.86	0.0361
C <sub>2</sub> H <sub>6</sub> NO <sub>6</sub> P	170.992	9.219	HILIC	ESI-	7.17	2.84	0.0023
C <sub>12</sub> H <sub>6</sub> Cl <sub>2</sub> NOP <sub>3</sub>	342.902	9.239	HILIC	ESI-	6.78	2.76	0.0013
C <sub>10</sub> H <sub>7</sub> ClNO <sub>14</sub> P	430.930	9.054	HILIC	ESI+	6.78	2.76	0.0789
C <sub>10</sub> H <sub>8</sub> ClN <sub>9</sub> O <sub>5</sub>	369.034	9.046	HILIC	ESI+	6.77	2.76	0.0473
C <sub>16</sub> H <sub>30</sub> N <sub>2</sub> O <sub>14</sub>	474.169	8.739	HILIC	ESI-	6.60	2.72	0.0669
C <sub>24</sub> H <sub>45</sub> N <sub>8</sub> O <sub>10</sub> P	636.299	1.299	HILIC	ESI-	6.57	2.71	0.0462
C <sub>3</sub> H <sub>7</sub> ClN <sub>3</sub> P <sub>3</sub> S	244.925	9.223	HILIC	ESI-	6.36	2.67	0.0042
C <sub>5</sub> H <sub>6</sub> ClN <sub>3</sub> S <sub>2</sub>	206.969	9.210	HILIC	ESI-	6.34	2.66	0.0023
C <sub>4</sub> H <sub>11</sub> ClNO <sub>9</sub> P	282.986	9.067	HILIC	ESI-	6.18	2.62	0.0028
C <sub>4</sub> H <sub>6</sub> N <sub>3</sub> O <sub>2</sub> PS <sub>2</sub>	222.965	9.055	HILIC	ESI+	6.13	2.61	0.07896
C <sub>11</sub> H <sub>16</sub> N <sub>4</sub> O <sub>2</sub> S	268.098	2.296	HILIC	ESI-	6.00	2.58	0.07036
C <sub>6</sub> H <sub>13</sub> NO <sub>9</sub>	243.058	7.601	HILIC	ESI-	5.83	2.54	0.02429
C <sub>6</sub> H <sub>13</sub> ClO <sub>6</sub>	216.039	9.584	HILIC	ESI-	5.78	2.53	0.0031
C <sub>3</sub> H <sub>3</sub> N <sub>5</sub> O <sub>8</sub> S	268.970	9.211	HILIC	ESI-	5.73	2.52	0.0027
D-Pantothenic acid	219.110	6.531	HILIC	ESI-	5.70	2.51	0.0959
gamma-Glu-gln	275.111	9.313	HILIC	ESI-	5.54	2.47	0.0272
C <sub>8</sub> H <sub>16</sub> Cl <sub>3</sub> N <sub>3</sub> O <sub>8</sub>	387.000	9.309	HILIC	ESI-	5.48	2.45	0.0462
D-(-)-Quinic acid	192.062	8.336	HILIC	ESI-	5.37	2.42	0.0057
C <sub>12</sub> H <sub>3</sub> ClN <sub>2</sub> O <sub>9</sub>	353.952	17.31	HILIC	ESI-	5.24	2.38	0.0445
Tiglylcarnitine	243.147	8.016	HILIC	ESI+	5.17	2.37	0.0789
C <sub>7</sub> H <sub>12</sub> N <sub>2</sub> O <sub>2</sub> P <sub>2</sub>	218.036	9.581	HILIC	ESI-	5.06	2.34	0.0020
C <sub>4</sub> H <sub>2</sub> Cl <sub>3</sub> N <sub>5</sub> P <sub>2</sub> S	318.858	9.225	HILIC	ESI-	5.03	2.33	0.0028
C <sub>16</sub> H <sub>18</sub> Cl <sub>2</sub> N <sub>4</sub> O <sub>14</sub>	560.020	8.866	HILIC	ESI-	4.88	2.28	0.0316
C <sub>9</sub> H <sub>13</sub> ClNOP	217.043	9.553	HILIC	ESI-	4.87	2.28	0.0023
C <sub>12</sub> H <sub>30</sub> N <sub>5</sub> O <sub>3</sub> P	323.209	1.572	HILIC	ESI-	4.74	2.24	0.0139
C <sub>4</sub> H <sub>14</sub> N <sub>2</sub> O <sub>5</sub> P <sub>2</sub>	232.038	10.58	HILIC	ESI-	4.57	2.19	0.0832
C <sub>5</sub> H <sub>6</sub> ClN <sub>5</sub>	171.030	5.117	HILIC	ESI-	4.54	2.18	0.0143
C <sub>9</sub> HCl <sub>2</sub> NO <sub>3</sub> P <sub>2</sub> S	334.853	9.064	HILIC	ESI+	4.47	2.16	0.0789
C <sub>2</sub> H <sub>3</sub> N <sub>8</sub> O <sub>10</sub> P <sub>3</sub> S <sub>5</sub>	551.779	6.528	HILIC	ESI-	4.15	2.05	0.0027
C <sub>6</sub> H <sub>10</sub> ClN <sub>2</sub> O <sub>9</sub> P	319.981	5.506	HILIC	ESI+	4.08	2.03	0.0830
C <sub>3</sub> H <sub>8</sub> Cl <sub>2</sub> N <sub>3</sub> OP <sub>3</sub> S	296.897	9.059	HILIC	ESI+	4.04	2.01	0.0789
Perfluoro-1-butanesulfonic acid	299.950	1.176	HILIC	ESI-	4.03	2.01	0.01963

C <sub>7</sub> H <sub>3</sub> ClO <sub>15</sub> S	393.887	17.32	HILIC	ESI-	4.02	2.00	0.0750
C <sub>8</sub> H <sub>24</sub> N <sub>8</sub> P <sub>2</sub> S	326.132	9.556	HILIC	ESI-	3.93	1.97	0.0028
C <sub>7</sub> H <sub>13</sub> ClO <sub>6</sub>	228.039	8.372	HILIC	ESI-	3.92	1.97	0.0377
C <sub>2</sub> H <sub>8</sub> N <sub>4</sub> O <sub>2</sub>	120.065	5.406	HILIC	ESI+	3.72	1.89	0.0789
cis-4-Hydroxy-D-proline	131.058	8.409	HILIC	ESI+	3.555	1.82	0.0963
2-Hydroxytetracosanoic acid	384.360	1.228	HILIC	ESI-	3.53	1.82	0.0383
C <sub>6</sub> H <sub>17</sub> NOP <sub>2</sub> S	213.051	9.153	HILIC	ESI+	3.25	1.70	0.0789
C <sub>7</sub> H <sub>15</sub> ClO <sub>7</sub>	246.050	8.273	HILIC	ESI-	3.13	1.64	0.0316
Olprinone	250.085	7.087	HILIC	ESI-	2.89	1.53	0.0935
C <sub>2</sub> H <sub>3</sub> ClN <sub>8</sub> O	190.011	8.932	HILIC	ESI-	2.84	1.51	0.0113
C <sub>3</sub> H <sub>7</sub> ClN <sub>10</sub>	218.055	7.955	HILIC	ESI-	2.80	1.48	0.0228
C <sub>5</sub> H <sub>7</sub> N <sub>8</sub> PS <sub>2</sub>	273.998	8.353	HILIC	ESI-	2.61	1.38	0.0459
Ro 20-1724	278.163	2.200	HILIC	ESI-	2.52	1.33	0.0375
2-Deoxyhexopyranose	164.067	7.644	HILIC	ESI-	2.50	1.32	0.0347
C <sub>6</sub> H <sub>16</sub> ClOP <sub>3</sub>	232.009	8.950	HILIC	ESI-	2.42	1.27	0.0439
C <sub>7</sub> H <sub>12</sub> Cl <sub>2</sub> N <sub>4</sub> O <sub>12</sub> P <sub>2</sub> S <sub>2</sub>	539.874	8.888	HILIC	ESI-	2.35	1.23	0.0445
C <sub>8</sub> H <sub>16</sub> ClN <sub>6</sub> O <sub>4</sub> PS <sub>2</sub>	390.011	8.831	HILIC	ESI-	2.33	1.22	0.0470
NS1800000	183.052	2.173	HILIC	ESI-	2.29	1.19	0.0869
δ-Ribono-1,4-lactone	148.036	9.698	HILIC	ESI-	2.21	1.15	0.0725
C <sub>7</sub> H <sub>12</sub> ClN <sub>8</sub> O <sub>5</sub> P	354.034	8.858	HILIC	ESI-	2.20	1.13	0.0530
C <sub>7</sub> H <sub>9</sub> N <sub>4</sub> P <sub>3</sub>	242.005	7.667	HILIC	ESI-	2.18	1.12	0.0861
C <sub>4</sub> H <sub>11</sub> ClN <sub>2</sub> OP <sub>2</sub> S	231.976	7.694	HILIC	ESI-	2.15	1.10	0.0365
Diphenol glucuronide	286.068	7.317	HILIC	ESI-	0.467	-1.09	0.0593
C <sub>6</sub> H <sub>7</sub> NO <sub>5</sub>	173.031	9.645	HILIC	ESI-	0.460	-1.12	0.0356
C <sub>11</sub> H <sub>2</sub> Cl <sub>3</sub> P <sub>3</sub>	331.842	9.747	HILIC	ESI-	0.449	-1.15	0.0700
C <sub>12</sub> H <sub>5</sub> N <sub>7</sub> O	263.055	6.619	HILIC	ESI-	0.435	-1.19	0.0171
C <sub>6</sub> H <sub>7</sub> Cl <sub>2</sub> OP <sub>3</sub>	257.909	9.743	HILIC	ESI-	0.432	-1.21	0.0478
C <sub>3</sub> H <sub>4</sub> ClN <sub>2</sub> O <sub>4</sub> P <sub>3</sub>	259.907	9.742	HILIC	ESI-	0.428	-1.22	0.0521
3-Phosphonoxy pyruvic acid	183.976	9.743	HILIC	ESI-	0.424	-1.23	0.0478
Indoprofen	281.105	1.904	HILIC	ESI-	0.416	-1.26	0.0401
Pyridoxine phosphate	249.040	6.621	HILIC	ESI-	0.413	-1.27	0.0935
C <sub>4</sub> H <sub>6</sub> Cl <sub>2</sub> O <sub>6</sub>	219.953	9.748	HILIC	ESI-	0.413	-1.27	0.0498
C <sub>3</sub> H <sub>8</sub> O <sub>11</sub> P <sub>2</sub>	281.954	9.744	HILIC	ESI-	0.407	-1.29	0.0380
L-Phenylalanine	165.078	6.694	HILIC	ESI-	0.339	-1.55	0.0439
trans-Aconitic acid	174.015	11.06	HILIC	ESI-	0.331	-1.59	0.0162
C <sub>7</sub> H <sub>14</sub> O <sub>6</sub> S	226.050	1.416	HILIC	ESI-	0.272	-1.87	0.0380

C <sub>8</sub> H <sub>9</sub> O <sub>2</sub> P <sub>3</sub>	229.982	10.87	HILIC	ESI-	0.266	-1.90	0.0340
C <sub>15</sub> H <sub>40</sub> N <sub>6</sub> O <sub>9</sub> P <sub>2</sub>	510.231	1.323	HILIC	ESI-	0.199	-2.32	0.0070
C <sub>25</sub> H <sub>56</sub> N <sub>2</sub> O <sub>11</sub> P <sub>2</sub> S	654.310	1.353	HILIC	ESI-	0.166	-2.58	0.0034
C <sub>3</sub> HN <sub>2</sub> PS <sub>2</sub>	159.931	2.298	HILIC	ESI-	0.164	-2.60	0.0380
C <sub>6</sub> H <sub>8</sub> N <sub>4</sub> P <sub>2</sub> S	229.993	7.357	HILIC	ESI-	0.162	-2.62	0.0425
C <sub>6</sub> H <sub>12</sub> O <sub>6</sub> S	212.034	1.558	HILIC	ESI-	0.146	-2.76	0.0256
C <sub>22</sub> H <sub>48</sub> N <sub>8</sub> O <sub>2</sub> S <sub>5</sub>	616.249	1.376	HILIC	ESI-	0.145	-2.78	0.0120
3-O-(3-Methylbutanoyl)-beta-D-fructofuranosyl 3-O-(2-methylbutanoyl)-4-O-(3-methylbutanoyl)-alpha-D-glucopyranoside	594.288	1.346	HILIC	ESI-	0.134	-2.89	0.0028
C <sub>11</sub> H <sub>18</sub> N <sub>2</sub> O <sub>6</sub>	274.116	8.512	HILIC	ESI+	0.132	-2.91	0.0827
C <sub>24</sub> H <sub>39</sub> ClN <sub>10</sub> O <sub>8</sub>	630.265	1.359	HILIC	ESI-	0.123	-3.02	0.0028
C <sub>9</sub> H <sub>7</sub> N <sub>4</sub> O <sub>3</sub> P <sub>3</sub> S	343.945	9.913	HILIC	ESI+	0.100	-3.32	0.0789
C <sub>29</sub> H <sub>55</sub> N <sub>4</sub> O <sub>7</sub> P <sub>3</sub>	664.330	1.263	HILIC	ESI-	0.091	-3.45	0.0003
C <sub>4</sub> H <sub>5</sub> N <sub>2</sub> O <sub>4</sub> P	175.999	10.87	HILIC	ESI-	0.084	-3.55	0.0211
C <sub>32</sub> H <sub>48</sub> O <sub>11</sub> S	640.294	1.366	HILIC	ESI-	0.075	-3.72	0.0028
6-(1-Hydroxyethyl)-3-(hydroxymethyl)-27-dioxabicyclo[4.1.0]hept-3-en-5-one	186.052	8.813	HILIC	ESI-	0.068	-3.86	0.0031
3138020	234.161	1.555	HILIC	ESI-	0.059	-4.08	0.0250
N-Acetylneuraminic acid	309.110	2.729	C18	ESI+	0.043	-4.52	0.0298
C <sub>10</sub> H <sub>12</sub> N <sub>10</sub> S	304.096	8.833	HILIC	ESI-	0.036	-4.77	0.0013
Benzyl methanoate	136.050	7.714	C18	ESI+	0.035	-4.82	0.0689
C <sub>15</sub> H <sub>24</sub> N <sub>2</sub> O <sub>3</sub> P <sub>2</sub> S	374.100	1.326	HILIC	ESI-	0.030	-5.01	0.0003
C <sub>27</sub> H <sub>56</sub> ClN <sub>6</sub> O <sub>8</sub> P <sub>3</sub> S	752.279	1.257	HILIC	ESI-	0.020	-5.58	0.0009
C <sub>29</sub> H <sub>59</sub> N <sub>6</sub> O <sub>10</sub> P <sub>3</sub> S	776.323	1.262	HILIC	ESI-	0.016	-5.91	0.0017
C <sub>14</sub> H <sub>14</sub> N <sub>4</sub> O <sub>7</sub>	350.084	12.03	HILIC	ESI-	0.015	-5.99	0.0003
C <sub>27</sub> H <sub>56</sub> N <sub>8</sub> O <sub>3</sub> S <sub>5</sub>	700.307	1.266	HILIC	ESI-	0.012	-6.27	0.0003
C <sub>33</sub> H <sub>56</sub> O <sub>17</sub>	724.352	1.306	HILIC	ESI-	0.011	-6.49	0.0003
C <sub>32</sub> H <sub>58</sub> ClN <sub>8</sub> O <sub>2</sub> P <sub>3</sub>	714.359	1.302	HILIC	ESI-	0.004	-7.74	0.0067

MW = Molecular weight; RT = retention time; FC = fold change;  $P_{adj}$  = FDR-adjusted  $P$  values calculated within each column-ion mode combination.

### **Genome composition of *C. michiganensis* 0317**

These inoculation experiments described above were performed with the pathogenic New York *C. michiganensis* 0317 isolate, which does not harbor plasmid pCM1 or the *celA* pathogenicity gene. In order to probe for *celA*-like homologues and other putative virulence genes, we used short read Illumina sequencing to generate a high coverage genome assembly. Using the MiSeq Illumina platform, we generated 0.5 Gb of output sequence, which provided 160x coverage of the assembled 3.36 Mb genome (Table 3.4). A *de novo* assembly of the *C. michiganensis* 0317 genome in was produced including 17 contigs with an N50 value of 803,811 and a BUSCO completeness score of 96.3% (Table 3.4).

The assembly was aligned to the reference genome, Cm382 and plasmid pCM2 to determine similarities and differences. Pulsed-field gel electrophoresis determined that *C. michiganensis* 0317 contained a 70 kb plasmid resembling pCM2 (Tancos et al., 2015), therefore we attempted to extract plasmid sequences present on contigs 6 and 11 to assemble into the pCM2-like plasmid (Fig. 3.10). Two approaches were used: (1) the program plasmidSPAdes, which assembles plasmids from whole genome sequencing data, and (2) a custom approach of diluting the reads 1:10 to encourage SPAdes and plasmidSPAdes to assemble the low-copy plasmid (Antipov et al., 2016). Both approaches were unsuccessful at extracting and assembling the plasmid sequences.

To identify similarities and differences in virulence factor composition, the assembly was compared to sequenced *C. michiganensis* genomes. The *C. michiganensis* 0317 genome was compared to Cm382, a pathogenic isolate CASJ002, and a non-pathogenic isolate CASJ009 using BRIG, which identified genomic regions unique to *C. michiganensis* 0317 (Fig. 3.11). Sequences of virulence genes from *C. michiganensis* 0317 were BLASTed against Cm382 to determine presence or absence and sequence similarity (Fig. 3.11). The genome of *C.*

*michiganensis* 0317 lacks *celA*, *ppaJ* and *phpB*, which were all located on the pCM1 plasmid of Cm382 (Fig. 3.11). All other hypothesized virulence genes from Cm382 were present in the genome of *C. michiganensis* 0317 and held high sequence similarity to those in Cm382 (Fig. 3.11).

The assembly was annotated using RAST and Prokka to detect bacterial enzymes capable of generating products detected in the metabolomic data through degradation of larger compounds. The tomatinase gene, *tomA*, encodes a functional tomatinase enzyme capable of hydrolyzing the host alkaloid  $\alpha$ -tomatine to tomatidine, which was the most significantly differentially accumulated metabolite in *S. lycopersicum* ‘Mt. Fresh’ sap from *C. michiganensis*-infected plants (Table 3.1). The *tomA* gene was detected on contig 6 at position 33523 to 35154 of the *C. michiganensis* 0317 genome, which shared 99% sequence similarity with the Cm382 tomatinase when aligned using BLASTn. The enzyme gamma-glutamyl transpeptidase catalyzes the transfer of the  $\gamma$ -glutamyl group from glutathione to  $\gamma$ -glutamylmethionine, the seventh-most significantly accumulated metabolites in *S. lycopersicum* ‘Mt. Fresh’ sap from *C. michiganensis*-infected plants (Table 3.1). The gamma-glutamyl transpeptidase encoding gene, *ggtA*, was detected on contig 2 at position 724835 to 727645 of the *C. michiganensis* 0317 genome, and the gene shared 99% sequence similarity with the Cm382 *ggtA* gene.

**TABLE 3.4.** Assembly statistics of *C. michiganensis* 0317 compared to NCPPB382

Strain	Length (bp)	GC content	# Contigs	N50	L50	Reference
<i>C. michiganensis</i> 0317	3,365,759	72.67%	17	803,811	2	This study
<i>C. michiganensis</i> NCPPB382	3,298,000	72.6%	-	-	-	(Gartemann et al., 2008)

bp = base pairs

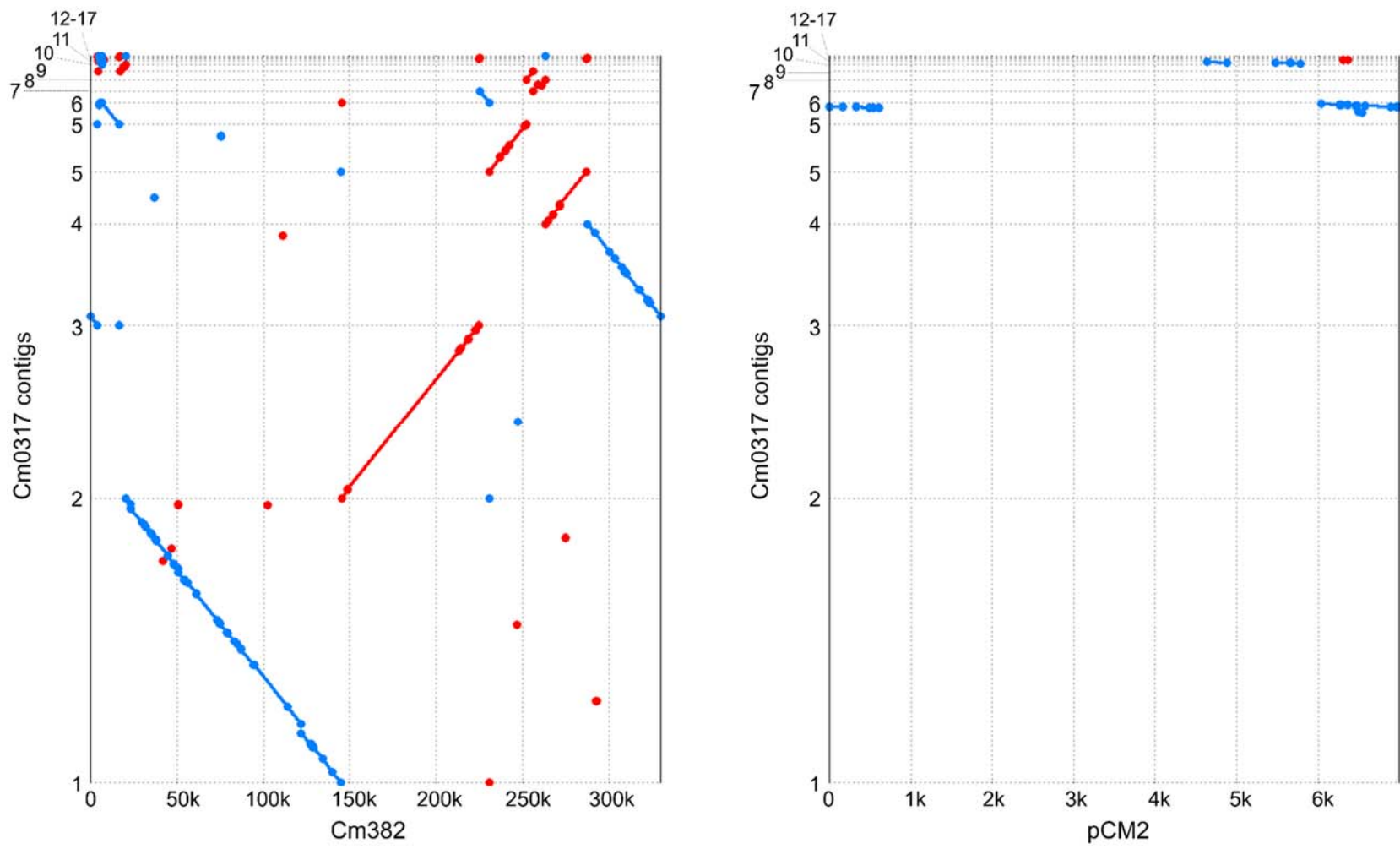
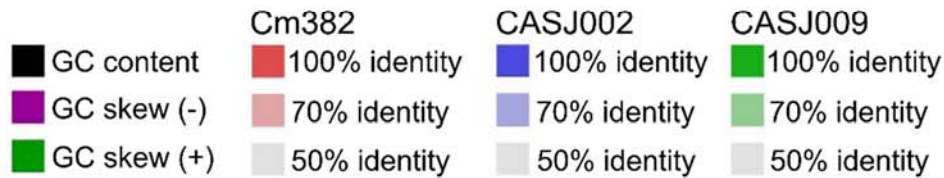
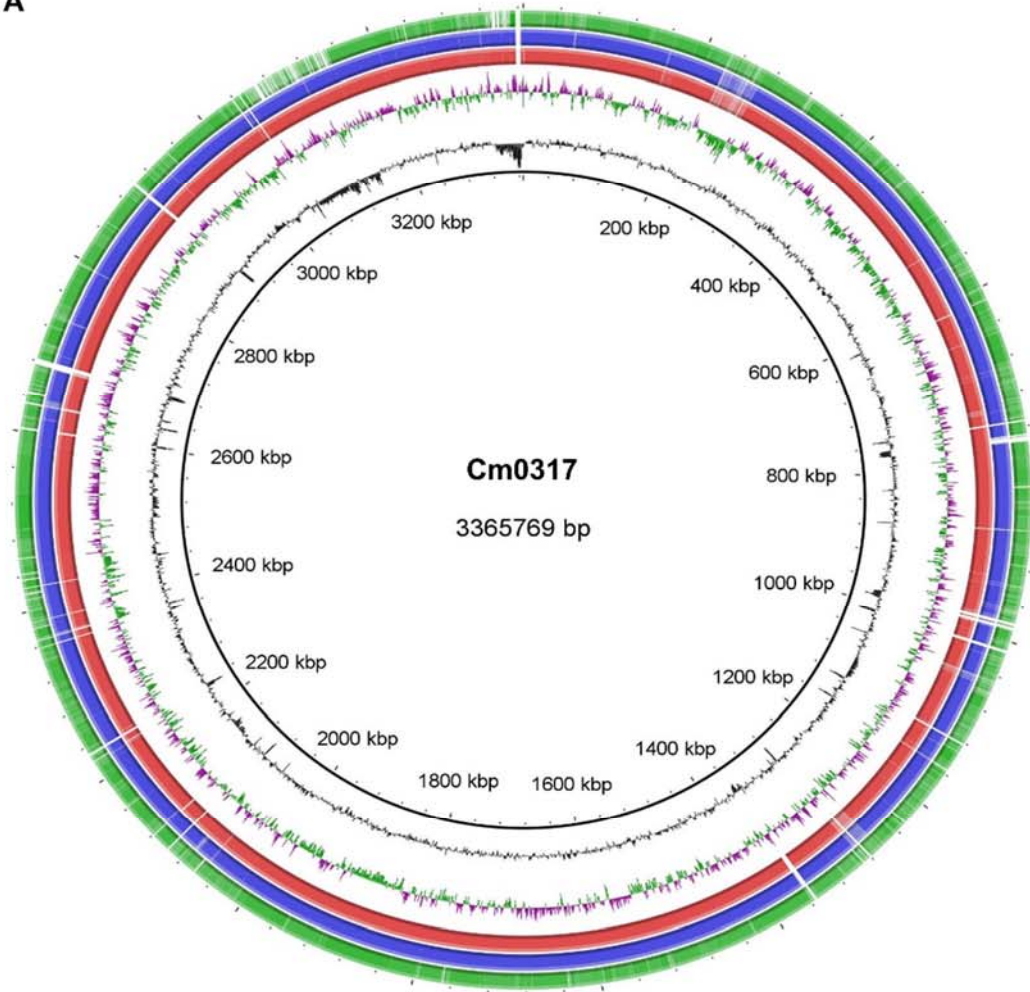


**FIGURE 3.10.** Genome-genome alignment dot plots between the *C. michiganensis* 0317 assembly, Cm382 (left), and pCM2 (right). Plots were generated using MUMmer 3.0. Dots represent nucleotide matches between genomes, and dots with lines highlight contiguous sequences that match between genomes. Red lines indicate matches that share the same strand directionality and blue lines are reverse complement matches.

A



B

	Cm382	Cm0317	Cm0317 Contig	% Sequence identity
<b>Chp family proteases</b>				
chpA	■	■	11	99.5
chpB	■	■	6	99.2
chpC	■	■	6	99.8
chpD	■	■	12	99.5
chpE	■	■	12	98.8
chpF	■	■	6	100
chpG	■	■	6	99.9
pat-1	■	■	11	86.6
phpA	■	■	11	74.6
phpB	■	■		
<b>Chymotrypsin-related serine proteases</b>				
ppaA	■	■	12	99.5
ppaB1	■	■	16	99.4
ppaB2	■	■	16	99.2
ppaC	■	■	11	99.9
ppaD	■	■	6	100
ppaE	■	■	6	99.6
ppaF	■	■	1	98.8
ppaG	■	■	2	99.8
ppaH	■	■	2	99.6
ppaI	■	■	2	99.6
ppaJ	■	■		
<b>Subtilase proteases</b>				
sbtA	■	■	6	99.7
sbtB	■	■	4	99.7
sbtC	■	■	4	99.7
<b>Cellulases</b>				
celA	■	■		
celB	■	■	4	98.9
celH	■	■	3	98.2
<b>Xylanases</b>				
xysA	■	■	2	99.2
xysB	■	■	2	99.7
<b>Pectinases</b>				
pgaA	■	■	3	99.9
pelA1	■	■	11	98.1
pelA2	■	■	6	99.1
<b>Transcriptional regulators</b>				
vatr1	■	■	3	99.4
vatr2	■	■	3	99.8
wcoP	■	■	1	98.4
<b>Others</b>				
gmdA	■	■	2	99.9
perf	■	■	4	99.7
srtA	■	■	3	99.8
tomA	■	■	6	99.7
expA	■	■	2	99.7

**FIGURE 3.11.** (A) Comparisons of the *C. michiganensis* 0317 genome with the chromosomes of Cm382, CASJ002, and CASJ009 generated using BLAST Ring Image Generator. The solid black line represents *C. michiganensis* 0317 and the jagged black line represents GC percentage. Purple and dark green jagged lines represent GC negative and positive skew, respectively. Genome comparisons between Cm382, CASJ002, and CASJ009 are depicted in red, blue, and green, respectively. (B) Virulence gene presence (green) or absence (red) comparisons between *C. michiganensis* 0317 and Cm382. Sequence similarity between virulence genes of each strain was determined using BLAST.

## ***DISCUSSION***

Bacterial canker of tomato continues to be an economically disruptive disease for tomato growers around the world. Breeding for complete resistance has thus far been unsuccessful, and there are limited strategies to control the pathogen once inside the xylem (Johannes et al., 2010; de León et al., 2011; Sen et al., 2014). Next generation technologies have been useful to improve our understanding of *C. michiganensis* biology and host-microbe interactions, which may provide important information for developing future breeding and control strategies (Coaker et al., 2004; Gartemann et al., 2008; Balaji et al., 2008; Hiery et al., 2013; Savidor et al., 2012; Thapa et al., 2017; Nandi et al., 2018; Peritore-Galve et al., 2020). However, we still do not fully understand how the pathogen affects the host xylem, and if xylem sap chemical changes differ during colonization of tolerant or susceptible hosts. The aim of these experiments was to identify metabolites that differentially accumulated during *C. michiganensis*-colonization of *S. lycopersicum* ‘Mt. Fresh’ and *S. habrochaites* LA2128. A secondary aim was to detect differences in metabolite concentration between *S. lycopersicum* and *S. habrochaites* sap from healthy plants that may be used as nutrient sources for the pathogen. Finally, we sequenced the genome of *C. michiganensis* 0317 – the pathogenic isolate used in these experiments that naturally lacks the pathogenicity factor CelA – to catalog virulence genes and begin to explore pathways potentially used to produce bacterially derived metabolites identified using untargeted metabolomics.

The bacterial canker pathogen is able to colonize the xylem of wild tomatoes without causing severe symptoms (Peritore-Galve et al., 2020). Sterilized sap from wild tomatoes sustains lower growth densities of *C. michiganensis* compared to sap from cultivated *S. lycopersicum* ‘Mt. Fresh’ (Peritore-Galve et al., 2020). We extracted xylem sap from *C.*

*michiganensis* and water-inoculated *S. lycopersicum* ‘Mt. Fresh’ and *S. habrochaites* LA2128 plants, using *S. habrochaites* LA2128 as the tolerant species for metabolomics. Sap from *S. habrochaites* LA2128 sustained the lowest density of *C. michiganensis* growth between *S. lycopersicum* and *S. arcanum* accessions, making it an interesting candidate to identify metabolites enriched in *S. lycopersicum* sap that may be carbon or nitrogen sources for *C. michiganensis* (Peritore-Galve et al., 2020).

To select plants whose sap would be used for metabolomics, we measured bacterial densities in sap, and sap flow. The pathogen colonizes to high densities in xylem and forms bacterial aggregates on annular rings and other xylem elements (Chalupowicz et al., 2011; Peritore-Galve et al., 2020). Harvested xylem sap contains high densities of planktonic *C. michiganensis* in both *S. lycopersicum* ‘Mt. Fresh’ and *S. habrochaites* LA2128, suggesting the bacteria are using the natural flow of xylem sap as a means to spread through the plant. The dense biofilms produced by the tomato wilt pathogen *R. solanacearum* restrict xylem sap flow, leading to wilt symptoms (Araud-Razou et al., 1998; Tran et al., 2016). Here we found that xylem sap flow was not significantly altered in *S. lycopersicum* despite leaflet wilt symptoms having developed. The pathogen could, however, be aggregating in petiole xylem vessels but in not stem xylem, which would cause leaflet wilt. Further studies are needed to understand the relationship between biofilm formation and bacterial canker symptoms.

Sap from healthy and *C. michiganensis*-infected plants from the susceptible tomato cultivar *S. lycopersicum* ‘Mt. Fresh’ and tolerant wild tomato accessions, *S. habrochaites* LA2128 were submitted for untargeted metabolomics analysis using C18 and HILIC columns in positive and negative ESI modes. This approach was used to detect the broadest array of metabolites, and to the best of our knowledge this is the most comprehensive dataset of tomato

xylem sap metabolites (Dixon and Pegg, 1972; Chellimi et al., 1998; Lowe-Power et al., 2018). The chemical composition of xylem sap of cultivated tomato species is poorly understood, and even less studied in wild tomato species. The effects of *C. michiganensis* colonization on xylem sap composition has not been studied before, therefore this exploratory approach was a first step towards understanding chemical changes in the xylem during early bacterial canker symptom development.

On the most fundamental level, *C. michiganensis* does alter the chemical composition of *S. lycopersicum* 'Mt. Fresh' xylem sap. Of the known compounds that were significantly differentially accumulated in sap from infected plants, the highest increased metabolite was tomatidine. Tomatidine is a steroidal alkaloid and the aglycone derivative of the defense molecule  $\alpha$ -tomatine (Friedman, 2013). The *C. michiganensis* genome contains a secreted tomatinase enzyme (TomA) that hydrolyzes  $\alpha$ -tomatine to tomatidine (Kaup et al., 2005; Gartemann et al., 2008; Savidor et al., 2012). High concentrations of  $\alpha$ -tomatine inhibit *in vitro* growth of *C. michiganensis*, but *tomA* mutants were not impaired in *in planta* colonization or virulence, suggesting that deglycosylation of  $\alpha$ -tomatine to tomatidine may be important in other processes such as fruit colonization, or may play a role in other plant physiological changes that occur during pathogen colonization (Kaup et al., 2005). The only known compound that was significantly reduced in concentration in sap from *C. michiganensis*-infected plants was the nucleoside analogue sangivamycin. Nucleoside analogues are antimicrobial compounds that have been widely studied in *Streptomyces* species and are antiviral drugs used in clinical settings (McCarty and Bandarian, 2008; Jordheim et al., 2013; Niu and Tan, 2015). This class of molecules are understudied in plants, but the reduction in sangivamycin concentration during infection may allow the pathogen to successfully colonize the xylem.

A majority of significantly differentially accumulated metabolites in infected *S. lycopersicum* 'Mt. Fresh' sap were negatively charged, hydrophobic compounds. The dipeptide  $\gamma$ -glutamylmethionine was the most increased known compound in this group. Gamma-glutamyl amino acids are typically degradation products of larger proteins. In human diseases, increased accumulation of  $\gamma$ -glutamyl amino acids, such as  $\gamma$ -glutamylmethionine, are a byproduct of degradation of the antioxidant glutathione by glutamyl transpeptidases (Franco et al., 2007; Kalhan et al., 2011). In plants, glutathione plays a critical role in quenching reactive oxygen species produced in response to pathogen detection; Arabidopsis plants lacking glutathione biosynthesis genes were more susceptible to bacterial and oomycete pathogens (Noctor et al., 1998; Parisy et al., 2007; Galant et al., 2011). The *C. michiganensis* reference genome and Cm0317 contain a gamma-glutamyltranspeptidase (GGT) expressed under nutrient-rich growth conditions that may play a role in catalyzing the transfer of the glutathione  $\gamma$ -glutamyl group to release glutamate for consumption (Gartemann et al., 2008; Peritore-Galve et al., 2019). The gastric bacterial pathogen *Helicobacter pylori* utilizes a GGT enzyme to consume glutathione, and the byproducts of this degradation contribute to host symptoms (Shibayama et al., 2007; Ricci et al., 2014). Metabolism of *C. michiganensis* may be an interesting route of research to better understand how this pathogen has adapted to the nutrient-poor xylem, and the GGT encoding gene, *ggtA*, might be a target for future functional studies.

To contrast how *C. michiganensis* infection affects xylem sap composition in a tolerant tomato genotype, we conducted the same untargeted metabolomics experiment with healthy and infected sap of *S. habrochaites* LA2128. Similar to *S. lycopersicum*, most of the metabolites that were significantly differentially accumulated were negatively charged hydrophobic molecules. However, the concentration of this class of molecules were lower in xylem sap from infected

plants relative to healthy *S. habrochaites* LA2128 plants. Comparisons of metabolites that significantly differentially accumulated in sap from each plant species determined that no sap metabolites shared patterns of differential accumulation in *C. michiganensis*-infected *S. habrochaites* and *S. lycopersicum* plants. However, there were some patterns in the types of *S. habrochaites* metabolites affected by pathogen infection. The known metabolite with the greatest decrease in concentration was pyroglutamic acid, an intermediate of glutathione synthesis and a precursor to glutamic acid (Palmer and Alpern 2010). Malic acid and trans-aconitic acid had significantly decreased concentrations in infected sap, possibly suggesting that the citric acid cycle (CAC) is affected in response to pathogen presence. Several enzymes in the CAC pathway are reduced in activity or completely inactivated due to oxidative stress responses, which are triggered by *C. michiganensis* presence in tolerant tomato breeding lines containing quantitative trait loci from *S. habrochaites* LA407 (Tretter and Adam-Vizi, 2000; Sweetlove et al., 2002; Coaker et al., 2004; Bolton et al., 2009). The intermediate N-acetyl-L-glutamic acid is a precursor to the production of urea, as well as the production of polyamines such as putrescine, which are crucial for tomato bacterial wilt symptom development (Lowe-Power et al., 2018; Blume et al., 2019). However, putrescine was not detected in these experiments. Finally, the antibacterial terpene sweroside and the antimicrobial compound sulfadimethoxine were decreased in concentration, which may allow for increased bacterial proliferation in the xylem (Kumarasamy et al., 2003; Dubey et al., 2009).

*Clavibacter michiganensis* grows to three-fold lower densities in *S. habrochaites* LA2128 sap relative to *S. lycopersicum* 'Mt. Fresh' sap (Peritore-Galve et al., 2020). We were interested in using this dataset to identify metabolites that might serve as carbon or nitrogen sources for the pathogen. Most metabolites that were present in significantly different concentrations between

species were negatively charged, hydrophilic compounds. The three metabolites that were most enriched in *S. lycopersicum* 'Mt. Fresh' sap relative to *S. habrochaites* LA2128 were the acidic compounds camphorsulfonic acid, 4-formyl-2-methoxyphenyl hydrogen sulfate and uric acid. The top three metabolites most enriched in *S. habrochaites* LA2128 sap relative to *S. lycopersicum* 'Mt. Fresh' were benzylmethanoate, N-acetylneuraminic acid, and 6-1-hydroxyethyl-3-hydroxymethyl-27-dioxabicyclo[4.1.0]hept-3-en-5-one. It is unclear whether *S. habrochaites* LA2128 is enriched in metabolites that have growth inhibitory properties towards *C. michiganensis*, or just has less available metabolites for bacterial consumption. Future work can study bacterial growth with individual compounds identified in this study to determine sap metabolites critical to *C. michiganensis* growth.

Untargeted metabolomics is a powerful tool to probe interactions between host and pathogen. It is estimated that 1.06 million metabolites exist across all known plant species, highlighting the difficulty of accurately identifying metabolites from mass spectral data (Afendi et al., 2011; Moghe and Kruse, 2018). Liquid chromatography – mass spectrometry for metabolite detection can provide the most wide array of metabolites that constitute the tomato sap metabolome, and fragmentation data of individual metabolites produced through DDMS2 mode can assist in more accurate identification; but further experiments are necessary for accurate identification and classification of compounds (Zamboni et al., 2015; Moghe and Kruse 2018). As public repositories increase the number of identified plant metabolites and computational resources are refined, MS matching will become more accurate (Dührkop et al., 2015; Moghe and Kruse, 2018). This experiment is a first step towards understanding differences in sap metabolites composition during *C. michiganensis* infection in tolerant and susceptible tomatoes. Future experiments will utilize targeted metabolomics approaches to measure precise

concentrations of metabolites of interest, and to use the sequenced genome to study bacterially derived compounds and identify enzymes capable of degrading larger products to generate metabolites detected in the dataset. Results from these studies will further our knowledge of *C. michiganensis*-tomato interactions that may lead to new management strategies.

### ***ACKNOWLEDGMENTS***

Thank you to Holly Lange and Chase Crowell for technical support, and the USDA-GRIN for wild tomato seed. Thank you to Elena Diaz Rubio at the Cornell Metabolomics core for processing and performing the untargeted metabolomics analysis. Special thank you to Liz Mahood and Gaurav Moghe for their support with metabolomics techniques and continued collaboration on this project.

### ***REFERENCES***

- Afendi, F. M., Okada, T., Yamazaki, M., Hirai-Morita, A., Nakamura, Y., Nakamura, K., Ikeda, S., Hiroki, T., Altaf-Ul-Amin, Md., Darusman, L. K., Saito, K., and Kanaya, S. 2012. KNApSAcK family databases: integrated metabolite–plant species databases for multifaceted plant research. *Plant Cell. Physiol.* 53:e1–e1.
- Alikhan, N.-F., Petty, N. K., Ben Zakour, N. L., and Beatson, S. A. 2011. BLAST Ring Image Generator (BRIG): simple prokaryote genome comparisons. *BMC Genomics.* 12:402.

- Almagro Armenteros, J. J., Tsirigos, K. D., Sønderby, C. K., Petersen, T. N., Winther, O., Brunak, S., von Heijne, G., and Nielsen, H. 2019. SignalP 5.0 improves signal peptide predictions using deep neural networks. *Nat. Biotechnol.* 37:420.
- Andrews, S. 2010. FastQC: a quality control tool for high throughput sequence data. Available online at: <http://www.bioinformatics.babraham.ac.uk/projects/fastqc>
- Antipov, D., Hartwick, N., Shen, M., Raiko, M., Lapidus, A., and Pevzner, P. A. 2016. plasmidSPAdes: assembling plasmids from whole genome sequencing data. *Bioinformatics.* 32:3380–3387.
- Araud-Razou, I., Vasse, J., Montrozier, H., Etchebar, C., and Trigalet, A. 1998. Detection and visualization of the major acidic exopolysaccharide of *Ralstonia solanacearum* and its role in tomato root infection and vascular colonization. *Eur. J. Plant Pathol.* 104:795–809.
- Arwiyanto, T., Sakata, K., Goto, M., Tsuyumu, S., and Takikawa, Y. 1994. Induction of tomatine in tomato plant by an avirulent strain of *Pseudomonas solanacearum*. *Jpn. J. Phytopathol.* 60:288–294.

- Aziz, R. K., Bartels, D., Best, A. A., DeJongh, M., Disz, T., Edwards, R. A., Formsma, K., Gerdes, S., Glass, E. M., Kubal, M., Meyer, F., Olsen, G. J., Olson, R., Osterman, A. L., Overbeek, R. A., McNeil, L. K., Paarmann, D., Paczian, T., Parrello, B., Pusch, G. D., Reich, C., Stevens, R., Vassieva, O., Vonstein, V., Wilke, A., and Zagnitko, O. 2008. The RAST server: rapid annotations using subsystems technology. *BMC Genomics*. 9:75.
- Balaji, V., Mayrose, M., Sherf, O., Jacob-Hirsch, J., Eichenlaub, R., Iraki, N., Manulis-Sasson, S., Rechavi, G., Barash, I. and Sessa, G. 2008. Tomato transcriptional changes in response to *Clavibacter michiganensis* subsp *michiganensis* reveal a role for ethylene in disease development. *Plant Physiol*. 146:1797–1809.
- Bankevich, A., Nurk, S., Antipov, D., Gurevich, A. A., Dvorkin, M., Kulikov, A. S., Lesin, V. M., Nikolenko, S. I., Pham, S., Prjibelski, A. D., Pyshkin, A. V., Sirotkin, A. V., Vyahhi, N., Tesler, G., Alekseyev, M. A., and Pevzner, P. A. 2012. SPAdes: a new genome assembly algorithm and its applications to single-cell sequencing. *J. Comput. Biol*. 19:455–477.
- Blume, C., Ost, J., Mühlenbruch, M., Peterhänsel, C., and Laxa, M. 2019. Low CO<sub>2</sub> induces urea cycle intermediate accumulation in *Arabidopsis thaliana*. *PLOS ONE*. 14:e0210342.
- Bolger, A. M., Lohse, M., and Usadel, B. 2014. Trimmomatic: a flexible trimmer for Illumina sequence data. *Bioinformatics*. 30:2114–2120.

- Bolton, M. D. 2009. Primary metabolism and plant defense—fuel for the fire. *Mol. Plant-Microbe Interact.* 22:487–497.
- Brettin, T., Davis, J. J., Disz, T., Edwards, R. A., Gerdes, S., Olsen, G. J., Olson, R., Overbeek, R., Parrello, B., Pusch, G. D., Shukla, M., Thomason III, J. A., Stevens, R., Vonstein, V., Wattam, A. R., and Xia, F. 2015. RASTtk: a modular and extensible implementation of the RAST algorithm for building custom annotation pipelines and annotating batches of genomes. *Sci. Rep.* 5:8365.
- Chalupowicz, L., Barash, I., Reuven, M., Dror, O., Sharabani, G., Gartemann, K.-H., Eichenlaub, R., Sessa, G., and Manulis-Sasson, S. 2017. Differential contribution of *Clavibacter michiganensis* ssp. *michiganensis* virulence factors to systemic and local infection in tomato. *Mol. Plant Pathol.* 18:336–346.
- Chong, J., Soufan, O., Li, C., Caraus, I., Li, S., Bourque, G., Wishart, D. S., and Xia, J. 2018. MetaboAnalyst 4.0: towards more transparent and integrative metabolomics analysis. *Nucleic Acids Res.* 46:W486–W494.
- Coaker, G. L., Willard, B., Kinter, M., Stockinger, E. J., and Francis, D. M. 2004. Proteomic analysis of resistance mediated by Rcm 2.0 and Rcm 5.1, two loci controlling resistance to bacterial canker of tomato. *Mol. Plant-Microbe Interact.* 17:1019–1028.

- Dalsing, B. L., Truchon, A. N., Gonzalez-Orta, E. T., Milling, A. S., and Allen, C. 2015. *Ralstonia solanacearum* uses inorganic nitrogen metabolism for virulence, ATP production, and detoxification in the oxygen-limited host xylem environment. mBio. 6 <http://mbio.asm.org/content/6/2/e02471-14>
- Dixon, G. R., and Pegg, G. F. 1972. Changes in amino-acid content of tomato xylem sap following infection with strains of *Verticillium albo-atrum*. Ann. Bot. 36:147–154.
- Dreier, J., Meletzus, D., and Eichenlaub, R. 1997. Characterization of the plasmid encoded virulence region *pat-1* of phytopathogenic *Clavibacter michiganensis* subsp. *michiganensis*. Mol. Plant-Microbe Interact. 10:195–206.
- Dubey, J. P., Lindsay, D. S., and Lappin, M. R. 2009. Toxoplasmosis and other intestinal coccidial infections in cats and dogs. Vet. Clin. North Am. Small Anim. Pract. 39:1009–1034.
- Dührkop, K., Shen, H., Meusel, M., Rousu, J., and Böcker, S. 2015. Searching molecular structure databases with tandem mass spectra using CSI:FingerID. Proc. Natl. Acad. Sci. U.S.A. 112:12580–12585.
- Fahy, E., Sud, M., Cotter, D., and Subramaniam, S. 2007. LIPID MAPS online tools for lipid research. Nucleic Acids Res. 35:W606-612.

- Fatima, U., and Senthil-Kumar, M. 2015. Plant and pathogen nutrient acquisition strategies. *Front. Plant Sci.* 6:750.
- Franco, R., Schoneveld, O. J., Pappa, A., and Panayiotidis, M. I. 2007. The central role of glutathione in the pathophysiology of human diseases. *Arch. Physiol. Biochem.* 113:234–258.
- Friedman, M. 2013. Anticarcinogenic, cardioprotective, and other health benefits of tomato compounds lycopene,  $\alpha$ -tomatine, and tomatidine in pure form and in fresh and processed tomatoes. *J. Agric. Food Chem.* 61:9534–9550.
- Galant, A., Preuss, M. L., Cameron, J. C., and Jez, J. M. 2011. Plant glutathione biosynthesis: diversity in biochemical regulation and reaction products. *Front. Plant Sci.* 2:45.
- Gartemann, K.-H., Abt, B., Bekel, T., Burger, A., Engemann, J., Flügel, M., Gaigalat, L., Goesmann, A., Gräfen, I., Kalinowski, J., Kaup, O., Kirchner, O., Krause, L., Linke, B., McHardy, A., Meyer, F., Pohle, S., Rückert, C., Schneiker, S., Zellermann, E. M., Pühler, A., Eichenlaub, R., Kaiser, O., and Bartels, D. 2008. The genome sequence of the tomato-pathogenic actinomycete *Clavibacter michiganensis* subsp. *michiganensis* NCPPB382 reveals a large island involved in pathogenicity. *J. Bacteriol.* 190:2138–2149.

- Godzien, J., Alonso-Herranz, V., Barbas, C., and Armitage, E. G. 2015. Controlling the quality of metabolomics data: new strategies to get the best out of the QC sample. *Metabolomics*. 11:518–528.
- Goodger, J. Q. D., Sharp, R. E., Marsh, E. L., and Schachtman, D. P. 2005. Relationships between xylem sap constituents and leaf conductance of well-watered and water-stressed maize across three xylem sap sampling techniques. *J. Exp. Bot.* 56:2389–2400.
- Gurevich, A., Saveliev, V., Vyahhi, N., and Tesler, G. 2013. QUASt: quality assessment tool for genome assemblies. *Bioinformatics*. 29:1072–1075.
- Hao, L., Greer, T., Page, D., Shi, Y., Vezina, C. M., Macoska, J. A., Marker, P. C., Bjorling, D. E., Bushman, W., Ricke, W. A., and Li, L. 2016. In-depth characterization and validation of human urine metabolomes reveal novel metabolic signatures of lower urinary tract symptoms. *Sci. Rep.* 6:1–11.
- Hao, L., Wang, J., Page, D., Asthana, S., Zetterberg, H., Carlsson, C., Okonkwo, O. C., and Li, L. 2018. Comparative evaluation of MS-based metabolomics software and its application to preclinical Alzheimer’s disease. *Sci. Rep.* 8:1–10.
- Hiery, E., Adam, S., Reid, S., Hofmann, J., Sonnewald, S., and Burkovski, A. 2013. Genome-wide transcriptome analysis of *Clavibacter michiganensis* subsp *michiganensis* grown in xylem mimicking medium. *J. Biotechnol.* 168:348–354.

Horai, H., Arita, M., Kanaya, S., Nihei, Y., Ikeda, T., Suwa, K., Ojima, Y., Tanaka, K., Tanaka, S., Aoshima, K., Oda, Y., Kakazu, Y., Kusano, M., Tohge, T., Matsuda, F., Sawada, Y., Hirai, Y. M., Nakanishi, H., Ikeda, K., Akimoto, N., Maoka, T., Tkahashi, H., Ara, T., Sakurai, N., Suzuki, H., Shibata, D., Neumann, S., Iida, T., Tanaka, K., Funatsu, K., Matsuura, F., Soga, T., Taguchi, R., Saito, K., and Nishioka, T. 2010. MassBank: a public repository for sharing mass spectral data for life sciences. *J. Mass Spectrom.* 45:703–714.

Jahr, H., Dreier, J., Meletzus, D., Bahro, R., and Eichenlaub, R. 2000. The endo- $\beta$ -1,4-glucanase CelA of *Clavibacter michiganensis* subsp. *michiganensis* is a pathogenicity determinant required for induction of bacterial wilt of tomato. *Mol. Plant-Microbe Interact.* 13:703–714.

Jordheim, L. P., Durantel, D., Zoulim, F., and Dumontet, C. 2013. Advances in the development of nucleoside and nucleotide analogues for cancer and viral diseases. *Nat. Rev. Drug Discov.* 12:447–464.

Kalhan, S. C., Guo, L., Edmison, J., Dasarathy, S., McCullough, A. J., Hanson, R. W., and Milburn, M. 2011. Plasma metabolomic profile in nonalcoholic fatty liver disease. *Metabolism.* 60:404–413.

- Karp, P. D., Billington, R., Caspi, R., Fulcher, C. A., Latendresse, M., Kothari, A., Keseler, I. M., Krummenacker, M., Midford, P. E., Ong, Q., Ong, W. K., Paley, S. M., and Subhraveti, P. 2019. The BioCyc collection of microbial genomes and metabolic pathways. *Brief Bioinform.* 20:1085–1093.
- Kaup, O., Gräfen, I., Zellermann, E.-M., Eichenlaub, R., and Gartemann, K.-H. 2005. Identification of a tomatinase in the tomato-pathogenic actinomycete *Clavibacter michiganensis* subsp. *michiganensis* NCPPB382. *Mol. Plant-Microbe Interact.* 18:1090–1098.
- Kozukue, N., Han, J.-S., Lee, K.-R., and Friedman, M. 2004. Dehydrotomatine and alpha-tomatine content in tomato fruits and vegetative plant tissues. *J. Agric. Food Chem.* 52:2079–2083.
- Kumarasamy, Y., Nahar, L., Cox, P. J., Jaspars, M., and Sarker, S. D. 2003. Bioactivity of secoiridoid glycosides from *Centaureum erythraea*. *Phytomedicine.* 10:344–347.
- Kurtz, S., Phillippy, A., Delcher, A. L., Smoot, M., Shumway, M., Antonescu, C., and Salzberg, S. L. 2004. Versatile and open software for comparing large genomes. *Genome Biol.* 5:R12.
- Lenth, R. V. 2016. Least-Squares Means: The R Package lsmeans. *J. Stat. Softw.* 69:1–33.

- de León, L., Siverio, F., López, M. M., and Rodríguez, A. 2011. *Clavibacter michiganensis* subsp. *michiganensis*, a seedborne tomato pathogen: healthy seeds are still the goal. *Plant Dis.* 95:1328–1338.
- Lowe-Power, T. M., Hendrich, C. G., Roepenack-Lahaye, E. von, Li, B., Wu, D., Mitra, R., Dalsing, B. L., Ricca, P., Naidoo, J., Cook, D., Jancewicz, A., Masson, P., Thomma, B., Lahaye, T., Michael, A. J., and Allen, C. 2018. Metabolomics of tomato xylem sap during bacterial wilt reveals *Ralstonia solanacearum* produces abundant putrescine, a metabolite that accelerates wilt disease. *Environ. Microbiol.* 20:1330–1349.
- McCarty, R. M., and Bandarian, V. 2008. Deciphering deazapurine biosynthesis: pathway for pyrrolopyrimidine nucleosides toyocamycin and sangivamycin. *Chem. Biol.* 15:790–798.
- Moghe, G. D., and Kruse, L. H. 2018. The study of plant specialized metabolism: challenges and prospects in the genomics era. *Am. J. Bot.* 105:959–962.
- Nandi, M., MacDonald, J., Liu, P., Weselowski, B., and Yuan, Z.-C. 2018. *Clavibacter michiganensis* ssp. *michiganensis*: bacterial canker of tomato, molecular interactions and disease management. *Mol. Plant Pathol.* 19:2036–2050.
- Niu, G., and Tan, H. 2015. Nucleoside antibiotics: biosynthesis, regulation, and biotechnology. *Trends Microbiol.* 23:110–119.

Noctor, G., Arisi, A.-C. M., Jouanin, L., Kunert, K. J., Rennenberg, H., and Foyer, C. H. 1998.

Glutathione: biosynthesis, metabolism and relationship to stress tolerance explored in transformed plants. *J. Exp. Bot.* 49:623–647.

Overbeek, R., Olson, R., Pusch, G. D., Olsen, G. J., Davis, J. J., Disz, T., Edwards, R. A.,

Gerdes, S., Parrello, B., Shukla, M., Vonstein, V., Wattam, A. R., Xia, F., and Stevens, R.

2014. The SEED and the Rapid Annotation of microbial genomes using Subsystems

Technology (RAST). *Nucleic Acids Res.* 42:D206-214.

Palmer, B. F., and Alpern, R. J. 2010. Metabolic acidosis. Chapter in *Comprehensive Clinical*

*Nephrology* (Fourth Edition), eds. Jürgen Floege, Richard J. Johnson, and John Feehally.

Philadelphia: Mosby, p. 155–166. Available at:

Parisy, V., Poinssot, B., Owsianowski, L., Buchala, A., Glazebrook, J., and Mauch, F. 2007.

Identification of PAD2 as a gamma-glutamylcysteine synthetase highlights the

importance of glutathione in disease resistance of Arabidopsis. *Plant J.* 49:159–172.

Peritore-Galve, F. C. Schneider, D. J., Yang, Y., Thannhauser, T. W., Smart, C. D., and

Stodghill, P. 2019. Proteome profile and genome refinement of the tomato-pathogenic

bacterium *Clavibacter michiganensis* subsp. *michiganensis*. *Proteomics.* 19:e1800224

Peritore-Galve, F. C., Miller, C., and Smart, C. D. 2020. Characterizing colonization patterns of *Clavibacter michiganensis* during infection of tolerant wild *Solanum* species.

Phytopathology. 110:574–581.

Ricci, V., Giannouli, M., Romano, M., and Zarrilli, R. 2014. *Helicobacter pylori* gamma-glutamyl transpeptidase and its pathogenic role. World J. Gastroenterol. 20:630–638.

Savidor, A., Teper, D., Gartemann, K.-H., Eichenlaub, R., Chalupowicz, L., Manulis-Sasson, S., Barash, I., Tews, H., Mayer, K., Giannone, R. J., Hettich, R. L., and Sessa, G. 2012. The *Clavibacter michiganensis* subsp. *michiganensis*–tomato interactome reveals the perception of pathogen by the host and suggests mechanisms of infection. J. Proteome Res. 11:736–750.

Scalbert, A., Brennan, L., Manach, C., Andres-Lacueva, C., Dragsted, L. O., Draper, J., Rappaport, S. M., van der Hooft, J. J., and Wishart, D. S. 2014. The food metabolome: a window over dietary exposure. Am. J. Clin. Nutr. 99:1286–1308.

Seeman, T. 2014. Prokka: rapid prokaryotic genome annotation. Bioinformatics. 30:2068-2069.

Sen, Y., van der Wolf, J., Visser, R. G. F., and van Heusden, S. 2014. Bacterial canker of tomato: current knowledge of detection, management, resistance, and interactions. Plant Dis. 99:4–13.

- Shibayama, K., Wachino, J., Arakawa, Y., Saidijam, M., Rutherford, N. G., and Henderson, P. J. F. 2007. Metabolism of glutamine and glutathione via gamma-glutamyltranspeptidase and glutamate transport in *Helicobacter pylori*: possible significance in the pathophysiology of the organism. *Mol. Microbiol.* 64:396–406.
- Siebrecht, S., Herdel, K., Schurr, U., and Tischner, R. 2003. Nutrient translocation in the xylem of poplar — diurnal variations and spatial distribution along the shoot axis. *Planta.* 217:783–793.
- Simão, F. A., Waterhouse, R. M., Ioannidis, P., Kriventseva, E. V., and Zdobnov, E. M. 2015. BUSCO: assessing genome assembly and annotation completeness with single-copy orthologs. *Bioinformatics.* 31:3210–3212.
- Sweetlove, L. J., Heazlewood, J. L., Herald, V., Holtzapffel, R., Day, D. A., Leaver, C. J., and Millar, A. H. 2002. The impact of oxidative stress on Arabidopsis mitochondria. *Plant J.* 32:891–904.
- Tancos, M. A., Chalupowicz, L., Barash, I., Manulis-Sasson, S., and Smart, C. D. 2013. Tomato fruit and seed colonization by *Clavibacter michiganensis* subsp. *michiganensis* through external and internal routes. *Appl. Environ. Microbiol.* 79:6948–6957.

- Tancos, M. A., Lange, H. W., and Smart, C. D. 2015. Characterizing the genetic diversity of the *Clavibacter michiganensis* subsp. *michiganensis* population in New York. *Phytopathology*. 105:169–179.
- Tancos, M. A., Lowe-Power, T. M., Peritore-Galve, F. C., Tran, T. M., Allen, C., and Smart, C. D. 2018. Plant-like bacterial expansins play contrasting roles in two tomato vascular pathogens. *Mol. Plant Pathol.* 19:1210–1221.
- Thapa, S. P., Pattathil, S., Hahn, M. G., Jacques, M.-A., Gilbertson, R. L., and Coaker, G. 2017. Genomic analysis of *Clavibacter michiganensis* reveals insight into virulence strategies and genetic diversity of a gram-positive bacterial pathogen. *Mol. Plant-Microbe Interact.* 30:786–802.
- Tran, T. M., MacIntyre, A., Hawes, M., and Allen, C. 2016. Escaping underground nets: extracellular DNases degrade plant extracellular traps and contribute to virulence of the plant pathogenic bacterium *Ralstonia solanacearum*. *PLOS Pathogens*. 12:e1005686.
- Tretter, L., and Adam-Vizi, V. 2000. Inhibition of Krebs cycle enzymes by hydrogen peroxide: a key role of  $\alpha$ -ketoglutarate dehydrogenase in limiting NADH production under oxidative stress. *J. Neurosci.* 20:8972–8979.

- Vidavsky, N., Kunitake, J. A. M. R., Diaz-Rubio, M. E., Chiou, A. E., Loh, H.-C., Zhang, S., Masic, A., Fischbach, C., and Estroff, L. A. 2019. Mapping and profiling lipid distribution in a 3D model of breast cancer progression. *ACS Cent. Sci.* 5:768–780.
- Wickham, H. 2009. *ggplot2: Elegant Graphics for Data Analysis*. New York: Springer-Verlag.
- Wishart, D. S., Feunang, Y. D., Marcu, A., Guo, A. C., Liang, K., Vázquez-Fresno, R., Sajed, T., Johnson, D., Li, C., Karu, N., Sayeeda, Z., Lo, E., Assempour, N., Berjanskii, M., Singhal, S., Arndt, D., Liang, Y., Badran, H., Grant, J., Serra-Cayuela, A., Liu, Y., Mandal, R., Neveu, V., Pon, A., Knox, C., Wilson, M., Manach, C., and Scalbert, A. 2018. HMDB 4.0: the human metabolome database for 2018. *Nucleic Acids Res.* 46:D608–D617.
- Zamboni, N., Saghatelian, A., and Patti, G. J. 2015. Defining the metabolome: size, flux, and regulation. *Mol. Cell.* 58:699–706.
- Zhang, H., Yohe, T., Huang, L., Entwistle, S., Wu, P., Yang, Z., Busk, P. K., Xu, Y., and Yin, Y. 2018. dbCAN2: a meta server for automated carbohydrate-active enzyme annotation. *Nucleic Acids Res.* 46:W95–W101.

## CHAPTER 4

### **Proteome profile and genome refinement of the tomato-pathogenic bacterium**

#### ***Clavibacter michiganensis* subsp. *michiganensis***

##### ***ABSTRACT***

The gram-positive bacterial pathogen *Clavibacter michiganensis* subsp. *michiganensis* (Cmm) causes bacterial canker of tomato, an economically impacting disease for tomato growers in New York, where annual outbreaks cause yield loss in infected fields with total crop loss in some locations. The systemic nature of this bacterium makes it difficult to control with cultural or chemical methods, and there is currently no known resistance in tomato. Whole genome analysis has identified many potential genes involved in disease induction, and further analyses of the *in vitro* transcriptome, proteome, and *in vivo* ‘interactome’ have been studied. However, a more complete proteome profile will provide additional tools for researchers studying this pathogen and will enable improved annotation of the genome. Tandem mass spectrometry and bioinformatic analyses were used to identify the proteome profile of the sequenced strain, NCPPB382. A proteogenomic pipeline was created using strict filters to generate a highly accurate peptide dataset. These peptide-level data enabled the identification of twenty-six new coding regions, some of which were confirmed through reverse-transcription PCR. The data also supported extension of 59 ORFs and expression validation of 2,183 gene models. Data are available via ProteomeXchange with identifier PXD006787.

\*This chapter was published in: Peritore-Galve F.C., Schneider D.J., Yang Y., Thannhauser T.W., Smart C.D., and Stodghill P. (2019) Proteome profile and genome refinement of the tomato-pathogenic bacterium *Clavibacter michiganensis* subsp. *michiganensis*. *Proteomics*, 1800224. Supporting information not shown here is available online.

## **INTRODUCTION**

The gram-positive bacterial pathogen *Clavibacter michiganensis* subsp. *michiganensis* (Cmm) is the causal agent of bacterial canker of tomato (*Solanum lycopersicum*). This internationally quarantined bacterium can cause economic losses for growers in all tomato-growing regions by causing epidemics from contaminated seed and by entry through natural openings or wounds in the plant (de León et al. 2011; Chalupowicz et al. 2011; Tancos et al. 2013). The pathogen proliferates and spreads through the plant xylem, and at higher densities forms stem cankers, unilateral leaf wilt, and bird's-eye lesions on fruit, resulting in yield loss and reduced tomato fruit quality (Chalupowicz et al. 2011; Tancos et al. 2013; Nandi et al. 2018; Sen et al. 2014).

Recent studies have expanded our understanding of Cmm biology and virulence factors (Nandi et al. 2018). The first sequenced genome of Cmm, strain NCPPB382 (Cmm382), identified the *chp/tomA* 129-kb pathogenicity island (PAI). This island harbors serine proteases and cell wall degrading enzymes hypothesized to be involved in virulence, as well as a tomatinase enzyme that detoxifies the host-defense alkaloid  $\alpha$ -tomatine (Gartemann et al. 2008; Thapa et al. 2017). The *tomA* subregion also contains genes involved in uptake and metabolism of carbohydrates, as well as glycosyl hydrolases described as putative virulence factors (Gartemann et al. 2008; Thapa et al. 2017). Two plasmids, pCM1 and pCM2, were also identified in Cmm382 and are necessary for full virulence (Meletzus et al. 1993; Eichenlaub and Gartemann 2011). Subsequent 'omics analyses of Cmm have validated the annotated genome and provided evidence for expression of putative virulence genes (Gartemann et al. 2008; Savidor et al. 2012; Hiery et al. 2013). A recent comparative genomic study of 16 pathogenic Cmm isolates identified 13 core Sec-dependent secreted proteins (Thapa et al. 2017). The present

study matched novel genes in the Cmm382 genome to genes in the 16 recently sequenced Cmm isolates, validating the utility of proteogenomic approaches.

Proteogenomics uses custom protein sequence databases to identify novel peptides to improve genome annotations (Nesvizhskii 2014). This technique is used to refine genomes and discover protein-coding regions that may play a role in virulence or other important biological processes. Recently it was used to identify 30 new protein coding regions and extend the N-terminus of 50 previously annotated genes of the tomato bacterial spot pathogen *Xanthomonas euvesicatoria* (Abendroth et al. 2017). Six-frame (6F) translated databases of the genome are often used in proteogenomics for identification of novel peptides. This approach, paired with the standard 1% false discovery rate (FDR) cutoff has an unacceptably high probability of generating false positive hits to peptides in the dataset, resulting in misannotation of new genes (Krug et al. 2013). Therefore, stricter filtering criteria or confirmation through an orthogonal validation approach should be employed to reduce the likelihood of false-positive peptide identifications in a proteogenomic dataset. Genome annotation quality also affects sensitivity of novel peptide identification using a 6F database; genomes with more complete annotations are more likely to produce false-positive novel gene predictions (Zhang et al. 2015). Cmm382 has been studied to further understand the complex mechanisms of virulence, but global analyses have not been used to refine the genome, making it a candidate for proteogenomics (Nandi et al. 2018).

This dataset briefly describes the production and use of high-resolution Cmm382 proteomic data for reannotation and refinement of the reference genome. Proteomic data were generated through a 2D fractionation strategy of high pH reverse phase fractionation (hpRP) followed by low pH nanoliquid chromatography (HPLC), and tandem mass spectrometry (nano-

LC-MS/MS) of Cmm382 bacterial pellet and supernatant samples. MS/MS spectra were searched against a 6F translated database of the Cmm382, pCM1, and pCM2 Genbank genomes (AM711867, AM711865, and AM711866, respectively) (Figure X). Strict FDR cutoffs and filtering criteria were applied in order to greatly reduce the number of false positive peptides in the dataset for more precise reannotation (Zhang et al. 2015; Li et al. 2016, 2017). These data were used to improve the annotation of protein coding genes by identifying novel coding regions, extending annotated open reading frames (ORFs), and confirming protein expression for predicted gene models (Figure X) (Nesvizhskii 2014). Transcription of six proposed novel coding regions was confirmed using reverse transcription polymerase chain reaction (RT-PCR) (Figure X). All data are available through ProteomeXchange (<http://www.proteomexchange.org>) Consortium via the PRIDE partner repository with the dataset identifier PXD006787.

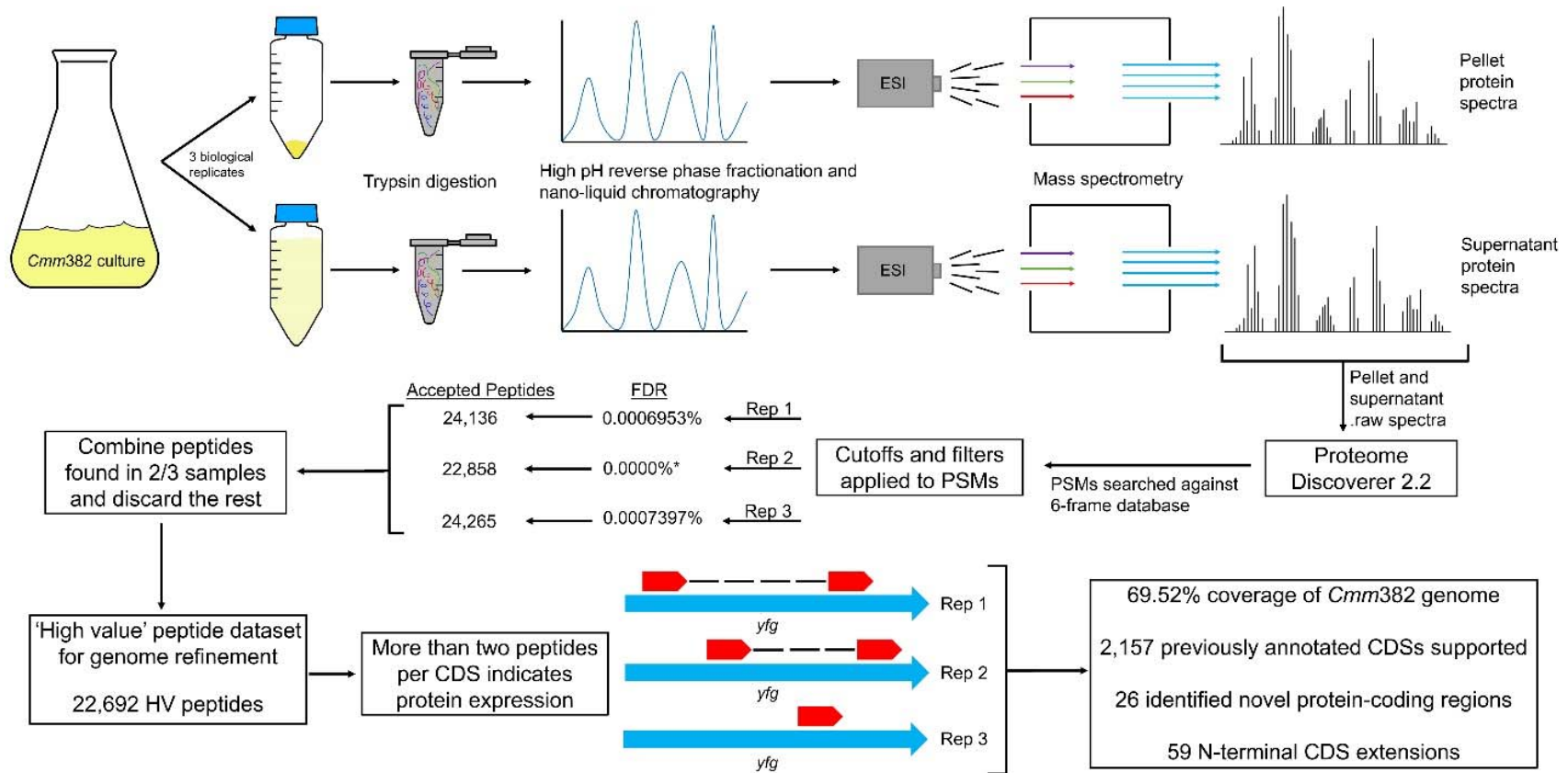


**Figure 4.1.** Visual abstract of sample preparations, shotgun proteomics, and filtering steps used to generate the *Cmm382* proteome and the high-value dataset for genome refinement. \* Following the FDR of biological replicate two denotes that the mass error was so low that Percolator (part of PD2.2) assigned  $q$ -values lower than  $7 \times 10^{-6}$ . Although the reported  $q$ -values are zero, they are not truly zero; the value reported by PD2.2 for this set of PSMs is most likely the result of very high scoring matches. Further information on PSMs, peptide matches, and database searching can be found in the supplemental information of the published article.

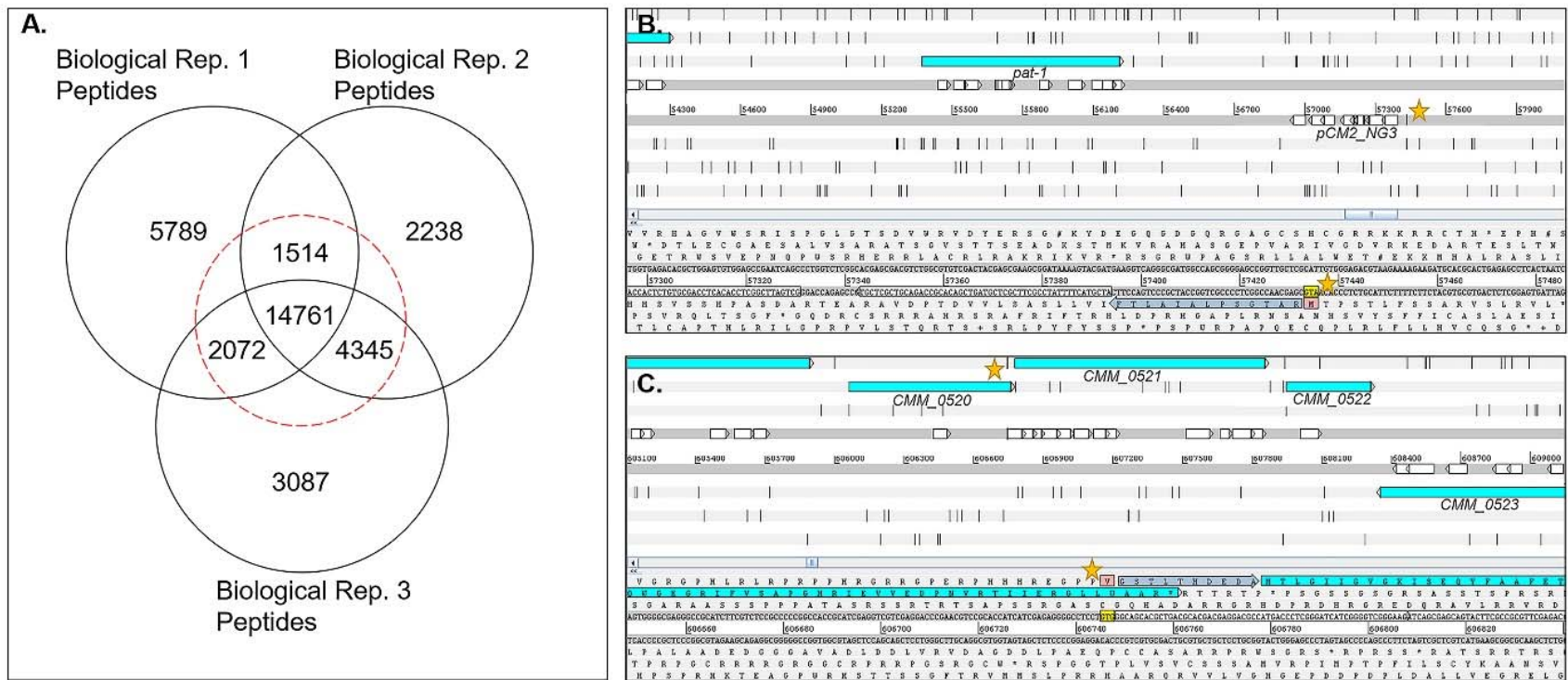


**Figure 4.2.** (A) Number of unique peptides from each biological sample and the number supported in the high-value peptide dataset (shown in dashed red circle). (B) Novel CDS identification: White boxes denote peptides from the high-value dataset mapped onto the sequence of pCM2 (AM711866) in a region with no previously annotated CDS. The yellow star highlights the position of the predicted start codon. (C) Gene extension modification of *CMM\_0521* in the chromosome (AM711867) showing the peptide that supports an upstream GTG as the start codon (yellow star) instead of the previously annotated ATG start codon.

## ***METHODS***

### **Culturing for protein extraction**

Cmm328 was cultured for 24 hours to early log phase at 160rpm at 28°C in a minimal medium containing (per liter) 0.25g MgSO<sub>4</sub>·7H<sub>2</sub>O, 0.5g KH<sub>2</sub>PO<sub>4</sub>, 2g K<sub>2</sub>HPO<sub>4</sub>, 10g sucrose, and 0.1g yeast extract (Alarcon et al. 1998; Gartemann et al. 2008). Supernatants were separated from bacterial cells (Figure 4.1) by centrifugation at 4°C for 15 minutes at 7,500 x G and filter sterilized using Corning 500mL 0.2um polyethersulfone (PES) filtration systems (Corning, NY). This experiment was replicated in triplicate to produce three biological samples of the pellet and supernatant samples for proteomic analysis.

### **Preparation of sample proteins and trypsin digest**

The cell pellet was resuspended in 4mL of lysis buffer consisting of 50mM Tris-HCl pH 8.0, 150mM NaCl, 1mM PMSF (phenylmethylsulfonyl fluoride), and 5mM EDTA (ethylenediaminetetraacetic acid). Using a French pressure cell press equipped with a Mini Cell (Thermo Spectronic, Pittsburgh, PA), the cells were disrupted in two cycles at 900PSI for 3 minutes per cycle. Cell debris was removed from the lysate by centrifugation at 4°C at 15,000 x G for 10 minutes. The proteins in the clarified cell lysate were precipitated by adding 10 volumes of 10% TCA (trichloroacetic acid)/acetone. Precipitation was carried out at -20°C for over 16 hours. A protein pellet was formed by centrifugation of the precipitate at 4°C, 15,000 x G for 15 minutes. The protein pellet was washed three times in cold acetone, air dried for 5 minutes, then stored at -20°C.

A volume of 500mL of the filtered culture supernatant was concentrated using Amicon Ultra centrifugal filter units (Millipore, Billerica, MA) with a 10K NMWL (nominal molecular weight limit) membrane. The supernatant was centrifuged at 4,000 x G at 4°C to a total volume

of 0.25mL. The supernatant proteins from the final 10K concentrate were precipitated by the addition of 10 volumes of 10% TCA/acetone. The precipitation was carried out at -20°C overnight. A protein pellet was formed by centrifugation of the precipitate at 4°C, 15,000 x G for 15 minutes. The protein pellet was washed twice in cold acetone, air dried for 5 minutes, then stored at -20°C.

Protein pellets from both the cell pellet and culture supernatant were resuspended in 6M urea/50 mM TEAB (triethylammonium bicarbonate). Proteins were reduced with DTT (dithiothreitol) at 5mM, and the cysteines were blocked with 10mM MMTS (methyl methanethiosulfonate). Urea concentration was lowered to less than 1M with 50 mM TEAB, and trypsin enzyme (Promega, Madison, WI) was added at a trypsin:protein ratio of 1:25. Digestion was carried out at 30°C for 18 hours. The peptides were isolated by solid phase extraction (SPE) c18 cartridges (Waters, Milford, MA) using a Supelco 12 position vacuum manifold prior to analysis. The eluted peptides were dried at reduced pressure and stored at -20°C prior to analysis.

### **First dimension high pH reverse phase fractionation and HPLC**

The high pH reverse phase (hpRP) chromatography was carried out using a Dionex UltiMate 3000 HPLC system (Sunnyvale, CA) with UV detection (214 nm) as described (Yang et al. 2011; Wang et al. 2011). Specifically, each sample was reconstituted in 175µl of buffer A [20 mM ammonium formate ( $\text{NH}_4\text{CHO}_2$ ), pH 9.5 in water], and loaded onto an XTerra MS C18 column (3.5 µm, 2.1x150 mm) (Waters, Milford, MA) with 20 mM  $\text{NH}_4\text{CHO}_2$ , pH 10 as buffer A and 85% ACN (acetonitrile)/15%  $\text{H}_2\text{O}$ /20 mM  $\text{NH}_4\text{CHO}_2$  as buffer B. The chromatography was carried out at 30°C and a flow rate of 200 µl/minute. The elution program involved a 39 minute linear gradient from 0-45% buffer B followed by a 3 minute ramp to 90% buffer B where it was held for 1 minute. Forty-eight fractions were collected at 1-minute intervals and pooled

based on the UV absorbance using a multi-fraction concatenation strategy to take maximum advantage of the analytical column's peak capacity (Yang et al. 2011; Wang et al. 2011). Six and twelve fractions were generated for each bacterial supernatant and pellet analyzed, respectively. The pooled fractions were dried at reduced pressure using a centrifugal concentrator and stored at -20°C until analyzed as described below.

### **Second dimension fractionation and tandem MS**

All of the fractions were reconstituted in 80  $\mu\text{L}$  of 2% ACN/0.5%  $\text{H}_2\text{CO}_2$  for nano-liquid chromatography-electrospray ionization-MS/MS analysis, that was carried out using an Orbitrap Fusion<sup>TM</sup> Tribrid<sup>TM</sup> mass spectrometer (Thermo-Fisher Scientific, San Jose, CA) equipped with a nanospray Flex Ion Source and coupled to a Dionex UltiMate3000RSLCnano system (Thermo, Sunnyvale, CA). Ten  $\mu\text{L}$  of each fraction was injected onto a PepMap C-18 RP nano-trap column (5  $\mu\text{m}$ , 100  $\mu\text{m}$  i.d. x 20 mm, Dionex) at 20  $\mu\text{L}/\text{minute}$  flow rate for on-line desalting. The analytical separation was carried out at 35°C and 300 nL/minute on a PepMap C-18 RP nano-column (2  $\mu\text{m}$ , 75  $\mu\text{m}$  x 15 cm). Eluent A consisted of an aqueous solution of 0.1%  $\text{H}_2\text{CO}_2$  and eluent B was 0.1%  $\text{H}_2\text{CO}_2$  in ACN. The column was equilibrated prior to the run at 5% Eluent B and the elution involved a 120-minute linear gradient from 5-35% B, followed by a 5-minute ramp to 90% B. The column was washed for 5 minutes at 90% B and then returned to initial conditions 25 minutes for equilibration. The Orbitrap Fusion was operated in a data dependent, positive ion mode with the spray voltage and source temperature set to 1.8 kV and 275°C, respectively. All mass analyzers were calibrated externally. The FT mass analyzer was used for MS1 scans to select multiply charged precursor ions for fragmentation followed by a 3 second "Top Speed" data-dependent CID of the selected ions in the linear ion trap using an activation time of 10 msec, a  $\pm 1.6$  m/z quadrupole isolation window, a threshold ion count of

10,000 and a normalized collision energy of 30%. MS survey scans were carried out at a resolving power of 120,000 (fwhm at  $m/z$  200) for the  $m/z$  range of 375-1575. Dynamic exclusion parameters were set at repeat count 1 with a 20 s repeat duration, an exclusion list size of 500, and a 40 s exclusion duration with  $\pm 10$  ppm exclusion mass window. All data were acquired under Xcalibur 3.0 operation software (Thermo-Fisher Scientific).

### **Search settings for MS and MS/MS spectra**

A 6-frame translated database of Cmm382, pCM1, and pCM2 from the Genbank accessions (AM711867, AM711865, and AM711866, respectively) was generated and used to search MS/MS spectra (<https://github.com/pvstodghill/peritore2018>). The search settings used in Proteome Discoverer 2.2 (Thermo-Fisher Scientific) were semi-tryptic with one missed cleavage, fixed methylthio modification of cysteine, and variable modification of methionine oxidation. The peptide mass tolerance and fragment mass tolerance values were 10 ppm and 0.4Da, respectively. The mean difference between theoretical and observed masses for every sample was less than 60 parts per billion.

### **FDR cutoff calculation and filters applied**

All results from all fractions of the pellet and supernatant were pooled by biological replicate prior to scoring. We selected a custom FDR cutoff for each biological replicate by calculating at what cutoff the estimated number of theoretical false discoveries was less than one. The PSM results for each replicate were ordered by q-value from smallest to largest. The data were then sorted to identify the PSM with the largest possible q-value ( $E_M$ ) for which the number of PSMs whose q-value was less than or equal to  $E_M$ , multiplied by  $E_M$  was less than one.  $E_M$  then became the FDR cutoff for that biological replicate. Non-unique peptides were discarded and PSMs found in two of three biological replicates were combined into the high value peptide

database.

## **Confirming transcription of new genes using Reverse Transcription-Polymerase Chain Reaction**

Cmm382 was cultured for 24 hours to early log phase at 160rpm at 28°C in Luria-Bertani medium as described in (Tancos et al. 2018). Full-length genomic DNA from Cmm382 was extracted with the MasterPure Gram-Positive DNA purification kit (Epicentre, Madison, WI) following manufacturer's instructions. Total RNA was extracted from 2mL of Cmm382 grown as described above using a ZR Fungal/Bacterial RNA MiniPrep kit (Zymo Research Corp., Irvine, CA). An off-column additional DNase treatment was performed using TURBO DNA-free DNase (Fisher Scientific; Pittsburgh, PA). Quantity and quality of DNA and RNA were determined with a NanoDrop ND 1000 (NanoDrop Technologies, Wilmington, DE) and a Qubit 2.0 Fluorometer (Invitrogen, Carlsbad, CA). Reverse transcription was performed with RNA to cDNA EcoDry Premix (random hexamers) (Clontech Laboratories, Inc., Mountain View, CA) using 300ng total RNA per reaction. One-tenth of the reverse transcription reaction volume of cDNA was used in a 25 µl PCR reaction using EmeraldAmp GT PCR Master Mix (Takara Bio, Inc., Otsu, Shiga, Japan) with primers designed to amplify *gyrB* or regions within novel protein-coding genes (Table 4.3). To ensure no DNA contaminants were in the RNA, negative controls were performed with 100ng total RNA as a template. Genomic DNA was used at 50ng per reaction with 10 µM of forward and reverse primers as a positive control (Figure 4.3). Amplifications were performed in a C1000 Touch Thermal Cycler (Bio-Rad Laboratories, Inc., Hercules, CA). PCR was performed in 25 µl reactions with the following parameters: preheat for 3 minutes at 95°C, 35 cycles at 95°C for 15 seconds, primer pair specific annealing temperature for 30 seconds (Table 4.3), extension at 72° for 30 seconds, final extension at 72°C for 5 minutes,

and held at 12°C. Amplicons were electrophoresed on 1% gels at 80V for 1 hour, followed by staining with GelRed (Biotium Inc., Hayward, CA).

## **RESULTS**

Cmm382 was cultured to early log phase in minimal medium as previously described (Alarcon et al. 1998; Fluegel et al. 2012; Hiery et al. 2013). Supernatants were separated from bacterial cell pellets through centrifugation (Figure 4.1) and filter sterilized. Three biological samples each of pellet and supernatant were submitted for shotgun proteomics. Subsequent steps included protein purification, trypsin digestion, hpRP, HPLC, and MS/MS. Mass spectrometry and MS/MS raw spectra were processed and searched using Sequest HT software within Proteome Discoverer 2.2 (PD2.2, Thermo) using a custom database generated from the 6F translation of the annotated genome. Custom search settings were applied and FDR cutoffs were calculated for each biological sample by requiring the number of theoretical false discoveries to be less than one (Figure 4.1). Non-unique peptides were discarded and data from all three biological replicates were combined into a “high value” (HV) peptide dataset (Figure 4.1 and Table 4.1). Gene models of Cmm382, pCM1, and pCM2 were required to be supported by at least two peptides independently derived from two out of three biological samples (Figure 4.1 and 4.2). To test the sensitivity of the filtering criteria used for the HV peptide dataset, a mock trypsin digestion of the 6F-translated database was carried out *in silico* using custom scripts (<https://github.com/pvstodghill/peritore2018>). The number of unique peptides identified in the resulting dataset was more than tenfold greater than in the HV dataset derived from biological samples (Table 4.1).

**Table 4.1.** Database and peptide search statistics

	Genomic database size (bp)	Amino acids in database	Number of unique peptides	Unique peptides mapped to known CDSs	Unique peptides mapped to novel CDSs
<i>In silico</i>	3,395,237	6,533,671	353,739	51,918 (14.56%)	511 (0.144%)
<b>Experimental ('High-value')</b>	3,395,237	6,533,671	22,692	22,547 (99.36%)	145 (0.0064%)

Peptides from the HV dataset supported expression of 2183 ORFs of Cmm382 (Figure 4.1), achieving 69.52% coverage of the improved genome. The same dataset provided evidence for 26 new protein-coding regions, 59 ORF N-terminal extensions, and the expression of a product encoded by a previously identified pseudogene (CMM\_PS\_19). ORFs with peptide-level evidence supporting new CDS annotations or N-terminal extension were assigned the most proximal canonical start codon using Artemis (Sanger Institute, Cambridge, UK) (Figure 4.2).

Of the 26 novel coding regions, 20 were on the chromosome, two in plasmid pCM1, and four in pCM2. BLASTP identified high sequence similarity of these products to proteins from *Clavibacter michiganensis* subspecies (Table 4.2). The genomic location of seven novel CDSs encoding proteins of unknown function was within the *chp/tomA* PAI, a region essential for disease induction (Table 4.2) (Chalupowicz et al. 2017). Previously unannotated coding regions on the chromosome outside of the *chp/tomA* PAI encoded mostly proteins of unknown function, many of which were identified in sequenced isolates from a recent bacterial canker outbreak in California (Thapa et al. 2017). Novel coding regions on the plasmids encoded proteins of unknown function, putative membrane proteins, or proteins with no known sequence similarity.

Transcription of six intergenic novel CDSs on both plasmids and the chromosome were confirmed using RT-PCR (Figure 4.3). Primers were designed to amplify internal regions of the

new genes and a housekeeping gene to detect complementary DNA derived from transcripts (Figure 4.3 and Table 4.3) (Tancos et al. 2015). Amplicons from the gDNA template were sequenced and all genes were correctly amplified, supporting the accuracy of our proteogenomic approach in identifying novel CDSs.

**Table 4.2.** Table of novel *Cmm382* and plasmid genes identified in this study

Gene name	Predicted position	Strand	Predicted protein length (aa)	Neighboring genes
New CDS in <i>Cmm382</i> chromosome				
<i>CMM_NG1</i> †	38178 - 39737	Forward	519	<i>CMM_0033...CMM_0034</i>
<i>CMM_NG2</i>	60856 - 60314	Reverse	180	<i>chpA...CMM_0046</i>
<i>CMM_NG3</i>	76081 - 76479	Forward	132	<i>chpF...CMM_0054</i>
<i>CMM_NG4</i>	80087 - 80263	Forward	58	<i>CMM_0056...CMM_0057</i>
<i>CMM_NG5</i>	95309 - 95641	Forward	110	<i>parX...CMM_0067</i>
<i>CMM_NG6</i>	111115 - 111552	Forward	145	<i>CMM_0073...CMM_0074</i>
<i>CMM_NG7</i>	116549 - 116223	Reverse	108	<i>CMM_0076...CMM_0077</i>
<i>CMM_NG8</i>	228988 - 229674	Forward	228	<i>CMM_0167a...CMM_0168</i>
<i>CMM_NG9</i>	504699 - 506195	Forward	499	<i>CMM_0426...CMM_0427</i>
<i>CMM_NG10</i>	555723 - 552277	Reverse	1148	<i>xthB...CMM_0476</i>
<i>CMM_NG11</i>	716112 - 716483	Forward	123	<i>CMM_0627...CMM_0628</i>
<i>CMM_NG12</i>	735208 - 735798	Forward	196	<i>CMM_0648...CMM_0649</i>
<i>CMM_NG13</i>	945437 - 944421	Reverse	338	<i>CMM_0828...wcoK</i>
<i>CMM_NG14</i>	1284804 - 1284926	Forward	40	<i>CMM_1122...sgaH</i>
<i>CMM_NG15</i> †	1611425 - 1611772	Forward	115	<i>CMM_1419...argE</i>
<i>CMM_NG16</i>	2190639 - 2190151	Reverse	162	<i>CMM_1940...CMM_1941</i>
<i>CMM_NG17</i>	2307160 - 2306783	Reverse	125	<i>CMM_2043...CMM_2044</i>
<i>CMM_NG18</i>	2600418 - 2599810	Reverse	202	<i>CMM_2295...CMM_2296</i>
<i>CMM_NG19</i> †	2615387 - 2614806	Reverse	193	<i>CMM_PS_21...moaE</i>
<i>CMM_NG20</i>	2759950 - 2759684	Reverse	88	<i>CMM_2449...CMM_2451</i>
New CDS in <i>Cmm382</i> plasmids				
<i>pCM1_NG1</i> †	5531 - 5692	Forward	53	<i>traG...pCM1_0006</i>
<i>pCM1_NG2</i> †	24206 - 24006	Reverse	66	<i>pin...pCM1_0026</i>
<i>pCM2_NG1</i>	28245 - 27733	Reverse	170	<i>pCM2_0029...pCM2_0030</i>
<i>pCM2_NG2</i>	32779 - 33063	Forward	94	<i>parA...pCM2_0034</i>
<i>pCM2_NG3</i>	56108 - 56380	Forward	90	<i>pat-1...pCM2_NG5</i>
<i>pCM2_NG4</i> †	57435 - 56893	Reverse	180	<i>pCM2_NG4...pCM2_NG6</i>

†Denotes new genes with expression confirmed by RT-PCR.

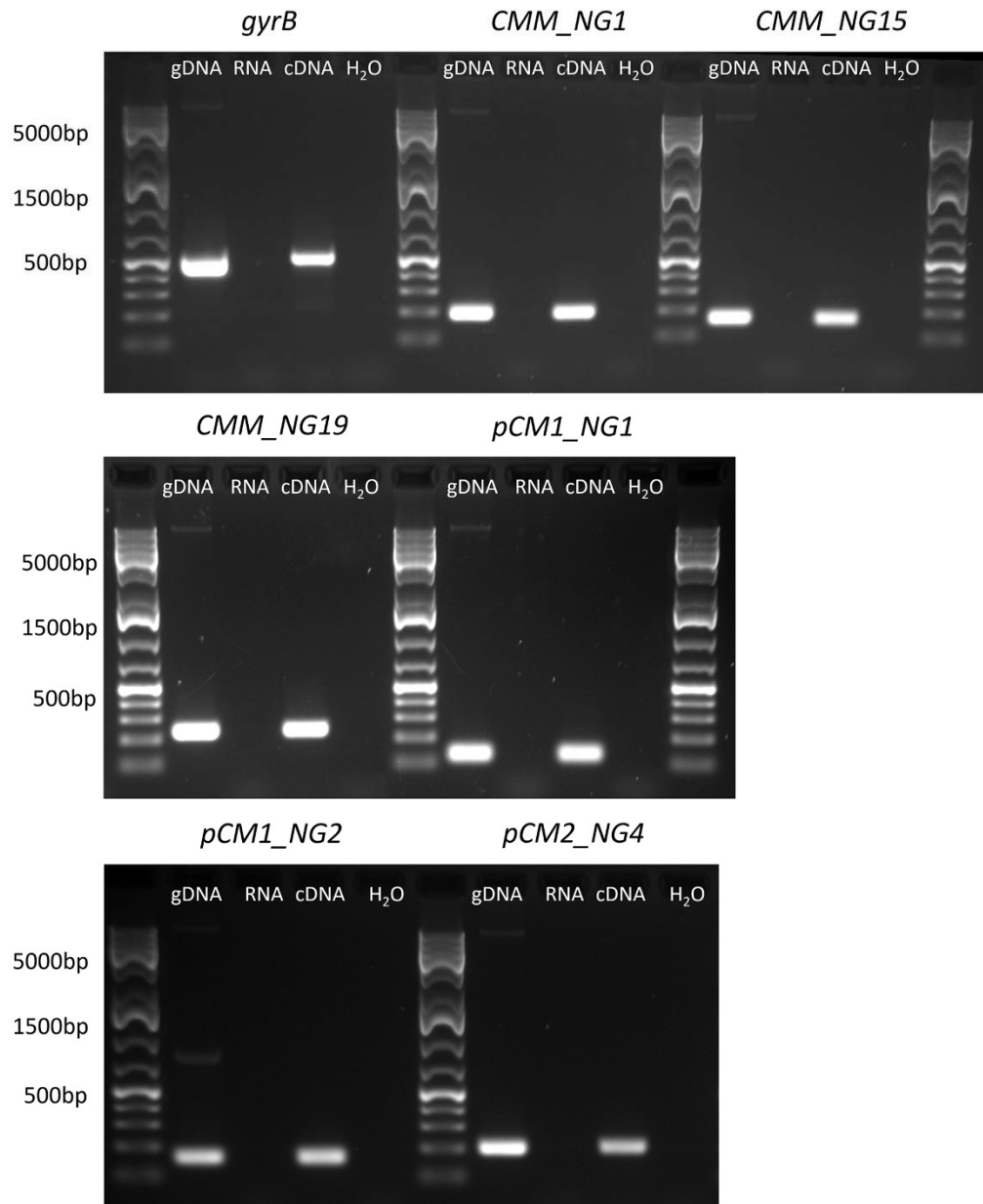


**Figure 4.3.** GelRed-stained agarose gel showing the expression analysis of selected novel coding regions *in vitro*. Reverse transcription-polymerase chain reaction (RT-PCR) products of Cmm382 along with positive (50ng genomic DNA) and negative controls (100ng total RNA and water). The constitutively expressed housekeeping gene *gyrB* was amplified using the same conditions. Thermo Scientific O'GeneRuler 1kb Plus DNA Ladder was used to measure fragment size.

**Table 4.3.** Oligonucleotides used in this study

Name	Sequence (5'-3')	Locus tag	Gene location	T <sub>m</sub> (°C)	Amplicon size (bp)	Reference
GyrB	F:ACCGTCGAGTTCGACTACGA R:CCTCGGTGTTGCCSARCTT	<i>CMM_0006</i>	Chromosome	60	525	Tancos et al., 2015
Ch_G1	F:GCGCTCACGTATCTGAATGA R:GTTCCACCCCGTAGAAGTGA	<i>CMM_NG1</i>	Chromosome	56	193	This study
Ch_G2	F:CTCTGGTTCACCACGAAGC R:CAGGTCATCCAGCAGTTCAC	<i>CMM_NG15</i>	Chromosome	56	161	This study
P1_G3	F:GTCGACACTCCCGCTGGT R:GGGTAGAAGCGAACCTCTCC	<i>pCM1_NG2</i>	pCM1	56	158	This study
P2_G4	F:ACATTTGTGCCCAGAAGTCC R:TCAAGTAGAGCTGCGAGCAA	<i>pCM2_NG4</i>	pCM2	56	202	This study
Ch_G7	F:AATCGTCTACGCCAGACCAC R:GTACCGGGCATCCATACATC	<i>CMM_NG19</i>	Chromosome	56	237	This study
P1_G8	F:GGACTIONGACCCGAGGTC R:CCAAGATGCTGTCCACTGTC	<i>pCM1_NG1</i>	pCM1	56	113	This study

## ***DISCUSSION***

Discovery of unannotated protein-coding regions through proteogenomics is useful for refining genomes, which in turn may provide genetic insight into virulence and the biology of Cmm and other plant pathogens. High-resolution accurate spectra (MS1: 120 000 fwhm, +/- 54ppb) and fragmentation data (MS2: +/- 0.4Da) were generated and searched against a 6F-translated database of Cmm382. Strict filtering criteria were applied to produce highly accurate peptide predictions. Different manipulations of FDR and downstream filters have been used to reduce the number of false positive peptides identified from a dataset (Zhang et al. 2015; Li et al. 2016, 2017). However, here we use a strategy that adjusts the FDR cutoff as a function of the number of theoretical false positives. This approach yields enough peptides to achieve 69.52% coverage of the genome and to identify 26 new coding regions, and extend 59 ORFs. Confirming transcription of a subset of these new genes by RT-PCR provided further evidence that the filtering criteria used were effective. The 5'-most proximal start codon was assigned for every new coding region and for genes requiring extension. We were unable to assign canonical start codons for four gene extensions. This may suggest that those genes utilize a start codon other than ATG, GTG, or TTG, in Cmm. Start codon usage is currently unstudied in *Clavibacter* and may be an interesting avenue of research to uncover the genetics of this gram-positive pathogen. Discovery of new ORFs in the *chp/tomA* PAI and on the plasmids may contribute to identification of new Cmm virulence factors. Evidence for new genes and correction of previously annotated genes will be used to improve the Cmm382 Genbank reference genome, and future studies will be aimed at functional characterization of proteins of biological interest.

## ***ACKNOWLEDGEMENTS***

The authors acknowledge funding from Cornell AgriTech and USDA Federal Capacity Funds. The authors thank members of the Smart lab and Angela Kruse for helpful discussions and critical reading of the manuscript. Mention of trade names or commercial products in this publication is solely for the purpose of providing specific information and does not imply recommendation or endorsement by the USDA. USDA is an equal opportunity provider and employer. This article has been contributed to by US Government employees and their work is in the public domain in the USA.

## ***REFERENCES***

- Abendroth, U., Adlung, N., Otto, A., Grüneisen, B., Becher, D., and Bonas, U. 2017. Identification of new protein-coding genes with a potential role in the virulence of the plant pathogen *Xanthomonas euvesicatoria*. *BMC Genom.* 18:625
- Alarcon, C., Castro, J., Munoz, F., Arce-Johnson, P., and Delgado, J. 1998. Protein(s) from the gram-positive bacterium *Clavibacter michiganensis* subsp. *michiganensis* induces a hypersensitive response in plants. *Phytopathology.* 88:306–310.
- Chalupowicz, L., Barash, I., Reuven, M., Dror, O., Sharabani, G., Gartemann, K.-H., Eichenlaub, R., Sessa, G., and Manulis-Sasson, S. 2017. Differential contribution of *Clavibacter michiganensis* ssp. *michiganensis* virulence factors to systemic and local infection in tomato. *Mol. Plant Pathol.* 18:336–346.

- Chalupowicz, L., Zellermann, E.-M., Fluegel, M., Dror, O., Eichenlaub, R., Gartemann, K.-H., Savidor, A., Sessa, G., Iraki, N., Barash, I., Manulis-Sasson, S. 2011. Colonization and movement of GFP-labeled *Clavibacter michiganensis* subsp. *michiganensis* during tomato infection. *Phytopathology*. 102:23–31.
- Eichenlaub, R., and Gartemann, K.-H. 2011. The *Clavibacter michiganensis* subspecies: molecular investigation of gram-positive bacterial plant pathogens. *Annu. Rev. Phytopathol.* 49:445–464.
- Fluegel, M., Becker, A., Gartemann, K.-H., and Eichenlaub, R. 2012. Analysis of the interaction of *Clavibacter michiganensis* subsp. *michiganensis* with its host plant tomato by genome-wide expression profiling. *J. Biotechnol.* 160:42–54.
- Gartemann, K.-H., Abt, B., Bekel, T., Burger, A., Engemann, J., Flügel, M., Gaigalat, L., Goesmann, A., Gräfen, I., Kalinowski, J., Kaup, O., Kirchner, O., Krause, L., Linke, B., McHardy, A., Meyer, F., Pohle, S., Rückert, C., Schneiker, S., Zellermann, E. M., Pühler, A., Eichenlaub, R., Kaiser, O., Bartels, D. 2008. The genome sequence of the tomato-pathogenic actinomycete *Clavibacter michiganensis* subsp. *michiganensis* NCPPB382 reveals a large island involved in pathogenicity. *J. Bacteriol.* 190:2138–2149.
- Hiery, E., Adam, S., Reid, S., Hofmann, J., Sonnewald, S., and Burkovski, A. 2013. Genome-wide transcriptome analysis of *Clavibacter michiganensis* subsp. *michiganensis* grown in xylem mimicking medium. *J. Biotechnol.* 168:348–354.

- Krug, K., Carpy, A., Behrends, G., Matic, K., Soares, N. C., and Macek, B. 2013. Deep coverage of the *Escherichia coli* proteome enables the assessment of false discovery rates in simple proteogenomic experiments. *Mol. Cell. Proteomics*. 12:3420–3430.
- de León, L., Siverio, F., López, M. M., and Rodríguez, A. 2011. *Clavibacter michiganensis* subsp. *michiganensis*, a seedborne tomato pathogen: healthy seeds are still the goal. *Plant Dis.* 95:1328–1338.
- Li, H., Joh, Y. S., Kim, H., Paek, E., Lee, S.-W., and Hwang, K.-B. 2016. Evaluating the effect of database inflation in proteogenomic search on sensitive and reliable peptide identification. *BMC Genom.* 17:1031.
- Li, H., Park, J., Kim, H., Hwang, K.-B., and Paek, E. 2017. Systematic comparison of false-discovery-rate-controlling strategies for proteogenomic search using spike-in experiments. *J. Proteome Res.* 16:2231–2239.
- Meletzus, D., Bermphol, A., Dreier, J., and Eichenlaub, R. 1993. Evidence for plasmid-encoded virulence factors in the phytopathogenic bacterium *Clavibacter michiganensis* subsp. *michiganensis* NCPPB382. *J Bacteriol.* 175:2131–2136.

- Nandi, M., MacDonald, J., Liu, P., Weselowski, B., and Yuan, Z.-C. 2018. *Clavibacter michiganensis* ssp. *michiganensis*: bacterial canker of tomato, molecular interactions and disease management. *Mol. Plant Pathol.* 19:2036–2050.
- Nesvizhskii, A. I. 2014. Proteogenomics: concepts, applications and computational strategies. *Nat. Meth.* 11:1114–1125.
- Savidor, A., Teper, D., Gartemann, K.-H., Eichenlaub, R., Chalupowicz, L., Manulis-Sasson, S., et al. 2012. The *Clavibacter michiganensis* subsp. *michiganensis*–tomato interactome reveals the perception of pathogen by the host and suggests mechanisms of infection. *J. Proteome Res.* 11:736–750.
- Sen, Y., van der Wolf, J., Visser, R. G. F., and van Heusden, S. 2014. Bacterial canker of tomato: current knowledge of detection, management, resistance, and interactions. *Plant Dis.* 99:4–13.
- Tancos, M. A., Chalupowicz, L., Barash, I., Manulis-Sasson, S., and Smart, C. D. 2013. Tomato fruit and seed colonization by *Clavibacter michiganensis* subsp. *michiganensis* through external and internal routes. *Appl. Environ. Microbiol.* 79:6948–6957.

- Tancos, M. A., Lange, H. W., and Smart, C. D. 2015. Characterizing the genetic diversity of the *Clavibacter michiganensis* subsp. *michiganensis* population in New York. *Phytopathology*. 105:169–179.
- Tancos, M. A., Lowe-Power, T. M., Peritore-Galve, F. C., Tran, T. M., Allen, C., and Smart, C. D. 2018. Plant-like bacterial expansins play contrasting roles in two tomato vascular pathogens. *Mol. Plant Pathol.* 19:1210–1221.
- Thapa, S. P., Pattathil, S., Hahn, M. G., Jacques, M.-A., Gilbertson, R. L., and Coaker, G. 2017. Genomic analysis of *Clavibacter michiganensis* reveals insight into virulence strategies and genetic diversity of a gram-positive bacterial pathogen. *Mol. Plant-Microbe Interact.* 30:786–802.
- Wang, Yuexi, Yang, F., Gritsenko, M. A., Wang, Yingchun, Clauss, T., Liu, T., et al. 2011. Reversed-phase chromatography with multiple fraction concatenation strategy for proteome profiling of human MCF10A cells. *Proteomics*. 11:2019–2026.
- Yang, Y., Qiang, X., Owsiany, K., Zhang, S., Thannhauser, T. W., and Li, L. 2011. Evaluation of different multidimensional LC-MS/MS pipelines for isobaric tags for relative and absolute quantitation (iTRAQ)-based proteomic analysis of potato tubers in response to cold storage. *J. Proteome Res.* 10:4647–4660.

Zhang, K., Fu, Y., Zeng, W.-F., He, K., Chi, H., Liu, C., et al. 2015. A note on the false discovery rate of novel peptides in proteogenomics. *Bioinformatics*. 31:3249–3253.

## CONCLUSIONS AND FUTURE STUDIES

Bacterial canker of tomato continues to be an economically devastating disease for growers worldwide with limited management strategies once the bacterium is introduced into a field or greenhouse (de Leon et al. 2011; Sen et al. 2015). The pathogen affects all aerial parts of the plant, causing leaflet wilt, stem and petiole cankers, leaf blisters, and bird's-eye lesions on fruit (de Leon et al. 2011; Sen et al. 2015; Nandi et al. 2018). The goals of this thesis were to study colonization patterns of *Clavibacter michiganensis* in xylem and fruit tissues of diverse *Solanum* hosts, and to understand the effects of colonization on symptom development and host molecular responses. The results of these studies can guide future investigations into the genetics of *C. michiganensis* pathogenicity and host-microbe interactions, with the hopes that a comprehensive understanding of *C. michiganensis*-host interactions can assist resistance-breeding efforts.

### ***Clavibacter michiganensis* colonization of wild *Solanum* species**

In chapter one we compared how *C. michiganensis* colonizes the vascular system of tolerant wild tomato accessions *S. habrochaites* LA2128, *S. arcanum* LA2157, and *S. arcanum* LA2172 compared to susceptible cultivated tomato, *S. lycopersicum* 'Mt. Fresh' (Sen et al. 2015; Peritore-Galve et al. 2020). Inoculations were also performed with the hypervirulent expansin mutant,  $\Delta$ CmEXLX2, to see if it could increase symptom severity in wild tomato genotypes relative to the wildtype strain (Tancos et al. 2018). *In planta* inoculations determined that wild tomato genotypes developed fewer symptoms relative to cultivated *S. lycopersicum*.  $\Delta$ CmEXLX2 was capable of inducing severe wilt symptoms in only one of the wild tomato genotypes, *S. arcanum* LA2172, while the wildtype *C. michiganensis* strain caused few to no wilt symptoms (Peritore-Galve et al., 2020). Spread and population density of the bacterial

strains were measured, which determined that pathogen density in wild tomatoes was reduced at 5 and 10 cm from the inoculation site. Bacterial density was  $10^{10}$  CFU per g tissue at the inoculation site and distally in *S. lycopersicum* plants, meaning that pathogen spread is limited in wild tomato species. To delve deeper into how the pathogen may be limited in systemic spread, plants were inoculated with an eGFP-expressing isolate to track radial spread in vascular bundles. Using laser-scanning confocal microscopy, we quantified intravascular spread 21 days post inoculation (dpi) and found that the pathogen was restricted mainly to protoxylem vessels in the vascular systems of wild tomato plants. In contrast, at 21 dpi *C. michiganensis* had spread to all vascular tissues including xylem fibers, tracheary elements, and parenchyma cells in *S. lycopersicum* plants. Together, these observations suggest that *C. michiganensis* is reduced in its ability for intravascular spread in wild tomatoes, potentially through the inability to macerate xylem tissues. Reduced spread between vessels may explain the lower bacterial populations at sites distal from the inoculation site in wild tomato plants. It is interesting to note that although high rates of intravascular spread was capable of explaining differences in wilt symptom development between wild and cultivated tomato plants, the hypervirulent expansin mutant demonstrated reduced intravascular spread relative to the wildtype strain in the two genotypes that it caused increased symptoms in, *S. lycopersicum* ‘Mt. Fresh’ and *S. arcanum* LA2172. These contrasting findings underscore the importance of CmEXLX2 in symptom development, which merits future study of its targets and function.

Since xylem sap is presumably the main nutrient source for *C. michiganensis* during vascular infection, we tested the ability for the pathogen to grow in sap. The bacterium grew to the highest densities in sap from cultivated species, but we were surprised to learn that it grew to the second highest densities in sap from *S. arcanum* LA2157, which was asymptomatic during

infection and harbored the lowest bacterial populations *in planta*. In contrast, it grew to very low densities in *S. habrochaites* LA2128 sap, but was capable of growing to densities up to  $10^8$  *in planta* (Peritore-Galve et al. 2020). These results led us to hypothesize that host-pathogen interactions occur in the xylem sap that can affect pathogen colonization, serving as an impetus for the experiments in chapter 3. I was also interested in the ability for the pathogen to form biofilm-like aggregates *in vitro* when cultured in sap from wild tomatoes. This pathogen forms dense aggregates when cultured in tomato xylem sap, but not in nutrient-rich or minimal medium *in vitro* (Chalupowicz et al. 2012; Tancos et al. 2018). We found that *in vitro* aggregation was growth-dependent when cultured in sap from wild and cultivated tomatoes (Peritore-Galve et al. 2020). Unpublished studies from the Smart lab tested the effect of modifying the pH of xylem mimicking medium on *C. michiganensis* aggregation *in vitro* and found that lowering the pH had modest effects on bacterial aggregation, whereas adding xylem sap greatly increased the density of *C. michiganensis* aggregates (Crowell et al., 2014). This result and the result of aggregation experiments with wild tomato sap might suggest that there is a chemical cue in xylem sap that influences *C. michiganensis* aggregation, and thus biofilm formation. Since aggregation and biofilm formation are critical for other vascular bacterial pathogens (reviewed in Rapicavoli et al. 2018 and Lowe-Power et al. 2018), this area of research is an interesting avenue for understanding *C. michiganensis* biology and pathogenicity.

The third and final aim of this study was to test if *C. michiganensis* caused symptoms when inoculated onto wild tomato fruit. Wild tomato fruit are small and green, and are morphologically very different from cultivated *S. lycopersicum* fruit. We found that *C. michiganensis* caused similar bird's-eye lesions on wild tomatoes, although there were slight differences in lesion size and shape (Peritore-Galve et al. 2020). Bird's-eye lesions on *S.*

*habrochaites* LA2128 fruit were raised lesions that, when imaged, seemed to be raised due to host cell proliferation. The accession *S. arcanum* LA2157 was completely asymptomatic when *C. michiganensis* was introduced into the vascular system, but developed severe symptoms both in the number of lesions and diameter of lesions when *C. michiganensis* was inoculated onto fruit. This finding highlights differences in host-microbe interactions based not only on host genotype, but also on the types of tissues tested.

### **Fruit development and ethylene-responsiveness affect symptom development**

Previous studies had determined that mature tomato fruit develop less severe symptoms compared to fruit inoculated with bacterial pathogens during early developmental stages (Medina-Mora et al. 2001; Tancos et al. 2013). That same phenomenon was also observed in wild tomato fruit inoculated with *C. michiganensis* in experiments described in chapter one (Peritore-Galve et al. 2020). Although we knew that fruit ceased developing symptoms around maturity, we did not have a precise developmental window. The aim of this chapter was to understand the connection between tomato fruit size at inoculation and symptom severity when inoculated with *C. michiganensis* and two additional bacterial pathogens of tomato, *Pseudomonas syringae* pv. tomato (bacterial speck), and *Xanthomonas gardneri* (bacterial spot). Since the hormone ethylene is intricately linked in tomato development and ripening, tomato mutants impaired in ethylene production and perception were inoculated (Klee and Giovannoni 2011). We determined that symptom severity to these pathogens is not linear to fruit size; symptom development begins when fruit are inoculated at approximately 0.2 cm diameter, then symptom severity peaks in fruit inoculated between 1 to 1.5 cm diameter, and fruit cease developing symptoms when inoculated around 3 cm diameter, although this varied by tomato genotype and by pathogen.

The ethylene-responsive mutant *Nr* develops reduced wilt symptoms when *C. michiganensis* is inoculated into the vascular system (Balaji et al. 2008). In contrast, *Nr* fruit developed more severe bird's-eye lesions and were susceptible until 3.5 cm diameter, whereas the wildtype tomato background was only susceptible until 3.0 cm diameter. The ethylene-responsive mutant *Gr* developed symptoms at larger sizes when inoculated with *P. syringae* pv. tomato and *X. gardneri* in comparison to the wildtype background. The ethylene synthesis and responsive mutant *Cnr* developed significantly fewer symptoms when inoculated with any of the three pathogens at several fruit sizes. We still do not fully understand the relationship between ethylene and fruit symptom severity, but these tomato genotypes can be used to further probe host-pathogen interactions with these three bacterial phytopathogens.

How bacteria cause symptoms on fruit and their routes of entry remain unknown. Trichome bases that are exposed because of natural shedding or mechanical damage have been proposed as a route of entry for bacterial pathogens, but bacterial entry through these apertures has not been directly observed (Getz et al. 1983). We observed a reduction of symptom severity and complete abolishment of symptom development as fruit development nears the end of the immature green stage and enters green mature stage, when they begin ripening (Pesaresi et al., 2014). During early development, fruit undergo rapid cell division and as a result need a flexible cutin membrane to allow for rapid organ growth (Fishman et al. 2002; Bertin et al. 2003, 2007; Bargel and Neinhuis 2005; España et al. 2014; Martin and Rose 2014). As fruit reach the green mature stage, they cease cell division and begin cell elongation, during which the cutin membrane becomes more rigid and chemical changes involved in ripening occur (Bargel and Neinhuis 2005; España et al. 2014). The observation that ethylene mutants follow the general cycle of peak and cessation of susceptibility might suggest that other developmental processes

play a role in fruit symptom severity during early development. The connection between trichome shedding and fruit symptoms is unclear, as trichomes of *S. habrochaites* LA2128 and *S. arcanum* LA2172 were not shed during fruit development, but they still showed a similar pattern of symptom development (unpublished data). Both host processes and pathogen routes of entry that contribute to fruit symptom severity merit future investigations.

### **Chemical changes in xylem sap composition of tolerant and susceptible tomato plants during *C. michiganensis* infection**

Results from chapter one determined that *C. michiganensis* is less able to systemically colonize wild tomato xylem in comparison to cultivated tomato (Peritore-Galve et al. 2020). Additionally, the bacterium grows to lower densities in wild tomato xylem sap than in cultivated tomato sap. We were interested in using untargeted metabolomics to understand what molecular responses occur in xylem sap as a result of *C. michiganensis* infection in wild and cultivated tomatoes, and what metabolites were different between wild and cultivated tomato sap that may supplement *C. michiganensis* growth. Xylem sap was harvested from *C. michiganensis* and water-inoculated *S. lycopersicum* ‘Mt. Fresh’ and *S. habrochaites* LA2128 plants 12 dpi and used for untargeted metabolomic analysis. To select samples for LC-MS analysis, sap flow and CFU per ml sap was measured. Those data determined that *C. michiganensis* has no significant effect on sap flow rate near the site of inoculation on the stem during early symptom development. Other wilt pathogens such as *Ralstonia solanacearum* and *Fusarium* species occlude xylem vessels through pathogen-derived structures and host responses such as tyloses, gels, and embolisms, reducing water conductivity (VanderMolen et al. 1983; Fry and Milholland 1990; Pérez-Donoso et al. 2007; Venturas et al. 2017). Although our data suggest that symptomatic *S. lycopersicum* plants can develop symptoms without reducing conductivity, future

investigations should study how sap flow and transpiration rates are altered during the course of bacterial canker symptom development. Furthermore, the unique unilateral wilt symptoms during early infection suggest that only some leaflets and xylem vessels are affected, therefore local obstructions in petiole vessels might contribute to wilt.

Untargeted metabolomics analysis revealed that both *S. lycopersicum* and *S. habrochaites* xylem sap is significantly altered in the presence of *C. michiganensis*. In sap from infected *S. lycopersicum* 'Mt. Fresh' plants, many differentially accumulated metabolites were negatively charged hydrophobic molecules that increased in concentration. In infected sap from *S. habrochaites* LA2128 plants, the majority of significantly differentially accumulated metabolites were negatively charged hydrophobic compounds that decreased in concentration. Comparisons of metabolite composition between healthy sap samples of each species determined that negatively charged, hydrophilic compounds were the class of metabolite that were mostly differentially abundant. This initial experiment identified compounds by their molecular weight and retention times using LC-MS, but these identifications are merely estimates. Ongoing work with collaborators includes increasing fragmentation data of metabolites to more accurately classify compounds that are differentially accumulated during infection and between healthy saps of different species (Moghe and Kruse 2018). Future work will confirm differential accumulation of specific metabolites using targeted metabolomic approaches, and will aim to understand the role of those compounds during symptom development and in pathogen metabolism.

### **Proteome profile and genome refinement of the reference strain of *C. michiganensis***

We collaborated with USDA researchers to generate a high-resolution proteome of *C. michiganensis* NCPPB382 pellet and supernatant proteins. Data from both pellet and supernatant

samples were combined to create a proteogenomics pipeline, where peptide sequences were used to validate and refine the reference genome (Nesvizhskii 2014). Through this approach, we achieved 70% coverage of genome, supporting translation of 2,157 genes, and extending the N-terminus of 59 protein-coding genes (Gartemann et al., 2008; Peritore-Galve et al. 2019). Additionally, we identified 26 novel protein-coding sequences in the plasmids, pathogenicity island, and other areas of the chromosome. Newly identified genes that are proximal to putative virulence genes (e.g. CMM\_NG2, CMM\_NG3, and pCM2\_NG3, next to *chpA*, *chpF*, and *pat-1*, respectively) can be future targets for functional characterization studies (Peritore-Galve et al. 2019). The proteogenomic pipeline that we generated can also be applied to proteomic data from other bacterial phytopathogens to identify previously unannotated protein-coding regions. This approach could also be used to understand differences in the *C. michiganensis* proteome when cultured in xylem sap. Those data could then be applied to the metabolomics study to provide evidence for bacterial enzymatic activity that support bacterial colonization and virulence

## **Future studies**

### Ch. 1: Wild tomato tolerance

- *Clavibacter michiganensis* was impeded in acropetal spread in the vascular system of wild tomatoes (Peritore-Galve et al., 2020). A recent *Ralstonia solanacearum* colonization study used grafted resistant and susceptible tomato genotypes to identify four crucial ‘bottlenecks’ (root colonization, acropetal spread from roots to shoots, vascular bundle colonization, and spread to apoplast tissues) that restrict pathogen spread, leading to increased plant resistance (Planas-Marquès et al., 2020). Furthermore, vascular resistance to Stewart’s wilt and Goss’s wilt of maize (caused by *Pantoea stewartii* and *Clavibacter nebraskensis*, respectively) occurs through the deposition of dense matrices in the xylem, restricting movement of the pathogen (Mbofung et al., 2016; Doblás-Ibáñez et al., 2020). It would be interesting to graft roots, scions, and stem

segments of tolerant wild tomatoes to cultivated susceptible tomatoes to study the link between pathogen spread and host resistance. Although we did not observe occlusions in the xylem of wild tomato species at 12 days post inoculation (Peritore-Galve et al., 2020), a more in-depth microscopic analysis of the pathogen colonizing tolerant tomato genotypes during different stages of disease progression might reveal barriers affecting bacterial spread.

- *Solanum habrochaites* LA2128 fruit infected with *C. michiganensis* developed raised bird's-eye lesions, that when imaged under a dissecting microscope were raised above the fruit compared to lesions on other genotypes (Peritore-Galve et al., 2020). This phenotype may be due to host cell proliferation. A first step in approaching this question would be to probe sequenced *C. michiganensis* genomes for opine synthesis genes that might induce host cell proliferation.
- Preliminary studies of sap flow presented in chapter 3 showed that there was no significant change in the amount of sap collected when *S. lycopersicum* cv. Mt Fresh and *S. habrochaites* LA2128 plants were 12 days post inoculation. Further experiments testing sap flow rate and transpiration rates of wild and susceptible tomato genotypes during different stages of infection may provide more information on how *C. michiganensis* affects the host xylem. Xylem embolisms and cavitations can also be measured through anatomical, hydraulic, and imaging methods, since this host response may affect wilt symptom development (Gullo 1991).

## Ch. 2: Ethylene tomatoes

- The reference genome, *C. michiganensis* NCPPB382 previously had not been reported to contain cutinase-encoding genes (Gartemann et al., 2008). Through proteogenomic refinement, we identified a chromosomal cutinase enzyme that shares high sequence similarity with a cutinase identified in *C. michiganensis* 0317, the isolate sequenced in chapter 3 (Peritore-Galve et al., 2019). These cutinases contain 37-amino acid-long signal peptides for secretion through the secretory pathway. In fact, most of the peptides from the NCPPB382 proteome that matched to the cutinase were identified from supernatant samples, supporting expression and secretion of this

cutinase during early log growth phase in lysogeny broth (Peritore-Galve et al., 2019). The next steps to follow up on this study would be to search for cutinases in other *Clavibacter* species, tomato-infecting Xanthomonads, and *Pseudomonas syringae* pv. tomato and align those sequences. Structural prediction of these cutinases could be used to test homology with fungal cutinases from tomato-pathogenic fungi. This would be interesting to compare since bacterial pathogens infect fruit during early development (Peritore-Galve, Ch. 2), and fungi such as *Botrytis cinerea* infect fruit after the fruit have ripened (Isaacson et al., 2009). Cutin wax chemical composition and density change during development, so bacterial and fungal cutinases may have distinct targets (Leide et al., 2007; Mintz-Oron et al., 2008). Functional analyses of the cutinase-encoding gene in *C. michiganensis* should include fruit and leaf inoculations since the cutinase may affect leaf surfaces that lead to the white blister phenotype (Chalupowicz et al., 2017).

- A similar project from the plant angle could be to inoculate fruit from a variety of cultivated tomato genotypes to test their relative susceptibility. Density and composition of the cuticular layer and epicuticular waxes can then be tested on fruit from genotypes that are the most and least susceptible. This would provide a more tangible target for breeding against bacterial disease severity in tomato fruit.
- Other bacterial virulence factors can be tested for their contributions to fruit colonization and symptom development. In *C. michiganensis* NCPPB382, there is a plasmid free derivative, Cm100, and a pathogenicity island-free derivative, Cm27, that are non-pathogenic when inoculated into tomato xylem (Chalupowicz et al., 2012, 2017). Inoculating these strains on tomato fruit would be good first step to understanding the genetic repertoire necessary for fruit symptom development and the genomic position of those genes (ie. plasmid-encoded, on the PAI, or non-PAI chromosome). The tomatinase-encoding gene *tomA* is in the PAI and was not necessary for colonization or symptom induction when *tomA*-mutant strains were inoculated into the plant vasculature (Kaup et al., 2005). The bacterial growth suppressing alkaloid  $\alpha$ -tomatine is

present at a very high concentration during early development, and is reduced drastically during development and ripening (Mintz-Oron et al., 2008). Therefore, the *C. michiganensis* tomatinase may be crucial for infecting tomato fruit but not xylem.

### Ch. 3.: Metabolomics

- The next step in this study is to increase data dependent MS2 fragmentation data through future LC-MS runs. These data will allow us to use network analyses of differentially accumulated metabolites for accurate prediction of their structures and classes. It would be interesting to analyze changes in sap composition between healthy and *C. michiganensis*-infected plants to predict degradation of metabolites that could be consumed by the pathogen. We can use the genome to generate a metabolic model of the bacterium in xylem sap, similar to what has been done with *R. solanacearum* and *Xylella fastidiosa* (Peyraud et al., 2016; Gerlin et al., 2020).

### *Clavibacter michiganensis* biofilms

- *Clavibacter michiganensis* forms biofilm-like aggregates during colonization of the plant xylem (Chalupowicz et al., 2012; Peritore-Galve et al., 2020). The pathogen contains no canonical pili, chemotaxis, or flagella-encoding genes (Gartemann et al., 2008). Recent genomic resources for *C. michiganensis* and other *Clavibacter* species can be used to probe for curli, adhesin, and pili-encoding genes that can be targets for functional analyses.
- The bacterium forms dense aggregates *in vitro* in the presence of xylem sap, but not when cultured in minimal medium, xylem-mimicking medium, or lysogeny broth (Chalupowicz et al., 2012; Peritore-Galve et al., 2020). Adjusting the pH of artificial media had non-significant effects on bacterial attachment, supporting the notion that xylem sap contains a chemical cue that causes the pathogen to form aggregates (Crowell et al., 2014). It would be interesting to delineate the chemical cue in xylem sap, as well as understand the transcriptional regulation underlying *C. michiganensis* aggregation.

- pH has been shown to have effects on bacterial cell division and cell size in *Escherichia coli* and *Salmonella enterica* (Castanheira et al., 2017; Mueller et al., 2020). *Clavibacter michiganensis* is subject to different pH environments in the xylem and in fruit tissues. Despite preliminary evidence suggesting xylem sap pH does not affect aggregation, this topic remains unstudied and may be an interesting avenue to understand the pathogen's biology.

#### Non-pathogenic *C. michiganensis*:

- Very little is known about non-pathogenic *C. michiganensis* isolates. Inoculation experiments with non-pathogenic isolates expressing eGFP could see if these strains are capable of colonizing xylem to high densities, and capable of spreading from protoxylem to metaxylem and surrounding tissues. An interesting question to ask with these isolates would be, are non-pathogenic *C. michiganensis* strains capable of spreading to tomato seeds? Comparing the ability for pathogenic and non-pathogenic isolates to spread into developing seed may point to fitness benefits associated with pathogenicity.

#### Persistence:

- Fruit are inoculated with  $10^9$  CFU per mL, although not an entire milliliter of bacterial suspension is placed on small fruit. Despite hundreds of thousands to millions of bacteria being present on the fruit, only tens to hundreds of bird's-eye lesions develop. This may signify that only a percentage of bacteria cause symptoms on fruit. This phenotype suggests bacterial persistence, in which only a subset of the inoculated *C. michiganensis* population is causing symptoms, possibly through differences in gene expression. The reference genome NCPPB382 contains genes (*CMM\_0135* and *CMM\_1809*) associated with the production and regulation of guanosine pentaphosphate (pppGpp), which plays a critical role in modifying bacterial transcription during nutrient and environmental stress conditions (Atkinson et al., 2011). These genes could play a role in persistence signaling or activation of virulence-associated transcription factors (*vatr1* and *vatr2*), making them an interesting target for functional analysis (Savidor et al., 2014).

## **REFERENCES**

- Atkinson, G. C., Tenson, T., and Hauryliuk, V. 2011. The RelA/SpoT homolog (RSH) superfamily: distribution and functional evolution of ppgpp synthetases and hydrolases across the tree of life. *PLOS One*. 6:e23479.
- Balaji, V., Mayrose, M., Sherf, O., Jacob-Hirsch, J., Eichenlaub, R., Iraki, N., Manulis-Sasson, S., Rechavi, G., Barash, I., and Sessa, G. 2008. Tomato transcriptional changes in response to *Clavibacter michiganensis* subsp. *michiganensis* reveal a role for ethylene in disease development. *Plant Physiol*. 146:1797–1809.
- Bargel, H., and Neinhuis, C. 2005. Tomato (*Lycopersicon esculentum* Mill.) fruit growth and ripening as related to the biomechanical properties of fruit skin and isolated cuticle. *J. Exp. Bot*. 56:1049–1060.
- Bertin, N., Génard, M., and Fishman, S. 2003. A model for an early stage of tomato fruit development: cell multiplication and cessation of the cell proliferative activity. *Ann. Bot*. 92:65–72.
- Bertin, N., Lecomte, A., Brunel, B., Fishman, S., and Génard, M. 2007. A model describing cell polyploidization in tissues of growing fruit as related to cessation of cell proliferation. *J. Exp. Bot*. 58:1903–1913.

- Castanheira, S., Cestero, J. J., Rico-Pérez, G., García, P., Cava, F., Ayala, J. A., Graciela Pucciarelli, G., and García-del Portillo, F. 2017. A specialized peptidoglycan synthase promotes *Salmonella* cell division inside host cells. *mBio*. 8:e01685-17.
- Chalupowicz, L., Zellermann, E.-M., Fluegel, M., Dror, O., Eichenlaub, R., Gartemann, K.-H., Savidor, A., Sessa, G., Iraki, N., Barash, I., and Manulis-Sasson, S. 2012. Colonization and movement of GFP-labeled *Clavibacter michiganensis* subsp. *michiganensis* during tomato infection. *Phytopathology*. 102:23–31.
- Chalupowicz, L., Barash, I., Reuven, M., Dror, O., Sharabani, G., Gartemann, K.-H., Eichenlaub, R., Sessa, G., and Manulis-Sasson, S. 2017. Differential contribution of *Clavibacter michiganensis* ssp. *michiganensis* virulence factors to systemic and local infection in tomato. *Mol. Plant Pathol*. 18:336-346.
- Crowell, R. C., Tancos, M. A., and Smart, C. D. 2014. Effects of pH and tomato sap on biofilm formation for the vascular pathogen *Clavibacter michiganensis* subsp. *michiganensis*. Unpublished abstract presented at Geneva Summer Scholar Symposium.
- Doblas-Ibáñez, P., Deng, K., Vasquez, M. F., Giese, L., Cobine, P. A., Kolkman, J. M., King, H., Jamann, T. M., Balint-Kurti, P., De La Fuente, L., Nelson, R. J., Mackey, D., and Smith, L. G. 2020. Dominant, heritable resistance to Stewart's Wilt in maize is associated with an enhanced vascular defense response to infection with *Pantoea stewartii*. *Mol. Plant-Microbe Interact*. 32:1581-1597.

- España, L., Heredia-Guerrero, J. A., Segado, P., Benítez, J. J., Heredia, A., and Domínguez, E. 2014. Biomechanical properties of the tomato (*Solanum lycopersicum*) fruit cuticle during development are modulated by changes in the relative amounts of its components. *New Phytol.* 202:790–802.
- Fishman, S., Bertin, N., and Génard, M. 2002. Cell division and cessation of cell proliferation in growing fruit. *Acta Hortic.* 584:125–131.
- Fry, S. M., and Milholland, R. D. 1990. Response of resistant, tolerant and susceptible grapevine tissues to invasion by the Pierce's Disease bacterium, *Xylella fastidiosa*. *Phytopathology.* 80:66–69.
- Gartemann, K.-H., Abt, B., Bekel, T., Burger, A., Engemann, J., Flügel, M., Gaigalat, L., Goesmann, A., Gräfen, I., Kalinowski, J., Kaup, O., Kirchner, O., Krause, L., Linke, B., McHardy, A., Meyer, F., Pohle, S., Rückert, C., Schneiker, S., Zellermann, E. M., Pühler, A., Eichenlaub, R., Kaiser, O., and Bartels, D. 2008. The genome sequence of the tomato-pathogenic actinomycete *Clavibacter michiganensis* subsp. *michiganensis* NCPPB382 reveals a large island involved in pathogenicity. *J. Bacteriol.* 190:2138–2149.
- Gerlin, L., Cottret, L., Cesbron, S., Taghouti, G., Jacques, M. A., Genin, S., and Baroukh, C. 2020. Genome-scale investigation of the metabolic determinants generating bacterial fastidious growth. *mSystems.* 5:e00698-19

- Getz, S., Fulbright, D. W., and Stephens, C. T. 1983. Scanning electron microscopy of infection sites and lesion development on tomato fruit infected with *Pseudomonas syringae* pv. tomato. *Phytopathology*. 73:39–43.
- Gullo, M. A .L. O. 1991. Three different methods for measuring xylem cavitation and embolism: a comparison. *Ann. Bot.* 67:417-424.
- Isaacson, T., Kosma, D. K., Matas, A. J., Buda, G. J., He, Y., Yu, b., Pravitasari, A., Batteas, J. D., Stark, R. E., Jenks, M. A., and Rose, J. K. 2009. Cutin deficiency in the tomato fruit cuticle consistently affects resistance to microbial infection and biomechanical properties, but not transpirational water loss. *Plant J.* 60:363-377.
- Kaup, O., Gräfen, I., Zellermann, E. M., Eichenlaub, R., and Gartemann, K.-H. 2005. Identification of a tomatinase in the tomato-pathogenic actinomycete *Clavibacter michiganensis* subsp. *michiganensis* NCPPB382. *Mol. Plant-Microbe Interact.* 18:1090-1098.
- Klee, H. J., and Giovannoni, J. J. 2011. Genetics and control of tomato fruit ripening and quality attributes. *Annu. Rev. Genet.* 45:41–59.

Leide, J., Hildebrandt, U., Reussing, K., Riederer, M., and Vogg, G. 2007. The developmental pattern of tomato fruit wax accumulation and its impact on cuticular transpiration barrier properties: effects of a deficiency in a beta-ketoacyl-coenzyme A synthase (LeCER6). *Plant Physiol.* 144:1667-1679.

de León, L., Siverio, F., López, M. M., and Rodríguez, A. 2011. *Clavibacter michiganensis* subsp. *michiganensis*, a seedborne tomato pathogen: healthy seeds are still the goal. *Plant Dis.* 95:1328–1338.

Lowe-Power, T. M., Khokhani, D., and Allen, C. 2018. How *Ralstonia solanacearum* exploits and thrives in the flowing plant xylem environment. *Trends Microbiol.* 26:929–942.

Martin, L. B. B., and Rose, J. K. C. 2014. There's more than one way to skin a fruit: formation and functions of fruit cuticles. *J. Exp. Bot.* 65:4639–4651.

Mbofung, G. C. Y., Sernett, J., Horner, H. T., and Robertson, A. E. 2016. Comparison of susceptible and resistant maize hybrids to colonization by *Clavibacter michiganensis* subsp. *nebraskensis*. *Plant Dis.* 100:711-717

Medina-Mora, C. M., Hausbeck, M. K., and Fulbright, D. W. 2001. Bird's-eye lesions of tomato fruit produced by aerosol and direct application of *Clavibacter michiganensis* subsp. *michiganensis*. *Plant Dis.* 85:88–91.

- Mintz-Oron, S., Mandel, T., Rogachev, I., Feldberg, L., Lotan, O., Yativ, M., Wang, Z., Jetter, R., Venger, I., Adato, A., and Aharoni, A. 2008. Gene expression and metabolism in tomato fruit surface tissues. *Plant Physiol.* 147:823-851
- Moghe, G. D., and Kruse, L. H. 2018. The study of plant specialized metabolism: challenges and prospects in the genomics era. *Am. J. Bot.* 105:959–962.
- Mueller, E. A., Westfall, C. S., and Levin, P. A. 2020. pH-dependent activation of cytokinesis modulates *Escherichia coli* cell cise. *PLOS Genet.* 16:e1008685.
- Nandi, M., Macdonald, J., Liu, P., Weselowski, B., and Yuan, Z.-C. 2018. *Clavibacter michiganensis* ssp. *michiganensis*: bacterial canker of tomato, molecular interactions and disease management. *Mol Plant Pathol.* 19:2036–2050.
- Nesvizhskii, A. I. 2014. Proteogenomics: concepts, applications and computational strategies. *Nat Meth.* 11:1114–1125.
- Pesaresi, P., Mizzotti, C., Colombo, M., and Masiero, S. 2014. Genetic regulation and structural changes during tomato fruit development and ripening. *Front. Plant Sci.* 5:124

- Pérez-Donoso, A. G., Greve, L. C., Walton, J. H., Shackel, K. A., and Labavitch, J. M. 2007. *Xylella fastidiosa* infection and ethylene exposure result in xylem and water movement disruption in grapevine shoots. *Plant Physiol.* 143:1024–1036.
- Peritore-Galve, F. C., Miller, C., and Smart, C. D. 2020. Characterizing colonization patterns of *Clavibacter michiganensis* during infection of tolerant wild *Solanum* species. *Phytopathology.* 110:574–581.
- Peritore-Galve, F. C., Schneider, D. J., Yang, Y., Thannhauser, T. W., Smart, C. D., and Stodghill, P. 2019. Proteome profile and genome refinement of the tomato-pathogenic bacterium *Clavibacter michiganensis* subsp. *michiganensis*. *Proteomics.* 19:1800224.
- Peyraud, R., Cottret, L., Marmiesse, L., Gouzy, J., and Genin, S. 2016. A resource allocation trade-off between virulence and proliferation drives metabolic versatility in the plant pathogen *Ralstonia solanacearum*. *PLOS Pathog.* 12:e1005939
- Planas-Marquès, M., Kressin, J. P., Kashyap, A., Panthee, D. R., Louws, F. J., Coll, N. S., and Valls, M. 2020. Four bottlenecks restrict colonization and invasion by the pathogen *Ralstonia solanacearum* in resistant tomato. *J. Exp. Bot.* 71:2157-2171.
- Rapicavoli, J., Ingel, B., Blanco-Ulate, B., Cantu, D., and Roper, C. 2018. *Xylella fastidiosa*: an examination of a re-emerging plant pathogen. *Mol. Plant Pathol.* 19:786–800.

- Savidor, A., Chalupowicz, L., Teper, D., Gartemann, K.-H., Eichenlaub, R., Manulis-Sasson, S., Barash, I., and Sessa, G. 2014. *Clavibacter michiganensis* subsp. *michiganensis* Vatr1 and Vatr2 transcriptional regulators are required for virulence in tomato. *Mol. Plant-Microbe Interact.* 27:1035-1047.
- Sen, Y., van der Wolf, J., Visser, R. G. F., and van Heusden, S. 2015. Bacterial canker of tomato: current knowledge of detection, management, resistance, and interactions. *Plant Dis.* 99:4–13.
- Tancos, M. A., Chalupowicz, L., Barash, I., Manulis-Sasson, S., and Smart, C. D. 2013. Tomato fruit and seed colonization by *Clavibacter michiganensis* subsp. *michiganensis* through external and internal routes. *Appl. Environ. Microbiol.* 79:6948–6957.
- Tancos, M. A., Lowe-Power, T. M., Peritore-Galve, F. C., Tran, T. M., Allen, C., and Smart, C. D. 2018. Plant-like bacterial expansins play contrasting roles in two tomato vascular pathogens. *Mol. Plant Pathol.* 19:1210–1221.
- VanderMolen, G. E., Labavitch, J. M., Strand, L. L., and DeVay, J. E. 1983. Pathogen-induced vascular gels: ethylene as a host intermediate. *Phys. Plant.* 59:573–580.

Venturas, M. D., Sperry, J. S., and Hacke, U. G. 2017. Plant xylem hydraulics: what we understand, current research, and future challenges. *J. Int. Plant Biol.* 59:356–389.

## APPENDIX 1

### **Assessing the role of the uncharacterized OLD nuclease in *Xanthomonas campestris* pv. *campestris***

#### ***ABSTRACT***

Black rot of crucifers is an economically devastating bacterial disease with a worldwide distribution. This disease is caused by the gamma-proteobacterium *Xanthomonas campestris* pv. *campestris* (Xcc). The causal agent is often seed-borne, leading to the contamination of seedlings and transplants. Secondary inoculum can enter through hydathodes or plant wounds, where the pathogen colonizes the low nutrient xylem. We hypothesized that the uncharacterized Overcoming Lysogenization Defect (OLD) nuclease would play a role in Xcc virulence during host colonization. We identified New York isolates that naturally contained or lacked the *old* gene to conduct knockout and knock-in experiments to characterize *in vitro* growth and biofilm aggregation, *in planta* virulence and colonization density. Through genomic analyses of the *old* gene, we determined that the gene is located on a putative genomic island and has sequence similarity to a recently characterized antiphage defense system. Follow-up experiments will focus on testing the potential role of OLD in antiphage defense and establishing the role of OLD nucleases in diverse bacteria.

## ***INTRODUCTION***

New York State is among the top five producers of cabbage in the USA. Crop yields can be significantly reduced by black rot of crucifers caused by the gamma-proteobacterium *Xanthomonas campestris* pv. *campestris* (Xcc) (USDA NASS, 2017). Black rot is the most economically damaging bacterial disease of cabbage in NY and worldwide, sometimes leading to total crop loss in the field during warm and wet growing seasons. The bacterium can be seed borne with latent infections developing in seedlings, but it can also be dispersed through water from wind-blown rain or general irrigation (Lange et al. 2015). The pathogen can enter through plant wounds and hydathodes, colonizing the vascular system, leading to v-shaped leaf lesions (Sutton and Williams 1970b; Cerutti et al. 2017). Bacteria then spread to the stem vascular tissue, plugging the xylem vessels through aggregation and production of extracellular polysaccharides, ultimately leading to plant death (Sutton and Williams 1970a, 1970b). Despite this pathogen posing a serious threat to growers for over a century there are still only limited strategies for control. Therefore, a deeper understanding of Xcc biology may lead to development of new management strategies through resistance breeding and agricultural products.

Pathology studies of Xcc have focused on extracellular polysaccharides that are crucial for disease induction (Sutton and Williams 1970a, 1970b; Chou et al. 1997; Dharmapuri and Sonti 1999; Qian et al. 2005; Lu et al. 2007). Biofilms and bacterial signaling mediated through cyclic di-GMP have also been demonstrated to play a role in host colonization and virulence (Dow et al. 2003; Ryan et al. 2011). The bacterium employs a type III secretion system to translocate effector proteins into host cells that are necessary for full virulence, avirulence, and colonization in *Brassica* hosts (Jiang et al. 2009; Vicente and Holub 2013).

The objective of this study was to characterize the Overcoming Lysogenization Defect (OLD) nuclease of Xcc. We hypothesized that the OLD protein would play a role in biological processes associated with host colonization and virulence. This family of enzymes was first identified and characterized in bacteriophage P2, where it interferes with bacteriophage lambda growth in P2 lysogens of *E. coli*, and was capable of killing recombinational repair (*recB* and *recC*) mutants in *E. coli* following P2 infection (Lindahl et al. 1970; Myung and Calendar 1995). *In silico* analyses have identified OLD nucleases in other human and plant pathogenic bacteria such as *Klebsiella pneumoniae*, *Ralstonia solanacearum*, *Yersinia pestis*, *Pantoea ananatis*, and *Vibrio cholera* (Schiltz et al. 2019). Presence of the *old* gene was essential for *Salmonella typhimurium* growth in under high temperature stress (Khatiwara et al. 2012).

Crystal structures of OLD proteins revealed two distinct classes: Class 1 OLD proteins are encoded by single *old* genes, whereas class 2 OLD proteins are 50aa longer and associated with a downstream UvrD/PcrA/Rep-like helicase (Schiltz et al. 2019, 2020). Class 2 *old* genes, such as the ones identified in Xcc strains contain an N-terminal ATPase domain and C-terminal Topoisomerase/primase (Toprim) catalytic domain that functions through the two-metal cleavage system (Schiltz et al. 2019). The ATPase domain has not been solved for class 2 OLD proteins, but the class 1 ATPase domain was crystallized and solved from the thermophilic bacterium *Thermus scotoductus* (Schiltz et al. 2020). Class 1 ATPase domains had structural homology to ABC ATPase superfamily proteins, which includes proteins involved in DNA double strand break repair (Schiltz et al. 2020). In the gastric pathogen *Helicobacter pylori*, UvrD was necessary for repairing damaged DNA, an important process to maintain genomic integrity during host colonization (Kang and Blaser 2006). Recently a systematic analysis of antiphage defense systems in bacteria identified class 2 OLD and UvrD proteins from *Bacillus cereus* as

the novel antiphage system ‘Gabija’, and demonstrated its ability to reduce the number of plaques caused by *Siphoviridae* phages (Doron et al. 2018).

In this study we identified the genomic position of *old* and *uvrD*, and generated knockout and knock-in *old* gene mutants in New York isolates naturally containing or lacking *old*. We tested these mutants for *in vitro* growth and biofilm aggregation, *in planta* virulence and host colonization, and began to test for phage-related phenotypes.

## ***MATERIALS AND METHODS***

### **Bacterial strains and growth conditions**

Strains Xcc08092 and Xcc0471 used in this study were isolated from black rot outbreaks in New York in 2008 and 2004, respectively (Lange et al. 2015). Xcc isolates and *E. coli* strains used in this study (Table A1.1) were incubated for 24 hours at 28°C in Lysogeny Broth (LB) medium (Miller, 1972). When necessary, LB medium was supplemented with antibiotics gentamicin (40 µg/ml), kanamycin (100 µg/ml), or streptomycin (100 µg/ml) (Fisher Scientific; Pittsburgh, PA).

### **Plasmid construction**

The native promoter and full-length Xcc08092 *old* gene was amplified with primers Old\_ *Xba*I-F/R containing artificial *Xba*I cut sites on both 5’ and 3’-ends (Table A1.2). A 2200bp PCR product was generated and subsequently cloned into the pBS60 vector (Morello and Collmer 2009), yielding the complementation plasmid pBS60*old* (Table A1.1). A 1011bp streptomycin (Sm<sup>R</sup>) resistance gene (*aadA1*) with FRT flanks from pCPP5242 (Kvitko et al. 2007) was amplified with artificial 5’ and 3’ *Bsi*WI restriction sites using primers SmR\_ *Bsi*WI-FR (Table A1.2), then cloned into a pBS60*old* vector to yield pBS60*old*Sm<sup>R</sup> (Table A1.1 and A1.2). The 3701bp fragment containing the *old* gene disrupted by the Sm<sup>R</sup> cassette was excised

and ligated into the single *Bsi*WI site of vector *pk18mobsacB* (Kvitko and Collmer 2011) to yield *pk18mobsacB::oldSmR* using *E. coli* Zymo 5 $\alpha$  (Zymo Research Inc., Irvine, CA) grown on LB supplemented with kanamycin and X-gal for blue-white selection (Table A1.1).

**TABLE A1.1.** Bacterial strains and plasmids used in this study

Strain or Plasmid	Description <sup>†</sup>	References/Source
<b>Strains</b>		
<i>Xanthomonas campestris</i> pv. <i>campestris</i>		
Xcc08092	Wildtype virulent New York isolate containing <i>old</i> and <i>uvrD</i>	(Lange et al., 2016)
Xcc08092 $\Delta$ <i>old</i>	Xcc08092 mutant strain with disrupted <i>old</i> gene	This study
Xcc08092 $\Delta$ <i>old</i> - Complement	Xcc08092 $\Delta$ <i>old</i> transformed with pBS60 <i>old</i> complement vector	This study
Xcc08092 $\Delta$ <i>old</i> - EV	Xcc08092 $\Delta$ <i>old</i> transformed with pBS60 vector (empty vector control)	This study
Xcc0471	Wildtype virulent New York isolate lacking <i>old</i>	(Lange et al., 2016)
Xcc0471: <i>old</i> -1	Xcc0471 transformed with pBS60 <i>old</i> complement vector	This study
Xcc0471: <i>old</i> -2	Second Xcc0471 transformant with pBS60 <i>old</i> complement vector	This study
Xcc0471: <i>old</i> -3	Third Xcc0471 transformant with pBS60 <i>old</i> complement vector	This study
Xcc0471-EV-1	Xcc0471 transformed with pBS60 vector (empty vector control)	This study
Xcc0471-EV-2	Second Xcc0471 transformant with pBS60 vector (empty vector control)	This study
Xcc0471-EV-3	Third Xcc0471 transformant with pBS60 vector (empty vector control)	This study
Xcc8004	Wildtype virulent sequenced isolate lacking <i>old</i> gene	(Qian et al., 2005)
Xcc0454	Wildtype virulent New York isolate containing <i>old</i>	(Lange et al., 2016)
Xcc0538	Wildtype virulent New York isolate containing <i>old</i>	(Lange et al., 2016)
Xcc10104	Wildtype virulent New York isolate containing <i>old</i>	(Lange et al., 2016)
Xcc12049	Wildtype virulent New York isolate containing <i>old</i>	(Lange et al., 2016)
Xcc13069	Wildtype virulent New York isolate containing <i>old</i>	(Lange et al., 2016)
<i>Escherichia coli</i>	Wildtype virulent New York isolate containing <i>old</i>	(Lange et al., 2016)
Zymo 5 $\alpha$ (DH5 $\alpha$ )	Cloning strain	Zymo Research

<b>Plasmids</b>		
pBS60	Expression vector; Gm <sup>R</sup> ; 4.9 kb	(Swingle et al., 2008; Morello and Collmer, 2009)
pBS60 <i>old</i>	Full length <i>old</i> and promoter region cloned into pBS60; Gm <sup>R</sup> ; 7.1 kb	This study
pCPP5242	Plasmid containing streptomycin resistance gene <i>aadA1</i> ; Sm <sup>R</sup> ; 3.2 kb	(Kvitko et al., 2007)
pBS60 <i>old</i> Sm <sup>R</sup>	pBS60: <i>old</i> ::Sm <sup>R</sup> cassette; Gm <sup>R</sup> Sm <sup>R</sup> ; 8.6 kb	This study
pk18mobsacB	Suicide vector; Km <sup>R</sup> ; 5.7 kb	(Kvitko and Collmer 2011)
pk18mobsacB:: <i>old</i> Sm <sup>R</sup>	Disrupted <i>old</i> ::Sm <sup>R</sup> cassette cloned into pk18mobsacB; Km <sup>R</sup> Sm <sup>R</sup> ; 9.4 kb	This study

†Gm<sup>R</sup>, Gentamicin acetyltransferase; Km<sup>R</sup>, aminoglycoside (kanamycin) phosphotransferase; Sm<sup>R</sup>, aminoglycoside adenyltransferase

### **Transformation and isolation of mutant and complement strains**

Plasmid DNA was extracted from *E. coli* Zymo 5*a* containing pBS60*old* and pk18mobsacB::*old*Sm<sup>R</sup> vectors using the EZNA X-press plasmid DNA mini kit according to manufacturer's instructions (Omega Bio-Tek; Norcross, GA). Electrocompetency and electroporation was performed with a modified version of the protocol from White and Gonzalez 1995. Electrocompetent *Xcc* cells were prepared by inoculating 4mL of liquid LB with *Xcc* then growing for 24 hours at 28°C at 200rpm then transferring those 4mL of LB into 250mL of Nutrient Broth (NB) medium and incubating for 24 hours at 28°C rotating at 160rpm. Cultures were then placed on ice for 10 minutes then transferred into cold 50mL Falcon tubes and centrifugated at 4602 x g for 15 minutes at 4°C. Supernatants were carefully poured out and the pellet was washed in 25mL cold, sterile water, followed by another centrifugation at 4602 x g for 10 minutes at 4°C. Cells were resuspended in 10mL cold Electroporation Buffer (EPB; 10% sterile glycerol in sterile ddH<sub>2</sub>O) then transferred to 15mL Falcon tubes and centrifuged at

maximum speed for 5 minutes at 4°C. Supernatants were again poured out and pellets were resuspended in 0.5mL of cold EPB. Fifty microliter aliquots were transferred into 1.5mL Eppendorf tubes and stored at -80°C or used immediately.

For electroporation, 1-3µg plasmid DNA in <6ul water or elution buffer was added to 50ul of electrocompetent cells. Plasmid DNA and cells were mixed gently with a pipette and transferred to a cold 2mm electroporation cuvette on ice. Electroporation was performed with one pulse at 2.5kVs (12kV/cm) for 5 milliseconds then 600ul super optimal broth with catabolite repression (SOC) was immediately placed into the cuvette to recover the cells. This suspension was transferred to a 1.5mL Eppendorf tube then recovered for 3 hours shaking at 28°C and 220rpm. After 3 hours, cells were plated on LB medium with appropriate antibiotics and incubated overnight at 28°C.

The plasmid *pk18mobsacB::oldSm<sup>R</sup>* was electroporated into the wildtype Xcc08092 strain to produce the *old* knockout strain, Xcc08092Δ*old* (Table A1.1). Putative knockout transformants were plated on LB medium supplemented with streptomycin and 10% sucrose (1M) to counter-select for double-crossover mutants (Kvitko and Collmer 2011). Sucrose resistant colonies were transferred to LB amended with streptomycin and incubated overnight. The *old* gene of Xcc08092Δ*old* was PCR amplified and sequence verified with OldNuc-F/R, SmR-F/R, Xcc\_LFlank-F/R, and Xcc\_RFlank-F/R primers to ensure the correct placement of the disrupting Sm<sup>R</sup> cassette.

The complementation (pBS60*old*) and empty (pBS60) vectors were electroporated into Xcc08092Δ*old* and wildtype Xcc0471, which naturally lacked *old*, to yield the complementation and empty vector strains, Xcc08092Δ*old*-Comp, Xcc08092Δ*old*::EV, Xcc0471::*old*, and Xcc0471::EV. Mutants were grown 1-2 days on LB medium amended with gentamicin (40µg ml<sup>-1</sup>

<sup>1</sup>) and/or streptomycin (100µg ml<sup>-1</sup>) and selected colonies were PCR amplified to confirm the presence of the vector and *old* gene. Transformation with pBS60*old* and pBS60 was performed twice to yield three mutant transformants (Table A1.1).

### **PCR analysis and RNA expression**

Chromosome integrations and plasmid constructs were confirmed using gene-specific PCR and product sequencing (Table A1.2). Genomic DNA was extracted using the MasterPure Gram-positive DNA purification kit (Epicentre, Madison, WI) according to the manufacturer's instructions. Amplification was performed in a C1000 Touch Thermal Cycler (Bio-Rad Laboratories, Inc., Hercules, CA) using EmeraldAmp GT PCR Master Mix (Takara Bio Inc., Otsu, Shiga, Japan). Genomic DNA concentration for PCR was 50 ng per reaction with 10 µM of forward and reverse primers (Table A1.2). PCR was performed in 25 µl reactions with the following parameters: preheat for 3 minutes at 95°C, 34 cycles at 95°C for 15 seconds, primer pair specific annealing temperature for 30 seconds, primer pair-specific extension time at 72° (Table A1.2), final extension at 72°C for 5 minutes, and held at 12°C. Amplicons were electrophoresed on 1% gels at 80V for 1 hour, stained with GelRed (Biotium Inc., Hayward, CA) and visualized with UV light. PCR products were purified with the DNA Clean & Concentrator – 5 kit (Zymo Research Inc., Irvine, CA) according to manufacturer's instructions. Purified PCR products were sequenced on a 3730XL DNA Analyzer (Applied Biosystems, Foster City, CA) at the Cornell University Life Sciences Core Laboratories Center and sequences were aligned to the XccB100 reference genome (NCBI accession: NC\_010688.1).

Total RNA was extracted from 6 mL of Xcc grown as described above using the ZR Fungal/Bacterial RNA MiniPrep kit according to manufacturer's instructions (Zymo Research Corporation). An additional off-column DNase treatment was performed using TURBO DNA-

free DNase according to manufacturer's instructions (Fisher Scientific). Quantity and quality of DNase-treated RNA was determined with a NanoDrop ND1000 (NanoDrop Technologies, Wilmington, DE) and a Qubit 2.0 Fluorometer (Invitrogen, Carlsbad, CA). Reverse-transcription (RT) was performed with RNA to cDNA EcoDry Premix (random hexamers) (Clontech Laboratories, Inc. Mountain View, CA) using 300 ng total RNA per reaction. One-tenth of the RT reaction volume of cDNA was used in a 25  $\mu$ l PCR reaction using EmeraldAmp GT PCR Master Mix with primers XccTH3R and OldIntB, designed to amplify an internal region of the *old* gene, as well as primers designed to amplify internal regions of the housekeeping genes *dnak* and *gyrB* as controls (Table A1.2). To ensure no DNA contaminants were in the RNA, negative controls were performed with 100 ng total RNA as a template. Genomic DNA was used at 50 ng per reaction as a positive control. Products were electrophoresed on 1% gels at 90V for 45 minutes, stained with GelRed and visualized with UV light.

#### **DNA-hybridization for *old* gene detection and confirmation**

Three  $\mu$ g of *SphI*-HF (NEB, Ipswich, MA) digested genomic DNA of strains Xcc08092, Xcc0471, Xcc0471::*old*, and Xcc8004 overnight. Digested genomic DNA was then electrophoretically separated on a 1% agarose gel in 1x Tris-acetate-EDTA buffer at 35V for 15 hours in a cold room held at 4°C. Subsequent washes in 0.25M HCl and 1x Southern Base solution (20 g NaOH, 175.3 g NaCl, 2 L H<sub>2</sub>O) were performed. DNA was transferred to an Amersham Hybond-N+ membrane through upward capillary movement (GE Healthcare, Little Chalfont, United Kingdom).

The full-length *old* gene with partial upstream and downstream regions (2230bp) was amplified from Xcc08092 using the OldNuc-FR primers (Table A1.2) and cleaned using Zymo Clean and Concentrate – 5. An alkaline phosphatase group was added to the *old* gene amplicon

as a probe using Amersham<sup>TM</sup> AlkPhos Direct Labelling Reagents (GE Healthcare).

Hybridization and fluorescent detection with Amersham<sup>TM</sup> CDP-Star Detection Reagent (GE Healthcare) were performed as described by the manufacturer, then imaged using a BioRad ChemiDoc MP Imaging system (Bio-Rad Laboratories, Inc.).

**TABLE A1.2.** Oligonucleotides used in this study

Name	Sequence (5'-3') <sup>†</sup>	Target <sup>€</sup>	Purpose	T <sub>m</sub> (°C)	Extension time (min)	Size (bp)	Reference
<b>OldNuc</b>	F: GATTGGGTGCTTGTCGAAGT R: AGCAGCAAACAATGCGAAC	<i>Xcc old</i>	Verification/ Sequencing	66	2.5 min	2217	This study
<b>Old_XbaI</b>	F: ACAGCGTCTAGAGATTGGGTGCTTGTCGAAGT R: AGACAGTCTAGAAGCAGCAAACAATGCGAAC	<i>Xcc old</i>	Cloning	66	2.5 min	2200	This study
<b>SmR_BsiWI</b>	F: ACAGCGCGTACGGTGTAGGCTGGAGCTGCTTC R: ACAGCGCGTACGATGGGAATTAGCCATGGTCC	Sm <sup>R</sup>	Cloning	69	1 min	1011	This study
<b>pBS60-UP</b>	F: TGTGGAATTGTGAGCGGATA	Upstream of <i>old</i>	Sequencing	55	*	NA	This study
<b>pBS60-DOWN</b>	R: GGGCACCAATAACTGCCTTA	Downstre am of <i>old</i>	Sequencing	55	*	NA	This study
<b>XccTH3</b>	F: CCACCGCTAACGACAATCCT R: GGGATGTTGAGTCCTTCGGG	<i>Xcc old</i>	Verification	63	1 min	368	This study
<b>OldIntT</b>	F: ATCAATCACGCAATCGTTGA	<i>Xcc old</i>	Sequencing	NA	*	NA	This study
<b>OldIntB</b>	F: TCAACGATTGCGTGATTGAT	<i>Xcc old</i>	Sequencing	NA	*	NA	This study
<b>SmR</b>	F: GTGTAGGCTGGAGCTGCTTC R: ATGGGAATTAGCCATGGTCC	Sm <sup>R</sup>	Verification/ Sequencing	60	1.5 min	1478	This study
<b>Xcc_LFlank</b>	F: GAGCACGTGTGAGTCCCACA R: GATGCCATCGCGTAGCGTC	Upstream of <i>old</i>	Verification/ Sequencing	60	2 min	1694	This study
<b>Xcc_RFlank</b>	F: GATCCTAGAAATTCTCATTTACGTCCCCG R: TCAGCGTTGTCTCAACTTGG	Downstre am of <i>old</i>	Verification/ Sequencing	62	1.5 min	1129	This study
<b>Xcc_DnaK</b>	F: GGTATTGACCTCGGCACCAC R: ACCTTCGGCATAACGGGTCT	<i>dnaK</i>	Expression analysis	60	1 min	1034	(Fargier et al. 2011; Lange et al. 2015)
<b>Xcc_GyrB</b>	F: TGC GCGGCAAGATCCTCAAC R: GCGTTGTCCTCGATGAAGTC	<i>gyrB</i>	Expression analysis	60	1 min	1051	(Fargier et al. 2011; Lange et al. 2015)
<b>OldIntB</b>	F: TCAACGATTGCGTGATTGAT	<i>Xcc old</i>	Expression analysis	63	*	2550	This study

<sup>†</sup>Underline denotes restriction enzyme cut site. <sup>€</sup>Sm<sup>R</sup>, aminoglycoside adenylyltransferase. \* Extension time based on complementary primer.

### ***In vitro* growth and biofilm attachment**

Wildtype and mutant Xcc strains were cultured in LB medium for 24 hours as described above. Bacterial suspensions (1 mL) were pelleted at 4602 x g for 4 minutes, washed and centrifuged, then resuspended to OD<sub>600</sub> = 0.1 in sterile water. Ten µl of bacterial suspensions from each of three CFUs were inoculated into individual wells (n=12/strain) of a 96-well Falcon tissue culture plate containing 190 µl of LB medium (Corning Inc., Corning, NY). The plate was incubated at 28°C shaking in a BioTek microplate reader (Winooski, VT). Optical density was measured at 590nm every 2 hours for 48 hours (Tancos et al. 2018; Peritore-Galve et al. 2020). The mean area under the growth curve was calculated and significant differences between *in vitro* growth rates of mutants and their corresponding wildtype strain were tested with analysis of variance (ANOVA) (P<0.05) followed by Tukey's pairwise comparisons (P<0.05) using the R package agricolae, using R v. 3.3.2 (R Foundation for Statistical Computing, Vienna, Austria) (de Mendiburu 2016). The experiment was performed three times.

Bacterial strains were grown in LB for 24 hours as described above, pelleted at 3041 x g for 12 minutes, and resuspended in sterile water to an OD<sub>600nm</sub> = 0.8. Bacterial suspensions (5 µl) were added to individual wells of a 96-well Falcon tissue culture plates (Corning, Inc.) containing 95 µl of LB medium. Twelve replicates per strain from three independent CFUs (4 wells per CFU) were included, with 12 water-inoculated wells as a negative control. Plates were briefly shaken and statically grown at 28°C for seven days. After incubation, each of the wells in each of the 96-well plates were stained with 25 µl of 0.1% crystal violet for 25 minutes at room temperature, followed by two washes with 200 µl sterile water then blotted on paper towels and incubated at 60°C for 1 hour (Davey and O'Toole 2000; Tran et al. 2016; Tancos et al. 2018; Peritore-Galve et al. 2020). Crystal violet was solubilized by adding 100 µl of 30% acetic acid,

followed by brief agitation and quantifying the absorbance at 590 nm using the BioTek microplate reader (Davey and O'Toole 2000; Tran et al. 2016; Tancos et al. 2018; Peritore-Galve et al. 2020). Significant differences were tested with ANOVA ( $P < 0.05$ ) followed by Tukey's pairwise comparisons ( $P < 0.05$ ) using the R package agricolae in R v. 3.3.2 (R Foundation for Statistical Computing, Vienna, Austria) (de Mendiburu, 2016). The experiment was performed three times.

### **Disease severity and *in planta* bacterial populations**

The susceptible cabbage cultivar 'Surprise' (*Brassica oleraceae*) was planted in a custom Cornell potting mix composed of peat, perlite, and vermiculite in a 4:1:1 ratio supplemented with Osmocote slow release fertilizer (Scotts Miracle-Gro Co., Marysville, OH), and grown in the greenhouse with a 16-h light/8-h dark photoperiod. Plants were arranged into three randomized blocks with three plants to be inoculated with each genotype per block and one water-inoculated plant per block. Strains of Xcc were cultured and adjusted to an  $OD_{600nm} = 0.1$  in sterile water as described above. Bacterial strains were inoculated into 6-week-old cabbages by clipping the edge of three fully expanded leaves of nine plants ( $n=27$  leaves per strain) with scissors dipped in bacterial suspension (Dow et al. 2003; Lange et al. 2015). Disease severity was scored 14 days post inoculation (dpi) by measuring lesion length and dividing that by the length of the leaf from the cut site to where leaf tissue ceased forming on the petiole to produce a lesion ratio (Dow et al. 2003). Statistical analyses were performed with a linear mixed effects model with lesion ratio as the response, strain, plant, leaf number, and the interactions between strain and plant, and strain and leaf as main effects. Block was included as a random effect. This analysis was performed with the lme4 and emmeans packages in R v. 3.3.2 (Bates et al. 2015; Lenth 2016). Significant differences ( $P < 0.05$ ) between mutants and their corresponding wildtype strain were

tested using Tukey's pairwise comparisons. The experiment was performed twice. The knock-in experiment was performed once with the second transformants (*Xcc0471:old-2* and *Xcc0471-EV-2*) and once with the third transformants (*Xcc0471:old-3* and *Xcc0471-EV-3*).

*In planta* bacterial populations were quantified at 14 dpi by collecting leaf punches (n=27 per bacterial strain) from the tip of the v-shaped lesion of the third leaf using a cork borer (14mm diameter). Leaf punches were pooled by plant (n=9 pooled leaf punches per strain) and homogenized in 1 mL sterile water with a sterile 5 mm stainless steel grinding bead (Qiagen, Valencia, CA) in a TissueLyser (Retsch, Newtown, PA) at 30 Hz for 3 minutes (Lu et al. 2007). Serial dilutions were performed with the homogenized suspension and plated onto either yeast-dextrose-calcium carbonate (YDC) agar (for wildtype strains or negative controls), or LB medium amended with streptomycin and/or gentamicin, then incubated at 28°C for 3-5 days. Bacterial density was measured as colony forming units per gram of tissue (CFU g<sup>-1</sup>) as calculated below:

$$\frac{\left(\frac{\text{Number of CFUs}}{\text{Volume plated } (\mu\text{l}) * \text{dilution factor}}\right)}{\left(\frac{\text{Weight of sample (g)}}{\text{Volume of original homogenate } (\mu\text{l})}\right)}$$

Significant differences between *in planta* populations of mutants and their corresponding wildtype were assessed using ANOVA, followed by Tukey's HSD (P<0.05) with the package agricolae in R v. 3.3.2 (de Mendiburu, 2016). *In planta* population experiments were performed twice. The experiment was performed once with second knock-in transformants, *Xcc0471:old-2* and *Xcc0471-EV-2*.

### **Gene neighborhood analysis**

To survey the genes surrounding *old* and *uvrD* in *Xcc* we analyzed the following full length genomes available on NCBI: *XccB100* (NC\_010688.1), *Xcc8004* (NC\_007086.1),

Xcc33913 (NC\_003902.1) and XccCN03 (NZ\_CP017308.1). Whole genomes and genomic regions were aligned using the progressiveMauve algorithm in Geneious 11.1.3 (Darling et al., 2004; Darling et al., 2010).

## RESULTS

### Identification and genetic manipulation of *old* in New York isolates of Xcc

We used a genetic approach to study the OLD protein in Xcc. New York *Xanthomonas* isolates (n=7) were tested for the presence of the *old* gene using degenerate primers, which identified it in isolates: 0454, 0538, 08092, 10104, 12049, and 13069 (data not shown) (Table A1.1). Two isolates were selected for further studies: Xcc08092, which contained *old* with a neighboring *uvrD* gene, and Xcc0471, which naturally lacked *old*. Since we did not have genome sequences that could be analyzed for dissimilar *old* sequences, we used Southern blotting to confirm the presence or absence of *old* in Xcc08092 and Xcc0471 using the sequenced reference strain, Xcc8004, as a negative control.

The *old* gene was disrupted with an antibiotic resistance cassette in the virulent isolate, Xcc08092. The *old* gene and its native promoter region were inserted into the virulent isolate Xcc0471 naturally lacking *old*. The knockout strain was complemented with the same vector used to express *old* in Xcc0471, and an empty vector was used as a control in both knockout and knock-in experiments (Table A1.1). As expected, the *old* gene was expressed in Xcc08092, Xcc08092 $\Delta$ *old*-Comp, and Xcc0471:*old*, and not expressed in Xcc0471, Xcc08092 $\Delta$ *old* or the empty vector strains Xcc08092 $\Delta$ *old*-EV and Xcc0471-EV (Fig. A1.1.).

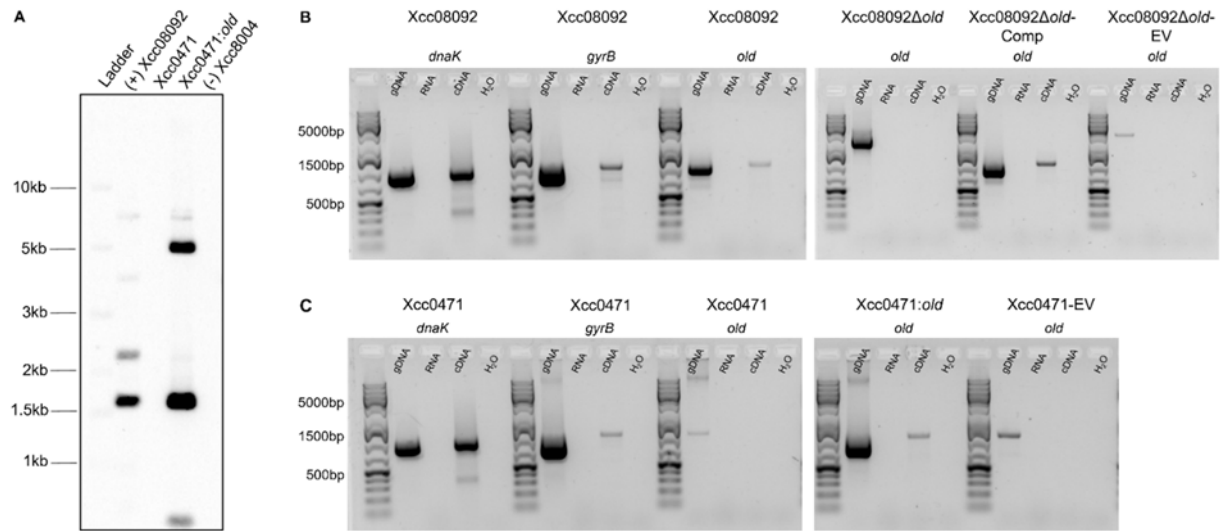


**FIGURE A1.1.** (A) Southern blot hybridization of *old* gene in *SphI* digested genomic DNA of Xcc08092 (positive control), Xcc0471, Xcc0471:*old* (additional positive control), and Xcc8004 (negative control). (B) Expression analysis of *old* gene in Xcc08092 and knockout strains using Reverse Transcription-Polymerase Chain Reaction (RT-PCR). (C) Expression analysis of *old* in Xcc0471 and knock-in strains. The *dnaK* and *gyrB* genes were used as positive controls for expression, and RNA and water were used as negative controls for contamination.

### ***In vitro* growth analysis and biofilm attachment**

We assessed growth rates of *old* mutants in nutrient rich LB medium to test for growth related phenotypes. There were no significant differences in growth rate between Xcc08092 and Xcc08092 $\Delta$ *old* ( $P=0.169$ ) (Fig. A1.2A&B). Complement and empty vector strains of Xcc08092 $\Delta$ *old* grew at significantly slower rates but achieved the same densities around 30 hours of growth. Knock-in experiment strains exhibited similar growth trends, with reductions in growth rate in both Xcc0471:*old* and Xcc0471-EV compared to wildtype, but still achieving similar densities around 35 hours (Fig. A1.2A&B). These phenotypes were corroborated by growth rate experiments in greater LB liquid volumes in Erlenmeyer flasks (data not shown).

The ability for Xcc mutant and wildtype strains to aggregate *in vitro* was tested through static growth for seven days then staining and quantifying the optical density of aggregated bacteria. The knock in strain Xcc0471:*old* had reduced aggregates relative to wildtype ( $P=0.015$ ) (Fig. A1.2C). The empty vector control Xcc0471-EV was not significantly different from either the wildtype strain or the overexpression strain ( $P=0.08$  and  $P=0.76$ , respectively) (Fig. A1.2C). There were no significant differences in aggregation between wildtype Xcc08092 and mutant strains in the knockout experiment (Fig. A1.2C).

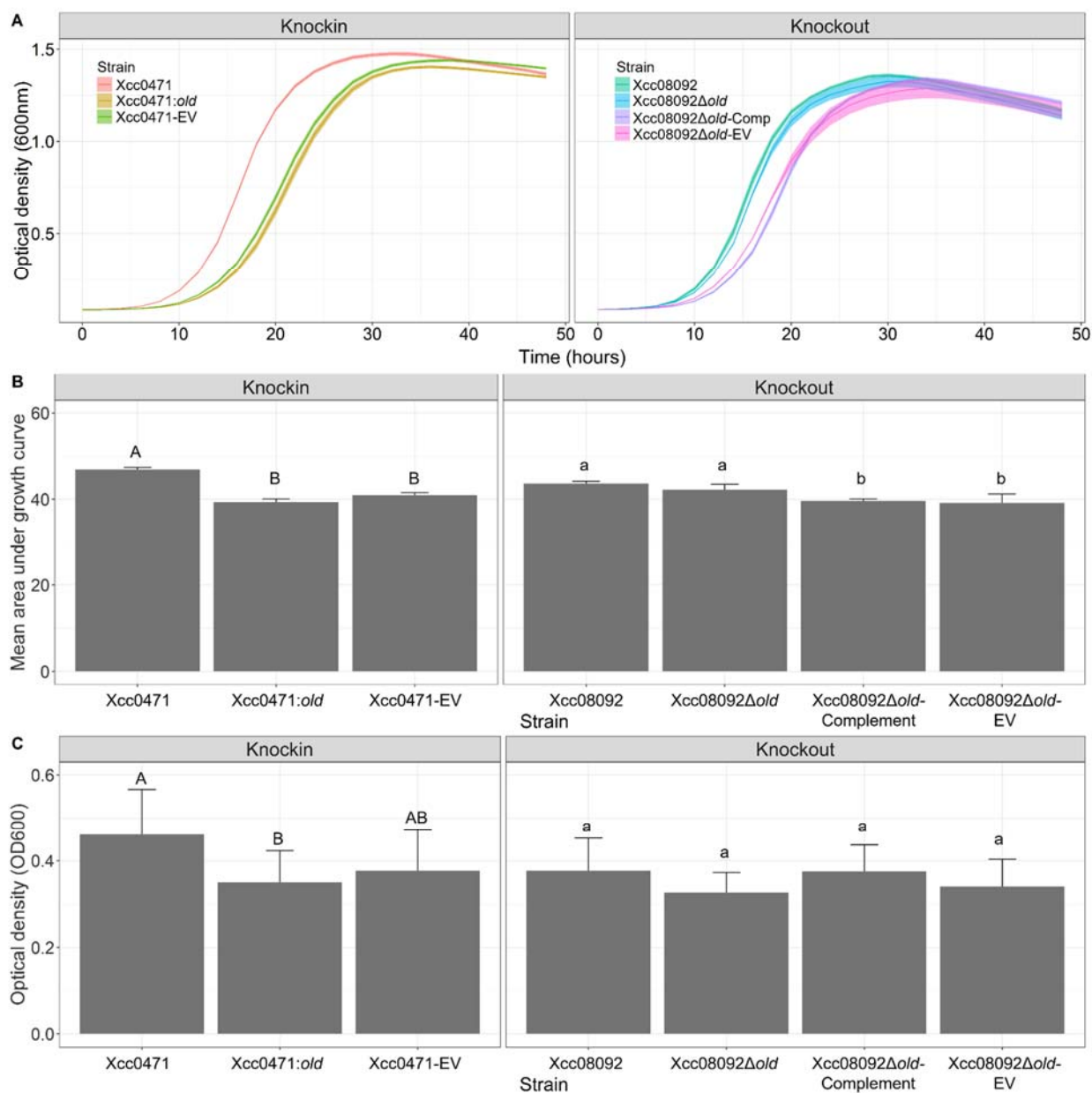


**FIGURE A1.2.** (A) Growth rates of Xcc0471 (left) and Xcc08092 (right) strains from knock-in and knockout experiments. Shaded areas correspond to the 95% confidence interval. (B) Mean area under the growth curve. (C) Mean optical density of aggregated bacteria in 96-well tissue culture plates after 7 days of static growth. Bars in all graphs correspond to one standard deviation, and letters denote significant differences ( $P < 0.05$ ) calculated using Tukey's pairwise comparisons.

### **Overexpression of the *old* gene reduces disease severity and *in planta* growth in Xcc0471**

To assess the potential role of *old* in disease severity, cabbage plants from the cultivar ‘Surprise’ were clip inoculated and lesions were measured 15 dpi. Plants inoculated with Xcc08092, mutant, complement, and empty vector control strains in the knockout experiment exhibited no significant difference in disease severity as measured by the length of the v-shaped lesion relative to leaf length ( $P < 0.05$ ) (Fig. A1.3A). In contrast, disease severity of the overexpression strain Xcc0471:*old* was reduced by half of that observed in plants inoculated with wildtype Xcc0471 ( $P < 0.0001$ ) (Fig. A1.3A&C). Disease severity of the empty vector control, Xcc0471-EV, was not significantly different from the wildtype strain ( $P = 0.094$ ) (Fig. A1.3A&C). Similar results were observed when plants were inoculated with Xcc0471:*old-2*, Xcc0471-EV-2, and Xcc0471:*old-3* and Xcc0471:EV-3 (data not shown).

To assess the effect of the *old* gene mutations and overexpression on growth *in planta* population density of Xcc strains was measured at the tip of the v-shaped lesion. There were no significant differences in population density between wildtype and mutant strains in the knockout experiment ( $P < 0.05$ ) (Fig. A1.3B). However, the knock-in strain Xcc0471:*old* grew to significantly lower population densities ( $6.3 \times 10^6$  CFU  $g^{-1}$ ) compared to wildtype Xcc0471 ( $2.2 \times 10^7$  CFU  $g^{-1}$ ) ( $P = 0.0046$ ) (Fig. A1.3B). The empty vector control, Xcc0471-EV, colonized to similar densities ( $2.8 \times 10^7$  CFU  $g^{-1}$ ) as the wildtype strain (Fig. A1.3B). The experiment was repeated with plants inoculated with the second transformant Xcc0471:*old-2* and the empty vector control Xcc0471-EV-2. Colonization density was also significantly lower between Xcc0471:*old-2* and Xcc0471, but not between Xcc0471 and Xcc0471-EV-2 (data not shown).

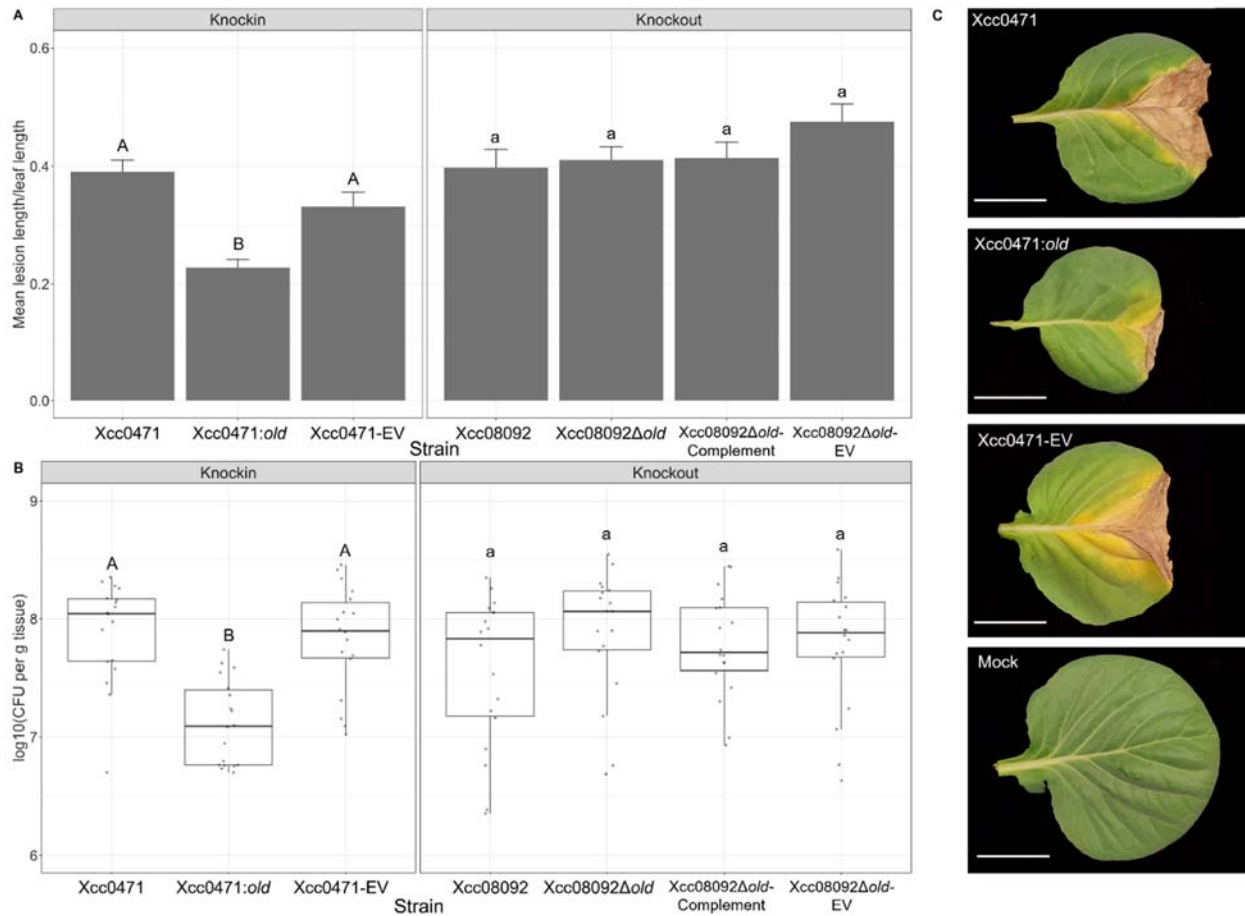


**FIGURE A1.3** (A) Disease severity of Xcc0471 knock-in and Xcc08092 knockout strains calculated by measuring lesion length and dividing by the leaf length. Bars correspond to standard error of the mean. (B) *In planta* population density from tissue excised at the tip of the v-shaped lesion. Data shown is pooled from two independent experiments. (C) Characteristic v-shaped lesions of black rot on cabbage cultivar ‘Surprise.’ White bars correspond to five centimeters. Letters in graphs denote significant differences ( $P < 0.05$ ) calculated using Tukey’s pairwise comparisons.

### **The *old* gene is present on a highly variable genomic island**

Insights on genetic function can often be found through the analysis of surrounding genes. Three publicly available sequenced strains that contained or lacked the *old* gene were analyzed. The *old* gene was present in the sequenced strains XccB100 and XccCN03, but not in other reference strains such as Xcc33193 and Xcc8004. The gene was located on a genomic island 79kb in XccB100 and 88kb in XccCN03, termed *Xanthomonas* variable region 13 (XVR13) in both strains. This genomic island is flanked by transfer RNA encoding genes and contained different GC (60%) content relative to the rest of these two genomes (65% GC) (Fig. A1.4). The *old* gene was proximal to *uvrD* and an IS5 family transposase gene on the antisense strand of XccB100, and was flanked by hypothetical protein-encoding genes on the sense strand of XccCN03 (Fig. A1.4). The XVR13 island is present in Xcc8004 and Xcc33913 but is different in length and genetic composition. In Xcc33913, the island is 32kb, and in Xcc8004 is 100kb (Fig. A1.4). In all four genomes, XVR13 contains transposase-encoding genes, phage related genes, and genes involved in conjugative transfer, partitioning and replication of plasmids (Fig. A1.4). The XVR13 region of Xcc8004 and Xcc33913 also contains avirulence and virulence-related genes involved in the formation of the type IV secretion system (Fig. A1.4).

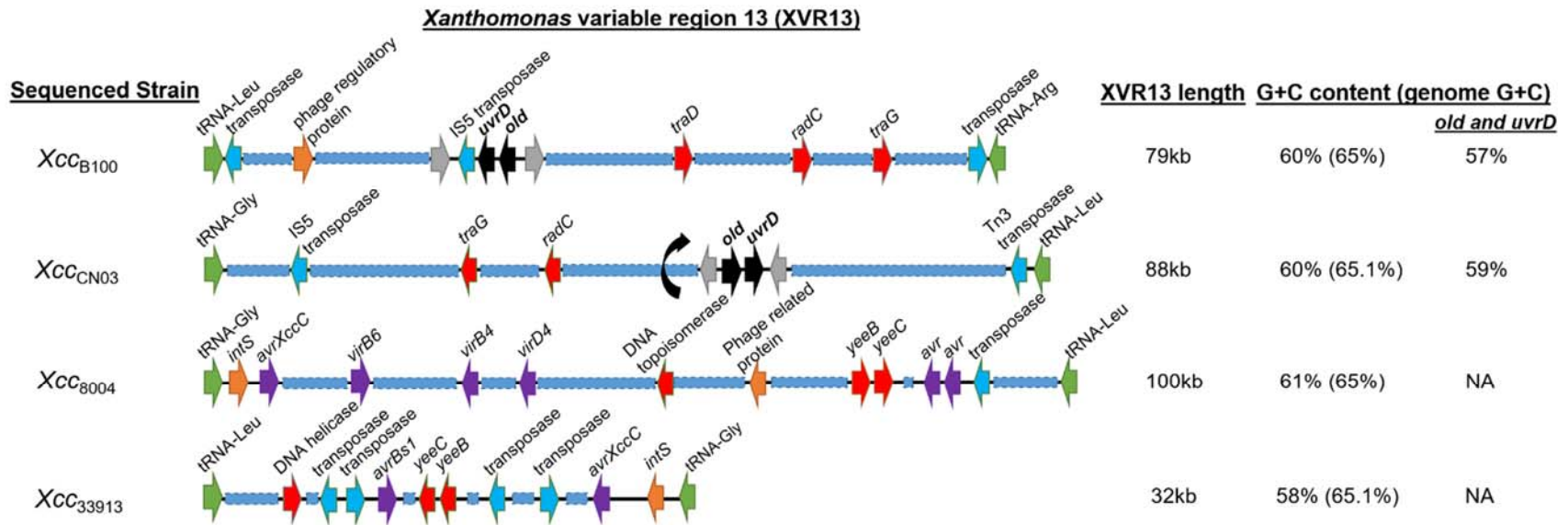


**FIGURE A1.4** Graphical depiction of the XVR13 region of XccB100, XccCN03, Xcc8004, and Xcc33913. The *old* and *uvrD* genes (black arrows) are present in XccB100 and XccCN03, and flanked by transposase (blue arrows) or hypothetical protein-encoding genes (grey arrows). Genes involved in DNA processes are in red, phage-related genes in orange, virulence-related genes in purple, and tRNA-encoding genes in green. Blue dashed rectangles represent areas containing CDSs encoding hypothetical proteins and proteins of unknown function not depicted in this graphic.

## ***DISCUSSION***

Despite our recently improved understanding of the structure of OLD proteins, we have little information on what roles OLD nucleases and the associated UvrD helicase play in bacteria. We hypothesized that OLD might play roles in DNA activities during nutrient and host-response stress on the pathogen during host colonization. To test this hypothesis, we identified New York isolates of Xcc that contained and did not contain the *old* gene, and generated knockout and knock-in mutants, complementation, and control strains. The *old* gene was present in 6 out of 7 isolates tested. These strains had previously been assorted into unique haplotypes using a multi locus sequence analysis approach (Lange et al. 2015). Isolates that either contained or lacked the *old* gene were all from unique haplotypes as determined through MLSA; however, those that contained *old* clustered under the NY Xcc subpopulation A and Xcc0471 and reference strain Xcc33913 that both lacked *old* clustered in NY Xcc subpopulation B (Lange et al. 2015). The *uvrD* gene that is typically associated with class 2 OLD was identified and partially sequenced in Xcc08092. Furthermore, RT-PCR experiments confirmed that *old* was expressed under nutrient rich growth conditions in Xcc08092 that naturally contained the gene. The association between population structure and presence or absence of the *old* gene remains unknown, but these results paired with the location of *old* in the XVR13 genomic island in sequenced strains highlights genomic variability within Xcc populations.

The function of *old* in bacteria is currently unknown. We assessed the phenotypes of knockout or knock-in mutants in several experiments. First, *in vitro* growth rates were determined for all strains in nutrient rich media. Knocking out the *old* gene caused no significant differences in growth rate, but overexpressing the *old* gene in the knockout mutant or Xcc0471 led to a delay in growth rate relative to wildtype. We predicted that the plasmid pBS60 might

contribute to delayed growth rates *in vitro*, so we included an empty vector control, which indeed shared the same delay in growth rate. Although the growth rates were slower between strains with the pBS60 plasmid and plasmid-free strains, saturation of growth was achieved between 30-35 hours. Therefore, we included the empty vector strains as controls for all experiments. *In vitro* aggregation of Xcc strains grown statically for seven days was determined through the crystal violet staining assay. Knocking out the *old* gene had no significant effect on aggregation *in vitro*, but overexpressing *old* in Xcc0471:*old* led to a reduction of aggregates. Bacterial nucleases can inhibit biofilm formation in conditions that are not conducive for successful colonization through the degradation of extracellular DNA, a component of some bacterial biofilms (Whitchurch et al. 2002; Tang et al. 2011; Beenken et al. 2012; Jakubovics et al. 2013). These nucleases may also be crucial for the dispersal of motile bacteria from mature biofilms to seek new areas for colonization (Berne et al. 2010). The role of nucleases and extracellular DNA on Xcc biofilms has not been studied, and this phenotype suggests that OLD may have an effect on biofilm-related aggregation.

We had hypothesized that the *old* gene may be important during pathogen colonization of cabbage xylem. Plants were clip inoculated with mutant and wildtype strains to assess disease severity and colonization density. Knocking out the *old* gene had no effect on disease severity or *in planta* colonization density, suggesting that OLD is not essential for Xcc during the stress of colonization and disease induction. Overexpression of *old* in Xcc0471 led to a reduction of disease severity and colonization density. The empty vector control strain achieved similar populations and disease severity as the wildtype, suggesting that *old* may reduce the fitness of Xcc0471 during host colonization and disease induction. Since the *old* gene is associated with a *uvrD* helicase, it is possible that overexpression of *old* without the helicase may lead to negative

fitness phenotypes under stressful conditions.

A genome-wide study of Xcc isolates collected in China identified 27 variable genomic regions, among which XVR13 was identified near the terminus of chromosome replication flanked by tRNA and integrase genes (He et al. 2007). This region had highly variable genetic content within the isolates tested in that study, and between the genomes analyzed in this study (He et al. 2007). The location of the island paired with varying genetic composition suggests that XVR13 has undergone multiple insertion and deletion events (He et al. 2007). The *old* and *uvrD* genes were located in the XVR13 region in XccB100 and XccCN03. In Xcc33913 and Xcc8004 the XVR13 island contained avirulence genes *avrXccC*, *avrXccE1* and *avrBsI*, and *virB* genes involved in the formation of the type IV secretion system (He et al. 2007). Recently, a systematic study of bacteria described new antiphage defense systems including *old* and *uvrD* as the putative anti-*Siphoviridae* system ‘Gabija’ (Doron et al. 2018). Horizontal gene transfer facilitated by genomic islands allow bacteria to adapt to different stressors (Juhas et al. 2009). The XVR13 genomic island has variable genetic content between strains and if the *old* gene plays an antiphage defense role, then the island may be a defense or virulence island based on the isolate tested (Juhas et al. 2009; Makarova et al. 2011; Doron et al. 2018).

In conclusion, we do not have a full understanding of the role of OLD in Xcc, but we know that the gene is non-essential for growth in nutrient rich media or during black rot disease. However, expressing the *old* gene into a strain that does not contain it reduces *in vitro* aggregation, *in planta* disease severity, and colonization density. Finally, *old* and *uvrD* are located in a highly variable genomic island, which may contain genes involved in virulence or antiphage defense depending on the isolate. Future studies will focus on testing the potential role of OLD in antiphage defense, and understanding the association between *old* and *uvrD* in class 2

OLD systems.

### ***ACKNOWLEDGEMENTS***

This work was supported by a School of Integrative Science Schmitta-Novak Small Grant and USDA Federal Capacity Funds through the New York State Agricultural Experiment Station. Thank you to Alvin Han, Holly Lange, Rachel Kreis, and Taylere Hermann for technical support and advice on working with Xcc and cabbage; Zoë Dubrow for support on Southern blotting; and Josh Chappie and Carl Schiltz for stimulating discussions about OLD. Thank you to Bryan Swingle and Alan Collmer for providing knockout and expression vectors, and to the Swingle lab for providing me with bench space in Ithaca where I could work.

### ***REFERENCES***

- Bates, D., Mächler, M., Bolker, B., and Walker, S. 2015. Fitting linear mixed-effects models using lme4. *J. Stat. Softw.* 67:1–48.
- Beenken, K. E., Spencer, H., Griffin, L. M., and Smeltzer, M. S. 2012. Impact of extracellular nuclease production on the biofilm phenotype of *Staphylococcus aureus* under *in vitro* and *in vivo* Conditions. *Infect. Immun.* 80:1634–1638.
- Berne, C., Kysela, D. T., and Brun, Y. V. 2010. A bacterial extracellular DNA inhibits settling of motile progeny cells within a biofilm. *Mol. Microbiol.* 77:815–829.

- Cerutti, A., Jauneau, A., Auriac, M.-C., Lauber, E., Martinez, Y., Chiarenza, S., Leonhardt, N., Berthomé, R., and Noël, L. D. 2017. Immunity at cauliflower hydathodes controls systemic infection by *Xanthomonas campestris* pv *campestris*. *Plant Physiol.* 174:700–716.
- Chou, F.-L., Chou, H.-C., Lin, Y.-S., Yang, B.-Y., Lin, N.-T., Weng, S.-F., and Tseng, Y. H. 1997. The *Xanthomonas campestris gumD* gene required for synthesis of xanthan gum is involved in normal pigmentation and virulence in causing black rot. *Biochem. Biophys. Res. Commun.* 233:265–269.
- Davey, M. E., and O’Toole, G. A. 2000. Microbial biofilms: from ecology to molecular genetics. *Microbiol. Mol. Biol. Rev.* 64:847–867.
- Dharmapuri, S., and Sonti, R. V. 1999. A transposon insertion in the *gumG* homologue of *Xanthomonas oryzae* pv. *oryzae* causes loss of extracellular polysaccharide production and virulence. *FEMS Microbiol. Lett.* 179:53–59.
- Doron, S., Melamed, S., Ofir, G., Leavitt, A., Lopatina, A., Keren, M., Amitai, G., and Sorek, R. 2018. Systematic discovery of antiphage defense systems in the microbial pangenome. *Science* 359:eaar4120

- Dow, J. M., Crossman, L., Findlay, K., He, Y. Q., Feng, J. X., and Tang, J. L. 2003. Biofilm dispersal in *Xanthomonas campestris* is controlled by cell-cell signaling and is required for full virulence to plants. *Proc. Natl. Acad. Sci. U. S. A.* 100:10995–11000.
- Fargier, E., Saux, M. F.-L., and Manceau, C. 2011. A multilocus sequence analysis of *Xanthomonas campestris* reveals a complex structure within crucifer-attacking pathovars of this species. *Syst. Appl. Microbiol.* 34:156–165.
- He, Y.-Q., Zhang, L., Jiang, B.-L., Zhang, Z.-C., Xu, R.-Q., Tang, D.-J., Qin, J., Jiang, W., Zhang, W., Zhang, X., Liao, J., Cao, J. R., Zhang, S. S., Wei, M. L., Liang, X. X., Lu, G. T., Feng, J. X., Chen, B., Chen, J., and Tang, J. L. 2007. Comparative and functional genomics reveals genetic diversity and determinants of host specificity among reference strains and a large collection of Chinese isolates of the phytopathogen *Xanthomonas campestris* pv. *campestris*. *Genome Biol.* 8:R218.
- Jakubovics, N. S., Shields, R. C., Rajarajan, N., and Burgess, J. G. 2013. Life after death: the critical role of extracellular DNA in microbial biofilms. *Lett. Appl. Microbiol.* 57:467–475.

Jiang, W., Jiang, B.-L., Xu, R.-Q., Huang, J.-D., Wei, H.-Y., Jiang, G.-F., Cen, W. J., Liu, J., Ge, Y. Y., Li, G. H., Su, L. L., Hang, X. H., Tang, D. J., Lu, G. T., Feng, J. X., He, Y. Q., Tang, J. L. 2009. Identification of six type III effector genes with the PIP box in *Xanthomonas campestris* pv. *campestris* and five of them contribute individually to full pathogenicity. *Mol. Plant-Microbe Interact.* 22:1401–1411.

Juhas, M., van der Meer, J. R., Gaillard, M., Harding, R. M., Hood, D. W., and Crook, D. W. 2009. Genomic islands: tools of bacterial horizontal gene transfer and evolution. *FEMS Microbiol. Rev.* 33:376–393.

Kang, J., and Blaser, M. J. 2006. UvrD Helicase Suppresses Recombination and DNA Damage-Induced Deletions. *J. Bacteriol.* 188:5450–5459.

Khatiwara, A., Jiang, T., Sung, S.-S., Dawoud, T., Kim, J. N., Bhattacharya, D., Kim, H. B., Ricke, S. C., Kwon, Y. M. 2012. Genome scanning for conditionally essential genes in *Salmonella enterica* Serotype Typhimurium. *Appl. Environ. Microbiol.* 78:3098–3107.

Kvitko, B. H., and Collmer, A. 2011. Construction of *Pseudomonas syringae* pv. tomato DC3000 mutant and polymutant strains. *Methods Mol. Biol.* 712:109–128.

- Kvitko, B. H., Ramos, A. R., Morello, J. E., Oh, H.-S., and Collmer, A. 2007. Identification of harpins in *Pseudomonas syringae* pv. tomato DC3000, which are functionally similar to HrpK1 in promoting translocation of type iii secretion system effectors. *J. Bacteriol.* 189:8059–8072.
- Lange, H. W., Tancos, M. A., Carlson, M. O., and Smart, C. D. 2015. Diversity of *Xanthomonas campestris* isolates from symptomatic crucifers in New York State. *Phytopathology.* 106:113–122.
- Lenth, R. V. 2016. Least-squares means: the R package lsmeans. *J. Stat. Softw.* 69:1–33.
- Lindahl, G., Sironi, G., Bialy, H., and Calendar, R. 1970. Bacteriophage lambda; abortive infection of bacteria lysogenic for phage P2. *Proc. Natl. Acad. Sci. U. S. A.* 66:587–594.
- Lu, G.-T., Ma, Z.-F., Hu, J.-R., Tang, D.-J., He, Y.-Q., Feng, J.-X., and Tang, J. L. 2007. A novel locus involved in extracellular polysaccharide production and virulence of *Xanthomonas campestris* pathovar *campestris*. *Microbiology.* 153:737–746.
- Makarova, K. S., Wolf, Y. I., Snir, S., and Koonin, E. V. 2011. Defense islands in bacterial and archaeal genomes and prediction of novel defense systems. *J. Bacteriol.* 193:6039–6056.

Miller, J. H. 1972. *Experiments in Molecular Genetics*. Cold Spring Harbor, New York: Cold Spring Harbor Laboratory

de Mendiburu, F. 2016. *Agricolae: statistical procedures for agricultural research*. <https://cran.r-project.org/web/packages/agricolae/index.html>

Morello, J. E., and Collmer, A. 2009. *Pseudomonas syringae* HrpP is a type III secretion substrate specificity switch domain protein that is translocated into plant cells but functions atypically for a substrate-switching protein. *J. Bacteriol.* 191:3120–3131.

Myung, H., and Calendar, R. 1995. The old exonuclease of bacteriophage P2. *J. Bacteriol.* 177:497–501.

Peritore-Galve, F. C., Miller, C., and Smart, C. D. 2020. Characterizing colonization patterns of *Clavibacter michiganensis* during infection of tolerant wild *Solanum* species. *Phytopathology.* 110:574-581

Qian, W., Jia, Y. T., Ren, S. X., He, Y. Q., Feng, J. X., Lu, L. F., Sun, Q., Ying, G., Tang, D. J., Tang, H., Wu, W., Hao, P., Wang, L., Jiang, B. L., Zeng, S., Gu, W. Y., Lu, G., Rong, L., Tian, Y., Yao, Z., Fu, G., Chen, B., Fang, R., Qiang, B., Chen, Z., Zhao, G. P., Tang, J. L., and He, C. 2005. Comparative and functional genomic analyses of the pathogenicity of phytopathogen *Xanthomonas campestris* pv. *campestris*. *Genome Res.* 15:757–767.

Ryan, R. P., Vorhölter, F. J., Potnis, N., Jones, J. B., Van Sluys, M. A., Bogdanove, A. J., and Dow, J. M. 2011. Pathogenomics of *Xanthomonas*: understanding bacterium-plant interactions. *Nat. Rev. Microbiol.* 9:344–355.

Schiltz, C. J., Adams, M. C., and Chappie, J. S. 2020. The full-length structure of *Thermus scotoductus* OLD defines the ATP hydrolysis properties and catalytic mechanism of Class 1 OLD family nucleases. *Nucleic Acids Res.*

Schiltz, C. J., Lee, A., Partlow, E. A., Hosford, C. J., and Chappie, J. S. 2019. Structural characterization of Class 2 OLD family nucleases supports a two-metal catalysis mechanism for cleavage. *Nucleic Acids Res.* 47:9448–9463.

Sutton, J. C., and Williams, P. H. 1970a. Comparison of extracellular polysaccharide of *Xanthomonas campestris* from culture and from infected cabbage leaves. *Can. J. Bot.* 48:645–651.

- Sutton, J. C., and Williams, P. H. 1970b. Relation of xylem plugging to black rot lesion development in cabbage. *Can. J. Bot.* 48:391–401.
- Swingle, B. S., Thete, D., Moll, M., Myers, C. R., Schneider, D. J., and Cartinhour, S. Characterization of the PvdS-regulated promoter motif in *Pseudomonas syringae* pv. tomato DC3000 reveals regulon members and insights regarding PvdS function in other pseudomonads. *Mol. Microbiol.* 68:871-889
- Tancos, M. A., Lowe-Power, T. M., Peritore-Galve, F. C., Tran, T. M., Allen, C., and Smart, C. D. 2018. Plant-like bacterial expansins play contrasting roles in two tomato vascular pathogens. *Mol. Plant Pathol.* 19:1210–1221.
- Tang, J., Kang, M., Chen, H., Shi, X., Zhou, R., Chen, J., and Du, Y. 2011. The staphylococcal nuclease prevents biofilm formation in *Staphylococcus aureus* and other biofilm-forming bacteria. *Sci. China Life Sci.* 54:863–869.
- Tran, T. M., MacIntyre, A., Hawes, M., and Allen, C. 2016. Escaping underground nets: extracellular DNAses degrade plant extracellular traps and contribute to virulence of the plant pathogenic bacterium *Ralstonia solanacearum*. *PLOS Pathogens.* 12:e1005686.

Vicente, J. G., and Holub, E. B. 2013. *Xanthomonas campestris* pv. *campestris* (cause of black rot of crucifers) in the genomic era is still a worldwide threat to brassica crops. *Mol. Plant Pathol.* 14:2–18.

Whitchurch, C. B., Tolker-Nielsen, T., Ragas, P. C., and Mattick, J. S. 2002. Extracellular DNA required for bacterial biofilm formation. *Science.* 295:1487–1487.

White, T. J., and Gonzalez, C. F. 1995. Electroporation of *Xanthomonas*. In *Electroporation Protocols for Microorganisms, Methods in Molecular Biology™*, Humana Press, p. 135–141.

Yao, G. W., Duarte, I., Le, T. T., Carmody, L., LiPuma, J. J., Young, R., and Gonzalez, C. F. 2017. A broad-host-range tailocin from *Burkholderia cenocepacia*. *Appl. Environ. Microbiol.* 83:e03414-16.

## APPENDIX 2

### **Diversity Preview Weekend 2018 Extension Report**

#### **Introduction to diversity in STEM**

Representation of people from diverse backgrounds in the workplace creates a better atmosphere and increases overall productivity. Studies have also shown that diverse groups are more apt to solve problems in comparison to homogenous groups. Here diversity is defined as differences in racial demographics, cultural and ethnic identities, ability, sexuality, gender, first generation and economic status. Although many axes of diversity exist, this report mainly focuses on ethnic and racial diversity. Graduate education has even lower rates of enrollment by underrepresented minority (URM) students than at the undergraduate level. Therefore, efforts must be focused at encouraging URM students to apply to graduate programs to increase diversity in science, technology, engineering and mathematics (STEM) fields. However, the work does not end there; training academics on effective mentoring, reducing biases in the admissions process, and hiring faculty from URM backgrounds must be prioritized to create an inclusive environment in which URM students can succeed.

The first step is to understand the current diversity of graduate students from URM backgrounds in the USA, Cornell University, and within the School of Integrative Plant Sciences (SIPS). According to the 2006-2016 Graduate Enrollment and Degrees report by the Council of Graduate Schools, the percentage of ethnic/racial URM student enrollment in graduate programs in 2016 was a cumulative 33.5% (Fig. A2.1). The breakdown is: bi/multiracial, 3%; Latinx/Hispanic, 10.9%; Native American/Alaska Native, 0.5%; Asian, 7.1%; Black/African American, 11.8%; and Native Hawaiian/Pacific Islander, 0.2% (Fig. A2.1). These low percentages are in stark contrast to the 60.7% of students who self-identified as white entering

graduate programs in 2016 (the other 5.9% was accounted by those who did not provide Race/Ethnicity) (Fig. A2.1). This report did not include data on first-generation, socioeconomic, sexuality and gender, or ability status. These data can provide a background with which we can analyze URM demographics in graduate programs at Cornell.

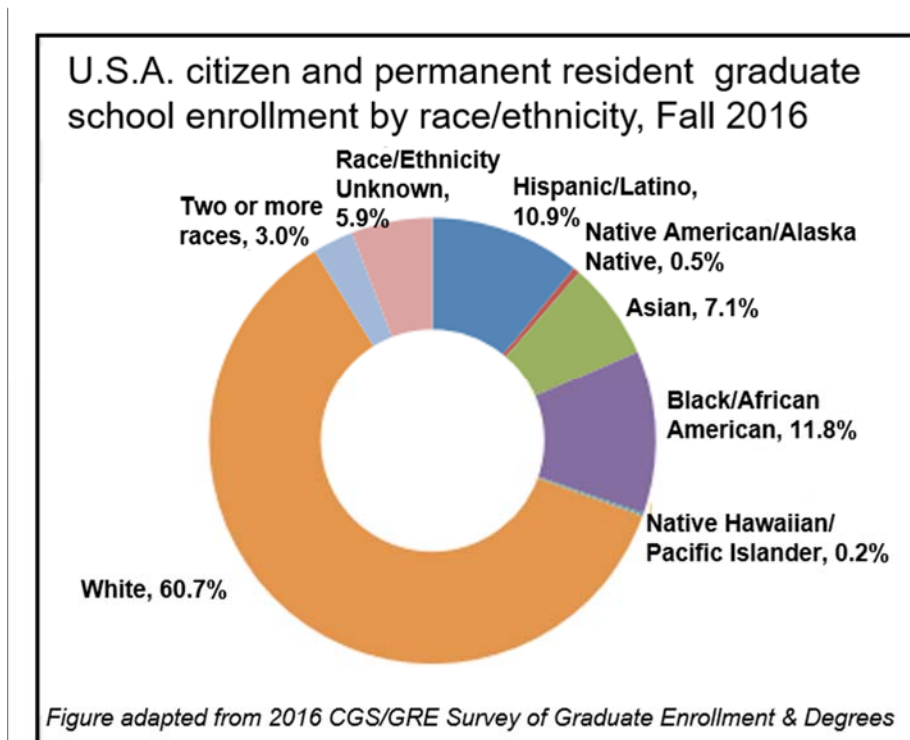


**FIGURE A2.1.** Nation-wide statistics of graduate school enrollment by race and ethnicity. Figure adapted from the Council of Graduate Schools “Graduate Enrollment and Degrees: 2006 to 2016” report.

[http://cgsnet.org/ckfinder/userfiles/files/CGS\\_GED16\\_Report\\_Final.pdf](http://cgsnet.org/ckfinder/userfiles/files/CGS_GED16_Report_Final.pdf)

Cornell University strives to be an inclusive institution by recruiting a diverse student body. Graduate and professional student data surveyed by the Cornell University Graduate School in 2017 reported that 17% of new and enrolled graduate students self-identified as URM (including Asian, Black/African American, Latinx/Hispanic, Native American, and multi-racial students) (Fig. A2.2). This is less than half of what is reported as the average national percentage

of URM students (39.4 %) enrolling in graduate programs by the Council of Graduate Schools (Fig. A2.1). Furthermore, 42.7% of new and enrolled Cornell graduate and professional students were International (of any race/ethnicity), and the remaining 31.4% as white (A2.2). There was a 6.2% gender disparity with more males enrolling and already at Cornell in comparison to females (Fig. A2.2). These statistics did not include information on non-binary or trans students. In racial/ethnic demographic surveys the distinction between USA URM students and international students is important because of the systemic educational and societal barriers that URM students face in the USA. This separation does not mean that international students do not face substantial barriers in their home countries and in the USA. Statistics on sexuality, socioeconomic and first-gen, or disability statuses were not reported in this survey.

SIPS has partnered with the non-profit Gender at work to undergo an internal gender and diversity audit with the aim of identifying barriers impeding recruitment of diverse students, staff, post-docs, and faculty. At the faculty level, 88% self-identified as white; 9% as Asian; 1% as Hispanic/Latinx; and 1% as Native American/Alaska Native with a gender split of 69% male and 31% female professors (Fig. A2.3). In 2017, the percentage of international students was 31.8%, with USA citizens making up the other 68.2% (Fig. A2.3). This is in contrast with the average enrollment of international students at Cornell of 47% (Fig. A2.4). The survey data of SIPS graduate students enrolled in 2017 was less racially/ethnically diverse than that of Cornell as a whole: white 78.4%, Black/African American 0%, Native American/Indigenous 0%, Latinx/Hispanic 11.4%, Asian, 2.3%, Multicultural-Non-URM 2.3%, Multicultural-URM 1.1%, Unreported, 4.5% (Fig. A2.4).

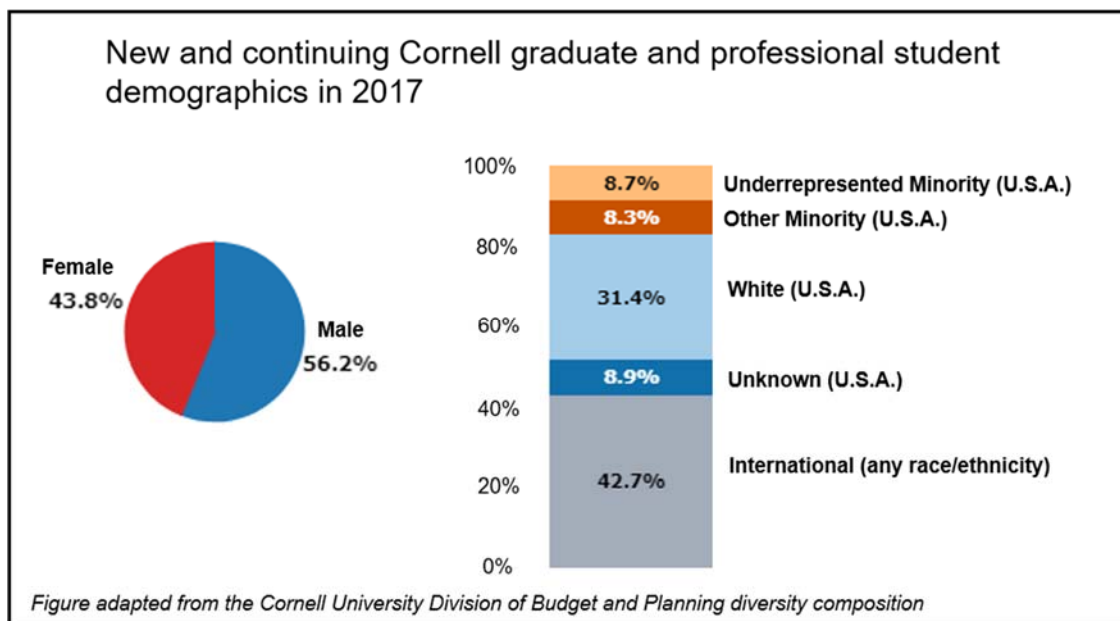


**FIGURE A2.2.** Binary gender and race/ethnicity/international demographics of Cornell graduate and professional students in 2017. Figure adapted from the Cornell University Division of Budget and Planning diversity composition dashboard.

[http://irp.dpb.cornell.edu/tableau\\_visual/diversity-composition-dashboard](http://irp.dpb.cornell.edu/tableau_visual/diversity-composition-dashboard)

Gender parity of graduates was almost equal, with 48% of enrolled SIPS grads identifying as female (Fig. A2.4). Survey data from SIPS demonstrates a disparity between national and Cornell-wide percentages of graduate diversity and that recorded in SIPS, and confirms that SIPS is overwhelmingly white. The stark decline from 48% enrolled graduate students self-identifying as women to 31% self-identified women faculty highlights the leaky pipeline in academia, which is indicative of systemic issues that women face in higher education. The internal audit is currently working to identify and correct barriers and systemic issues within the school that could alleviate these systemic issues.

Unfortunately, the lack of diversity within SIPS is common for postsecondary

educational programs in agricultural sciences. Lack of inclusivity in agricultural sciences as well as unfavorable images of agriculture have been suggested as barriers for URM enrollment in agricultural education programs (Wiley et al., 1997). Furthermore, Cornell faces the barrier of being an Ivy League institution, which has historically been exclusionary to URM students and is inaccessible for lower income students. On a personal note: I spoke with academic and non-academic Latinx colleagues about how URM students might not find agriculture as ‘attractive’ of a field as other areas of research, which was discussed by Wiley and colleagues. There is a notion that “URM students simply are not interested in agriculture,” which I have heard several times here at Cornell and at other institutions. This simply is not true. Agriculture is a way of life for Latinxs along the Borderlands of the USA and Mexico, all across Mexico, Central America, South America, and the Caribbean. Violence against Latinx, Black/African American, and Indigenous farmers paired with US imperialism has led to removal of land ownership and labor exploitation of Black and Indigenous people of color (POC) and non-POC Latinxs (Wimberly et al., 2018; Anzaldúa 1987). Recently, Leah Penniman, the co-founder of Soul Fire Farms in upstate New York, spoke at Cornell about her new book *Farming while Black* (<https://youtu.be/x31POPHF6bl>). In her book and talk, she discussed how Indigenous and West African peoples pioneered many of the common farming techniques and practices used in the past and present. She also stated that 14 percent of farmers in the USA were Black in 1920, which has dropped to less than 2 percent in 2019 due to racist policies, violence, segregation, the jim crow south, and other systemic barriers perpetrated by the US government (Penniman 2018; “Why have Americas Black farmers disappeared?”).

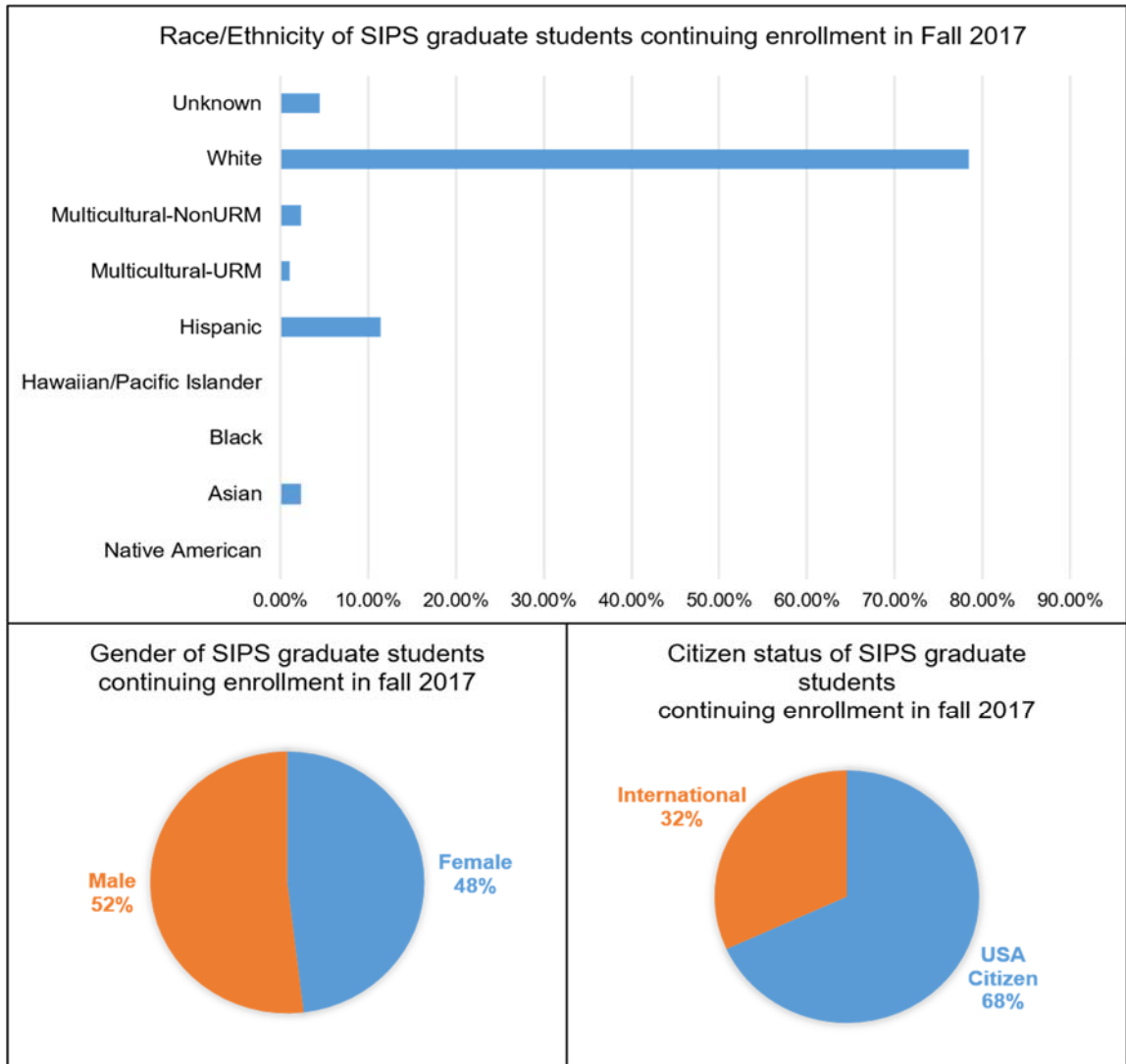


**FIGURE A2.4.** Racial/Ethnic (top), gender (bottom left), and international status (bottom right) of graduate students enrolled in SIPS programs in 2017. Data were collected and arranged by the SIPS administration in collaboration with Gender at Work. Full version can be accessed here:

<https://sips.cals.cornell.edu/sites/sips.cals.cornell.edu/files/shared/SIPS%20Diversity%20Data%20-%20Fall%202017%20%28002%29.pdf>

To address the notions that URM students are not interested in agriculture we need to incorporate non-revisionist histories of agriculture and policies that have shaped socio-political

issues around agriculture into undergraduate, graduate, and faculty education. This, paired with holistic admissions processes, better mentorship training, and facilitated discussions surrounding race/ethnicity, gender, sexuality, ability, economic status, and citizenship status can begin to improve diversity, equity and inclusion in SIPS graduate programs at Cornell.

### **Inception and expansion of the Diversity Preview Weekend**

In 2017, graduate students from the departments of Ecology and Evolutionary Biology (EEB) and Neurobiology and Behavior (NBB) identified low numbers of applications from URM students as being one of the major barriers for their departments being diverse at the graduate student level. They predicted that this might be because of differences in rates of exposure, access to resources, and network connections of qualified URM students. In order to address this issue, they created the 2017 Diversity Preview Weekend (DPW), which was hosted from April 20-23<sup>rd</sup> on the Ithaca campus. This program invited 22 high-achieving students from URM backgrounds who would benefit from graduate student guidance to strengthen their ability to create a highly competitive graduate school application. The aim was to encourage the students through workshops on interviewing, application timeline, fellowships, *curriculum vitae* creation, and personal statements. Along with the workshops, attendees had the opportunity to have mock interviews with professors, tour the campus, and to have formal and informal conversations with graduate students and professors about topics ranging from research to personal life in postgraduate studies.

This program was expanded in 2018 by the partnership of the departments of EEB, Entomology, and the School of Integrative Plant Science (SIPS), whose students also identified low application numbers from URM students as a contributor to the lack of graduate student diversity. Planning began during the summer of 2017, where we began to publicize the event

through various outlets including an official Cornell Diversity Preview Weekend website (<http://www.cornelldpw.org/>), Facebook page, Twitter account (@Cornell\_DPW), and through email contacts from graduate students' undergraduate institutions, Historically Black Colleges and Universities, Hispanic Serving Institutions, Native American Colleges, Women's Colleges, identity-related professional societies, and beyond. Applications were opened in October of 2017 with a deadline of December 1<sup>st</sup>. This deadline was extended for students in Puerto Rico who had much difficulty accessing an online connection to send their application materials after hurricane Maria. Applications consisted of a 1-page personal statement, *curriculum vitae*, unofficial transcript, and one letter of recommendation.

Eighty-three total applications were submitted, among those only 79 were complete. This was an almost four-fold increase from the 2017 pilot year, where 44 applications were submitted. Applications that were not fits for the program based on academic interests not aligning (e.g. applications where they solely talked about attending medical school), or students who had already been accepted to a graduate program were politely rejected with personalized emails as to why they were not accepted. The remaining applications were sent to 24 graduate student reviewers from EEB, Entomology, and SIPS. Four people, two of which were within the field that the student was interested in, and two from external departments/school reviewed each application. Applications were reviewed with six criteria ranked from 1-5 with 1 being "do not accept" and 5 being "accept." The criteria were as follows:

1. Research Interest Fit: Does the applicant's stated research interest align with the chosen field? (e.g. if the applicant is interested in psychology, this is not a good fit.)
2. Motivation and Demonstrated Interest: Is the applicant committed to pursuing a graduate education in their field of interest? How have they demonstrated this commitment?

3. Demonstrated Ability to Succeed: How has the applicant achieved success in academic and/or non-academic spheres? (i.e. Has the applicant overcome adversity or been successful in a way that may speak to their ability to complete a graduate program? This may include successes outside of research or the classroom.)
4. Experience and Relevant Coursework: What research experience has the applicant had? Relative to courses available at their institution (i.e. the courses available at a liberal arts college and an R1 university are different), has the student maximized enrollment in courses related to their field of interest?
5. Need or Impact of Attendance: How might attendance at this preview weekend impact the student's ability to successfully apply to graduate school in the future?
6. Other or Intangibles: Are there other facets of this application not covered in 1-5 that you wish to discuss?

The admissions committee met in person for in-depth discussions about the merits of each applicant, and decided to give precedence to students in their junior or senior years and to students who were already strong applicants, but who would benefit greatly from added guidance and encouragement through this program. Applicants who were rejected were sent personalized emails explaining why they were rejected, and they were encouraged to apply to DPW2019. We explicitly stated in the emails that students could reach out to us to receive the feedback on their applications in order to strengthen their personal statements, CVs, etc. for future programs. In total, 40 students from 15 different states, Guam, and Puerto Rico (Fig. A2.5) were accepted for DPW2018.

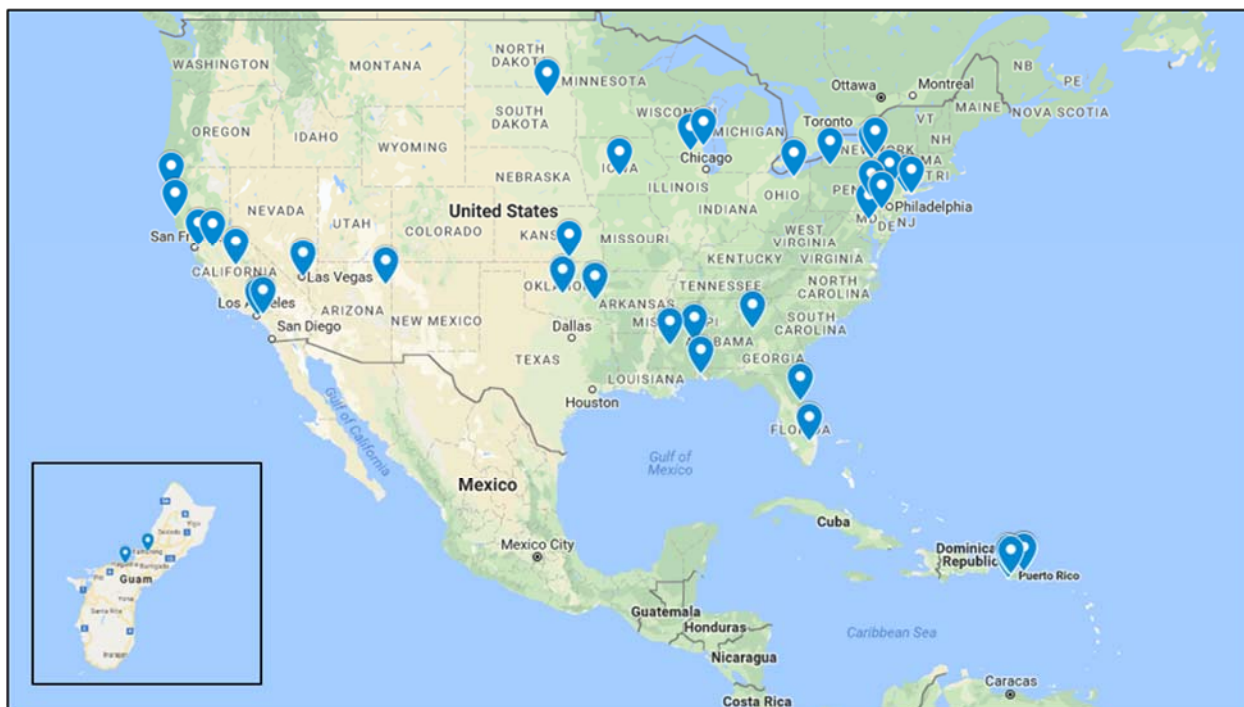


FIGURE A2.5. Where DPW2018 attendees were from. Guam not to scale.

### March 8<sup>th</sup>, DPW2018: Day 1

Beginning the morning of March 8<sup>th</sup>, the students began arriving and registering for the event at a centralized location in Corson-Mudd Hall. Graduate student volunteers also made trips to airports in Ithaca and Syracuse to pick up the attendees. There we provided the students with schedules and other materials for the weekend, as well as graduate school application information provided by the Cornell Graduate School. Students had a half-day to explore the campus, talk to graduate students, and meet each other in an informal setting. The first evening we had a relaxed dinner with opening remarks introducing ourselves and speaking about what DPW aims to achieve. Graduate students were critical in being able to bring the students to and from campus. In order to reduce costs of the weekend, graduate students offered up spare rooms, inflatable beds, and couches for the DPW students to stay during the weekend event.

**March 9<sup>th</sup>, DPW2018: Day 2**  
**Workshop 1: Graduate School Resources and Support for URM Students**



**FIGURE A2.6.** Anitra Douglas-McCarthy introduces the basics of graduate school during the first workshop.

The second day started with a presentation and interactive discussion on general aspects of graduate school led by Anitra Douglas-McCarthy, the Cornell Graduate School Director of Recruitment (Fig. A2.6). Anitra introduced concepts of what a graduate degree can do for educational development and how that influences job opportunities, as well as what should be expected from a graduate program (i.e. more independence and responsibility, in-depth studies of a field, etc.). How to choose the right graduate program was a theme in this presentation; a tip that attendees found helpful was that school rankings matter less than the support (mentorship, educational, and financial) that can be received from a program. Other factors for choosing the right program included reputation, size of institution, cost, geographic location, admissions criteria, available resources, future career options, support system for graduate students, and

professional development opportunities. Anitra also spoke about differences between MPS, MS, and PhD degrees, specifically about how each degree is structured, what kind of funding is most common for each degree, and how they prepare you for different career trajectories. Personal feedback from students informed me that some of them had not heard about MPS degrees and were not aware of common differences in funding between MS and PhD degrees. Information on graduate studies at Cornell was also presented. Anitra finished by talking about the application process and materials, developing an application timeline, and funding available.

### **Workshop 2: How to interview**

This workshop was organized and run by Janani Hariharan (SIPS) and Natalie Hofmeister (EEB) with contributions from Kass Urban-Mead (Entomology), John McMullen (Ento), Lizzie Lombardi (Ento), Eugene Law (SIPS), and Jenny Uehling (EEB). Presenters described the interview process by introducing the idea of starting with a practiced “elevator pitch” as a response to the question “tell me about yourself.” Presenters introduced a rough guide for elevator pitches as starting with present (what are you doing right now?), past (what have you done? What skills did you gain?), and future (why do you want this particular opportunity?). Each of the contributors then gave rehearsed elevator speeches to demonstrate how good and bad pitches sound, then the session broke out for students to work on their own speeches and practice with graduate students and attendees.

The presenters had previously sent a poll out to faculty to get a sense of what faculty expect in an interview. The top three important criteria that faculty identified for interviewees hoping to join their lab are (1) that they had read the PIs research website, (2) were generally familiar with their research area, and (3) had read at least some of their papers. Criteria that was less important to faculty were to have a well-developed understanding of where the field is

heading, having done work in their field, and having published papers in their field. Traits that were most important for faculty were intelligence, research experience, curiosity, ability to describe research interests, collegiality, and excitement. This is in contrast to GPA, work experience, and GRE scores, which were less important to the polled faculty.

Asking questions to the interviewer was identified as one of the most important aspects of an interview. Presenters talked about three different areas that should be asked about during the interview process: program, student resources, and social life. They encouraged students to ask faculty about their opinions of the graduate program, its strengths and weaknesses, and their perceived direction of the program. For student resources, they made sure students knew to ask about how students are typically funded, average time to completion, and availability of professional development programs. The social life category included asking about how the stipend supports cost of living in the area, how active the lab is outside of work, and whether or not there is a graduate student association for the department. The session was ended on the encouraging note that professors once sat in the prospective graduate student's seat and that the interviewers are there because they want to get to know the candidate!

### **Faculty meetings**

After department/school-specific lunches, students broke off to have 30-minute one-on-one meetings with faculty. The goal of these meetings was for students to talk to professors about research and to discuss graduate studies in science. In a post-DPW survey, many faculty reported having interesting and engaging discussions during the meetings, and the attendees expressed much enthusiasm about being able to meet with professors and have them talk about their research interests.

## Facility tours



**FIGURE A2.7.** Top image: SIPS Assistant Director Magdalen Lindeberg gives a tour of the Liberty Hyde Bailey Conservatory. Bottom left: Entomology students tour the insect collection at the Dyce Lab. Bottom right: EEB students visit the Cornell Lab of Ornithology and see the amazing diversity of preserved bird specimens.

After four meetings with faculty members, students went on facility tours specific to each discipline (Fig. A2.7). SIPS students visited the plant transformation facility and were given a tour guided by Matthew Willmann. The group was set to visit the hydroponics facility at Kenneth Post Laboratory with a tour from Horticulture graduate student Erica Hernandez, but snow and rain made us change plans. Magdalen Lindeberg led a guided tour through the Liberty Hyde Bailey Conservatory, where the students learned about Welwitschia, titan arum, and the Victoria lily. EEB students took tours at the Lab of Ornithology, and Entomology students toured the insect collections at the Dyce lab.

### **SIPS social, dinner and lightning talks**

The SIPS-specific portion of the evening was concluded with a social and dinner including faculty, staff, post-docs, visiting scientists, graduate students, and DPW attendees. After the dinner, 5-minute lightning talks were presented by Horticulture section graduate student Haley Rylander, Soil and Crop Science section (SCS) post-doc Roli Wilhelm, and SCS section graduate student Eugene Law. EEB and Entomology graduate students and professors also presented their research during lightning talks at their dinner. Among those were Prof. Kelly Zamudio (EEB), graduate student Matt Boucher (Entomology), and graduate student Collin Edwards (EEB).



**FIGURE A2.8.** Top: Graduate student Eugene Law (SIPS) gives a lightning talk on his agronomic research on perennial grains. Bottom left: Prof. Kelly Zamudio talks about her research on diversification and conservation of neotropical frogs. Bottom right: Graduate student Matt Boucher speaks about his research on spread of a bacterial plant pathogen by insects.

## March 10<sup>th</sup>, DPW2018: Day 3

### Workshop 3: applying for fellowships



**FIGURE A2.9.** Graduate students Lauren Brzozowski and Kate Eisen give advice on writing the NSF-GRFP.

Day 3 started out with a presentation on applying for fellowships, with a heavy focus on the NSF-Graduate Research Fellowship (GRFP), by Lauren Brzozowski (SIPS) and Kate Eisen (EEB). They began by giving a broad overview on what scholarships, fellowships, and grants are and what they mean for graduate careers. They then honed in on the NSF-GRFP, briefly touching on the eligibility and requirements, thinking about projects, contacting faculty, the writing process, and their own experiences. Attendees asked many questions about what the review process looks like from the reviewer standpoint, which led to a discussion about writing the GRFP for a broad audience given that reviewers can come from different academic disciplines. The main takeaways for having a successful application were: (1) well defined intellectual merits and broader impacts; (2) creative, original, and transformative concepts; (3) well-reasoned and organized basis for activity, and a way of assessing success; (4) qualifications of individual and organization for activities; (5) adequate resources and support at the institution or through collaborations. In personal communication with several students, they expressed

gratitude for breaking down the difference between fellowships, grants, and scholarships and spoke about how they did not realize that STEM graduate studies were mostly funded through these sources. Many students were also interested in how to apply for other external grants, which will be added to the workshop curriculum for the coming years.

#### **Workshop 4: Writing your personal statements**

Several weeks before the event, we contacted the attendees and asked them to bring a prepared personal statement for this interactive workshop. This included the 1-page statement that they wrote for their DPW application or a statement they planned to use for REUs, internships, or graduate school applications. Graduate students Amelia Weiss (EEB), Erin Larson (EEB), and Cinnamon Mittan (EEB) organized this workshop, and were assisted by seven other graduate students who served as personal statement reviewers. The workshop began with a presentation on what a personal statement is, how it can help you expand on your CV, give a picture of you as a person and researcher, and how it can help show that you have what it takes to be a graduate student. They presented a general structure of personal statements tailored to graduate school applications:

- Intro
  - Narrative hook (often an anecdote)
- Recent Past
  - Post-high school
  - Influential classes/mentors
  - Research experiences
- Future
  - Plans

- Including specific graduate program details
- Conclusion that bookends narrative



**FIGURE A2.10.** Students learning about how to create an effective personal statement through a presentation and peer review.

The presenters emphasized that each personal statement should be tailored to each school and should link back to the research statement. Cinnamon used the “evolution” of her personal statement drafts as an example to talk about how whole paragraphs are often condensed into one sentence during the editing process, and how to use ideas drawn from those paragraphs to “show not tell” experiences critical to why you are pursuing graduate studies. The presentation ended on the importance of having many people from different backgrounds read writing pieces to improve the statement.

Post-presentation, students broke out into small groups with two graduate student editors who read each statement and gave personal feedback on what they liked about the statement and how it can be improved. After the initial graduate student edits, attendees had the opportunity to read each other's' work and give peer feedback. Through having the students work with each other, we hope to create a network where they feel comfortable contacting each other for future peer review of their graduate school applications.

### **Workshop 5: Crafting a CV**



**FIGURE A2.11.** Graduate students Rey Cotto Rivera, Anyi Mazo Vargas, and Nick Fletcher give feedback on students' CVs.

Workshop 5 was organized and presented by Emily Funk (Entomology), Nick Fletcher (EEB), Katie Holmes (Entomology), Kara Fikrig (Entomology), Rey Cotto Rivera (Entomology), and Anyi Mazo Vargas (Entomology). This session was organized in a similar fashion as the personal statement workshop, with a presentation followed with a breakout session for feedback on CVs. The presentation revolved mostly around what to include in a CV and in how to order information to make it 'flow'. The example CV flow given was education, research interest (optional), research experience, publications and presentations, teaching experience,

volunteer/extracurricular experience, grants/fellowships/awards, and relevant skills. For individual feedback, we asked the attendees to bring an updated CV or the CV they were asked to submit as part of their application package for feedback from graduate students and peer reviewers.

### **Discussion: Culture and identity in natural sciences**

This session was a closed-door, round-table discussion in small groups about what it meant to be in STEM coming from a marginalized community. Graduate students who are trained facilitators, including Stephanie Aguilon (EEB), Elena Michel (SIPS), Eugene Law (SIPS), and John McMullen (Entomology) joined each table to direct the discussions. Students were very receptive to this session and found it to be a space where they could talk about how stressful the weekend events had been thus far, and the increased pressure given that Cornell is an Ivy League institution. A significant event that happened during the facility tours earlier in the weekend was discussed: in two individual events, white male Cornell students shoved two African-American male DPW students out of the way on the sidewalk. The students who this happened to did not express much concern about these events, but other students in the program were angry and felt that they had been targeted given the recent acts of violence towards students of color on Cornell's campus and across the country. These conversations served as an outlet for the attendees to voice their concerns and opinions about their educational journeys so far and were able to relate to each other's struggles on a personal level.

## Graduate student research fair



**FIGURE A2.12.** Aerial view of the research fair

The idea of the research fair was to have graduate students from all areas of study to bring physical samples of their research to stimulate conversation about research and the type of tools and systems they use in their day-to-day work. This was a great way to highlight the diversity of disciplines available for study at Cornell without exclusively using posters and PowerPoint presentations. The LGBT Resource Center and Mann Library also set up tables to talk about the various resources and support that they offer the graduate community.

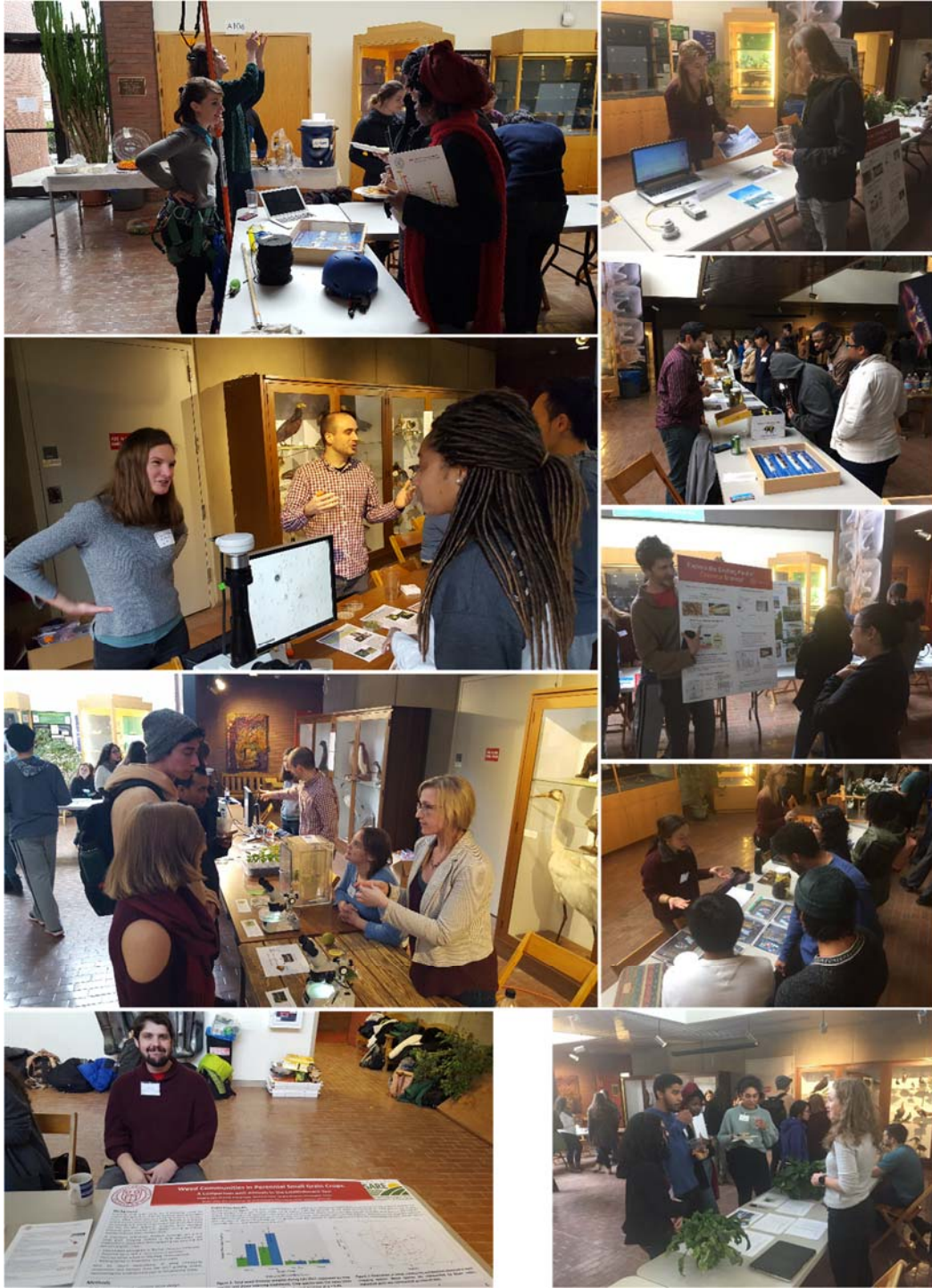


**FIGURE A2.13.** Graduate students from all disciplines show research samples or poster presentations.

## Graduate student life talks

The day was wrapped up with dinner and a graduate student life talk presented by Kristen Brochu (Entomology), Jon Hughes (EEB), and me. This talk was an EEB graduate student recruitment tradition where they send out a survey to graduate students to gather answers to serious and funny questions and turn it into a comedic outlet for tired recruits (in this case attendees). We used the presentation to talk about where graduate students come from, the type of research they do, how much coffee they drink, showcase funny lab traditions, embarrassing field picture stories, and why we chose to study at Cornell. A word bubble was made from the responses to the survey question “why did you choose to come to Cornell?” and the biggest words were “best” and “people.”



**FIGURE A2.14.** Graduate student life talks (left) and the word cloud from graduate students on why we chose Cornell (right). Word cloud provided by Jon Hughes.

## March 11<sup>th</sup>, DPW2018: Day 4

### Day 4: Closing remarks

The last half-day was used to thank the attendees and organizers for making DPW a wonderful weekend. Many of the graduate student hosts gave the attendees tours around campus and Ithaca before driving them to the airports. The attendees also used this time to create a large Facebook group with everyone that came in order to stay in touch and to keep each other accountable for their successes in undergrad and graduate school.

## Weekend statistics and outcomes

### 2017: 22 attendees

Three students from the 2017 cohort interviewed for graduate school in EEB at Cornell during spring of 2018, all were extended offers. One of the students has decided to come to Cornell, another to a program at Princeton University, and the other at UC-Santa Cruz.

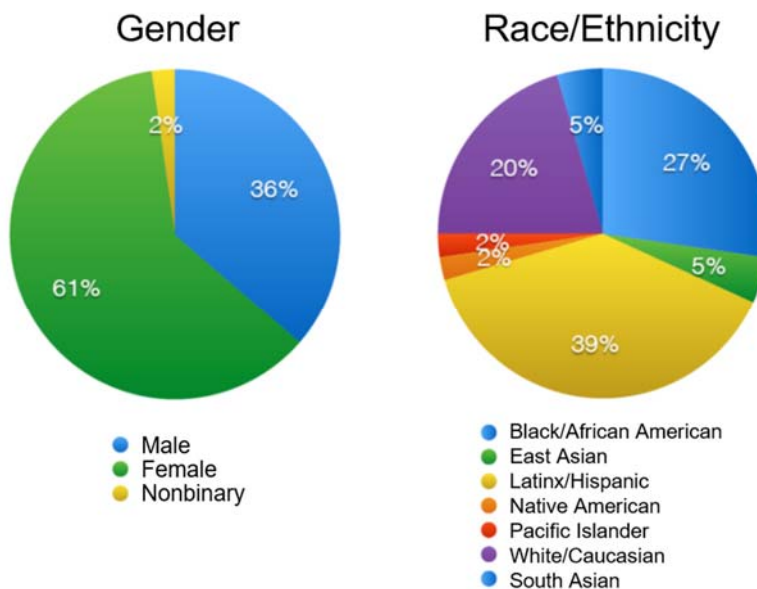


**FIGURE A2.15.** Pie chart statistics on gender and race/ethnicity of DPW 2017 attendees. Data were collected and analyzed by Suzanne Pierre and Cait McDonald.

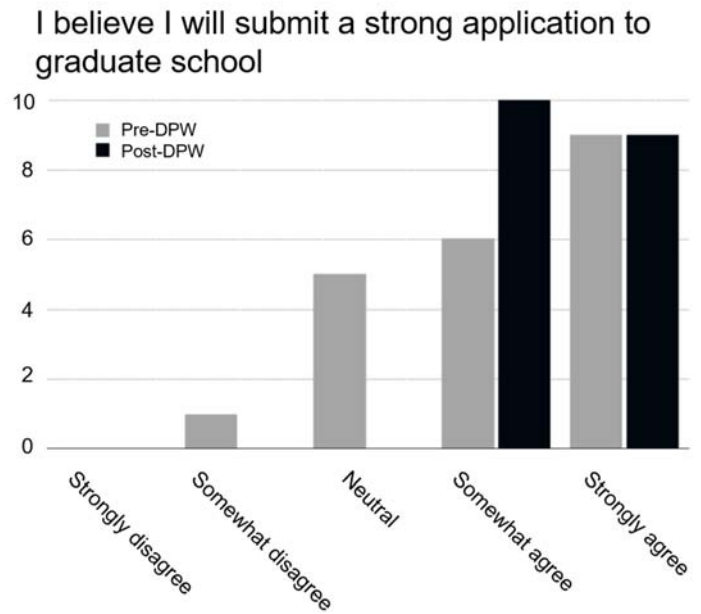
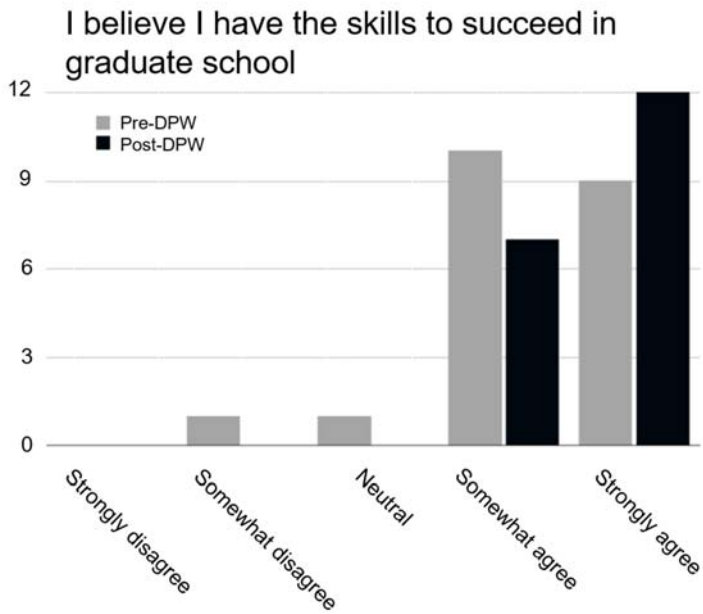
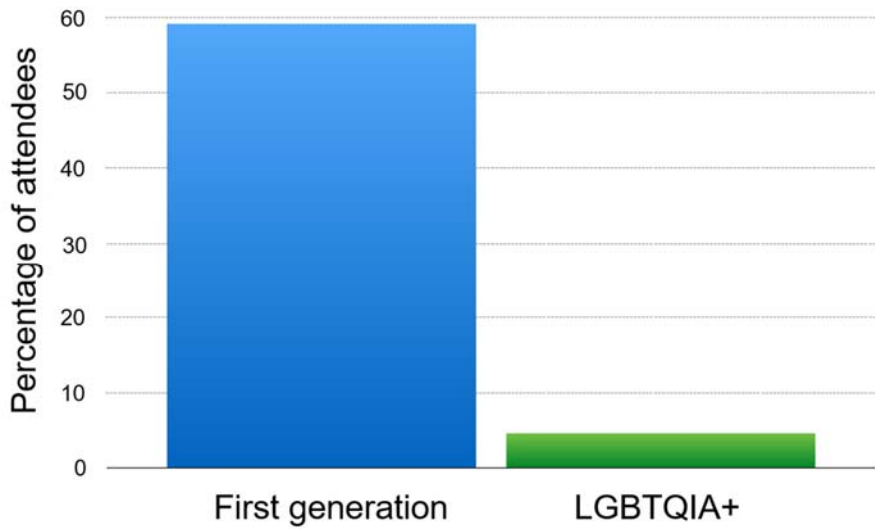


**FIGURE A2.16.** Bar charts on percentage of first-gen and sexuality identities of DPW2017 attendees (top). Bar charts showing pre- and post-weekend survey results. Data were collected and analyzed by Suzanne Pierre and Cait McDonald.

### I plan to apply to a PhD program at Cornell

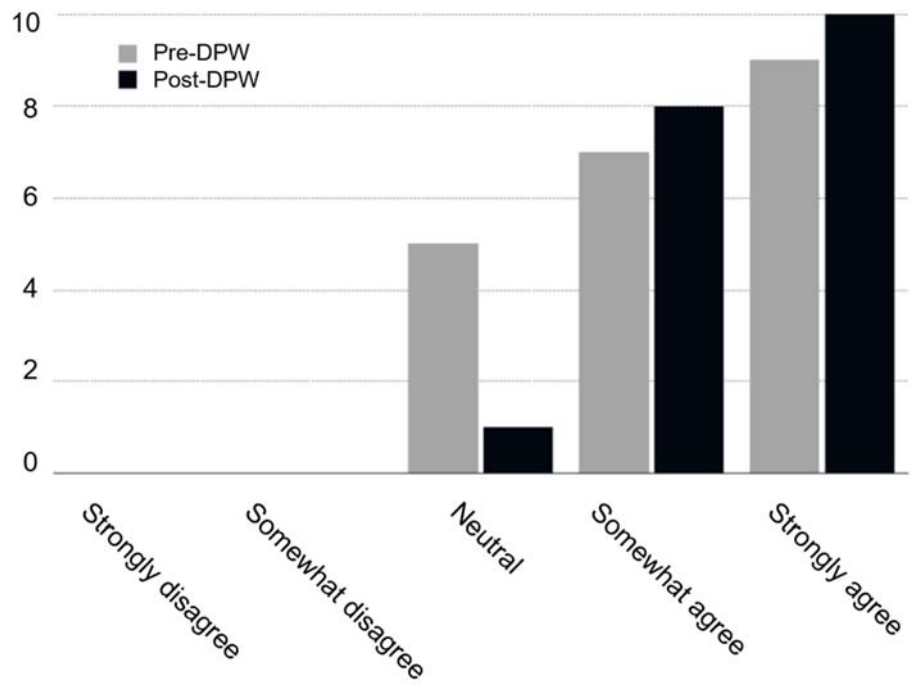


**FIGURE A2.17.** Bar charts showing pre- and post-weekend survey results of the number of students planning on applying to PhD programs at Cornell. Data were collected and analyzed by Suzanne Pierre and Cait McDonald.

**2018: 40 attendees**

A follow-up survey for 2017 and 2018 years was conducted in 2019. Of 62 DPW attendees in 2017 and 2018, 32 (52%) had entered graduate programs (22 PhD, 9 MS, 1 PharmD) at: Arizona State University, Binghamton University, Boston University, Colorado State University, Cornell (8 students), CUNY City College of New York, Massachusetts Institute of Technology, Princeton University (2 students), Ohio State University, University of California-Davis (3 students), UC-Los Angeles, UC-San Francisco, UC-Santa Barbara (2 students), University of Chicago, University of Massachusetts-Amherst, University of Minnesota (2 students), University of Wisconsin-Madison, University of Washington, University of Wyoming and Villanova University.

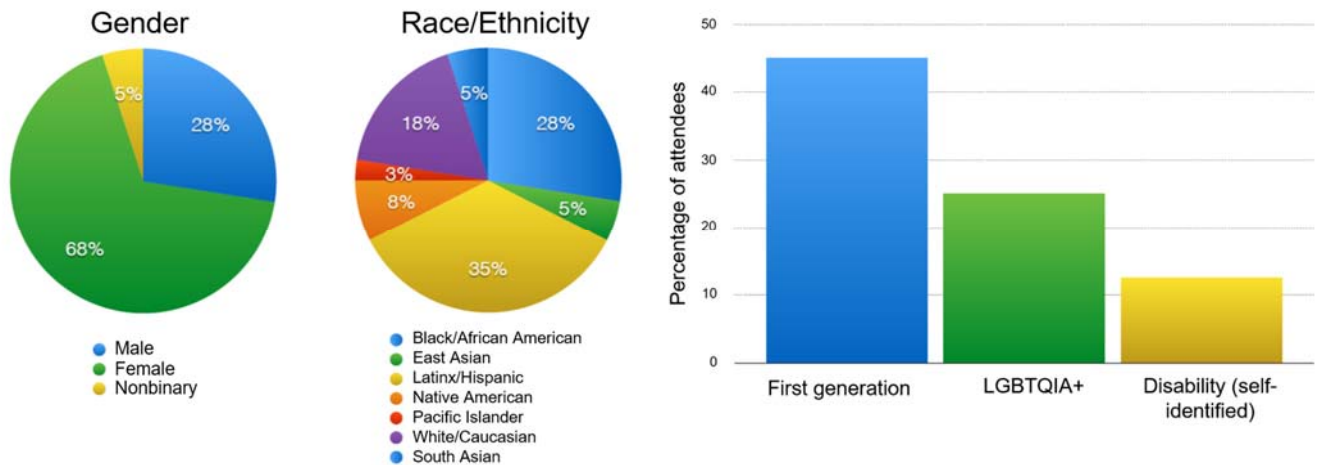


**FIGURE A2.17.** Demographic percentages

of DPW2018 attendees by gender, race/ethnicity, first generation, LGBTQIA+, and ability statuses. Data were collected and analyzed by Stephanie Aguillon.

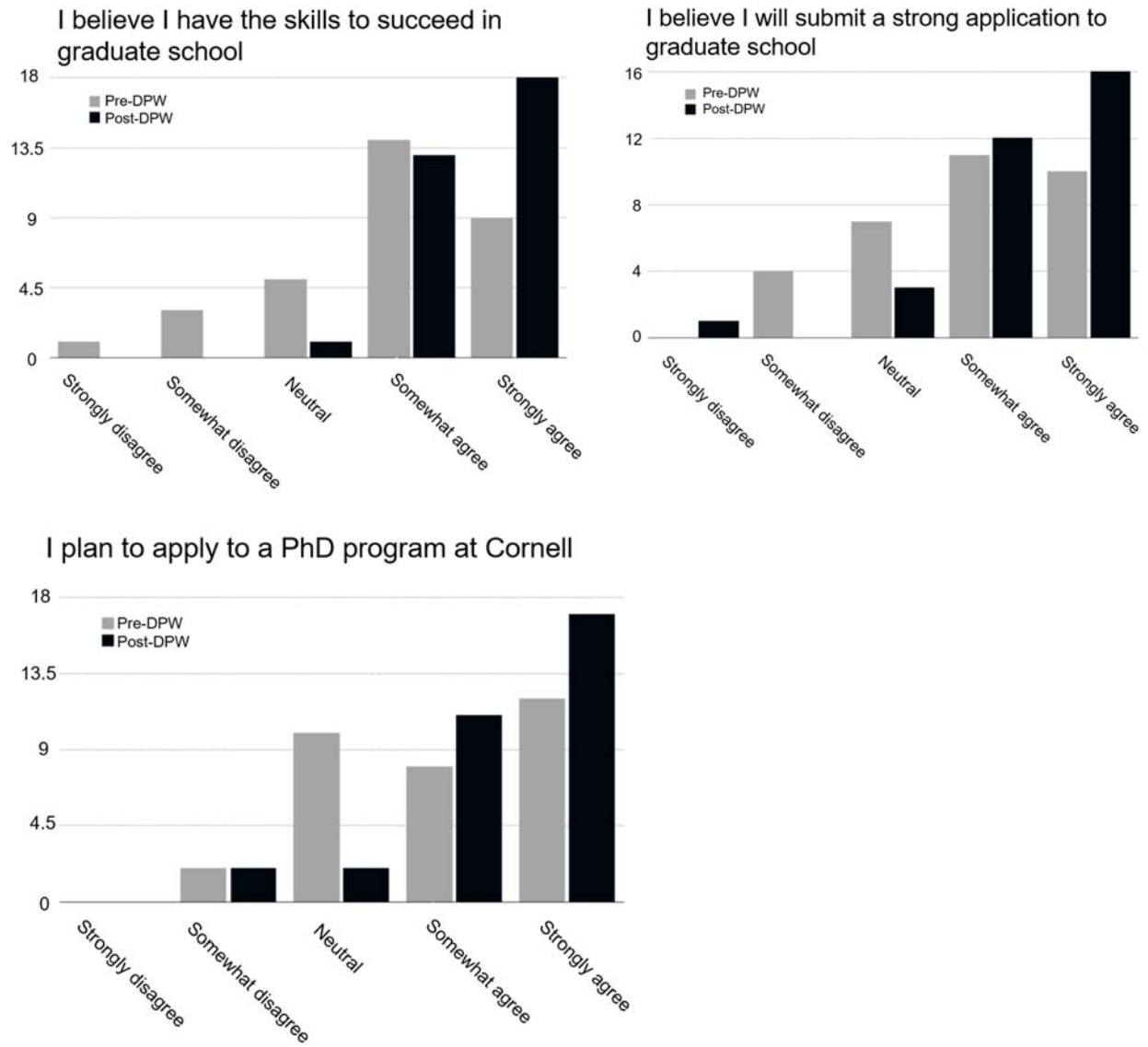


**FIGURE A2.18.** Bar charts showing pre- and post-weekend survey results from DPW2018 attendees. Data were collected and analyzed by Stephanie Aguilon.

## ***ACKNOWLEDGEMENTS***

This event could not have happened without the incredible effort by graduate students. I

apologize in advance to anyone I have missed in these acknowledgements:

DPW 2018 was funded through Director's funds from the School of Integrative Plant Science, the Office of Inclusion and Student Engagement, departmental funds from EEB and Entomology, and GPSA funds from the Entomology graduate student association. Special thank you to the administrators who helped make this event a success, including Anitra Douglas-McCarthy, Chris Smart, Tara Reed, and Tracy Holdridge. 2017 DPW data was collected, analyzed, and plotted by Suzanne Pierre and Cait McDonald. 2018 data was collected, analyzed and plotted by Stephanie Aguilon.

Founders: Suzanne Pierre and Cait McDonald

Co-leaders 2018: Julia Miller, Nick Segerson, Michelle Laterrade, Chris Peritore Galve, Amelia Weiss, Stephanie Aguilon, Kass Urban-Mead, and John McMullen

Social media: Natalie Hoffmeister, Kaitlin Deutsch, Mischa Olson

Tech support: Gregor Siegmund, Lindsay Fennel

Advertising: Anyi Mazo Vargas, Olivia Graham, Christopher Tarango

Admissions: Michelle Wong, Nick Mason, Erin Larson, Lina Arcila Hernandez, Cinnamon Mittan, Stephanie Aguilon, Amelia Weiss, Tim Luttermoser, Mary Centrella, Leticia Smith, Redhika Ravikumar, Laura Figueroa, Kass Urban-Mead, Michelle Laterrade, Lauren Brzozowski, Eugene Law, Janani Hariharan, Breanne Kisselstein, Adriana Hernandez, Nick Segerson, Mischa Olson, Julia Miller, Chris Peritore Galve

Travel and Housing: Kate Eisen, Nelson Milano, Lauren Brzozowski

Weekend Logistics: Chris Peritore Galve, Michelle Laterrade, Julia Miller, Angela Kruse, Jenny

Wilson, Penelope Lindsay, Jenny Uehling, David Chang van Oordt, Lily Twining, Radhika Ravikumar, Kaitlin Deutsch, Ashley Fersch, Zoe Getman-Pickering, Kara Andres

Faculty meeting and speaker organizing: Ben Johnson, Lizzie Lombardi, Tim Luttermoser, Anyi Mazo Vargas, Eugene Law, Al Kovaleski

Pre/Post-Weekend Materials: Emily Funk, Katie Holmes

Hosts: Zoe Dubrow, Mike Fulcher, Martha Sudderman, Juana Munoz Ucros, Ann Bybee-Finley, Arielle Johnson, Greg Vogel, Elena Michel, Max Fishman, Angela Kruse, Hannah Swegarden, Roberto Lozano, Chris Hernandez, Sam Bosco, Lauren Brzozowski, Julia Miller, Nick Segerson, Behrooz Azimzadeh, Kavya Krishnan, Andy Read, Jenna Hershberger, Michelle Laterrade, Emily Funk, Erin Larson, Gregor Siegmund, Cinnamon Mittan, Collin Edwards, Ethan Bass, Natalie Hofmeister, David & Tram, Lizzie Lombardi, Tom Ryan, Jenny Uehling, Amelia Weiss, Charlotte Levy, Keeley MacNeill, Kate Eisen, Jacob Elias, Anyi Mazo Vargas, Katie Holmes, Kara Fikrig, Kaitlin Deutsch, Paige Muniz, John McMullen, Zoe Getman-Pickering, Rey Cotto Rivera

All photos included in this report were taken by Natallie Hoffmeister, Stephanie Aguillon, Michelle Laterrade, Chris Peritore Galve, and Craig Cramer.

## **REFERENCES**

Anzaldúa, G. 1987. *Borderlands / La Frontera: The New Mestiza*. Aunt Lute Books.

Penniman, L. 2018. *Farming while Black: Soul Fire Farm's practical guide to liberation on the land*. Chelsea Green Publishing.

Sewell, S. Why have Americas Black farmers disappeared? *The Guardian*, 29 April 2019, <https://www.theguardian.com/environment/2019/apr/29/why-have-americas-black-farmers-disappeared>

Wiley, Z. Z., Bowen, B. E., Bowen, C. F., and Heinsohn, A. L. 1997. Attitude formulation of ethnic minority students towards the food and agricultural sciences. *J. Agric. Educ.* 38:21-29

Wimberly, C., Martínez, J., Muñoz, D., and Cavazos, M. 2018. Peons and progressives: race and boosterism in the lower Rio Grande Valley, 1904-1941. *WHQ.* 49:437-463